

DISS. ETH. NO. 25570

**FUNCTIONALIZATION OF LIGNOCELLULOSIC MATERIALS  
FOR NOVEL MEMBRANES IN OIL-WATER SEPARATION  
TECHNOLOGY**

A thesis submitted to attain the degree of  
DOCTOR OF SCIENCES of ETH ZURICH  
Dr.sc. ETH Zurich

presented by

*Marta Esther Vidiella del Blanco*

*MSc in Chemical Engineering, Universitat Ram3n Llull*

born on 23.08.1991

citizen of Spain

accepted on the recommendation of

Prof. Dr. I. Burgert (examiner)

Prof. Dr. L. Bergstr3m (co-examiner)

Prof. Dr. M. 3sterberg (co-examiner)

2018

© by Marta Esther Vidiella del Blanco

All rights reserved.

No part of this volume may be reproduced, stored in retrieval system or transmitted in any form or by any means, electronic, mechanical, photocopying recording or otherwise, without the prior written permission of the publishers.

Printed by the Reprozentrale, ETH Zürich, Switzerland

Water is critical for sustainable development and the eradication of poverty and hunger, and is indispensable for human development, health and wellbeing.

*- United Nations*



## Acknowledgments

I grew with the thought that our society could leave at a high technological level while taking care of the environment. With that thought I decided to study Chemical Engineering so that one day I could contribute to making this change. This PhD thesis brought me the opportunity of developing an environmentally friendly material which would help create a cleaner environment - covering my wishes. From the very beginning I faced my PhD thesis with great passion and joy. What I did not know is that it would give me much more than I expected and this was thanks to all the people that contributed to it.

First of all I would like to thank Prof. Ingo Burgert for giving me the opportunity to do my Doctoral Studies in his group. For having the chance of working on such an interesting topic and fascinating material. This last three years allowed me to grow professionally in topics and techniques I had not known about before and also personally through organizing conferences, learning to communicate my work to others and supervising students.

I would like to express my gratitude to Dr. Etienne Cabane who supervised me for the last three years. Having different backgrounds (polymer chemist and chemical engineer), we often had different ideas on how to approach the various topics of this thesis. However, this led to a lot of very fruitful discussions and expanded my horizon making this work so rewarding.

I would also like to thank Prof. Lennart Bergström and Prof. Monika Österberg for kindly accepting the position as co-examiners of my thesis.

This work would have not been possible without my students: Davide Tanadini, Jacob Kjellmann and Vera Gomez, who were always dedicated and reliable for which I am extremely thankful. I am specially grateful to Vera, who in spite of her young age showed to be a great professional, hard working, and reliable person. I really enjoyed supervising her and wish her all the best in the future.

I would like to thank my co-authors Eric Fischer, Luiz Grafulha, and Tobias Keplinger for all their work which contributed very much to the work in this thesis. I

## ACKNOWLEDGMENTS

---

specially would like to thank Tobias for introducing me into Raman spectroscopy, for his patience and help despite my "horrible" fluorinated polymer and for sharing his passion for this technique with me. I also would like to extend my gratitude to Dr. Zeltner for the very useful input on SI-AGET-ATRP and being always opened for discussion. Special thanks go to Asel Maria Aguilar and Dr. Kunze for their EM support. Thanks to all the people in the workshop that helped produce my separation holder, specially to Mr. Jenni and Mr. Meierhans. Also, working with wood, someone needed to prepare my samples. I could not have had more competent people than Mr. Schnider and Dr. Hass.

The office was always a comfortable place to go back to in stormy days and this was thanks to the colleagues I shared the space with, thanks Merve, Chiara, Samuel and Beni. The time spent during my PhD would not have been the same without all the friends and colleagues I shared the time with. Thank you Nicole, Nadia, Gemma, Danilo, Eric, Jan, Antoine, Christian, Marion, Maria, Tobias, Moritz, Stefano, Chiara, Merve, Paola, Philippe, to name a few. Also to my friends back in Spain, who despite the distance were always opened for support and motivation. Special thanks goes out to my flatmates: Rushd, Giacomo and Matthias. Thank you for always making me feel at home.

Without the love and support of my family I would not be who and where I am right now. Thank you for being there for me in every step that I took over the last years of my life. For the constant support, advice, drive and motivation given, specially during the rough times, and sharing the joy with me in the good moments.

Finally, Peter thank you for your constant support, encouragement, patience, and advice over these years. For always being there when I needed you and keeping things in perspective when I did not know how to continue. This accomplishment would not have been possible without you.

## Abstract

With a steady growth in world population and increasing pollution, drinking water is becoming a scarce resource. The main pollutant in water is oil, mostly due to anthropogenic causes. This creates a need for novel oil/water separation devices. In order to decrease the need for oil production and transport, in this work, we proposed the use of bio-based lignocellulosic materials with anisotropic hierarchical porous structure, such as wood, for oil/water separation. Throughout its evolution, the wood structure has been optimized by nature for water and nutrient transport, and mechanical stability of the tree. This makes it an eligible bio-based material for oil/water separation.

We first tested spruce wood cross sections and found out that they could be used in their native state for free oil/water separation. The separation is based on capillary forces, and it operates with high efficiencies, high fluxes, and low fouling. However, in order to separate oil/water emulsions, modification of the wood structure was shown to be necessary, since for oil repellency, low surface energy of the repelling material is needed.

In the next step, we functionalized wood cross sections with a hydrophilic polyelectrolyte domain and a hydrophobic fluorinated domain, to allow for oil/water emulsions separation. These well-defined domains with opposite wettabilities were obtained through the grafting of block copolymers with amphiphilic properties via AGET-SI-ATRP.

We investigated the solvent influence on the spatial distribution of the polymer-modification in the wood scaffold. We showed that by using dichloromethane (a poor wood-swelling solvent) we could limit the reaction of the initiator to the lumen/cell wall interface, in the first micrometers of the samples. Contrarily, pyridine (a good wood-swelling solvent) transported the initiator inside the cell wall, and deep inside the wood sample (confirmed by Raman and FTIR spectroscopy).

These results were reflected on the homopolymerization of the superhydrophilic polyelectrolyte ([2-(Methacryloyloxy)ethyl]trimethyl ammonium chloride - METAC) and the superhydrophobic (2,2,2-Trifluoroethyl methacrylate - TFEMA)

monomers, which showed polymer distributions similar to the macroinitiator. To produce two distinct polymer domains, we grafted a block copolymer consisting of a charged superhydrophilic polymer (poly([2-(Methacryloyloxy)ethyl]trimethyl ammonium chloride) - PMETAC) and a superhydrophobic and oleophobic polymer (poly(2,2,3,3,4,4,5,5-Octafluoro pentyl methacrylate) - POFPMA). The successful incorporation of the two monomers was confirmed by Raman and FTIR spectroscopy. While the grafting of PMETAC and POFPMA provide wood with either superhydrophilic or superhydrophobic properties, we showed that by combining these two monomers in different ratios to form a block copolymer, we could get intermediate wettability properties, ranging from superhydrophilic to highly hydrophobic.

Based on these results, first attempts on the separation of oil/water emulsions were conducted. A limitation for the separation of oil/water emulsions was found to be the size of the prepared oil droplets in water. The oil droplets produced were much smaller than the largest lumen size, and the modified wood could not be used for this challenging separation. The preparation of emulsions with larger droplet sizes and the determination of feasible separation parameters has to be addressed in future works.

Finally, we started to investigate the required settings for a continuous separation set-up. The study revealed the pressure constrains and design specifications needed for a possible scale-up. Given the low breakthrough pressure of our membrane a precise pressure control is required.

The work carried out within the frame of this thesis resulted in significant advances in the field of polymeric modification on bio-based lignocellulosic materials and bio-based oil/water separation devices, which can be a step forward towards a more sustainable world.



## Zusammenfassung

Mit einem stetigen Wachstum der Weltbevölkerung und zunehmender Verschmutzung wird Trinkwasser zu einer knappen Ressource. Der Hauptschadstoff im Wasser ist Öl, meist bedingt durch anthropogene Ursachen. Dies führt zu einem Bedarf an neuartigen Öl/Wasser-Trenngeräten. Um den Bedarf an Ölgewinnung und -transport zu verringern, haben wir in dieser Arbeit die Verwendung von biobasierten Lignozellulose-Materialien mit hierarchischer, anisotroper und poröser Struktur, wie beispielsweise Holz, zur Öl/Wasser-Trennung untersucht. Im Laufe ihrer Entwicklung wurde die Holzstruktur von Natur aus für den Wasser- und Nährstofftransport sowie die mechanische Stabilität des Baumes optimiert. Dies macht Holz potenziell zu einem geeigneten biobasierten Material für die Öl-Wasser-Trennung.

Zuerst haben wir Fichtenholzquerschnitte getestet und herausgefunden, dass sie im nativen Zustand zur freien Öl/Wasser-Trennung verwendet werden können. Die Trennung basiert auf Kapillarkräften und arbeitet mit hohen Wirkungsgraden, hohen Flussraten und geringer Verschmutzung. Um jedoch Öl/Wasser-Emulsionen zu trennen, erwies sich eine Modifikation der Holzstruktur als notwendig, da für die Ölabweisung eine geringe Oberflächenenergie des abweisenden Materials erforderlich ist.

Im nächsten Schritt funktionalisierten wir Holzquerschnitte mit einer hydrophilen Polyelektrolyt-domäne und einer hydrophoben fluorierten Domäne, um die Trennung von Öl/Wasser-Emulsionen zu ermöglichen. Diese gut definierten Domänen mit entgegengesetzten Benetzbarkeiten wurden durch das Pfropfen von Blockcopolymeren mit amphiphilen Eigenschaften über AGET-SI-ATRP gewonnen.

Wir untersuchten den Einfluss des Lösungsmittels auf die räumliche Verteilung der Polymermodifikation im Holzgerüst. Durch die Verwendung von Dichlormethan (einem schlechten Holzquellmittel) kann die Reaktion des Initiators auf die Lumen/Zellwandgrenzfläche in der Probe begrenzt werden. Im Gegensatz dazu transportierte Pyridin (ein gutes holzschwellendes Lösungsmittel) den Initiator in die Zellwand und tief in die Holzprobe (bestätigt

durch Raman- und FTIR-Spektroskopie).

Diese Ergebnisse spiegeln sich in der Homopolymerisation des superhydrophilen Polyelektrolyten ([2-(Methacryloyloxy)ethyl]trimethylammoniumchlorid - METAC) und der superhydrophoben (2,2,2-Trifluorethylmethacrylat - TFEMA)-Monomere wider, die eine dem Makroinitiator ähnliche Polymerverteilung aufwiesen.

Um zwei verschiedene Polymerdomänen herzustellen, haben wir ein Blockcopolymer gepfropft, das aus einem geladenen superhydrophilen Polymer (Poly([2-(Methacryloyloxy)ethyl] trimethylammoniumchlorid) - PMETAC) und einem superhydrophoben und oleophoben Polymer (Poly(2,2,3,3,3,4,4,5,5,5-Octafluoropentylmethacrylat) - POFPMA) besteht. Die erfolgreiche Einlagerung der beiden Monomere in das Holz wurde durch Raman- und FTIR-Spektroskopie bestätigt. Während die Pfropfung von PMETAC und POFPMA dem Holz entweder superhydrophile oder superhydrophobe Eigenschaften verleiht, haben wir durch die Kombination dieser beiden Monomere in unterschiedlichen Verhältnissen, ein Blockcopolymer generiert, mit dem eine mittlere Benetzbarkeit eingestellt werden kann, die von superhydrophil bis hochhydrophob reicht.

Basierend auf diesen Ergebnissen wurden erste Versuche zur Trennung von Öl-Wasser-Emulsionen durchgeführt. Eine Einschränkung für die Trennung von Öl/Wasser-Emulsionen wurde in der Größe der vorbereiteten Öltröpfchen in Wasser festgestellt. Die erzeugten Öltröpfchen waren wesentlich kleiner als die größte Lumengröße, und das modifizierte Holz konnte für diese anspruchsvolle Trennung daher nicht verwendet werden. Die Herstellung von Emulsionen mit grösseren Tröpfchengrößen und die Bestimmung realisierbarer Trennparameter muss in zukünftigen Arbeiten im Fokus stehen.

Abschliessend haben wir die erforderlichen Einstellungen für einen kontinuierlichen Separationsaufbau untersucht. Die Studie zeigte die Druckeinschränkungen und Entwurfsspezifikationen, die für ein mögliches Scale-up erforderlich sind. Aufgrund des geringen Durchbruchdrucks unserer Membran ist eine präzise Druckregelung erforderlich.

Die im Rahmen dieser Arbeit durchgeführten Arbeiten führten zu

signifikanten Fortschritten auf dem Gebiet der Polymermodifikation biobasierter Lignozellulose-Materialien und biobasierter Öl-Wasser-Trennvorrichtungen, die ein weiterer Schritt in Richtung einer nachhaltigeren Welt sein können.



# Table of Contents

Acknowledgements . . . . .	i
Abstract . . . . .	iii
Zusammenfassung . . . . .	v
<b>Table of Contents</b>	<b>ix</b>
<b>List of Figures</b>	<b>xiii</b>
<b>List of Tables</b>	<b>xvii</b>
<b>1 Introduction</b>	<b>1</b>
1.1 Motivation and Objectives . . . . .	1
1.2 Outline of the Thesis . . . . .	4
1.3 Wood Structure and Composition . . . . .	6
1.3.1 Hierarchical Wood Structure . . . . .	6
1.3.2 Wood Chemical Components and their Interaction . . . . .	11
1.4 Wood Modifications . . . . .	14
1.4.1 Common and new functional wood modification approaches	14
1.4.2 Controlled radical polymerization techniques . . . . .	18
1.5 Wood Membrane Characterization . . . . .	21
1.5.1 Electron Microscopy . . . . .	21
1.5.2 Raman and IR spectroscopy . . . . .	23
1.5.3 Contact angle . . . . .	24
1.6 Oil/Water Separation . . . . .	26
1.6.1 General problem . . . . .	27
1.6.2 Current technologies . . . . .	29
1.6.3 Alternatives . . . . .	33
1.7 Oil/Water Emulsions . . . . .	34
1.7.1 Emulsion Characterization . . . . .	35
<b>2 Underwater Superoleophobic Wood Cross Sections for Efficient Oil/Water</b>	

<b>Separation</b>	<b>39</b>
2.1 Introduction . . . . .	40
2.2 Results and Discussion . . . . .	42
2.2.1 Wood section Morphology . . . . .	42
2.2.2 Air and underwater wettability of spruce wood sections . . . . .	44
2.2.3 Capillary force-based separation (separation based on contrasting wetting properties) . . . . .	46
2.2.4 Separation of oil-water mixtures . . . . .	48
2.2.5 Other wood species . . . . .	50
2.3 Conclusions . . . . .	51
2.4 Experimental section . . . . .	52
Supplementary Information . . . . .	54
<b>3 Solvent-Controlled Spatial Distribution of SI-AGET-ATRP Grafted Polymers in Lignocellulosic Materials</b>	<b>61</b>
3.1 Introduction . . . . .	62
3.2 Results and Discussion . . . . .	64
3.2.1 Synthesis of W-Br macroinitiators: influence of reaction time, concentration, sample morphology, and solvent on the WPGs	66
3.2.2 Characterization of the BiBB distribution in wood . . . . .	67
3.2.3 Synthesis and characterization of wood-polymer materials . . . . .	71
3.3 Conclusions . . . . .	77
3.4 Experimental section . . . . .	78
Supplementary Information . . . . .	81
<b>4 Grafting of Amphiphilic Block Copolymers on Lignocellulosic Materials via SI-AGET-ATRP</b>	<b>91</b>
4.1 Introduction . . . . .	92
4.2 Results and Discussion . . . . .	94
4.2.1 Synthesis of the macroinitiator . . . . .	95
4.2.2 Homopolymerizations . . . . .	95
4.2.3 Copolymerization . . . . .	100
4.2.4 Wettability measurements . . . . .	106
4.3 Conclusions . . . . .	108
4.4 Experimental section . . . . .	109
Supplementary Information . . . . .	112

---

<b>5</b>	<b>Oil/Water Separation with Functionalized Wood-based Membranes</b>	<b>115</b>
5.1	Results and Discussion . . . . .	116
5.1.1	Characteristics of the wood-based membrane for oil/water separation . . . . .	116
5.1.2	Preliminary membrane characterization . . . . .	118
5.2	Conclusions . . . . .	122
5.3	Experimental section . . . . .	122
<b>6</b>	<b>Continuous Oil/Water Separation System</b>	<b>125</b>
6.1	Design of the separation system . . . . .	126
6.1.1	Lab-scale separation system . . . . .	126
6.1.2	Separation system scale-up for industrialization . . . . .	129
6.2	Conclusions . . . . .	130
<b>7</b>	<b>General Discussion and Conclusion</b>	<b>131</b>
7.1	Oil/water separation with native wood . . . . .	132
7.2	Tuning the wood's wettability through graft polymerization . . . . .	136
7.2.1	Control over the spatial distribution of the modifying polymer in wood . . . . .	137
7.2.2	Control over the copolymerization reaction . . . . .	141
7.3	Oil/water separation with functionalized wood-based membranes	146
7.4	From a batch lab-scale to a continuous industrial set-up . . . . .	147
<b>8</b>	<b>Outlook</b>	<b>151</b>
8.1	Future work . . . . .	152
8.2	Current limitation in the field of oil/water separation technologies .	153
8.3	Social impact of the work . . . . .	154
<b>9</b>	<b>References</b>	<b>155</b>
	<b>Curriculum Vitae</b>	<b>171</b>
	List of Publications . . . . .	173
	List of Conferences . . . . .	174





## List of Figures

1.1	Schematic representation of the wood structure. . . . .	8
1.2	Wood structure scheme of the different scale length. From the macrostructure (A), through the microstructure and ultrastructure (B) to the molecular level (C). . . . .	10
1.3	Schematic representation of the various possible routes for wood modification. . . . .	15
1.4	Modification distribution at the cellular level. (A) lumen filling, (B) lumen/cell wall interface, and (C) into the cell wall. . . . .	17
1.5	Controlled polymerization techniques, focusing in ATRP and its variant ARGET/AGET-ATRP. . . . .	19
1.6	Scheme of (a) normal ATRP reaction and (b) ATRP reaction with excess of reducing agent (AGET or ARGET). . . . .	20
1.7	Light scattering in Raman spectroscopy. . . . .	24
1.8	Schematic representation of the different contact angle measuring modes. . . . .	26
1.9	Oil pollution sources data for the world oceans. . . . .	28
1.10	Different processes of oil “weathering”. . . . .	29
1.11	Types of separation technologies with respect to the size of the rejected material. . . . .	30
1.12	Membrane separation configuration scheme. . . . .	31
1.13	Schematic representation of water-in-oil and oil-in-water emulsions. . . . .	34
2.1	Morphology of the spruce wood cross sections. . . . .	43
2.2	SEM images of wood cross section samples after circular saw cutting. . . . .	44
2.3	Wetting properties of the wood cross sections. . . . .	45
2.4	Illustration of the solid/water/oil system and Environmental Scanning Electron Microscopy (ESEM) images of the wood cross section. . . . .	47
S2.1	Calculation of probability distribution of the opened fibers. . . . .	55
S2.2	Breakthrough pressure evaluation. . . . .	56
S2.3	Average wood type distribution (EW and LW) by image processing. . . . .	56

S2.4 Images of the separation setup from the initial time to the end of the separation. . . . .	57
S2.5 Typical GC chromatograph of the permeate after the oil/water separation experiment. . . . .	58
S2.6 Water flow through wood cross sections cut with a circular saw. . .	58
S2.7 Morphology of the beech wood cross sections. . . . .	59
S2.1 Underwater oil sliding angle measurement for hexadecane . . . .	60
S2.2 ESEM image series of microtome wood saturation with water . . . .	60
S2.3 ESEM image series of circular saw cut saturation with water . . . .	60
S2.4 oil/water separation experiment with spruce wood . . . . .	60
S2.5 oil/water separation experiment with beech wood . . . . .	60
3.1 Scheme of the wood macro- and micro-scale with targeted initiator distribution and SI-AGET-ATRP reaction scheme. . . . .	64
3.2 Evolution of WPG (%) with respect to reaction time, using different BiBB concentrations, and EW/LW distributions. . . . .	66
3.3 Spatial distribution of the BiBB initiator molecule at the microstructure. 68	
3.4 Spatial distribution of the BiBB initiator molecule at the macrostructure. . . . .	70
3.5 Raman analysis of the samples modified by PTFEMA with both W-Br(Py) and W-Br(DCM) macroinitiator sets. . . . .	73
3.6 Raman analysis of the samples modified by PMETAC with both W-Br(Py) and W-Br(DCM) macroinitiator sets. . . . .	74
3.7 Macroscale distribution of the polymer modifications (TFEMA and METAC) using both W Br(Py) and W Br(DCM) macroinitiators. . . . .	75
S3.1 Wood swelling over time in pyridine and dichloromethane. . . . .	81
S3.2 SEM images of spruce wood cross-sections after treatment with solvents (Py and DCM). . . . .	82
S3.3 EDX elemental mapping results for TFEMA-polymerized samples in both BiBB sets of reaction (Py and DCM). . . . .	86
S3.4 WDX elemental mapping results for METAC-polymerized samples in both BiBB sets of reaction (Py and DCM). . . . .	87
S3.5 FTIR spectra of the different polymer modification (TFEMA and METAC monomers) in the two BiBB reacted sets (Py and DCM). . . .	88
4.1 Obtained weight percent gains of each homopolymer with respect to the targeted weight percent gains. . . . .	96
4.2 Monomer conversion of METAC under (A) different targeted degrees of polymerization and (B) different BiBB WPGs. . . . .	97

---

4.3	FTIR spectra of native wood (Ref) and the different wood modifications. . . . .	99
4.4	Average Raman spectra of the ROI on the homopolymerized samples W-PMETAC and W-PFOPMA. . . . .	100
4.5	GPC traces of PMETAC and PMETAC-b-POFPMA chains (reaction in solution). . . . .	102
4.6	WPG of POFPMA with respect to different PMETAC-modification concentrations. . . . .	104
4.7	Effect of the concentration of salt on the polymerization of OFPMA, in the case of the homo- and co-polymerizations. . . . .	105
4.8	FTIR and Raman spectra of the copolymerized samples. . . . .	107
4.9	Contact angles (CA) through the sessile drop method of the unmodified wood (Ref.) and the different wood modifications. . .	108
S4.1	FTIR spectra of native wood (Ref) and the BiBB-modified wood (W-Br). .	112
S4.2	NMR spectra of PMETAC and PMETAC-b-POFPMA chains (reacted in solution) . . . . .	113
5.1	Scheme of the oil/water separation on the block copolymerized wood scaffolds. . . . .	117
5.2	OCA and OSA for the three copolymer-modified wood-based membranes (Copolymer A, Copolymer B, and Copolymer C). . . .	118
5.3	White light microscopy images of the Tween20 vortex-produced emulsions before and after separation. . . . .	121
5.4	Emulsions droplet size of the SDS bath and probe sonication-produced emulsions, measured by small-angle light scattering. . .	121
6.1	Schematic representation of the wood holder system. Water and oil represented in blue and red, respectively. . . . .	127
6.2	P&ID of the pilot plant (continuous operation) in cycle test mode. .	128
6.3	Image of the lab-scale separation system. . . . .	128
6.4	Schematic representation of the possible scale-up membrane holder. . . . .	130



## List of Tables

1.1	Type of oil/water mixtures according to the droplet size of the dispersed phase. . . . .	34
S2.1	Breakthrough pressure parameters and results for different oils. . . .	57
3.1	Initiator and polymer weight percent gains in the wood samples. . .	75
S3.1	example of calculation for the esterification of 1 g of spruce wood with different equivalents of $\alpha$ -bromoisobutyryl bromide (BiBB) per AGU units. . . . .	84
S3.2	Estimation of cellulose substitution degree after reaction with BiBB.	85
S3.3	Targeted and estimated degrees of polymerization. . . . .	89

## Publication Contributions

This cumulative thesis is based on three published research articles. The author's contribution to the publications is described in the following part.

(I) Vidiella del Blanco, M., Fischer, E. J., and Cabane, E., *Underwater Superoleophobic Wood Cross Sections for Efficient Oil/Water Separation*, *Adv.Mater.Interfaces*, 2017, 4, 1700584.

Contribution: The author performed the experiments, characterizations (except GC-FID), evaluated and interpreted the raw data and wrote an elaborated version of the article.

(II) Vidiella del Blanco, M., Gomez, V., Grafulha, L.G.M., Keplinger, T., and Cabane, E., *Solvent-Controlled Spatial Distribution of SI-AGET-ATRP Grafted Polymers in Lignocellulosic Materials* (accepted in *Biomacromolecules*, DOI: 10.1021/acs.biomac.8b01393).

Contribution: The author planned and partially performed the experiments, all characterizations (except WDX), evaluated and interpreted the raw data and wrote an elaborated version of the article.

(III) Vidiella del Blanco, M., Gomez, V., Fleckenstein, P., Keplinger, T., and Cabane, E., *SI-AGET-ATRP Grafting of Block Copolymers with Amphiphilic Properties on Lignocellulosic Materials* (submitted).

Contribution: The author planned and partially performed the experiments, all characterizations (except NMR and GPC), evaluated and interpreted the raw data and wrote an elaborated version of the article.

## Co-authored publication (not part of the thesis)

Wang, Y., Yan, W., Frey, M., Vidiella del Blanco, M., Schubert, M., Adobes-Vidal, M., and Cabane, E., *Liquid-like SiO<sub>2</sub>-g-PDMS coatings on wood surfaces with underwater durability, anti-fouling, anti-smudge and self-healing properties*, *Adv. Sustainable Syst.* 2018, 1800070.

Contribution: The author characterized the samples through ESEM.

# Chapter 1

## Introduction

### 1.1. Motivation and Objectives

Water covers about 71% of the earth surface; it also exists in air, glaciers, and aquifers. It constitutes around 60 to 70% (adult) to 90 to 95% (fetus) of our body.<sup>1</sup> However, from all the water source only around 2.5% is fresh water and not all of it is drinkable as it can be and is polluted.<sup>2</sup> The quality of our water systems is synonym of our quality of life. In an always-growing population, with actual values above 7.6 billion, solutions to this issue need to be addressed.

From all the pollutants and contaminants in water, oil is by far the greatest contributor. Today's economy is mainly based on non-renewable resources. Oil and minerals are the main means of energy production and the composition of most goods we use in our daily life. The variety of chemicals, which can be produced from these two sources have made them highly attractive, contrarily to bio-based materials. However, this comes with consequences.

Due to the consumption of oil to produce energy and oil-based materials, oil needs to be extracted and transported all over the world. This has resulted in several oil spill accidents over the last decades.

These oil spill accidents in marine and aquatic ecosystems, although representing less than a 15% of the total oil pollution in water, have increased environmental awareness and led to tighter regulations.<sup>3</sup> Novel strategies to separate oil/water mixtures have become a global challenge. Given that traditional methods are limited concerning their energy costs, efficiency and complexity of the separation, new functional materials capable of overcoming

these barriers are highly desired.<sup>4-8</sup>

In the search for new alternatives, membranes (made from metal meshes and/or polymers) have recently emerged as a very promising approach to the oil pollution issue. These have advantages in terms of functional groups (allowing for trapping/repelling different pollutants), control over the membrane pore size (targeting different water treatment applications – for both chemical and pore exclusion separation) and are made of long-lasting materials. However, by using these types of materials it is possible to decrease the problem but not solve it. Since the materials are still mainly oil-based, there is still a need for the extraction and transportation of oil, which is the main cause of oil pollution in water. Moreover, these materials are produced in a bottom-up approach, which gives difficulties in the scale-up process.

Given the environmental impact of oil-based materials,<sup>9</sup> in order to decrease oil pollution, the need to exchange oil-based materials for bio-based materials is essential. In recent years, there has been a growing interest on utilizing bio-based materials. One type of bio-based material which use has increased is wood.

Wood is a highly valued material in the construction and furniture sector. Besides these important applications, it is usually considered only as a low-value material because wood is “pre-fabricated” by nature, i.e. it is not possible to assemble a new material for a specific purpose following the bottom-up (monomer to material) approach. For this same reason, it is rarely associated with advanced modern materials. This is mainly because its highly sophisticated hierarchical structure is often ignored. However, wood also has some other advantageous features. Together with the fact that wood already provides the scaffold to develop a variety of functional materials, the wood's naturally “pre-fabricated” structure also solves most of the common up-scaling problems.<sup>10</sup> In spite of these interesting underexploited properties, the applications of wood are currently limited due to the lack of



post-functionalization techniques.

Through this dissertation, a separation application will be addressed for wood, intending to produce a higher-value product. Wood stands for a highly porous material with excellent mechanical performance, and robustness in wet state. Furthermore, its abundance and renewable origin decrease the environmental impact, which is a timely advantage compared to oil-based products. Over the course of evolution, wood has adapted to satisfy various functions of the tree. Its development has led to a material that is optimized for long-distance water transport and has outstanding mechanical properties. Thanks to their hierarchical, porous structures, wood materials offer an ideal support for membrane technologies. However, they are lacking functional groups in order to compete with their main competitors, synthetic polymer and ceramic membranes.

The main goal of this thesis is to use the existing porous and anisotropic wood structure as a scaffold to design new functional materials, focusing on oil/water separation devices. The first aim was to use the natural anisotropic porous structure of wood to separate oil/water mixtures. Given the lack of functional groups in wood, it is probable that wood will not be capable of separating oil/water emulsions, which is possible with other devices available in the market. Therefore, functionalization of the wood scaffold to decrease the surface energy properties while still allowing the water to go through might be needed. In order to achieve this, the treated wood needs to be modified by introducing polymer chains into its cell and cell wall structure. The synthetic polymer chains should be grown directly from the wood polymers ensuring covalent attachment (for improved treatment stability) in the natural cell and cell wall scaffold. The final properties of the wood will depend on the chosen monomer, the grafted chain length and the overall composition (wood-polymer mass ratio). Therefore, an understanding of the modification reaction is needed in terms of location of the modification in the wood cell structure and a control

over the polymerization to achieve the desired wood-polymer ratios.

Once the polymerization reaction is well understood (in terms of reaction parameters) and with the right choice of monomers and monomer ratios, wood should be capable of not only separating oil/water mixtures but also oil/water emulsions.

In this way, we intend to, both solve a recurring problem by the use of a natural abundant renewable resource and expand the knowledge in the field of wood modification.

The main focus and goals of this thesis are:

- Producing a membrane from natural unmodified wood, which is capable of separating oil from water.
- Controlling the position of the polymer modification in the wood structure, as unmodified wood could not be capable of separating oil/water emulsions, thus chemical modifications are needed.
- Understanding of the copolymerization parameters, since a copolymerization is needed for the separation of oil/water emulsions.
- Finding the monomer ratio in the copolymerization that allows for oil/water emulsion separation in wood-based materials.
- Producing a wood-based membrane that is capable of separating oil/water emulsions.

### **1.2. Outline of the Thesis**

This cumulative thesis consists of three articles related to the utilization of wood as an oil/water separation material. For this, an understanding of the native wood structure, wood/water/oil interactions, and modification protocols to obtain an oleophobic/hydrophilic wood was needed.

Prior to the main publications, in this chapter (Chapter 1), an introduction to the

topic is briefly given. A general view of the wood hierarchical structure and its composition is discussed. Wood modification and characterization approaches are introduced together with different oil/water separation systems. Finishing with a general introduction of oil-in-water emulsions, their production and characterization.

In Chapter 2, the first article "Underwater Superoleophobic Wood Cross Sections for Efficient Oil/Water Separation" is presented. In this communication, we show how simple unmodified wood is capable of separating oil from water thanks to its hygroscopic properties and capillary forces, which allows it to retain water in its structure being able to repel the oil. The capillary forces formed by the tracheid lumina play an important role in this achievement. However, this only works for oil/water mixtures.

In Chapter 3, the second article "Solvent-Controlled Spatial Distribution of SI-AGET-ATRP Grafted Polymers in Lignocellulosic Materials" is introduced. When modifying wood for a certain application the position of the modification can play an important role. In this paper, the utilization of different solvents for tuning the position of the grafted chains into the cell wall structure is discussed. Given that SI-ATRP is a two-step process in which the initiator is firstly attached to the wood structure and then the polymer is grown from this initiator, the swelling properties of the solvent used during this first reaction where crucial for controlling the position of the polymer.

In Chapter 4, the third article "Grafting of Amphiphilic Block Copolymers on Lignocellulosic Materials via SI-AGET-ATRP" is presented. The grafting of different polymers into the wood structure results in a variation of the wood's wettability properties. In this paper the major challenge was to obtain a block copolymer consisting of an hydrophilic and an hydrophobic part. The protocol for this achievement and the characterization of the modified wood is discussed in the paper.

In Chapter 5, preliminary oil/water separation results for the modified wood are discussed. The preparation of stable emulsions and the difficulties of separating

them are explained.

In Chapter 6, a design of the continuous separation system and its possible scale-up is outlined. The limitations of the actual lab-scale system and possibilities of new designs are discussed.

In Chapter 7 a general discussion based on the individual conclusions of the previous chapters is given, for a better overlook of the thesis results. The results are contextualized in the frame of current state of the art.

Finally, in Chapter 8, an outlook with the possible next steps and the contributions of this thesis to the general field is given.

### **1.3. Wood Structure and Composition**

In this thesis, wood was used as a scaffold for oil/water separation systems. Starting by using only the wood for separating oil/water mixtures to modifying it to be able to separate oil-in-water emulsions. Even though hardwoods were also tested, mainly softwood species were used, in particular spruce (*Picea abies*).

#### **1.3.1. Hierarchical Wood Structure**

The hierarchical structure of wood comprises several length scales (ranging from macro- to nanostructure). This structure is optimized for fulfilling several needs of the tree: mechanical support, transport of water and nutrients, and storage and secretion of biochemicals. In the macrostructure of a tree, we can differentiate two main parts. The shoot (trunk, branches and leaves) and the roots (Figure 1.1).<sup>11,12</sup>

Different layers with specific functions form the trunk: outer bark (periderm and cortex), inner bark (phloem), vascular cambium, xylem (sapwood and heartwood), and pith. The function of the outer bark is to protect the trunk against weathering, fire, fungi attack and UV irradiation. The inner bark, which consists of living cells, is responsible for phloem sap transport. The vascular

cambium is a thin layer located between the phloem and the xylem. Its function is to produce cells through cell division for the phloem and the xylem (Figure 1.1). The xylem (wood) represents the biggest part of the trunk and can be divided for many wood species into sapwood and heartwood. Within the xylem, of many species, a typical year ring structure can be observed consisting of alternating regions of low- and high-density wood, earlywood and latewood, respectively (Figure 1.1). In the sapwood, the parenchyma cells are still alive (metabolically active) being able to synthesize biochemicals. Between the heartwood and the sapwood, there is a transition zone, which is crucial for the synthesis of extractives. These extractives, which are incorporated into the cell wall during the formation of (real) heartwood, are responsible for enhanced durability. Wood species differ significantly in their characteristic amount and composition of extractives. These determine the color of the wood, which roughly serves as an indicator of its durability.

Trees belong to the seed bearing plants, which can be divided into two main groups: softwoods or conifers (gymnosperms) and hardwoods or deciduous trees (angiosperms), see Figure 1.1. The difference in the microstructure between these two groups is notable. In terms of evolution, hardwoods are younger than softwoods, thus their structure is more complex. These have higher diversification of cell types, with different cell functions and chemistries, compared to softwoods. Whereas the anatomical differences in the general cellular structure between different kinds of wood (hardwoods and softwoods) can be very significant, the cell wall structure is relatively consistent.

Softwoods are mainly formed by tracheids (representing 90-95% of their structure), which are hollow cells with an average length of roughly 3 mm.<sup>13</sup> The hollow part of the cell, the lumen, can have a rectangular to hexagonal shape of 5-10  $\mu\text{m}$  in diameter for the latewood and 20-40  $\mu\text{m}$  in diameter for the earlywood.<sup>12</sup> The rest of the softwood structure is formed by ray cells (5-10%). Tracheids are mainly oriented in the longitudinal direction. They provide mechanical strength (especially the thick-walled latewood tracheids) and are responsible for water transport, which takes place mainly through

the large lumen cavities of the thin-walled earlywood tracheids. Contrarily, parenchyma ray cells run radially outwards from the pith to the bark. The rays ensure the synthesis, storage, and lateral transport of biochemicals as well as, to minor extend, water transport. Liquid transport between tracheids takes place through bordered pits. Between tracheids and ray parenchyma cells, the transport is carried out through half-bordered pits.

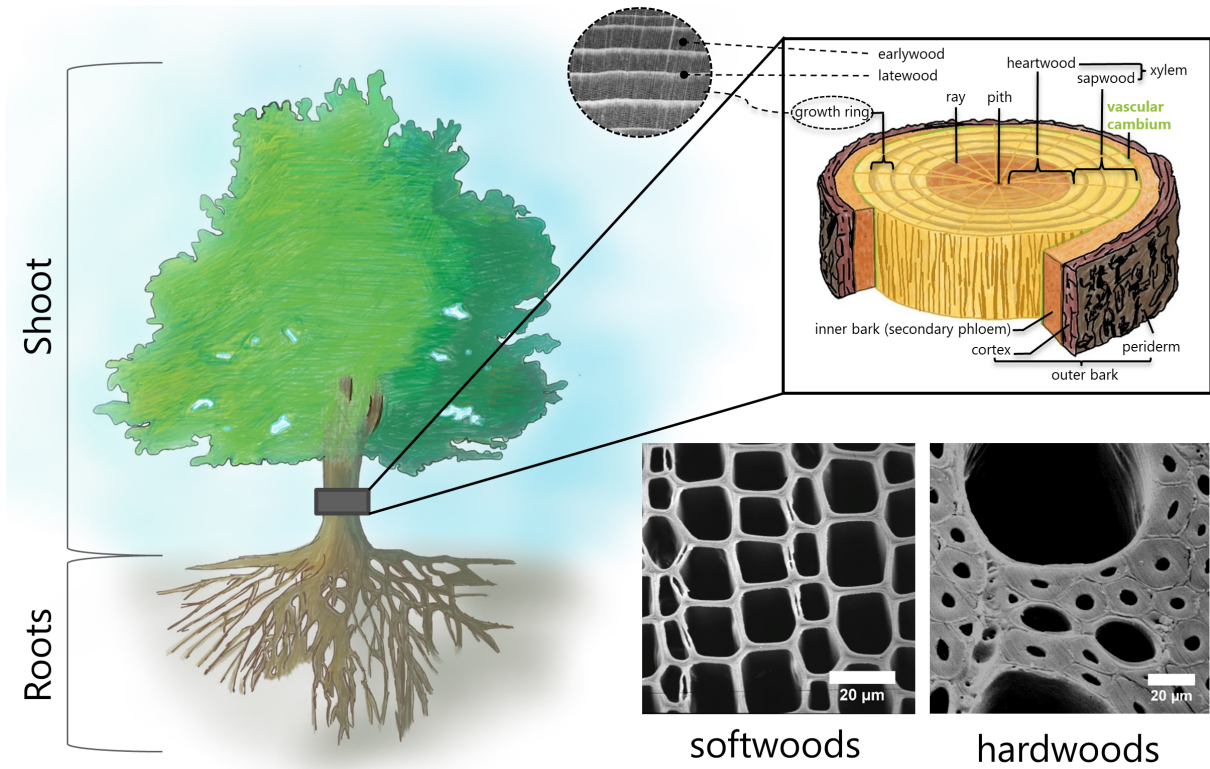


Figure 1.1: Schematic representation of the wood structure.

Hardwoods consist of a basic tissue of libriform fibers and fiber tracheids that serve for mechanical stability. Hardwood fibers are generally smaller and more compact than softwood tracheids. Their lumina is smaller and their walls are thicker.

The conducting elements in hardwood are the vessels. These often have large lumina and a specific distribution pattern across the growth ring. These patterns can be classified in three different groups: ring porous, semi-ring porous, and diffuse porous. In ring-porous woods, the transition from earlywood to latewood is abrupt, with vessel diameters decreasing substantially together with their distribution pattern. Contrarily, diffuse-porous hardwoods vessels either do not

differ significantly in size and distribution or the change is made gradually and no clear distinction can be made. It may happen that the vessel size and distributions fall into a pattern, which is described by neither of these two previous systems, this is the case for semi-ring porous hardwoods. The vessel's structure can be described as long pipes with lengths ranging from a few centimeters to up to several meters; they consist of a multitude of vessel elements with opened or perforated ends.<sup>14</sup>

As a defense mechanism caused by external factors or as a regular process during heartwood formation, the tree can irreversibly block the vascular pathways of the vessels in hardwoods. In most cases tyloses are formed that clog the vessels. Tyloses are parenchyma cells that grow into a vessel lumen forming a continuous protective layer. This natural mechanism can later affect water flow through the wood-based membrane scaffold.<sup>15-17</sup>

Both axial and radial parenchyma cells, which are short compact cells with stubby ends, are present in higher amounts in hardwoods than in softwoods.

Regarding the wood's ultrastructure, wood cells exhibit a layered wall structure consisting of a thin primary layer (P) and a thicker secondary wall composed by three sublayers (S1, S2, and S3), see Figure 1.2B. The layers of the secondary wall differ from each other with respect to their structure (angle of the cellulose microfibrils) and composition (varying quantities of cellulose, hemicellulose, and lignin). Adjacent cells are in contact with each other through a highly lignified layer (middle lamella - ML).

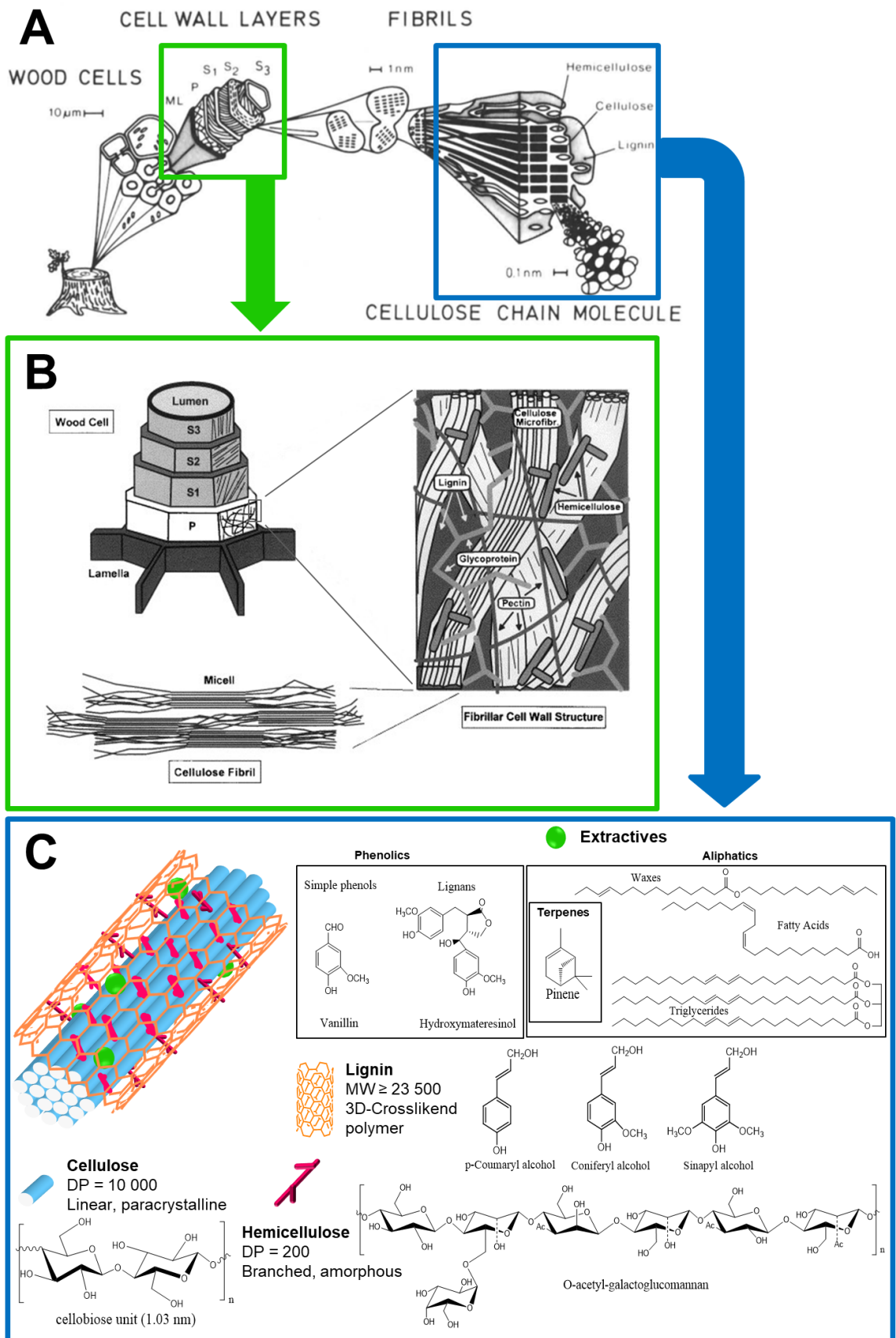


Figure 1.2: Wood structure scheme of the different scale length. From the macrostructure (A), through the microstructure and ultrastructure (B) to the molecular level (C).<sup>12,18,19</sup>



### 1.3.2. Wood Chemical Components and their Interaction

Wood is formed mainly by three main structural elements: cellulose, hemicellulose, and lignin. Further components, e.g. extractives, belong to the group of the so-called non-structural elements. The main molecular structures are represented in Figure 1.2C.

#### Cellulose

Cellulose is considered the most abundant biopolymer on earth, synthesized by plants, algae, animals, and bacteria. In wood, it represents approximately 40–45% of the dry substance in most wood species and is predominantly located in the secondary cell wall.

Cellulose is a homopolysaccharide build up through the polymerization of highly oriented  $\alpha$ -D-glucopyranose units joined by glycosidic bonds. These form microfibrils of semi-crystalline nature (crystalline and amorphous regions).

Cellulose chains are completely linear, with a tendency to form intra- and intermolecular hydrogen bonds. Due to its fibrous structure and the strong hydrogen bonds, cellulose is insoluble in most solvents. Its chemical and physical properties and supramolecular structure allows it to fulfill its function as the main structural component of the plant cell walls. The degree of polymerization (DP) of cellulose in wood is of about 10 000 glucose residues.

Crystalline cellulose can be characterized by X-ray diffraction analysis. In the chain direction, each repeating unit is a cellobiose residue (1.03 nm), and every glucose residue is accordingly displaced  $180^\circ$  with respect to its neighbors.<sup>11,19,20</sup>

#### Hemicellulose

Hemicelluloses are heterogeneous branched polysaccharide polymers, which are formed by various sugars (of C5 and C6 units). In wood, hemicelluloses represent between 20 and 30% of the dry weight of wood. Considerable differences exist between the content and composition of hemicelluloses in

the stem, branches, roots, and bark. Their most important mechanical role is the contribution to strengthening the cell wall through the interaction with cellulose (hydrogen bonding and van der Waals forces), and covalent bonds with lignin.<sup>12,21</sup>

They are build up from different monomeric sugar components: D-glucose, D-mannose, D-xylose, L-arabinose, and small amounts of L-rhamnose, D-glucuronic acid, 4-O-methyl-D-flucuronic acid, and D-galacturonic acid. These anhydro-sugar units can be subdivided into groups such as pentoses, hexoses, hexuronic acids, and deoxy-hexoses. The main unit can consist of a single homopolymer (e.g. xylans) or of one or more units forming heteropolymers (e.g. glucomannans). Glucomannans are the most abundant type of hemicelluloses in softwoods (20%), see Figure 1.2C. Some units can have side groups to the main backbone, e.g. 4-O-methylglucuronic acid, galactose. In contrast to cellulose, most hemicelluloses have a degree of polymerization of only 200.

Softwoods and hardwoods differ regarding both the percentage of total hemicellulose and the percentage of individual hemicelluloses and their composition. Concerning the non-glucosic sugar units present in wood, whereas softwoods have a high proportion of mannose units and more galactose units than hardwoods, hardwoods have a high proportion of xylose units and more acetyl groups than softwoods.<sup>11,12,19-23</sup>

### Lignin

After cellulose, lignin is the most abundant and important polymeric organic substance in the plant world. It was the incorporation of lignin what allowed plants to grow tall under terrestrial conditions. Lignin significantly increases the compressive strength allowing trees higher than 100 m to remain upright. Lignin is a characteristic chemical and morphological component of the tissues of higher plants such as gymnosperms and angiosperms. It is typically found in vascular tissues (tracheids in softwoods and in fibers, parenchyma cells and

vessels in hardwoods) where it provides the mechanical strength to maintain their structure from collapsing during liquid transport. Lignin is mostly present in high concentrations in the middle lamella layer and as part of the matrix of the wood cell walls.

Lignin represents between 20 to 40% of the dry weight of wood in softwoods and 18 to 25% of the dry weight of wood in hardwoods. Lignin is built up by phenylpropane units, which are mainly p-coumaryl alcohol, coniferyl alcohol, and sinapyl alcohol (see Figure 1.2C), linked together through a radical polymerization process.

The molecular weight of lignin varies greatly based on the method of extraction (milled wood lignin, cellulolytic enzyme lignin, enzymatic mild acidolysis lignin) but is estimated to range from 23 500 to 78 000 g/mol.<sup>24</sup> Lignin is closely linked with hemicelluloses to which it can form covalent bonds via ester and ether linkages. In contrast, there is no evidence of direct interaction between cellulose and lignin.<sup>11,19,20</sup>

### Extractives

As their name indicates, extractives are small organic and inorganic molecules that can be extracted from the wood structure by using polar and non-polar solvents. Their content and composition varies among wood species. Some species can have high amounts of extractives summing up to a 15% of the dry weight of wood. However, spruce only contains 3% of extractives in dry weight.

Extractives are not structural components of the cell wall and hence have no direct influence on the mechanical properties of wood. They are rather a protection element. They are responsible for high durability of the heartwood against microbial degradation (given their toxicity), and the dark color and odor of the wood.

Focusing on softwoods, extractives are mainly concentrated in resin canals and can be synthesized by parenchyma cells during heartwood formation.

The composition of extractives can be divided into phenols, aliphatics and terpenes.<sup>11</sup>

### 1.4. Wood Modifications

Wood has and still is widely used in the construction sector and furniture industry. Wood is a highly hygroscopic material that swells and shrinks as well as degrades due to fungi attack at high humidity contents. For practical reasons, there has been a large amount of research focused on the modification of wood in order to overcome its shortcomings and environmental flaws. Nevertheless, given the natural scaffold of wood, wood is also a good material for various applications, such as separation systems or electronic devices. In this section, the common wood modifications and new functional polymer techniques carried out on wood together with the specific techniques used during the course of this thesis are explained. A special emphasis is given on polymerization techniques.

#### 1.4.1. Common and new functional wood modification approaches

Common wood modification techniques (divided into chemical, surface, and thermal modification) have been of great use in improving the dimensional stability of wood. All techniques aim at reducing the water absorption of the wood material, in order to increase its durability and dimensional stability.<sup>14,25</sup>

Focusing on chemical modification, the different techniques can be grouped according to the chemistry performed on the wood. In most of the cases, the chemicals incorporated are covalently bond to the available -OH groups of the wood cell wall polymers (through esterification, etherification or silylation, see Figure 1.3). A long list of chemicals have been covalently bonded to the wood hydroxyl groups, which include but are not limited to anhydrides, acid chlorides, carboxylic acids, isocyanates, aldehydes, alkyl chlorides, lactones, nitriles, epoxides, and DMDHEU (dimethylol dihydroxyethyleneurea).<sup>14,26–29</sup>

The fabrication of wood-polymer composites has been one of the techniques used for dimensional stability. The wood-polymer composites material has been

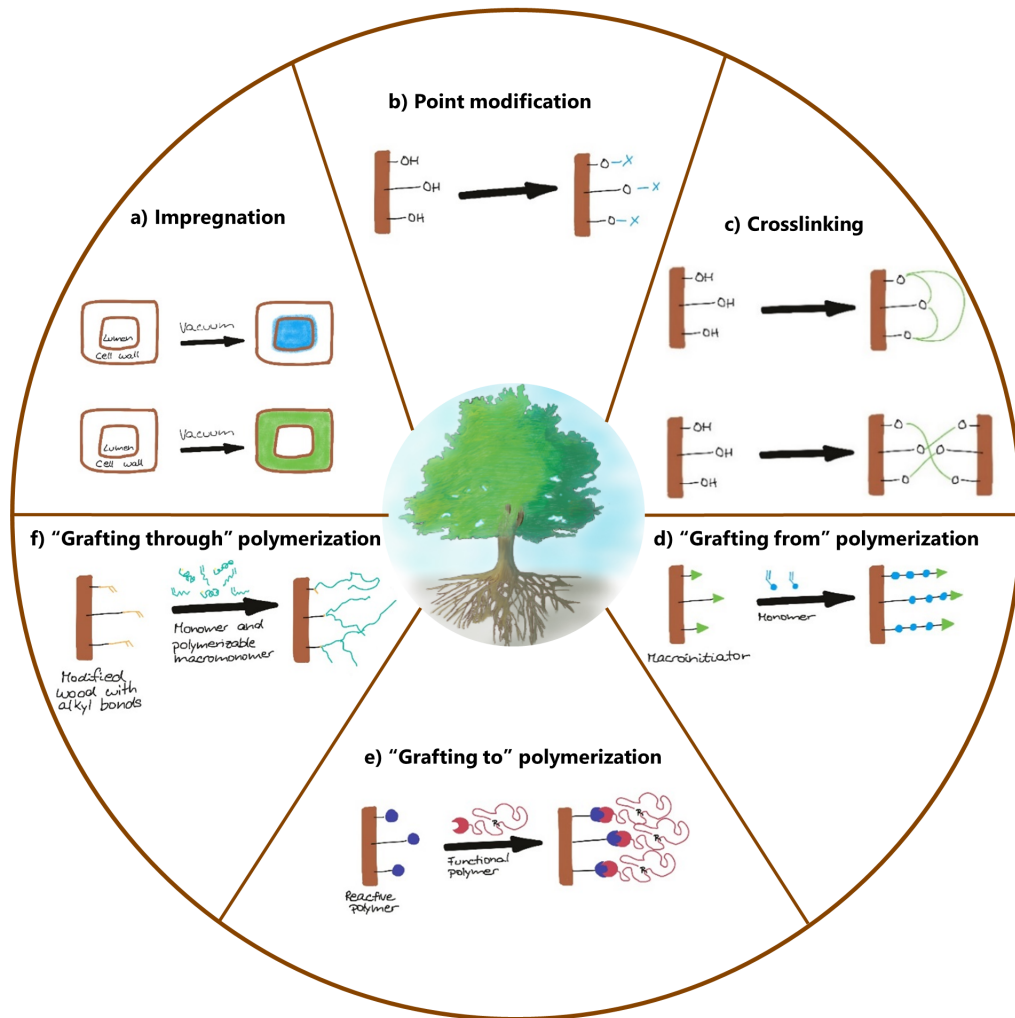


**Figure 1.3:** Schematic representation of the various possible routes for wood modification.

formed traditionally through the impregnation of either polymeric monomers (e.g. methacrylates, acrylates, styrene, or unsaturated polyesters) or thermoset resins (e.g., epoxy resin, phenol formaldehyde, urea formaldehyde, and melamine-formaldehyde resin) followed by in situ polymerization by radiation or catalyst-thermal treatment. Thermoset resin impregnation was shown to be in these cases more efficient in improving the wood dimensional stability than polymeric monomer impregnation; since the former was capable of reacting with the hydroxyl groups in the wood cell wall structure, whereas the latter could only react at the lumen/cell wall interface.<sup>30</sup>

In order to improve the impregnation of the polymer in the wood structure several studies have followed the approach of using multifunctional monomers such as  $\alpha$ -hydroxymethylacrylate (HEMA) and/or in situ formed diacrylate

crosslinking agents in the presence of an acid catalyst.<sup>30,31</sup>

Recent studies have shown that by using a good swelling solvent for the wood,<sup>32</sup> hydrophobic molecules (such as  $\epsilon$ -caprolactone) can be inserted into cell wall structure of the wood, doubling the dimensional stability of the wood.<sup>26</sup> The use of a good swelling solvent has also been used to polymerize styrene and N-Isopropylacrylamide into the wood cell wall structure for the same purposes.<sup>33</sup>

The position of the modification into the wood structure can be of great importance, not only for dimensional stability properties of the wood, where the modification should be on all the available -OH groups, and therefore into the cell wall), but also for other added-value applications.

One of these cases where the position of the modification might be important are in applications such as wood-hydrogels composites. In these cases, the purpose is opposite to the one for dimensional stability, as one would like to increase the interaction of water with the wood. Given that tracheid and vessel lumina are the largest voids in the wood structure, the aim of the modification should focus on filling the void to increase the hydrogen bonding interactions between the wood and water; increasing the water absorption capabilities of the wood.<sup>34</sup> Alternatively, more specific polymer distributions can be desired for certain applications, such as oil/water separation with wood.<sup>35</sup> Where in order to separate oil/water emulsions with wood, this one needs to be functionalized by polymer modification with a certain distribution in the wood cell wall, targeting a thick modification on the first micrometers of the wood surface and in the lumen/cell wall interface.

The different spatial distributions of the modification at the cellular level (microscopic level) can be seen in Figure 1.4.

Wood-polymer composites have been produced for improved dimensional stability for many years. However, the use of these traditional wood-polymer composites has been mainly limited to the fields of construction and furniture

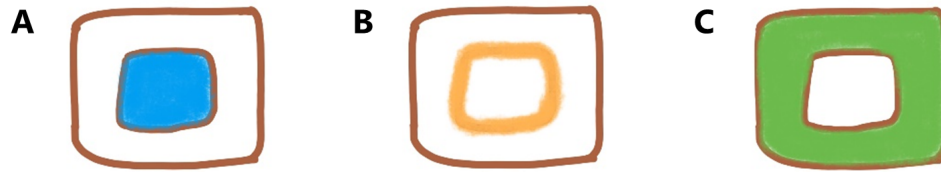


**Figure 1.4:** Modification distribution at the cellular level. (A) lumen filling, (B) lumen/cell wall interface, and (C) into the cell wall.

production. Nevertheless, polymer modification can also be used to produce added-value wood materials, using the natural hierarchical scaffold of wood of biological origin.

Although most publications have focused on the use of cellulose as a scaffold for several applications,<sup>36–42</sup> in recent years there has been a growing interest in polymer modification of wood-based materials for added-value applications. An example of a wood-based material for added-value applications can be the use of wood as a substrate for flexible light-emitting diode displays, in which wood powder was combined with different resins.<sup>43</sup> Alternatively, transparent wood for electronic applications was obtained using bulk wood directly, by firstly delignifying the wood and then impregnating with a resin.<sup>44</sup> Polyaniline-modified wood was created as a semiconducting composite material.<sup>45</sup> Wood–hydrogel composites were formed by reacting the hydroxyl groups available in the wood polymers and then crosslinking them with poly(N-isopropylacrylamide).<sup>34</sup> A pH sensitive wood was produced by polymerizing methacrylic acid (MAA) and 2-(dimethylamino)ethyl methacrylate (DMAEMA). These polymerizations resulted in higher wettability properties of the MAA modified wood samples than the DMAEMA modified samples under basic conditions, and the reverse behavior under acid conditions.<sup>46</sup>

Polymers have been also used to modify wood for oil water mixture separation. By delignifying the wood and curing an epoxy into the newly formed pores due to the absence of lignin, an hydrophobic/oleophilic wood was obtained.<sup>47</sup>

A polymerization technique used to introduce polymers in a controlled manner into the wood structure is surface initiated atomic transfer radical polymerization (SI-ATRP). This technique was used successfully on wood in several cases.<sup>33,48,49</sup>

During the course of this thesis, the use of this polymer modification technique (SI-ATRP) was extended to obtain a wood material that can be used as an oil/water separation device.

### 1.4.2. Controlled radical polymerization techniques

Radical polymerization allows for a higher variety of monomers compared to ionic polymerization. However, conventional free-radical polymerization (FRP) is characterized by a continuous production and consumption of active radical species. The statistical nature of FRP leads to typical dispersities of 1.5 or 2, depending on the mode of termination.<sup>50</sup>

On the contrary, reversible-deactivation radical polymerization (RDRP), also known as controlled/living radical polymerization (CRP), has allowed producing polymers with predefined molecular weights, relatively low dispersities, specific architectures, and various functionalities.<sup>51</sup> A leaving group, by producing a dormant species, reversibly deactivates the growing radical propagating species (i.e., active radical species). These dormant species can be re-activated through a stimulus. The process is similar for all CRP reactions techniques, differentiated by the form in which the dormant species are produced and consumed.<sup>52</sup> Through this technique, the concentration of radical propagating species is lower than in free radical polymerization conditions, with a 1-10% fraction of terminated chains, leading to lower termination of the active radical species. Moreover, the life of propagating species is extended by inserting dormant periods of around 1 minute after about 1 ms of activity. This extends the time needed for full polymerization but allows having a good control over the reaction.<sup>52-55</sup>

In the past years, the use and understanding of several CRP techniques has increased drastically. From the different CRP polymerization methods, atom transfer radical polymerization (ATRP) is one of the most extensively studied methods, due to its compatibility with a wide range of functional monomers and reaction conditions. Its utilization is steadily increasing since 1995 to today, as shown in Figure 1.5 (results of Scopus search engine on various CRP systems as of



September 15, 2018).

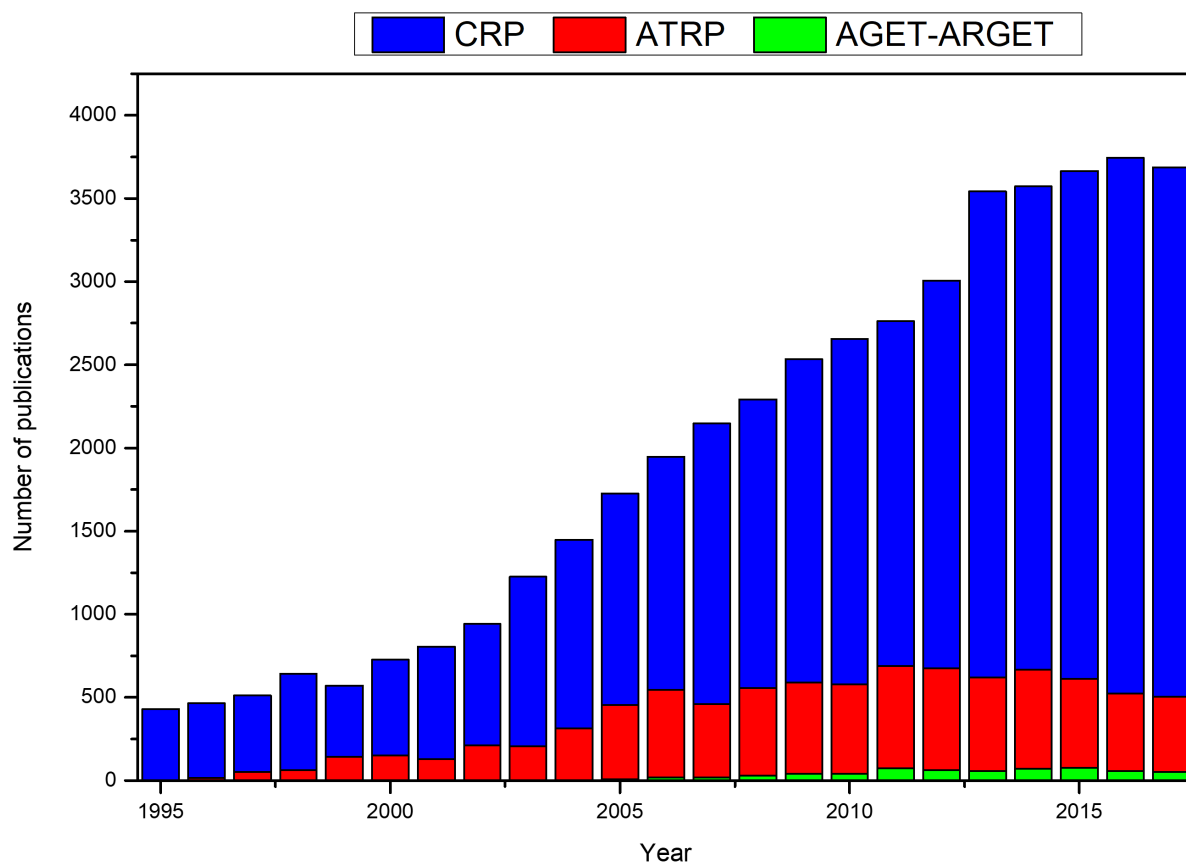
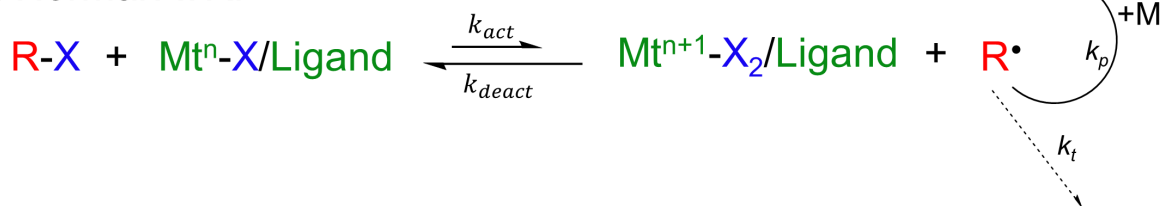


**Figure 1.5:** Controlled polymerization techniques, focusing in ATRP and its variant ARGET/AGET-ATRP.

As in all CRP techniques, the reaction process is controlled by the production of temporal dormant species; in this case, via a reversible redox process, which is catalyzed by a transition metal complex ( $M_t^{n+}X/\text{Ligand}$ ), being X another ligand or counter ion. To produce the radical, the transition metal complex undergoes a one-electron oxidation and the radical species is formed by the abstraction of a (pseudo)halogen atom (X) from the dormant species (R-X). The reversible redox reaction is controlled by two equilibrium constants, the rate constant of activation and deactivation, respectively. The polymer chains grow in a similar manner as in conventional FRP and are also terminated similarly by radical coupling and disproportionation. Several techniques have derived from ATRP, an example is activators generated by electron transfer (AGET), which follows the same principle as ATRP but in the presence of a reducing agent. This decreases the amount of catalyst needed and allows it to react under less oxygen free conditions. The scheme of both reactions is presented in Figure 1.6.

## a) Normal ATRP



## b) AGET-ATRP and ARGET-ATRP

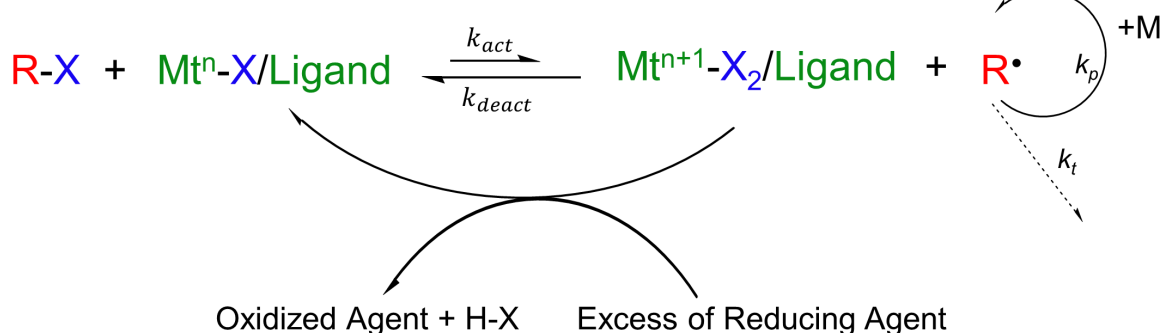


**Figure 1.6:** Scheme of (a) normal ATRP reaction and (b) ATRP reaction with excess of reducing agent (AGET or ARGET).<sup>54</sup>

The exact same principle is followed by a better known version: activators regenerated by electron transfer (ARGET), which is exactly the same as AGET but in this case very low amounts of the transition metal complex are used (< 500 ppm). Since normally no difference is being made between the two and the name ARGET is more spread through the scientific community, the search for obtaining Figure 1.5 was made for both AGET and ARGET.

Surface modification through the construction of polymer brushes has become of high importance, tailoring great advances in the surface and interface engineering field. Polymer brushes are individual chains covalently bonded to a solid interface, resulting in a thin polymer layer. They can be prepared from *grafting to*, *grafting from* or *grafting through* methods.<sup>34,56</sup> A highly used technique for grafting polymers onto solid surfaces is surface-initiated atom transfer radical polymerization (SI-ATRP). It follows the same principle as ATRP dividing, in this case, the reaction into two steps. In this approach, an initiator (with a halogen end) is grafted onto the surface of the solid in a first step. In the following step, polymer chains are grown from this covalently bonded initiator. SI-ATRP has enabled to control the grafting of polymers on existing materials to enhance their properties. This technique has been conducted on a wide range

of materials, from biological to synthetic, for various applications.<sup>42,48,57–59</sup>

With all these techniques in mind, during the course of this thesis, we have used SI-AGET-ATRP to introduce new functionalities into the wood structure, changing its wettability properties (see Chapter 4). From all the different available techniques SI-AGET-ATRP was chosen due to its compatibility to a wide range of monomers, high control over the reaction (essential feature in the creation of new functional materials from natural scaffolds), and, in particular with AGET, the need of less oxygen free conditions. This last feature can ease a possible scale-up of the reaction. Moreover, this technique has been previously successfully performed on wood.<sup>49</sup>

## **1.5. Wood Membrane Characterization**

In order to characterize wood and wood modifications, and to interpret the resulting properties, several characterization techniques were used. The techniques used in this thesis will be generally introduced in this section. When characterizing the chemical modifications in wood, specifically with polymers, some limitations need to be considered. Whereas, it is possible to locate the polymer modification in the wood structure with high resolution (e.g. via Raman), it is difficult or not possible to characterize the polymer modification by itself in terms of chain length, weight distribution, and type of copolymerization (block or random).

### **1.5.1. Electron Microscopy**

In electron microscopy (EM), an electron beam is used to image the sample either in reflection or transmission mode. In this thesis, scanning electron microscopy (SEM) and environmental scanning electron microscopy (ESEM) were used. These techniques allow visualizing and elementally analyzing the wood through scanning it with an electron beam, being capable of imaging the microstructure of the wood, wood modifications (e.g. polymer), and wettability effects from both native wood and modified wood.<sup>34,35,60–69</sup>

The main working principles of SEM and ESEM instruments are as follows: Typical electron sources are made from tungsten filaments (W), LaB<sub>6</sub> or CeB<sub>6</sub> crystals, or field emission guns. An electron beam is produced in the gun chamber. Inside, the acceleration voltage of the electron beam is controlled between the anode and the cathode. Once the electron beam leaves the gun chamber it is converged using several condenser lenses. An aperture objective helps control the beam current and spot size and the scanning coils set the scanning rate and magnification. Finally, the objective lens focuses the beam on the sample.

Images can be taken under low ( $3 \times 10^{-3}$  to  $1 \times 10^{-1}$  Pa) or high ( $1 \times 10^{-1}$  to  $1 \times 10^{-7}$  Pa) vacuum at the sample chamber. The higher the vacuum in the sample chamber, the higher the resolution that can be reached. Therefore, in order to obtain images with high spatial resolution (100 of nm – with a bulk sample), high vacuum has to be applied in the sample chamber. To image under high vacuum, given that the wood is not conductive, sputtering with a conductive layer is needed. Without sputtering, the wood sample suffers from charging and possible burning (degradation) of the wood sample. If high resolution is not required for the type of imaging desired, it is possible to image under low vacuum avoiding the need of sputtering the sample. Further increase of the resolution (10 of nm) can be achieved by imaging a thin slice (10  $\mu$ m thick) under low acceleration voltages.

Once the beam hits the sample there is an interaction between the electrons of the beam and the surface of the sample, which results in the emission of electrons (secondary (SE) or backscattered (BSE)) and X-rays. These interactions can provide different information about the sample. Some electrons are deflected through large angles or reflected by the atom nuclei (BSE); giving Z-contrast, which allows visualizing elements of higher atomic mass. These electrons, however, can also be affected by the topography of the sample, e.g. via shielding effect or border effect. Knocked electrons from the sample atoms due to the incident beam can escape at low energies (SE), which will give information about the samples morphology, topography, and shape. Furthermore, the beamed electrons can also cause the specimen atoms to

emit X-rays whose energy (EDX) and wavelength (WDX) are related to the specimen's elemental composition (known as characteristic X-rays); this will give elemental information of the sample composition.<sup>70,71</sup>

### **1.5.2. Raman and IR spectroscopy**

The use of Raman and infrared spectroscopy is of great interest due to the detailed chemical information they provide and, in the case of Raman, its resolution (diffraction-limited). They provide information regarding the cell wall structure, microfibril angle distribution in the different cell wall layers, lignin amount and composition as well as stress distribution within the plant fibers, and allow locating modifications with not only different elemental composition (like in EM) but also biopolymers in the cell structure.<sup>72–82</sup>

Both Raman and Infrared (IR) spectroscopy monitor molecular vibrations using different principles. Whereas, Raman spectroscopy is a scattering technique based on the Raman effect, it measures the inelastic scattering of a photon from a laser light source; IR spectroscopy measures the photon absorption, which is given when the molecule is excited to a higher vibrational energy level. Raman scattering is produced when light interacts with a molecule and polarizes its electron cloud. When nuclear motion is involved in this polarization, the energy from the light source (incident photon) will be transferred either to the molecule (Stokes) or from the molecule to the scattered photon (Anti-Stokes), see Figure 1.7. In Raman scattering, the energy of the scattered photon is different from the one of the incident photon (Raman-shift or Raman effect).

Contrarily, IR spectroscopy depends on changes in the molecule dipole moments. Thus, Raman and IR spectroscopy are complementary techniques, which through molecular vibration provide information regarding a given sample. This also means that they will have different resolution for different molecules. For instance, water gives a strong absorption band in the IR (due to its dipole), but only a weak Raman scattering.

Both techniques were used during the course of this thesis to provide

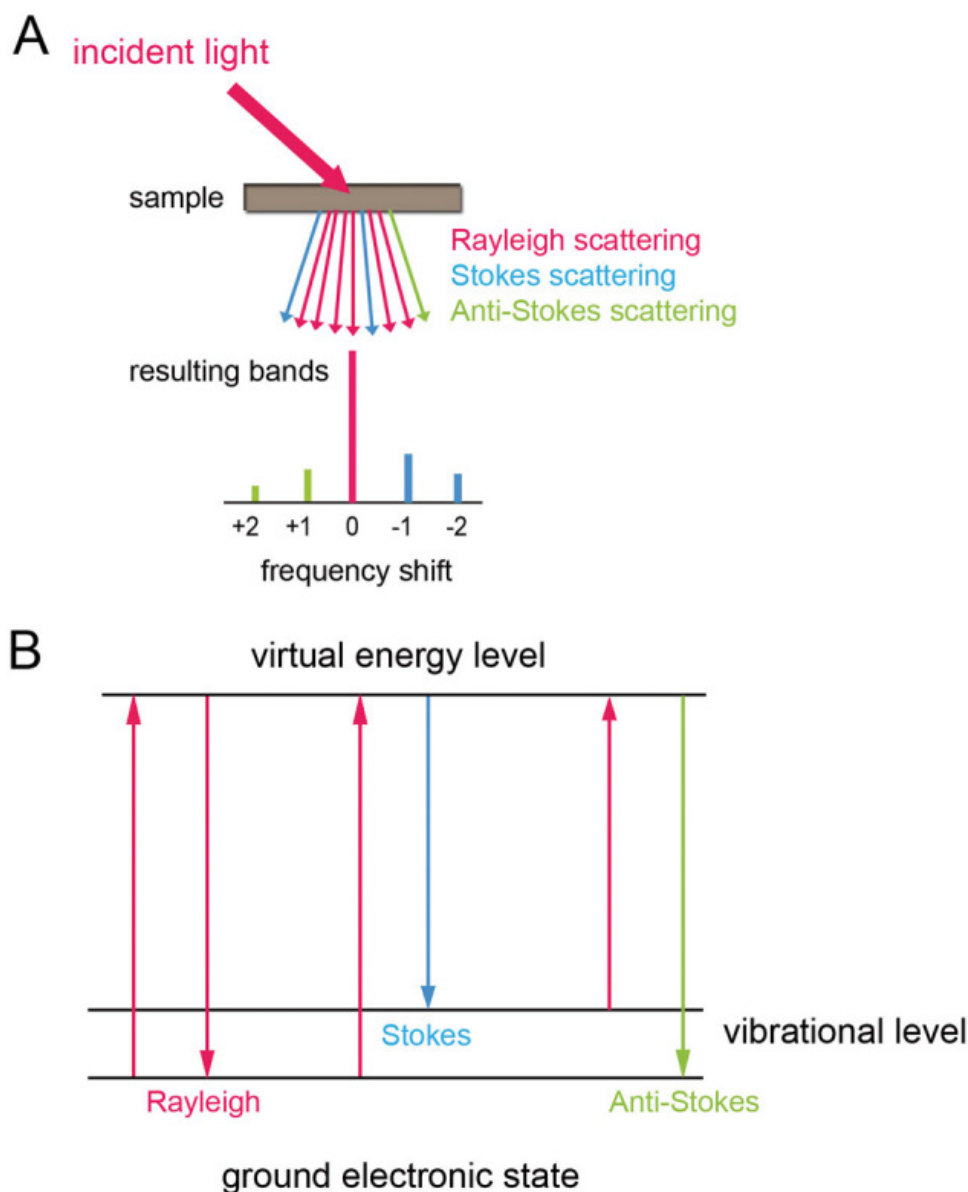


**Figure 1.7:** Light scattering in Raman spectroscopy. (A) Rayleigh, Stokes, and anti-Stokes scattering and the resulting frequency shift relative to the incident light. (B) Molecular energy levels corresponding to the type of light scattering.<sup>83</sup>

complementary information regarding the wood modifications.<sup>75,79</sup>

### 1.5.3. Contact angle

Contact angle measurements are intensively used in materials science to determine the wetting and adhesion properties of a material to a certain liquid. These properties play a very important role in many industrial processes. Through contact angle measurements, the surface energy of the material can also be estimated.<sup>84</sup> This is an important parameter to consider in the production of a

material for oil/water separation purposes.<sup>85</sup>

There are different methods for measuring the static contact angle of different solid materials and liquids. During the course of this thesis, the methods that were mainly used were sessile drop (SD) and captive bubble (CB). SD is the most widely used method, when characterizing the surface properties of a solid. In the SD method, the solid is in air (fluid) and a drop of the liquid that one wants to study is placed on the solid surface (see Figure 1.8). The angle formed between the liquid drop and the solid is the CA. However, due to the surface properties and structure of unmodified wood, the liquid drop experiences the effect of capillary forces of the wood structure and quickly spreads due to its wettability properties. These two effects make it difficult to obtain precise measurements through this method. For this reason, Rodríguez-Valverde et. al. recommend the use of captive bubble for porous materials such as wood and stone, when not modified, which diminishes these two effects.<sup>86</sup> Through the CB method, the material is soaked in the liquid, whose contact angle one wants to measure, and an air bubble (fluid) is placed on the wood surface from the lower side (see Figure 1.8). The angle between the air bubble and the material is measured. The complementary angle of the one obtained by the measurement is established as the contact angle of the liquid with the material.

Another type of contact angle, which is used to measure the adhesion properties of a material are sliding angle measurements (SA).<sup>87</sup> These type of measurements can be used to evaluate the adhesion of different oils onto the wood surface, therefore named as oil sliding angles (OSA). The same principle as in CB method is used for OSA measurements, with water as the liquid and the different oils as the fluid. Once the oil drop is placed onto the wood lower surface, the stage, in which the whole system is placed, is gradually tilted. The angle at which the fluid rolls off the solid surface is determined as the sliding angle. Sliding angle measurements can be used to measure the adhesion forces. These (sliding angle and adhesion forces) are an indirect proof of the amount of fouling a surface will suffer by the liquid being measured.

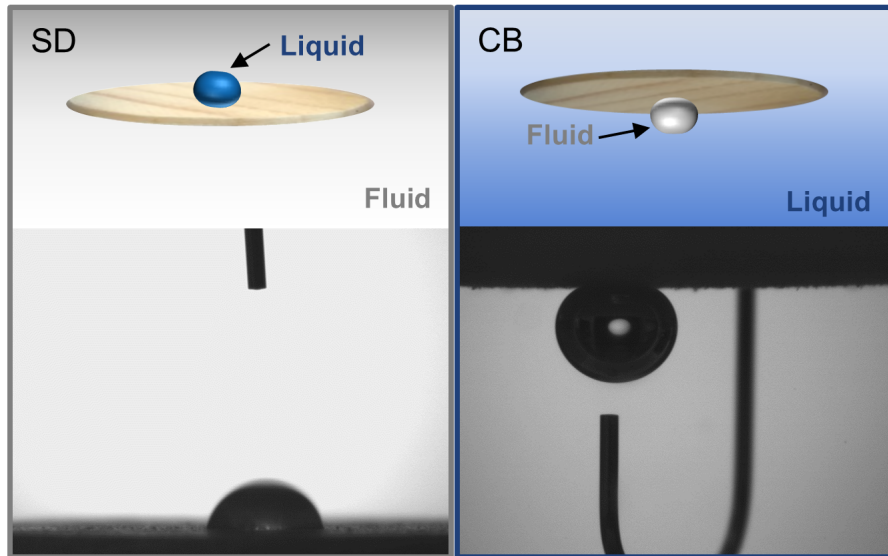


**Figure 1.8:** Schematic representation of the different contact angle measuring modes.

## 1.6. Oil/Water Separation

Oil is the greatest pollutant in water. The estimated tons of oil-waste released into the ocean vary greatly depending on the study; given that most of the oil enters the sea through non-point sources, such as industrial and domestic runoffs (sometimes grouped as “oil down the drain”).<sup>88</sup> The estimation ranges from 470,000 tons to a possible 8.4 million tons per year. The latest estimate is of 1.3 million tons per year of oil-waste released into the ocean, according to the 2003 book *Oil in the Sea III* by the U.S. National Research Council of the National Academy of Science (NRC), which is considered the authority on oil-spill data.<sup>5,89</sup>



### 1.6.1. General problem

When talking about oil-pollution in water the first images that come in mind are big oil spills with marine animals covered in a thick viscous carbon-dark liquid. However, surprisingly, oil spill accidents only represent between 10% and 14% of the total oil pollution in water. There are less expected sources that contribute to a higher extent. Some of the unexpected sources are e.g. from natural resources, like leakage from oil reservoirs placed under waterbeds (natural seeps), and most surprisingly the highest contribution source is oil down the drain. There are still some other, maybe, less surprising sources such as transportation and industrial contamination, which contribute to a higher extent than oil spills on polluting our water sources. The contribution percentage of the different sources varies greatly for every study (with a low variation on oil spill accidents and “oil down the drain” source). Depending on the region being studied, natural seeps happen in larger or smaller quantities. The areas where natural seeps occur are well known and monitored. Most sources agree that about 5-11% of the oil pollution comes from natural seeps. However, NRC published that they estimate 46% of oil pollution in North America comes from natural seeps, giving the Californian coast case as an example. In terms of “oil down the drain” pollution source, the amounts vary less going from 37% to 50% of the total pollution. This includes both industrial discharges and urban runoffs (represented as 45% in Figure 1.9). Shipping as an oil pollution source is agreed by most sources to represent between 24% and 33%. In the NRC report, shipping is considered together with “oil down the drain” source and represents only 37% altogether against the roughly 70% for most of the studies. What one can take from all this data is that it is normally very difficult to measure the real source of oil pollution and it is highly dependent on the region of the world being studied; however, it is evident that it is mainly an anthropologic sourced pollution. Figure 1.9 shows the data given by the world ocean review, which is a data study set representing the oceans of the entire world.<sup>3,5,88-91</sup>

When oil gets in contact with the environment, it undergoes several processes that change its physical and chemical properties. These processes are known

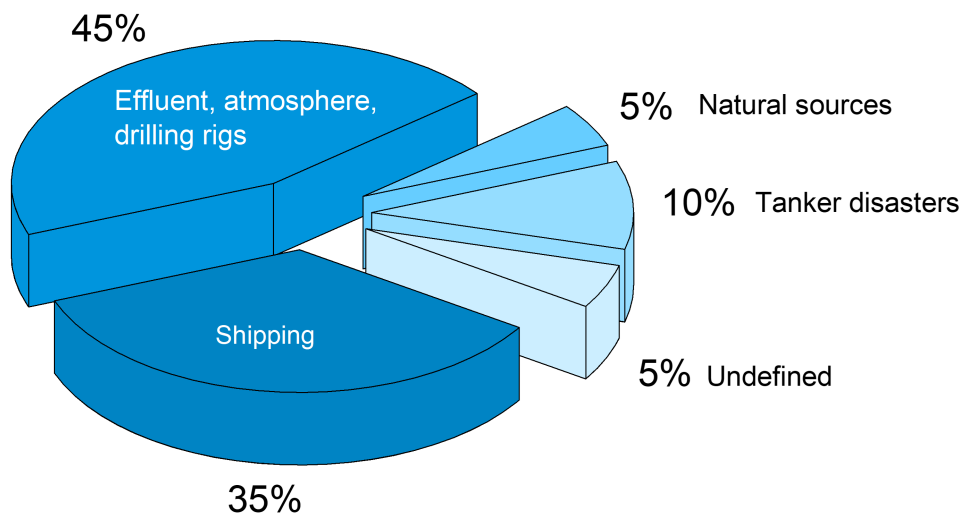


Figure 1.9: Oil pollution sources data for the world oceans.<sup>3</sup>

as “weathering” and occur at different rates; most of them taking place mainly as soon as the oil is released into the environment (see Figure 1.10). The rate of each process depends more on the type of oil rather than on the environment itself.

Crude oil is formed from more than 100 different molecules. The volatile molecules are the first to undergo “weathering”, short oligomers are broken into smaller compounds by bacteria and longer aliphatic chains remain longer without experiencing changes. If several volatile constituents compose the oil, these will evaporate at fast rates.

Another effect may be the spreading of the oil (oil slick), increasing the surface area exposed to the environment and speeding up the weathering process. The formation of dispersions (small oil droplets in a column of water) and emulsions (larger droplets of oil-in-water or water-in-oil) is due to the existence of bacteria and the salt concentration of the environment. Over time, the oil will suffer from photooxidation (breakage of the hydrocarbon chains due to the exposure of the sun) and dissolution.

Moreover, with time, bacteria also play an important role in the breakage of the hydrocarbon chain. Some parameters that might affect the bacteria growth and, thus, the rate of hydrocarbon breakage by bacteria would be the temperature, oxygen and nutrient supply for the bacteria, and the surface area

exposed (oil slicks).

As mentioned, oil pollution does not only exist in the form of oil/water mixtures but also as emulsions. Oil-in-water and water-in-oil emulsions represent a challenge for oil/water separation technologies and proved to be difficult with the simple unmodified wood system (Chapter 2). We intend to overcome this potential challenge through polymer modification of our wood scaffold, for which a good control over the reaction is needed (Chapter 3 and Chapter 4).

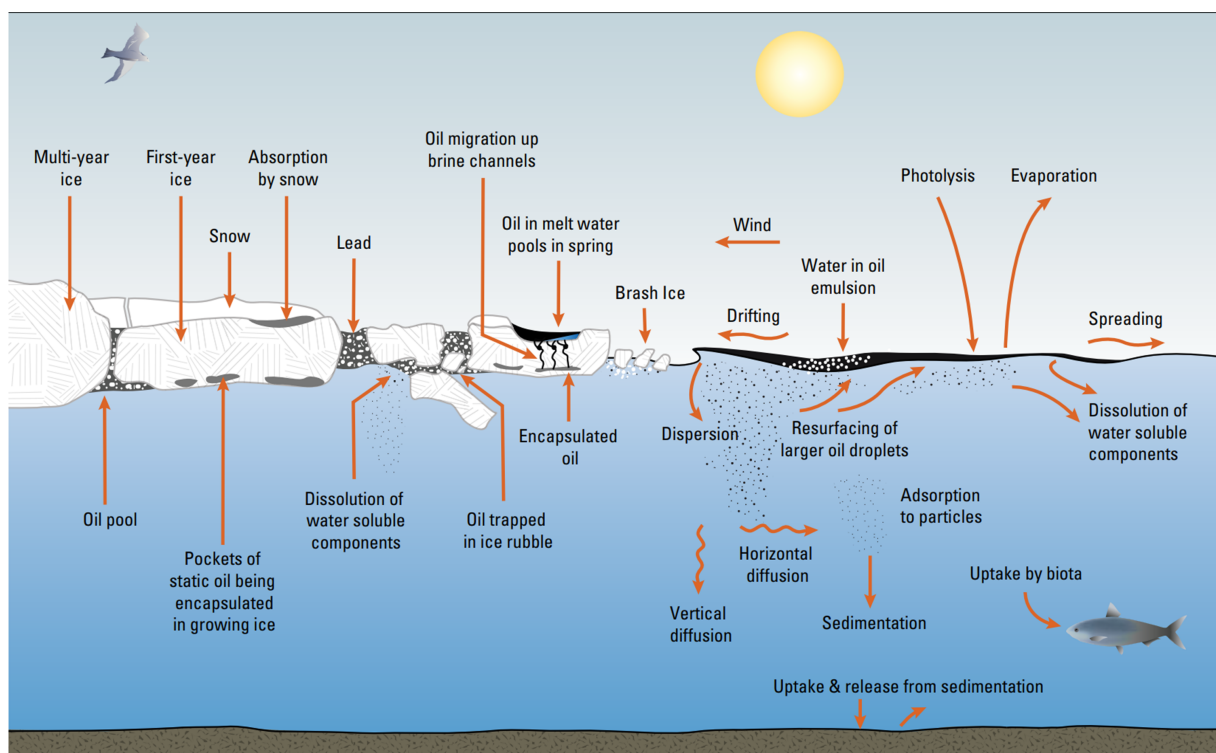


Figure 1.10: Different processes of oil "weathering".<sup>91</sup>

### 1.6.2. Current technologies

Due to oil spill accidents, awareness over the environmental impact of oil pollution in water has increased, leading to tighter regulations followed by great efforts to separate these two. Great focus has been put onto the production of inexpensive, low energy consumption, environmentally friendly and easy-to-use devices. Traditionally used methods (e.g. flocculation, gravitational separation, coagulation and air flotation) do not entirely fulfill these requisites (high energy and materials cost, low efficiency, and high complexity of the separation

system)<sup>7,8,92</sup>, for which new functional materials are being produced.

There are many different types of technologies for water treatment: bags, activated alumina, activated carbon, ceramic filters, UV filters, reverse osmosis, microfiltration, ultrafiltration, nanofiltration, etc. Depending on what needs to be separated or extracted from the water (e.g. suspended solids, viruses, bacteria, macromolecules (such as oil), or salts) and the size of the contaminant (from nano- to the macro-scale), filters and membranes are made in a wide variety of different sizes and with different chemical functionalities (see Figure 1.11). In membranes, the separation configuration can be either a cross-flow or a dead-end (see Figure 1.12).

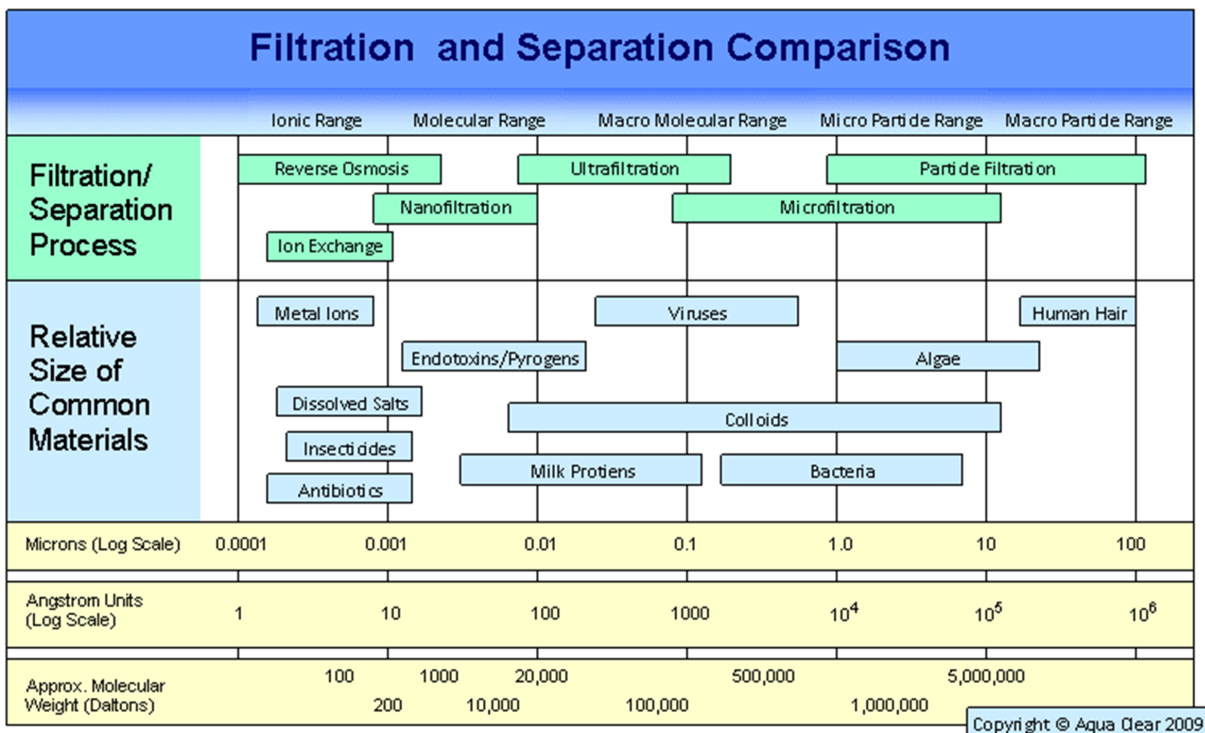
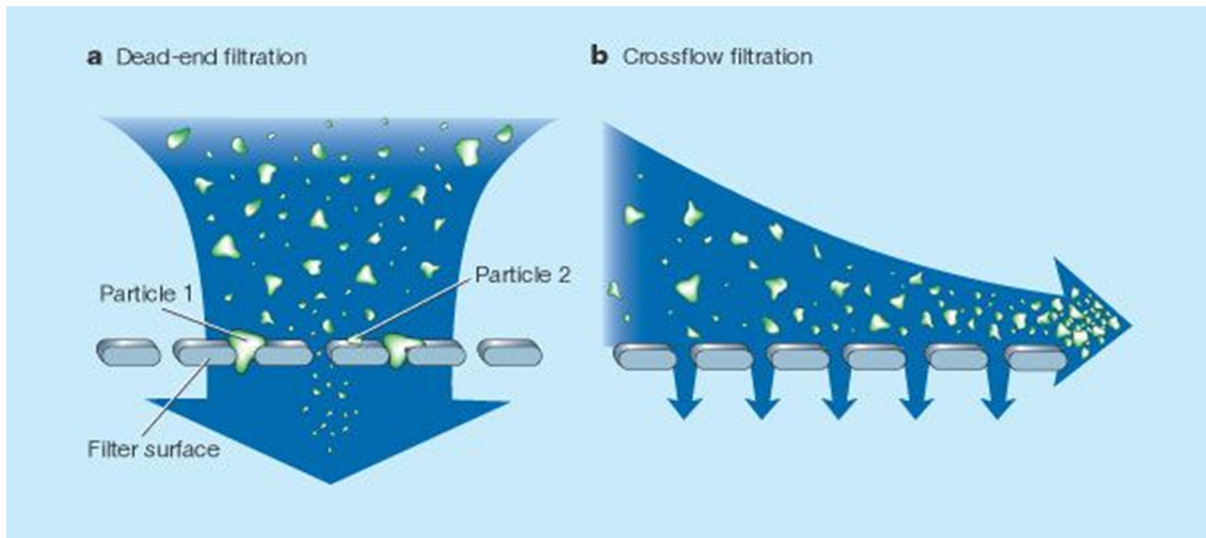


Figure 1.11: Types of separation technologies with respect to the size of the rejected material.<sup>93</sup>

In terms of oil/water separation, the devices used for this application can be divided into two categories: absorbent materials and filtration materials,<sup>95</sup> which do not absorb but repel contaminants. For the first case, given that the absorption of one liquid or another is limited, their efficiency tends to be low and large volumes of material are needed. The second group, separator materials, can be subdivided into two distinct groups: “oil-removing” materials and “water-removing” materials. In both cases, the efficiency is increased



**Figure 1.12:** Membrane separation configuration scheme.<sup>94</sup>

compared to the former group given that it is not limited by their size or absorption capacity. However, there are still some drawbacks. The “oil-removing” materials tend to have fouling problems since they let the oil through, while repelling water, suffering from different forms of clogging.<sup>96,97</sup> Contrarily, “water-removing” materials let water through and, therefore, suffer less from fouling, are anti-fogging, self-cleaning, and tend to achieve higher efficiencies.<sup>98,99</sup> Nevertheless, for the membrane to achieve this oleophobicity to separate oil-in-water emulsions ( $\leq 50 \mu\text{m}$ ) the use of fluorine chemistry is necessary.<sup>100</sup>

The performance of a membrane is evaluated according to several parameters: its efficiency in the rejection of the contaminant ( $R$ , see Equation 1.1); the pressure up to which the membrane is capable of rejecting the contaminant (breakthrough pressure ( $P_{B,th}$ ), see Equation 1.2);<sup>101,102</sup> and the flux it can achieve ( $Q_p$ , see Equation 1.3). Other commonly studied parameters are its transmembrane pressure ( $P_{TMP}$ , see Equation 1.4); and its permeability ( $k$ , see Equation 1.5). The operating flux can be increased by increasing the pressure (up to the breakthrough pressure); however, it increases energy costs.

$$R(\%) = \left(1 - \frac{C_p}{C_o}\right) \times 100 \quad (1.1)$$

where  $C_p$  is the concentration of the remaining oil in the permeate after separation and  $C_0$  is the initial concentration of oil in the feed.

$$P_{B,th} = \frac{2R\gamma_{12}}{D^2} \frac{1 - \cos(\theta)}{1 + 2(R/D)\sin(\theta)} \quad (1.2)$$

where  $2R$  represents the interspace between two pores (i.e., twice the cell wall thickness),  $2D$  is the pore diameter,  $\gamma_{12}$  is the interfacial tension between water and oil, and  $\theta$  is the oil contact angle on a wet wood surface.

$$Q_P = F_w \times A \quad (1.3)$$

where  $F_w$  is the flow through the membrane and  $A$  is the effective area of the membrane.

$$P_{TMP} = \frac{P_f + P_c}{2} - P_p \quad (1.4)$$

where  $P_f$  is the pressure at the feed,  $P_c$  the pressure of the concentrate and  $P_p$  the pressure of the permeate.

$$k = \frac{F_w}{P_{TMP}} \quad (1.5)$$

where  $F_w$  is the flow through the membrane and  $P_{TMP}$  is the transmembrane pressure.

A membrane can be operated in continuous with two different set-ups: either with the  $P_{TMP}$  or the flux ( $Q_p$ ) maintained constant. The transmembrane pressure tends to increase during operation due to fouling, which creates an increasing cake layer on the surface of the membrane. If the same pressure is applied, maintaining the  $P_{TMP}$  constant, this cake will decrease the flux. Contrarily, to overcome the resistance created by this cake, maintaining a constant flux, the pressure of the feed needs to increase, resulting on the increase of the  $P_{TMP}$ . Therefore, the fouling a membrane suffers can be monitored, by both operating conditions.<sup>103</sup>

### 1.6.3. Alternatives

Nature has inspired many of the materials produced for oil/water separation.<sup>104-106</sup> There are various surfaces in nature that are capable of repelling liquids (hydrophilic or lipophilic liquids) such as those from birds (feathers),<sup>107-109</sup> sea creatures (fish scales and clams),<sup>106,110,111</sup> insects (body and wings),<sup>112-116</sup> sand,<sup>117</sup> and plants (both leaves and flowers).<sup>114,118</sup> These materials can mainly separate oil/water mixtures. Researchers have been inspired by nature to produce new synthetic materials, which could be capable of separating oil from water with higher efficiencies and more challenging conditions, such as micro- to nano- oil-in-water emulsions. The list of these new synthetic materials includes sponges,<sup>119-124</sup> woven textiles,<sup>125-131</sup> meshes,<sup>132-134</sup> synthetic membranes (ceramic and polymer),<sup>135-141</sup> and foams.<sup>142-144</sup>

These different materials have advantages and drawbacks. Some of the biggest disadvantages are inherent to the separation configuration; e.g. low achievable efficiencies with sponges due to being absorbent materials. Others are the difficulty of the fabrication and stability of the scaffold modification, for instance, in meshes.

Our most direct competitor in the sense of configuration and efficiency ranges are polymer membranes. These achieve very high efficiencies under challenging conditions (nano-emulsion separation). The main drawback of these materials is related to the scale-up process, as a controlled growth over the polymeric membrane is complex, expensive and energy consuming. By using wood, we want to overcome this up-scaling problem while using a renewable resource.

## 1.7. Oil/Water Emulsions

The mixture of oil and water can be classified in three different groups according to the diameter size ( $d$ ) of the dispersed phase.<sup>101</sup>

**Table 1.1:** Type of oil/water mixtures according to the droplet size of the dispersed phase.

Name	Diameter ranges ( $d$ )
Free oil/water mixtures	$d > 150 \mu\text{m}$
Dispersions	$20 \mu\text{m} \leq d \leq 150 \mu\text{m}$
Emulsions	$d < 20 \mu\text{m}$

Emulsions can be naturally formed in nature, as mentioned previously in Section 1.6, through the weathering process that oil undergoes when entering the atmosphere. Oil/water emulsions can be classified in two subgroups: oil-in-water emulsions and water-in-oil emulsions depending on the liquid that forms the continuous phase (see Figure 1.13).

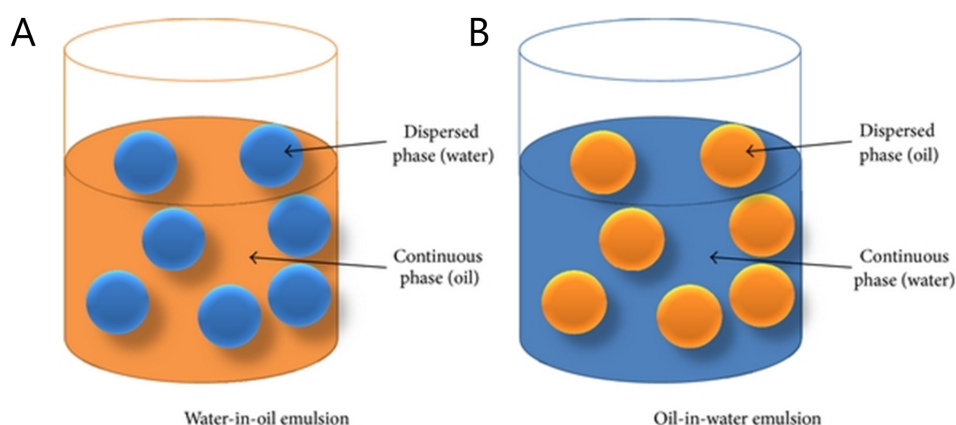


**Figure 1.13:** Schematic representation of water-in-oil and oil-in-water emulsions.<sup>144</sup>

Different techniques can be used for preparing emulsions. It is difficult to assign one technique as there are many relevant parameters in the emulsion preparation. Some of these parameters are the type of emulsifier used (anionic, cationic, and non-aionic), the hydrophilic-lipophilic balance (HLB) of the emulsifier, the shearing force given by the different techniques (stirring, vortex, sonication (bath and probe)), and the type of oil used and its solubility in water



(chain length dependence).

Important parameters for the preparation of emulsions are shear forces and stabilizers. When high shear is applied to a colloidal emulsion, the applied forces will lead to coalescence and breakage of the emulsion droplets. The particle size is then determined by the equilibrium of these two processes. When no shear is applied the size is determined by the stability of the emulsion, which can be described by the DLVO theory. The interaction of two particles is determined by their surface properties. There are two main contributions to this interaction. Van der Waals interactions are very short range attractive interactions and lead to an immediate coalescence of two droplets upon collision. Electrostatic interactions are long range repulsive interactions and decrease the possibility of such collisions. Electrostatic interactions are typically present, if the surface of a droplet is charged. If this is not originally the case, such charges may be introduced by the addition of surfactant, where the hydrophobic tail is miscible with the oil droplet, while the charge will orient itself towards the surface. Surfactants are a widely applied stabilization method for emulsions, which are produced through shear but without which would otherwise not be stable. Therefore, while shear can be used to obtain a controlled droplet size, surfactants can be used to stabilize it.<sup>145</sup>

### **1.7.1. Emulsion Characterization**

There are several techniques to characterize emulsions. A possible way is through light scattering of a laser beam, due to its collision with the droplets of the dispersed phase. The scattering angles depend on the size of the different droplets in the solution. During the course of this thesis, two of the most common techniques dynamic light scattering (DLS) and small-angle static light scattering (SASLS) were used.

Dynamic light scattering is based on the extraction of spectral information derived by time-dependent fluctuations of the light scattered from a specific volume of the sample. When a monochromatic coherent beam light hits the

particles in suspension, scattered light waves are spread out in all directions. Due to the randomness (Brownian motion) of the motion of the suspended particles, the interference can be stochastically constructive or destructive, resulting in stochastic light intensity signal. Moreover, the concentration of droplets in the area of study may vary. Therefore, the interference of the scattered waves in the far field region generates a net fluctuating scattered intensity. The size of the particle can be determined by the Stoke-Einstein equation, obtaining the hydrodynamic radius.<sup>146</sup>

Small-angle static light scattering is based on the angular dependency of the intensity to the size of the droplet. The measurements are performed by either fixing several detectors at the different scattering angles around the sample or by rotating one detector on a goniometer arm around the sample. Through this technique, it is possible to obtain information about size, structure, dynamics and even molecular weight of the sample. Different type of correlations can be used to obtain information regarding the different parameters. However, for emulsions we were only interested in the droplet sizes. Given that they are in the form of spheres the Mie theory can be used to characterize them.<sup>147</sup>

Dynamic light scattering can measure droplets of size ranges from the nanometer to few micrometers, whereas small-angle static light scattering detects droplets of sizes ranging from a few nanometers to hundreds of microns.<sup>148</sup>

In order to analyze the content of the emulsions gas chromatography with a flame-ionization detector (GC-FID), head-space gas chromatography (headspace GC), and high-performance liquid chromatography (HPLC) were used. These two techniques allowed for high accuracy of oil detection (at the ppm range). An international standard method is available for GC-FID (ISO 9377-2). However, due to historical and economical reasons there is no unified method to measure oil in water.<sup>149</sup>

Other less precise methods used are white light microscopy, comparison of the weight percent of oil before and after separation, transmittance, thermogravimetric analysis (TGA), ultraviolet-visible light (UV-Vis), Fourier transfer infrared spectroscopy (FTIR), and infrared spectrometer oil content analyzer.<sup>61,99,116,150-153</sup>



# Chapter 2

## Underwater Superoleophobic Wood Cross Sections for Efficient Oil/Water Separation

Functional surfaces with specific wettability are widely encountered in nature and have inspired the development of oil-repellent materials for oil/water separation. Despite some impressive results reported, materials combining high separation efficiency together with economical and easily scalable approaches and ideally based on renewable resources have yet to be reported. In this Communication, spruce (*Picea abies*) wood cross sections are proposed as oil/water separation systems. The natural wood anisotropic porous microstructure directs fluid transport, and the nature of the cell wall biopolymers results in superhydrophilicity and underwater superoleophobicity. Such wood membranes can separate water from oil with high efficiency (>99%) and high flux using only gravity and without the need for prior chemical modification of the wood scaffold. Wood also provides an intrinsic solution to scalability issues.

## 2.1. Introduction

In recent years, awareness of oil spill accidents in marine and aquatic ecosystems has increased, leading to tighter regulations. Water pollution, in particular due to oil contamination, is a global issue with adverse environmental impact; stressing the need to find novel strategies for efficient oil/water separation.<sup>4–6,8,154</sup>

Traditional approaches are plagued with high energy costs, a limited efficiency and the overall complexity of the separation processes.<sup>8,92,154</sup> Alternative separation techniques based on various porous materials such as polymer membranes,<sup>135,136</sup> woven textiles,<sup>101,125</sup> metal meshes,<sup>101,152,155–158</sup> sponges,<sup>63,119,120,159</sup> and foams<sup>142,143</sup> are more promising.

In the case of porous oil/water separation systems, the use of materials showing preferential wettability by one or the other liquid is particularly relevant; since the oil/water separation challenge is related to interfacial properties. Most of these so-called “oil-removing” materials are superhydrophobic and superoleophilic.<sup>135,159–161</sup> Even though they provide an adequate solution for oil/water separation, they have limited efficiency due to oil fouling. The adhesion of viscous oils to the filtration scaffold seriously affects membrane permeability and separation efficiency. Moreover, oil removal from the membrane must be done at a high environmental cost. Finally, hydrophobic-oleophilic membranes cannot be used for gravity-driven separation since the higher density water sits below the oil, preventing oil from passing through. Because of these drawbacks, oil-removing functional materials are now challenged by “water-removing” materials, which show a high affinity for water (superhydrophilicity) while having oil-repellent properties (superoleophobicity). However, such superoleophobic surfaces are very difficult to achieve, as demanding surface modifications are needed to obtain a specific surface roughness (ideally re-entrant structures) in combination with low surface energy chemicals (typically undesirable fluorinated polymers and surfactants). In addition, since the surface tension of oils is much lower than that of water, a

superoleophobic material is usually also superhydrophobic. It has also been shown that in many cases, a superoleophobic surface in air is superoleophilic under water.<sup>162</sup>

Jiang and co-workers proposed an alternative approach based on their observations of special wettability behaviors found in nature.<sup>106,163,164</sup> For example, fishes can avoid oil contamination in polluted waters thanks to their rough scales covered with mucus, which can trap a water layer at the interface. These types of solid/water/oil interface systems have two main advantages. Firstly, the water layer prevents contact between the oil and the solid material, decreasing the risks of contamination and fouling by oil. Secondly, this water layer repels oil and eliminates the need for fluorinated chemicals. Based on this concept, researchers developed water-removing materials that are successfully applied to oil/water separation problems.<sup>63,101,117,152,157,158,165</sup>

Despite the impressive results reported with this type of materials, a few drawbacks remain unaddressed. These systems are mostly obtained from synthetic polymers (foams, hydrogels, brushes) and metals, which provide the scaffold material for high mechanical stability. Their fabrication requires costly raw materials and sophisticated engineering. Moreover, to obtain the desired porosity, energy and chemicals are heavily involved. Altogether these drawbacks severely restrict large scale applications.

On the utilization of synthetic polymers, a recent study by Geyer et al. stresses out the ever increasing negative environmental impact of plastic wastes that nature cannot degrade or assimilate.<sup>9</sup> Bio-based and biodegradable polymers are an interesting alternative to synthetic polymers that could help solving this issue. In the field of oil/water separation, only few studies report on the utilization of bio-based materials, such as cellulose and chitosan, to manufacture membranes.<sup>9,128,166–171</sup> Hence, it is of great importance to develop new materials for oil/water separation that combine high separation efficiency with an economical and easily scalable approach, and ideally based on a renewable resource.

In this communication, we report on the utilization of native spruce wood cross sections with underwater superoleophobicity for oil/water separation. Wood is a well-known hygro-responsive material: it can absorb large quantities of water in a humid environment, and release it in a dry environment.<sup>172</sup>

Besides its peculiar hygro-responsive behavior, softwood has a typical 3D hierarchical structure constituted by aligned tracheids (hollow fibers) with cell walls mainly consisting of cellulose nanofibrils embedded within an amorphous matrix composed of lignin and hemicelluloses.<sup>11,173</sup> Wood is not only developed by the tree to support its growth towards light: it is also a vast vascular network used to transport water rich in nutrients from roots to leaves. Its hydrophilic nature and its natural hierarchical porosity suggest that wood may be an ideal candidate to be used as a water-removing material for oil/water separation purposes. In addition to its promising features – superhydrophilicity and anisotropic porous structure – wood also possesses several advantages making it highly competitive when compared to synthetic meshes, foams, and sponges. It is a highly abundant bio-sourced material, the manufacturing energy involved is limited to the classical wood processing operations, it has excellent mechanical properties and it intrinsically provides a solution to scalability.

## **2.2. Results and Discussion**

### **2.2.1. Wood section Morphology**

Figure 2.1 illustrates the morphology of a typical spruce wood cross section used in this work. In Figure 2.1b,c, the cross section cut reveals the anisotropic arrangement of the softwood fibers (tracheids). The latewood (LW – thick cell walls and narrow lumina) and earlywood (EW – thin cell walls and larger lumen area) regions are easily distinguishable.

For theoretical calculations, we assumed squared cells (the wood pores), with  $2D = 30 \mu\text{m}$  and  $2R = 5 \mu\text{m}$  for EW,  $2D' = 10 \mu\text{m}$  and  $2R' = 25 \mu\text{m}$  for LW (see Figure 2.1d). The complex wood microstructure is analogous to a vascular network, designed for fluid transport in the living tree. After it is felled and cut,



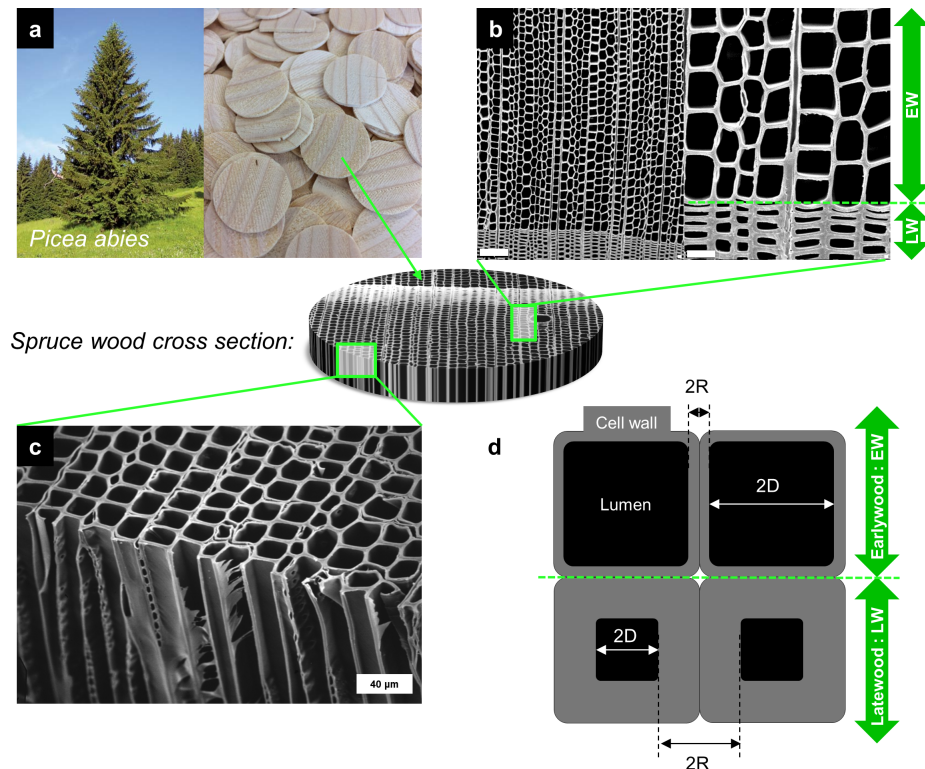


**Figure 2.1:** Morphology of the spruce wood cross sections. a) Photographs showing a Norway spruce tree (*Picea abies*) and the wood cross section discs ( $\varnothing$  20 mm, 1 mm thickness). b) and (c) Scanning Electron Microscopy (SEM) images of the wood cross sections after surface smoothing with a microtome knife. b) Truncated tracheids from top view, revealing the morphological difference between EW and LW cells (left scale bar: 100  $\mu$ m, right scale bar: 30  $\mu$ m). c) Tracheids from side view, showing the fiber alignment. d) Close up scheme of the EW and LW tracheids, with the relevant geometric parameters.

the main wood microfeatures, lumina and cell walls, are preserved. Spruce wood tracheids are about 3 mm in length. Providing that the cross sections are 1 mm thick, and assuming a random distribution of 3 mm long tracheids, the most probable scenario is that 66.6% of the hollow fibers will be cut opened from both ends (calculations in Supporting Information, S2.1). Therefore, the natural opened porous wood structure will allow the water to flow through the wood cross section during the separation process. In Figure 2.1b,c, wood surfaces smoothed with microtome cutting are shown, in order to better visualize the wood microstructure. In our experiments, we used wood discs directly obtained by circular saw cutting. It is well known that this processing step severely damages the wood fibers at the surface, possibly over several tens of microns.<sup>174</sup> As shown in Figure 2.2, the wood surfaces obtained after cutting are partially covered by folded cell wall fragments from shredded fibers. As we will see, this phenomenon does not affect the open porous structure of the wood cross

sections neither does it block the transport and permeation of fluids.

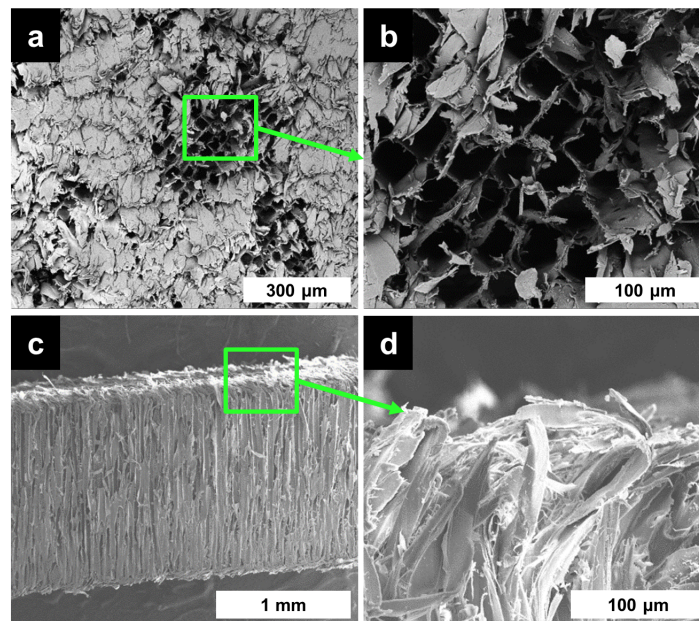


**Figure 2.2:** a,b) SEM images of wood cross section samples after circular saw cutting, showing shredded wood fibers, with torn and folded cell wall fragments partially covering luminal areas. c,d) The damage can extend up to several tens of microns in depth.

### **2.2.2. Air and underwater wettability of spruce wood sections**

To evaluate the performance of wood cross sections for oil/water separation purposes, we first investigated their wettability by measuring static and dynamic contact angles, both in air (with the sessile drop method) and underwater (with the captive bubble method). As shown in Figure 2.3a,b, the contact angles for both water and oils on a wood cross section cannot be measured in air. When a droplet of either liquid makes contact with the wood, it instantaneously spreads out and penetrates in the wood capillaries. Therefore, considering that the water and oil absorptions are extremely fast, the wood cross section surface in air may be qualified as superamphiphilic (both superhydrophilic and superoleophilic). In Figure 2.3c,d, underwater oil droplets (light and heavy oils) at the interface with the wood cross section are shown.

Both images display high contact angles, suggesting an oleophobic behavior. Indeed, the static oil contact angle values reported in Figure 2.3e range from  $141^{\circ}$  to  $155^{\circ}$ , being either superoleophobic or very close to this criterion. We conclude that the water-soaked wood cross sections show underwater

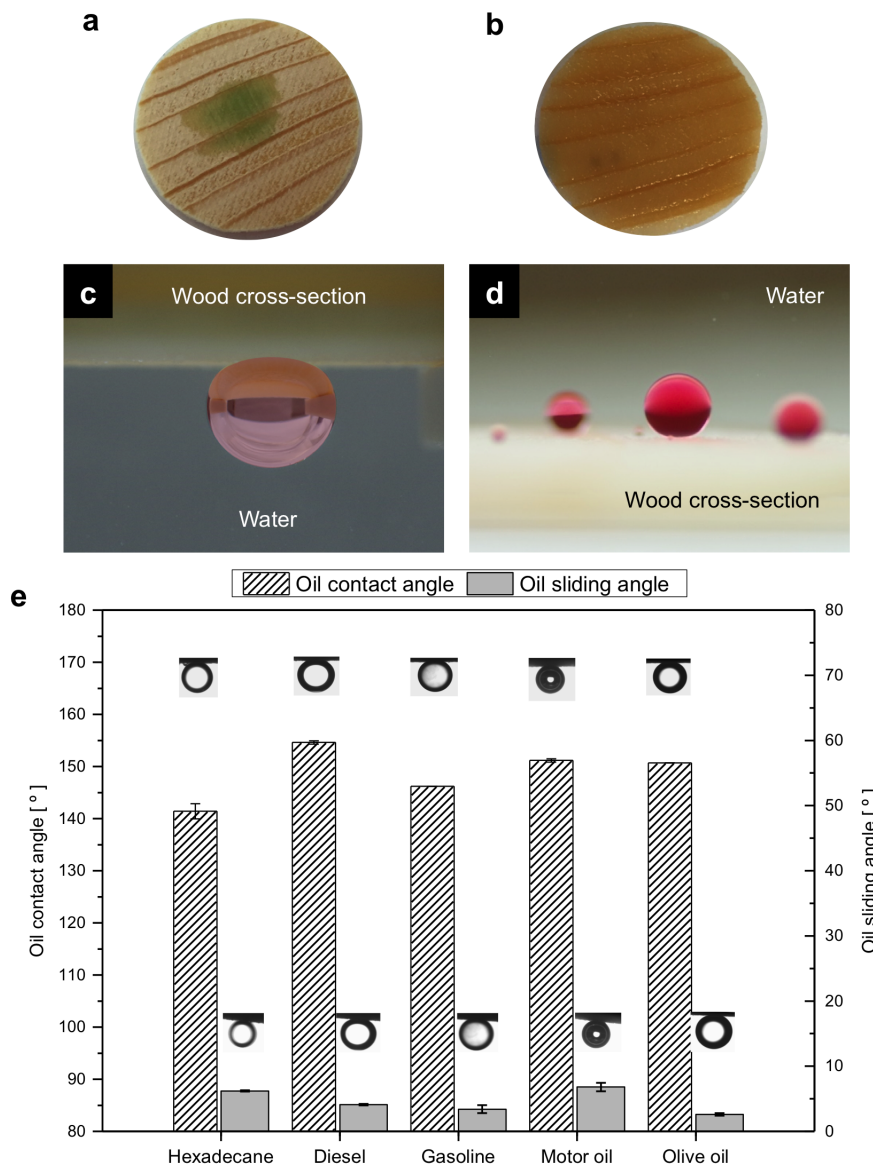


**Figure 2.3:** Wetting properties of the wood cross sections. *a,b*) respectively show the absorption of a water droplet and a hexadecane droplet on the opened wood porous structure in air. With contact angles below  $5^\circ$ , the surface is both superhydrophilic and superoleophilic. *c,d*) Photographs of dyed light and heavy oils (*c*) hexadecane, and (*d*) 1,2-dichloroethane) sitting on the water-immersed wood surface with high contact angles. *e*) Static and dynamic contact angle values for various oils in the wood/water/oil system, showing both the superoleophobic and the low oil adhesion properties of the wood cross sections.

oil-repellent behaviors for a wide range of oils, including both light and heavy oils. According to the dynamic contact angles shown in Figure 2.3e, all measured oil sliding angles (OSA) are below  $7^\circ$ . The small inserts illustrate the oil droplets easily rolling off the wood surface when the sample is slightly tilted (Movie S2.1, Supporting Information). The low OSA values obtained prove that the wet spruce wood surface displays very low oil adhesion levels. Together with the underwater superoleophobicity, these results indicate a clear potential for

its application in oil/water separation issues.

As schematized in Figure 2.4a, the underwater superoleophobicity is the result of a stable solid/water/oil three-phase system. The water/oil interface is obtained through the introduction of a lubricating or wetting phase inside the solid substrate. In our case, the wetting phase is water, and the solid substrate is wood. Wood is well known for its strong hygroscopic behavior resulting from the chemical nature of the cell wall biopolymers (cellulose, lignin, and hemicelluloses). The interactions between wood and water have been widely studied. In a first phase, water molecules penetrate the cell wall, where they are strongly bonded to hydroxyl functionalities. Further uptake leads to the fiber saturation point, where all cell walls are water saturated.<sup>11,172–175</sup> Afterwards, additional water – so-called “free water” – enters the structure filling up the cell lumina. This leads to a fully hydrated state, where the total weight uptake can exceed 200%. As the water soaks the wood preferentially, water is trapped in the wood hierarchical structure and stabilized in the lumina by capillary forces, forming a thin water film on the surface. This water film can be visualized on the ESEM images reported in Figure 2.4b-e (Movie S2.2 and S2.3, Supporting Information). Consequently, when an oil droplet approaches the surface, the water layer prevents contact between the wood substrate and the oil.<sup>176</sup> The composite solid/water/oil interface is therefore fully oleophobic without the need for fluorinated compounds to lower the surface energy.

### **2.2.3. Capillary force-based separation (separation based on contrasting wetting properties)**

The term “capillary phase separation” or “capillary force based separation” was coined to describe porous structures displaying a similar behavior, which were employed in separation processes.<sup>101,120,136,139,165,177</sup> Membranes designed to separate oil from water are characterized by their intrinsic efficiency (i.e. the percentage of oil repelled by the membrane), their flux, and by a maximum pressure – the breakthrough pressure  $P_B$  – above which the oil phase might be pushed inside the individual wood lumina, permeating through the membrane

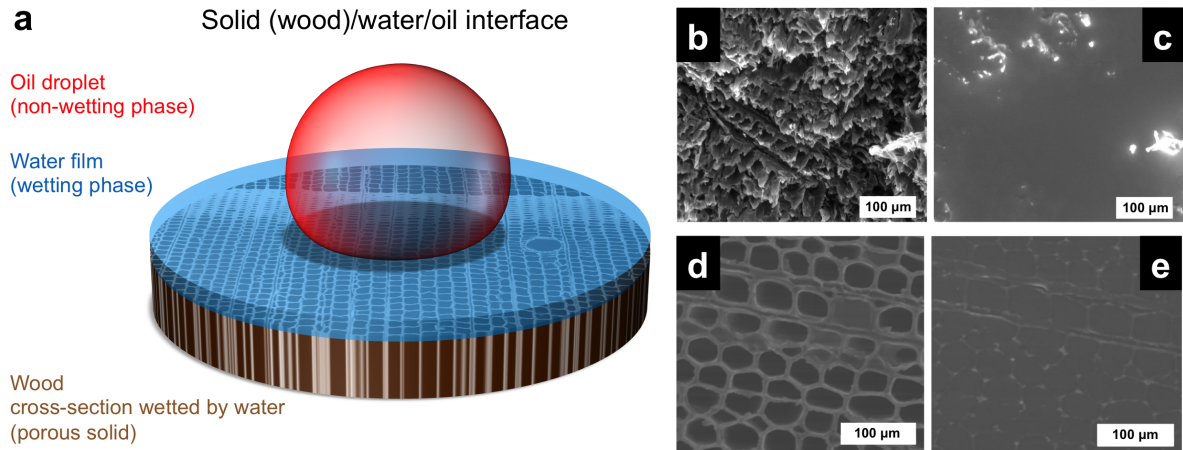


**Figure 2.4:** a) Illustration of the solid/water/oil system. Wood is preferentially wetted by water, forming a water film present at the interface which prevents the oil droplet to make contact with the wood surface. b) and c) Environmental Scanning Electron Microscopy (ESEM) images of the wood cross section cut with a circular saw, showing the water film forming on top of the wood microstructure (sample chamber at 3.30 Torr and 5.14 Torr respectively). d) and e) ESEM images of a microtomed wood surface in the dry and fully wetted states (sample chamber at 2.40 Torr and 4.25 Torr respectively).

(Figure S2.2, Supporting Information). In other words, if the pressure drop across the membrane is higher than  $P_B$ , the oil will flow through and the membrane will not be able to separate the oil from water. To demonstrate the potential of our system, we investigated all three characteristics. The solid/water/oil composite interface is described in Figure S2.2 (Supporting Information). Assuming a simple geometrical model for our wood scaffold (as shown in 2.1d), the theoretical pressure drop across the membrane may be expressed using Equation 2.1:<sup>101,178</sup>

$$P_{B,th} = \frac{2R\gamma_{12}}{D^2} \frac{1 - \cos(\theta)}{1 + 2(R/D) \sin(\theta)} \quad (2.1)$$

where  $2R$  represents the interspace between two pores (i.e. twice the cell wall thickness),  $2D$  is the pore diameter,  $\gamma_{12}$  is the interfacial tension between water and oil, and  $\theta$  is the oil contact angle on a wet wood surface. Experimentally,  $P_B$  is given by the maximum height of an oil column supported by the membrane, and can therefore be expressed by Equation 2.2:

$$P_{B,exp} = \rho g h_{max} \quad (2.2)$$

where  $\rho$  is the oil density,  $h_{max}$  is the maximum oil column height that the membrane can support, and  $g$  is the standard gravity. According to Equation 2.1, with a water/hexadecane interfacial tension of  $\gamma_{12} = 53.3 \text{ mJ m}^{-2}$ ,

an oil contact angle  $\theta = 141^\circ$ , and assuming a 100% EW cross section with an average pore diameter of  $2D = 30 \mu\text{m}$  and a cell wall thickness  $R = 2.5 \mu\text{m}$ , the  $P_{B,\text{th}}$  is 1.74 kPa.  $P_{B,\text{exp}}$  was measured with the experimental setup illustrated in Figure S2.2 (Supporting Information). We tested our wood membrane with hexadecane, obtaining a maximum height of 35 cm corresponding to a pressure of  $2.64 \pm 0.13$  kPa, which is significantly higher than the theoretical value.  $P_{B,\text{th}}$  was calculated based on the assumption that the wood cross sections solely consist of EW, with homogeneous pore sizes. In reality, as shown in Figure S2.3 (Supporting Information), our samples contain a small proportion of LW. Since the LW pores are smaller and the interspace between pores is larger,  $P_{B,\text{th}}$  would be much higher for a cross section consisting of 100% LW (calculated as 22.84 kPa). In our samples, the proportion of EW was estimated to be 86% using image analysis (Figure S2.3, Supporting Information). The contribution of the 14% LW explains the higher  $P_{B,\text{exp}}$ . To conclude, we found that the experimental value is in good agreement with the  $P_B$  values reported for other oil/water separation systems operating under similar external pressure conditions,<sup>101,132,152,179</sup> showing that our membranes have the proper stability to repel oil and to be used for oil/water separation. Pressure breakthrough values with the different oils are given in Table S2.1 (Supporting Information).

#### **2.2.4. Separation of oil-water mixtures**

In view of the special wettability of water and oils observed on the wet wood, and the adequate  $P_B$  value implying good stability, the ability of spruce wood cross sections to separate hexadecane from water was finally investigated. Free oil/water mixtures were separated using the experimental setup described in Figure S2.4 (Movie S2.4, Supporting Information). The round shaped, pre-wetted wood cross section was inserted between two glass tubes. A mixture of hexadecane and water was then poured into the upper tube. The wetting water phase has a higher density than hexadecane, permeating quickly through the wood disc with high flux (ca.  $3500 \text{ L m}^{-2} \text{ h}^{-1}$ ). On the other hand, because of the underwater superoleophobic behavior of the wet wood structure, when the oil phase reaches the interface, it is retained

above the membrane. The separation is performed without the use of external pressure, and only relies on gravity. Additional water/oil mixture can be poured, continuing the separation until the accumulated oil reaches the critical column height corresponding to  $P_B$ . The separation efficiency was quantitatively characterized by analyzing the oil contents after separation. The oil traces in the permeate were determined using gas chromatography. The separation efficiency was defined and calculated by the rejection coefficient  $R(\%)$  using Equation 2.3:

$$R(\%) = \left(1 - \frac{C_p}{C_o}\right) \times 100 \quad (2.3)$$

where  $C_p$  is the concentration of the remaining oil in the permeate and  $C_o$  is the initial concentration of oil in the feed. The separation efficiency for hexadecane was above 99.9% with a concentration of oil in the permeate lower than 7 ppm, illustrating the high separation efficiency of wood cross sections (a typical chromatograph is given in Figure S2.5, Supporting Information).

To further characterize the wood membranes, the water flux was measured. These experiments were performed maintaining a constant column of the feed of  $\approx 6$  cm and measuring the weight of permeated water per unit of time (Figure S2.6, Supporting Information). The high flux measured ( $3500 \text{ L m}^{-2} \text{ h}^{-1}$ ) can be achieved due to the opened structure and large pores of the wood cross sections. An increase in membrane thickness results in a significant decrease in flux (e.g., a 2 mm thick cross section gives a flux of  $1600 \text{ L m}^{-2} \text{ h}^{-1}$ ). The fiber length in spruce wood may explain this result. As discussed previously, there is a certain probability for a fiber to be open at both ends (with the ability to transport water across the wood membrane). This probability decreases with the thickness of the disc, i.e. a 2 mm thick disc contains more fibers closed at one end which results in water having to permeate through slower pathways (e.g. from one fiber to the other, through open pits).

We assume that the shredded fibers (see Figure 2.2) do not produce any “skin layer” effect since they are well separated from each other, leaving enough space for the water to flow through without restriction. The obtained

flux is significantly higher when compared to other porous systems such as ultrafiltration membranes, where skin layers are typically observed and represent an obstacle to the water flow.

### **2.2.5. Other wood species**

All woods are composed of high molecular weight compounds (cellulose, hemicelluloses, and lignin), and a smaller fraction of low molecular weight compounds (extractives and minerals). While the proportions and chemical composition of lignin and hemicelluloses may vary significantly in between softwoods and hardwoods, cellulose is uniformly present in all woods. Cellulose amounts for 40% to 50% (w/w), hemicelluloses for 20% to 30% and lignin for 20% to 30%. There is also a large diversity in amount (0.5% to 20%) and chemical composition of the extractives.

All woods are known to interact with water, however the rate of adsorption and the amount of water at equilibrium may significantly depend on the species, since wood wetting and swelling is directly related to both microstructure and chemical composition.

The chemical composition of a wood surface is directly linked to surface energy. The determination of surface energies of wood is particularly difficult, and results must be interpreted with caution.<sup>84,180–183</sup> According to literature, surface energies of different wood species (softwoods and hardwoods) only vary from 48 to 61 dynes/cm.<sup>180</sup> Therefore, it is likely that all woods would behave as water-removing materials and could be used to separate oil/water mixtures.

In terms of structure, wood morphology is likely to influence parameters such as flow rate, and pressure breakthrough. We have shown that beech wood (*Fagus sylvatica*), is also able to separate a model hexadecane/water mixture (see Movie S2.5, Supporting Information). The experimental conditions were identical: we simply replaced the spruce wood cross section by a beech wood cross section. The flux ( $6500 \text{ L m}^{-2} \text{ h}^{-1}$ ) was significantly higher for beech wood, and the pressure breakthrough of 2.12 kPa, is slightly lower in comparison



to spruce wood (2.64 kPa). This may be explained by differences in the microstructure. In beech wood, large vessels represent about 50% to 60% of the pores, and they have an average diameter of 60  $\mu\text{m}$  (see Figure S2.7, Supporting Information). It is therefore a better material for fluid transport in terms of flow rate, but this is at the expense of a lower pressure breakthrough.

### 2.3. Conclusions

In conclusion, we demonstrate that simple wood cross sections are both superhydrophilic and underwater superoleophobic with very low oil-sliding angles. This “water-removing” material is also endowed with natural anisotropic porosity, which provides an ideal scaffold for fluid transport. Due to these intrinsic properties, the native spruce wood scaffolds can separate various oils from water, with high efficiency, high flux, and resistance to fouling.

In addition, wood also possesses several advantages that make it highly competitive when compared to other oil/water separation devices. It is a highly abundant, readily available, and renewable bio-sourced material, it has good mechanical properties, and it does not require any chemical treatment for this application. We therefore propose an inexpensive, green, and scalable material for efficient oil/water separation. We anticipate that our wood membranes will offer a very practical solution to numerous oil pollution problems.

## 2.4. Experimental section

**Materials.** Norway spruce (*Picea abies*) cross sections (1 mm thick and 20 mm diameter) were prepared from large wood cross sections obtained by circular saw cutting. Throughout the experiments, the samples used had a similar EW/ LW distribution. Prior to any experiment, the samples were soaked in water under vacuum to assure they were in a fully hydrated state. The microtomed wood samples used for SEM imaging were smoothed by a rotary microtome equipped with a steel blade. The oils used were hexadecane (VWR technical, >99%), dodecane (Sigma-Aldrich, >99.9%), isopropanol (Sigma-Aldrich, >99.9%), gasoline, diesel, motor oil, and olive oil (obtained from local stores). Red dye Sudan III (Fluka A.G.) and blue dye Acid blue 129 (CIBA-GEIGY, >99%) were used to dye the oils and water respectively.

**Characterization.** The surface of the wood cut with a circular saw was observed by SEM (FEI Quanta 200FEG). The samples were sputtered with gold particles and attached to a stainless-steel sample holder with copper tape. Images of water condensation on wood samples with microtome and circular saw cuttings were acquired using ESEM (FEI Quanta 600 equipped with a Peltier cooling stage set at 2 °C). The chamber was operated at pressures ranging from 1 to 7 Torr to image the sample from dry to wet conditions. Oil contact angles and oil sliding angles were measured on a OCA20 (DataPhysics) instrument, installed in a climate room with 65% humidity, at 20 °C. Underwater measurements were performed using a glass cuvette filled with MilliQ water and the captive bubble technique.

**Separation experiments.** the wetted wood cross section (1 mm thick, 2 cm diameter) were placed between two glass tubes held by a clamp. A proper sealing was guaranteed by rubber O-rings. The oil/water mixtures (50% v/v) were poured simultaneously in the upper tube. The separation was driven only by gravity; no external pressure was applied. The flux was determined by measuring the incremental quantity of water passing through the membrane by unit of time and considering the effective separation area of the wood cross section (Ø 18 mm). The amount of oil in the permeate was analyzed by gas chromatography using an Agilent Technologies 7890B GC System equipped with an Inlet liner (Sky Liner, Split (Restek), deactivated glass with wool, 4 × 6.3 × 78.5 mm for Agilent GCs). The column used was a HP-5 (L: 30 m, ID: 320 µm and film thickness: 0.25 µm) from Agilent. A temperature ramp ranging from 40 to 300 °C (25 °C/min) was developed to obtain optimal separation. To avoid any possible artefacts when measuring the remaining oil with GC-FID, the dyes were not used for these experiments. For the pressure breakthrough measurement, the upper tube was replaced by a graduated glass cylinder. Oil was directly and slowly poured on the wetted wood cross section until the oil column height generated the breakthrough pressure. The experiments were performed five times with different wood disks.

## Acknowledgements

This research work was supported by the Swiss National Science Foundation (grant no 160041). The authors are grateful to Dr. Karsten Kunze from ScopeM at ETH Zürich, for his support on the SEM measurements, and to Asel Maria Aguilar Sanchez from the IFB department at ETH Zürich for her support in the ESEM measurements.

## Supplementary information

### S2.1: Estimating the percentage of fibers opened from both ends in a 1 mm wood cross section

When a 1 mm wood cross section is cut, some fibers might be opened from both ends – these fibers will let water through – and some fibers might be closed from one end, blocking the water flow (see Figure S2.1a). To estimate the percentage of tracheids opened from both ends in a 1 mm thick wood cross section, we reasoned on the basic scheme shown in Figure S2.1a,b. To simplify our model, we make the following assumptions: all the tracheids have the same length (3 mm), they are aligned perpendicularly to the cross section, and they are randomly distributed in the vertical direction.

Starting with one single fiber, we define the length of a tracheid  $d$  as 3 mm, and  $x$  is the thickness of our wood discs (Figure S2.1b). With these parameters we can formulate the probability that a single fiber is open as:

$$P(i) = \frac{(d - x)}{d}$$

Using this equation, if  $x$  is set to 1, 2 or 3 mm, then the probabilities to have a single fiber open from both ends are respectively 0.66, 0.33 and 0.

Since the probability of having each fiber opened from both ends is an independent event, if we consider a cross section with 100 fibers, we can calculate the compound probability for the 101 independent events using a binomial distribution. The resulting probability distribution shown in Figure 2.1c indicates that if we use a 1 mm thick wood cross section, the most probable scenario is that we will obtain 66.6% of the fibers opened from both ends.

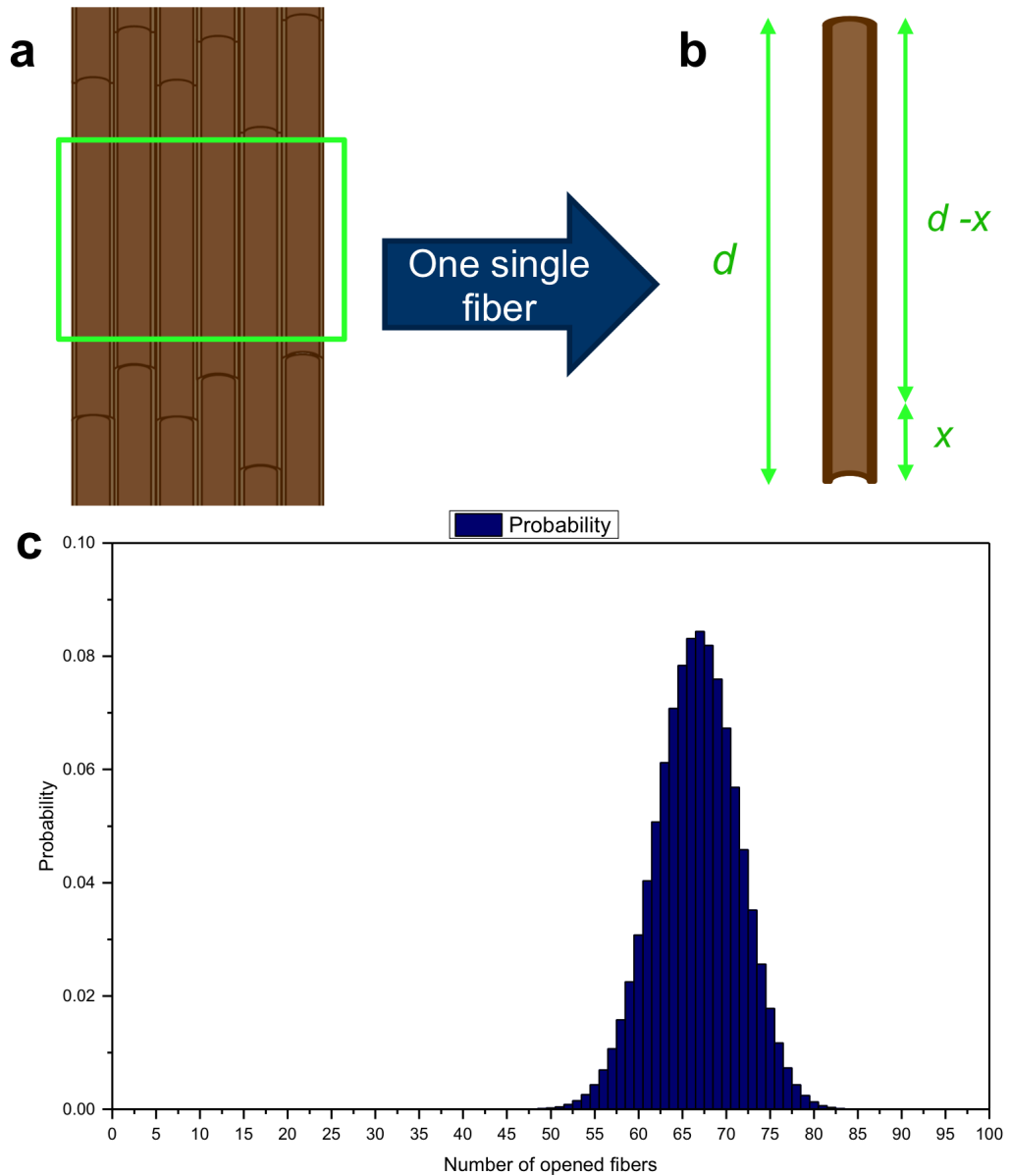


**Figure S2.1:** a) Representation of the randomly distributed tracheids in spruce wood. The dotted black line illustrates the 1 mm thick wood disc: the green fiber would be opened from both ends, and the red fiber would be opened only from one end. b) Representation of the parameters on a single fiber. c) Probability distribution of the opened fibers considering a thickness of 1 mm and a total of 100 fibers.

S2.2: Breakthrough pressure

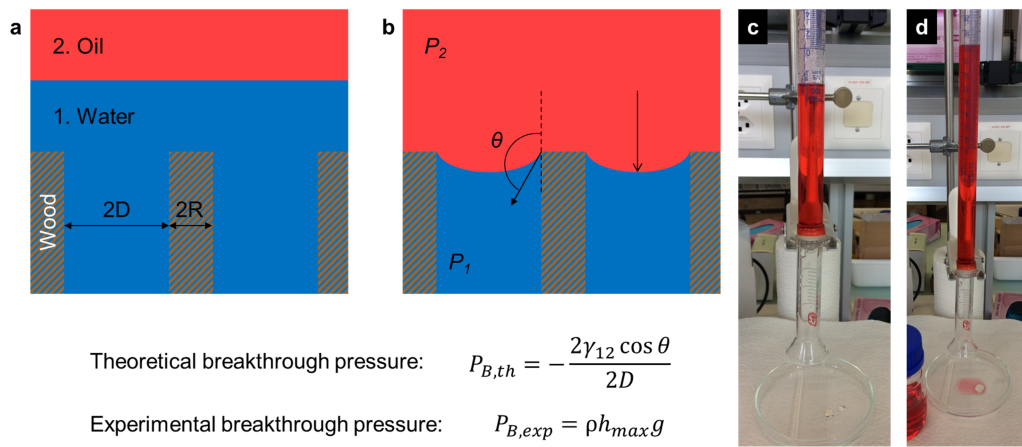


**Figure S2.2:** Breakthrough pressure evaluation. a) and (b) representation of the wood/water/oil system before and after the oil phase reaches the interface. c) and (d) illustrate the experimental setup built to measure the breakthrough pressure. In (d), the pressure generated by the hexadecane column reaches  $P_B$  and pushes the oil through the wood pores, which permeates. The equations used to calculate the theoretical and experimental pressure breakthrough are displayed.

S2.3: EW and LW proportion in the wood cross section

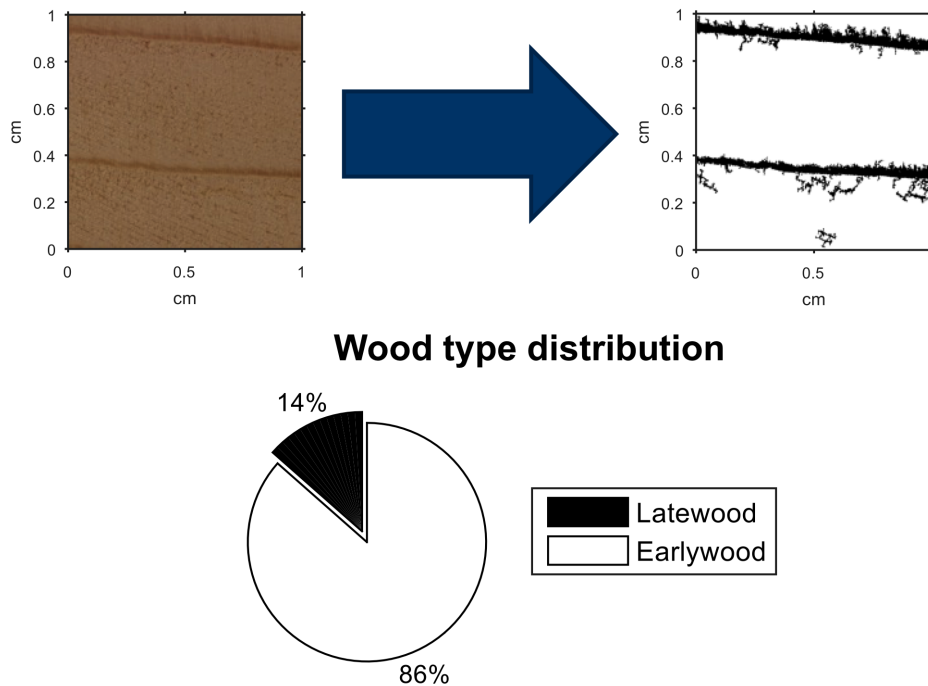


**Figure S2.3:** Average wood type distribution (EW and LW) by image processing with MATLAB 2015a from the spruce cross sections discs used in the study. Through image processing, we determined that the samples used in our experiment have an average 14% of latewood and 86% of earlywood, with a standard deviation of 3% (the analysis was done on 6 different discs).

**Table S2.1: Breakthrough pressure experimental values with the different oils**

*Table S2.1: Breakthrough pressure parameters and results for different oils.*

Oil	CA [°]	$\gamma_{12}$ [J m <sup>-2</sup> ]	$\rho_2$ [kg m <sup>-3</sup> ]	$h_{\max}$ [m]	$P_{B,th}$ [kPa]	$P_{B,exp}$ [kPa]
Hexadecane	142	0.053	770	0.35 ± 0.00	1.76	2.64 ± 0.00
Olive oil	151	0.016	900	0.21 ± 0.00	0.59	1.85 ± 0.03
Gasoline*	146	0.048	750	0.11 ± 0.03	1.64	0.86 ± 0.21
Motor oil	152	0.009	850	0.32 ± 0.00	0.33	2.64 ± 0.02
Diesel	155	0.030	840	0.21 ± 0.00	1.11	1.73 ± 0.00

\*The  $P_{B,exp}$  values for this oil show a high variability due to the inadequacy of the experimental material used to the type of oil.

#### S2.4: Separation set-up

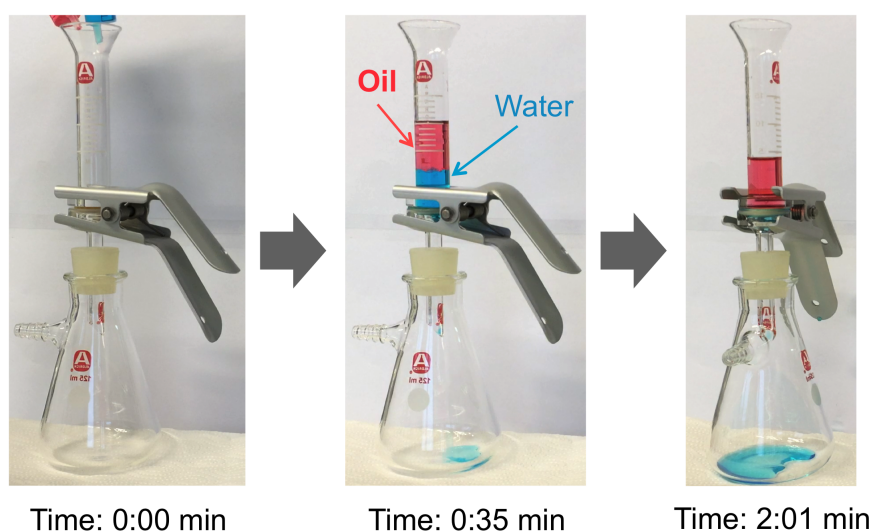


**Figure S2.4:** Images of the separation setup from the initial time to the end of the separation. While hexadecane is retained on top, the water flows through the membrane. For clarity's sake, oil was dyed red with Sudan III, and water was dyed blue with Acid blue 129.

### S2.5: Oil traces analysis with GC

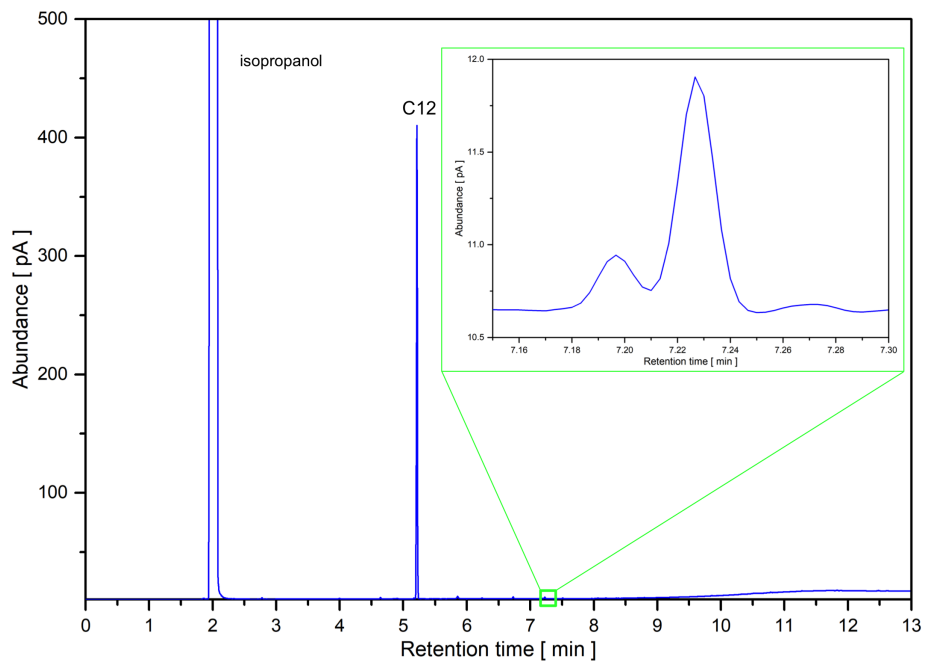


**Figure S2.5:** Typical GC chromatograph of the permeate after the oil/water separation experiment. Samples were diluted in isopropanol (retention time  $t_{R, \text{isopropanol}} = 2.04 \text{ min}$ ). Dodecane (C12) was used as internal standard ( $t_{R, \text{dodecane}} = 5.22 \text{ min}$ ). The insert shows the hexadecane (C16) peak ( $t_{R, \text{hexadecane}} = 7.23 \text{ min}$ ).

### S2.6: Flux measurements

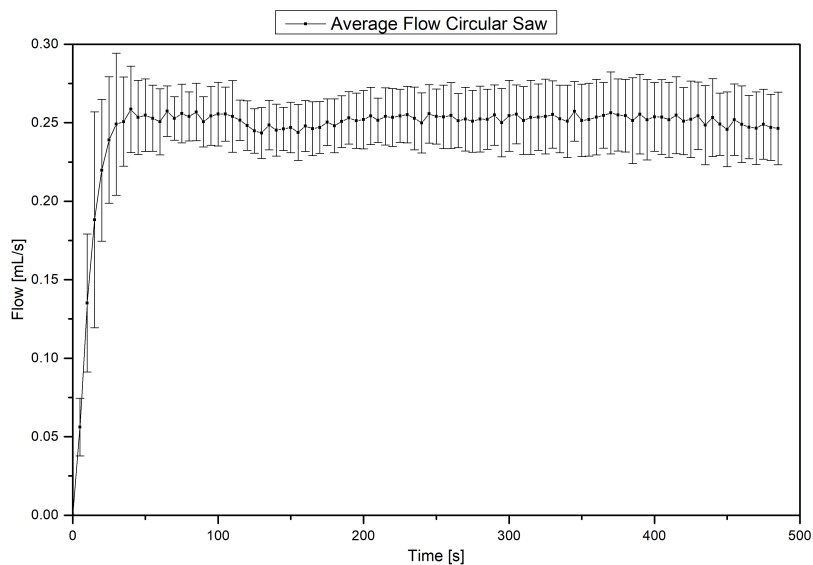


**Figure S2.6:** Water flow through wood cross sections cut with a circular saw. The average flow (with a constant water column of ca. 6 cm) is  $0.25 \text{ mLs}^{-1}$ . Considering our wood membranes with an effective filtration diameter of 18 mm, it corresponds to a flux of ca.  $3500 \text{ Lm}^{-2}\text{h}^{-1}$ . The average flow was obtained from the measurements of five different wood membranes.



### S2.7: Beech wood structure

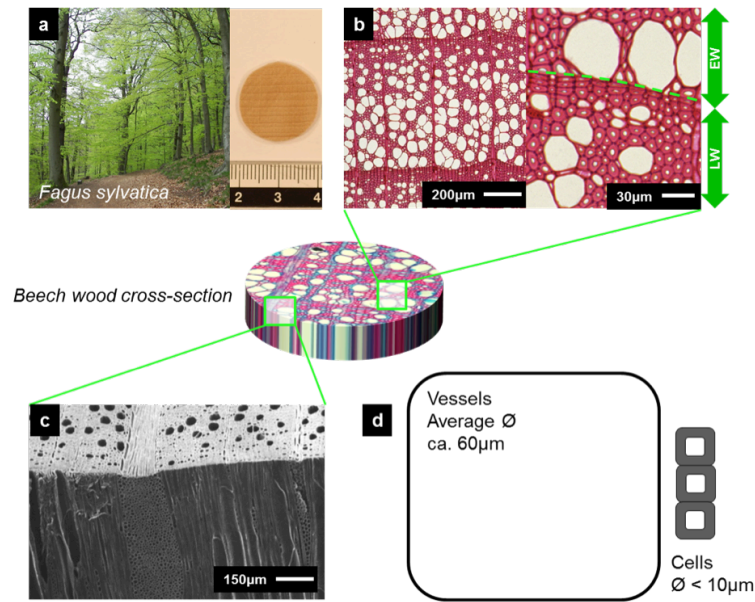


**Figure S2.7:** Morphology of the beech wood cross sections. a) Photographs showing a beech trees (*Fagus sylvatica*) and the wood cross section discs ( $\varnothing$  20 mm, 1 mm thickness). b) and (c) Optical microscopy and Scanning Electron Microscopy (SEM) images of the wood cross sections after surface smoothing with a microtome knife. b) Truncated vessels and cells from top view. c) Cells and vessels from side view, showing the fiber and vessel arrangement. d) Close up scheme of a typical vessel and cell diameter in beech wood.

**Movie S2.1:** *Underwater oil sliding angle measurement for hexadecane*

**Movie S2.2:** *ESEM image series of microtome wood saturation with water*

**Movie S2.3:** *ESEM image series of circular saw cut saturation with water*

**Movie S2.4:** *oil/water separation experiment with spruce wood*

**Movie S2.5:** *oil/water separation experiment with beech wood*

# Chapter 3

## Solvent-Controlled Spatial Distribution of SI-AGET-ATRP Grafted Polymers in Lignocellulosic Materials

In the current quest for the design of advanced complex materials, the functionalization of biological materials having hierarchical structures has been of high interest. In the case of lignocellulosic materials, various modification techniques have allowed to obtain materials with outstanding properties. However, the control over the spatial distribution of the modification inside the wood scaffold, which is an important parameter to obtain the desired properties, has yet to be understood. In this study, the use of solvents with different wood-swelling capabilities is proposed to control the spatial polymer-modification distribution inside the hierarchical wood structure. Wood cubes were functionalized via SI-AGET-ATRP using solvents with different wood-swelling capabilities. Spectroscopic (Raman and FTIR) and electron microscopy techniques showed that a good wood-swelling solvent as reaction media can transport the polymerization initiator molecule into the cell wall, allowing it to react with all the available -OH groups in the wood structure. Conversely, the use of a bad wood-swelling solvent limits the reaction to the available -OH groups at the lumen/cell wall interface. The subsequently added polymers grow from the available initiator sites and therefore show similar spatial distribution. This diffusion limitation is visible not only at the microscopic level (cellular structure) but also at the macroscopic level (over the length of the sample).

### 3.1. Introduction

Design principles inspired by nature are helping to manufacture new advanced materials with superior properties.<sup>184–186</sup> In particular, researchers have paid more and more attention to the complex hierarchical structures found in various biological materials. As shown by numerous recent publications, wood and wood-based materials have attracted a lot of interest in the materials science community.<sup>10,28,35,43,44,46,187–193</sup>

In most of these works, the wood structure is maintained and a chemical modification is needed to introduce new functionalities. Indeed, the properties of new wood-based materials can be greatly enhanced by the introduction of chemical compounds with specific functionalities. There exists a wide variety of chemistries to modify lignocellulosic materials. The chemicals incorporated into the wood structure can be covalently bonded to the available -OH groups in the wood cell wall polymers. A long list of chemical functionalities have been used to modify wood through covalent bonding with the -OH groups, which include but are not limited to, anhydrides, acyl chlorides, carboxylic acids, isocyanates, aldehydes, lactones, nitriles, epoxides, and DMDHEU (dimethylol dihydroxyethyleneurea).<sup>14,26–29</sup>

Wood may also be functionalized through the grafting of polymer chains.<sup>26,33,34,49,191</sup> Polymers are of special interest as they can provide wood with a higher variety of functional groups, when compared to modification by a single molecule. In addition to their chemical diversity, polymer properties depend on other parameters such as polymer chain length, polymer composition (copolymers), polymer architecture (linear, branched, star ...), which may also contribute to the final properties of the wood-polymer composite.

Besides considerations on the physicochemical properties of the modifying agents, a key parameter is their spatial distribution inside the wood structure. Wood is an anisotropic porous material with a hierarchical arrangement over several length scales. Therefore, regardless of the type of chemistry employed, the chemicals will reach different regions in the wood scaffold. At the microscale (cell and cell wall level), distribution of the modification may essentially target the lumen, the lumen/cell wall interface, or the cell wall.<sup>194</sup>

It is well known that the location of the modifying agent in the wood structure

has a crucial influence on the properties of the final material. As an example, the addition of hydrophobic components to wood will have different impacts on its dimensional stability according to their distribution. Native wood is subject to swelling and shrinkage due to the hygroscopic nature of the cell walls. If a hydrophobic polymer penetrates the cell wall and grafts on the cell wall hydroxyl groups, then the cell wall will be more hydrophobic, and the dimensional stability will highly increase. If the same hydrophobic polymer is now only filling up the lumen (initially a void space), then the transport of water inside wood is delayed, but it will eventually reach the unmodified cell wall. This will result in cell wall swelling and in a poor improvement of the dimensional stability.<sup>30</sup>

To be able to develop functional lignocellulosic materials with well-defined properties, we therefore need to control the spatial distribution of the modification. Until now, this proved to be highly challenging, because the wood structure is highly inhomogeneous, and the polymerization techniques used in wood were not selective enough. For this reason, we chose to modify wood with Surface-Initiated Atom Transfer Radical Polymerization (SI-ATRP). In general, polymer brushes can be prepared from *grafting to*, *grafting through*, or *grafting from* methods.<sup>27,56</sup>

For this study, a *grafting from* approach such as SI-ATRP was of particular interest. SI-ATRP has been conducted in a wide range of materials, from biological to synthetic, for various applications.<sup>42,48,49,195,196</sup> In this process, an initiator is first grafted onto the surface of a solid (or into the bulk of the material providing that the reagents can diffuse into it), yielding a macroinitiator. In the following step, polymer chains are grown from this covalently bonded initiator. Therefore, provided that the distribution of the initiator moiety can be controlled, we should be able to control the position of the grafted polymer, since the polymer chains only grow from the immobilized initiator.<sup>55</sup>

Although *grafting from* techniques have been applied to wood, the focus of these papers was not to show control over the polymer spatial distribution. Nevertheless, the work from Ermeidan et al. suggests that the solvent used for their Ring Opening Polymerization (ROP) approach in wood could influence the final polymer spatial distribution.<sup>26</sup> According to Mantanis et al.<sup>32</sup> the wood-swelling capability of a given solvent essentially depends on its molar volume, its basicity, and its hydrogen bonding capability.

Based on this former study and the work of Mantanis et al. who studied the swelling of wood with various organic solvents,<sup>32</sup> we investigated the effect of two different solvents on the final distribution of polymers in spruce wood samples. The modifications have been carried out using surface initiated activator generated by electron transfer atomic transfer radical polymerization (SI-AGET-ATRP) technique, a modified SI-ATRP technique. We used spectroscopy techniques (FTIR and Raman) as well as electron microscopy (SEM) to provide a detailed analysis of the distributions of both the initiator and the polymer into the cell wall structure (microscale), and through the entire wood sample (macroscale). We found out that by using solvents with different wood-swelling capabilities (pyridine and dichloromethane), we can control the distribution of the initiator in the wood scaffold (at both micro- and macro-scales), and consequently, we can control the position of the grafted polymer.

### 3.2. Results and Discussion

Figure 3.1 illustrates the morphology of spruce wood. The year rings shown in Figure 3.1 A are formed by a longitudinal arrangement of tracheids with different cell structures. The low-density regions are called earlywood (EW), with an average lumen size of  $36 \pm 7 \mu\text{m}$  and a cell wall thickness of  $4 \pm 0.75 \mu\text{m}$ ; and the high-density regions are called latewood (LW), with an average lumen size of  $8.5 \pm 5.54 \mu\text{m}$  and a cell wall thickness of  $5 \pm 2.5 \mu\text{m}$ .<sup>197</sup>

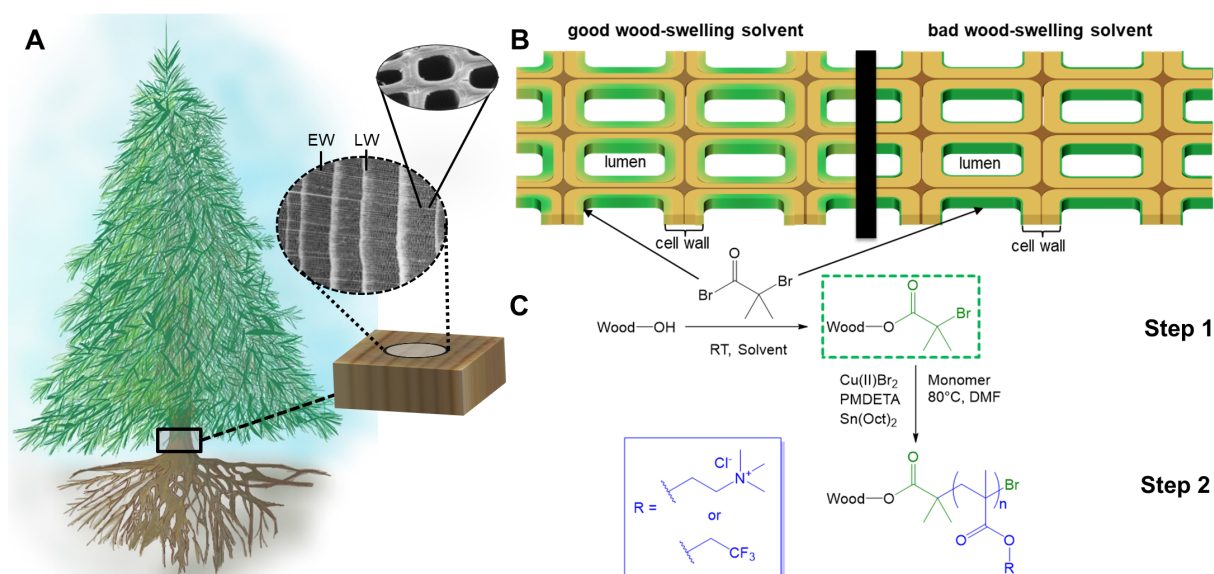


**Figure 3.1:** Scheme showing (A) the structure of spruce wood from macro- to micro-scale, (B) targeted initiator distribution into the wood structure and (C) SI-AGET-ATRP reaction process.

In most chemical wood modifications, a solvent is used to transport the reagents to the reaction sites (-OH groups). The transport of fluids in wood may occur through different pathways: from one cell to another via natural features (pits for instance), from lumen to cell wall via diffusion, and in the longitudinal direction through the middle lamellae and through cut open cell walls.<sup>198</sup> Although the importance of one or the other pathway is still debated, the nature of the solvent is widely accepted as a critical parameter determining the kinetics and the extent of wood impregnation and wood cell wall swelling.<sup>32</sup> Therefore, a possible way of controlling the distribution of chemicals in the wood structure is to use solvents with different swelling capabilities for the wood cell wall. According to the solvent system chosen, we targeted the distributions shown in Figure 3.1B: cell wall modification or decoration of the wood lumen/cell wall interface.

In this work, we modified wood cubes with a *grafting from* polymerization technique. SI-AGET-ATRP is a two-step reaction (see Figure 3.1C). In the first step,  $\alpha$ -Bromoisobutyryl bromide (BiBB) is covalently attached to the hydroxyl groups available in the wood cell walls, to obtain the wood macroinitiator (W-Br). In the second step, the desired polymer is grown from alkyl bromide moieties present in the macroinitiator. Since the polymer chains are directly initiated at the alkyl bromide sites, the control over the distribution of the attached BiBB moieties in wood should ensure control over the final position of the polymer brushes.

The interactions between wood and various organic solvents has already been investigated.<sup>32</sup> Based on the data provided by Mantanis et al., we selected a good and a bad wood-swelling solvent, respectively pyridine and dichloromethane, as reaction media for the esterification of wood hydroxyl groups with BiBB. By using two solvents with different wood-swelling properties, we expect to achieve two different distributions (shown in Figure 3.1B). In the case of pyridine, we expect to find BiBB deep inside the wood cell walls, while it should only decorate the lumen/cell wall interface in the case of dichloromethane. The swelling capability of DCM and Py were evaluated: spruce wood cubes were immersed in the two solvents, and the dimensional changes were measured. After equilibrium was reached, the cubes were swollen by 18.3% in Py, and 6.7% in DCM (see results Figure S3.1, in Supporting Information), thereby confirming the high swelling power of Py when compared to DCM.

### 3.2.1. Synthesis of W-Br macroinitiators: influence of reaction time, concentration, sample morphology, and solvent on the WPGs

As discussed previously, the covalent attachment of the alkyl halide compounds to the wood scaffold is a critical step for the control of the final polymer distribution. In a preliminary study, we investigated the influence of the reaction time, the BiBB concentration in solution, and the sample morphology on the final BiBB weight percent gain. As shown in Figure 3.2, and as reported already by Cabane et al.,<sup>33</sup> we observe a clear increase in WPG together with the increase of the reaction time and of the reactant's concentration.

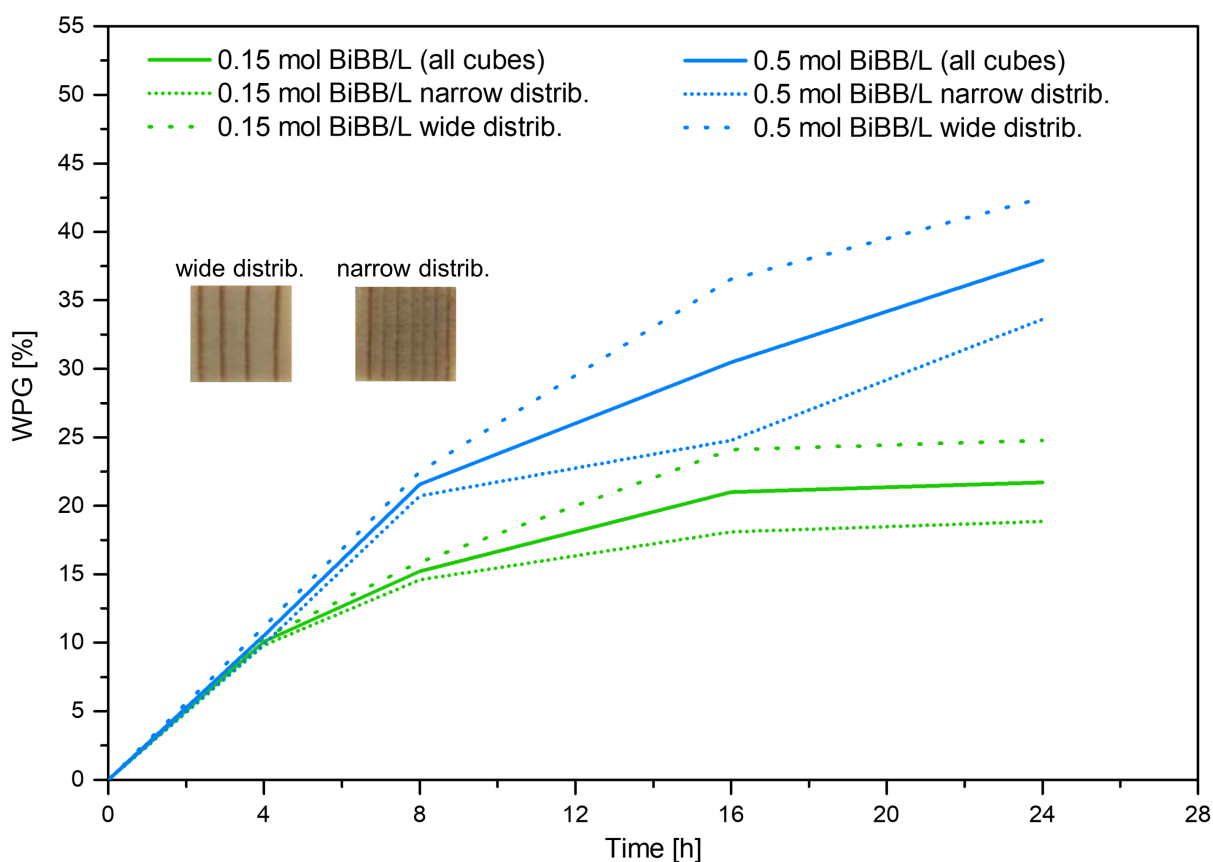


**Figure 3.2:** Evolution of WPG (%) with respect to reaction time, using different BiBB concentrations, and EW/LW distributions. For each reaction set, three samples of each year ring distributions were used. Pyridine was used as reaction media for all data sets.

More interestingly, Figure 3.2 shows that the macroscale morphology of the wood cubes has an effect on the final weight percent gains. The experiments were carried out using cubes with two types of wood year ring distributions. In one case the cubes have a higher fraction of EW (wide year ring distribution), and in the second set of samples, more year rings are present, meaning that the fraction of LW is higher (narrow year ring distribution). According to our experiments, we obtained higher WPGs with cubes containing a higher fraction



of EW. As mentioned previously, the diffusion of the pyridine solution into the cell wall is critical to ensure transport of BiBB compounds inside the cell wall, where they can react with wood hydroxyl groups. If the cell wall is thin (EW), the solution is likely to penetrate and fully swell the cell wall, providing good -OH accessibility and high WPGs. Conversely, the diffusion into thick cell walls (LW) is limited, thus a lower amount of -OH groups can be accessed, and the overall WPGs are lower. Considering these preliminary results, all reactions were performed with cubes having similar EW and LW proportions.

Finally, we investigated the effect of the solvent on the final WPG. A series of cubes were modified with two different solvents, pyridine and dichloromethane, for 20 and 24h respectively with all other conditions kept constant (room temperature, [BiBB] = 0.5 mol/L). We obtained 15% WPG for the DCM-modified cubes, and 25% WPG for the pyridine-modified cubes. We could therefore confirm that the BiBB WPG also depends on the solvent used. This was already observed by Cabane et al.,<sup>33</sup> and can be explained by the swelling ability of the different solvents used: a good solvent (such as pyridine) provides a better access to the wood cell wall -OH groups and subsequently a higher WPG, compared to a bad solvent system (such as DCM).

### **3.2.2. Characterization of the BiBB distribution in wood**

The distribution of the alkyl bromide in the wood structure was characterized at the “microscale” (i.e. cell wall level) using SEM and Raman microscopy, and at the “macroscale” (i.e. cube level) using FTIR spectroscopy.

The microscale characterization is reported in Figure 3.3. Brighter areas in the SEM images correspond to the presence of elements with higher atomic weight (Br in this case), contrasting with the darker areas where elements with lower atomic weight are present (C and O – major constituents of the wood biopolymers).

The Raman images are composed by the overlap of two images obtained from the same mapping. To obtain the first image, the aromatic skeletal vibration assigned to lignin (present in the cell wall but mainly in the compound middle lamellae (CML)) was integrated (1500 to 1700 cm) and is shown in red. The second image obtained from the integration of the C-Br vibration peak (270-330 cm<sup>-1</sup>) and shown in green, represents the distribution of the BiBB modification in the wood cell wall (the black area corresponds to the empty

lumen).

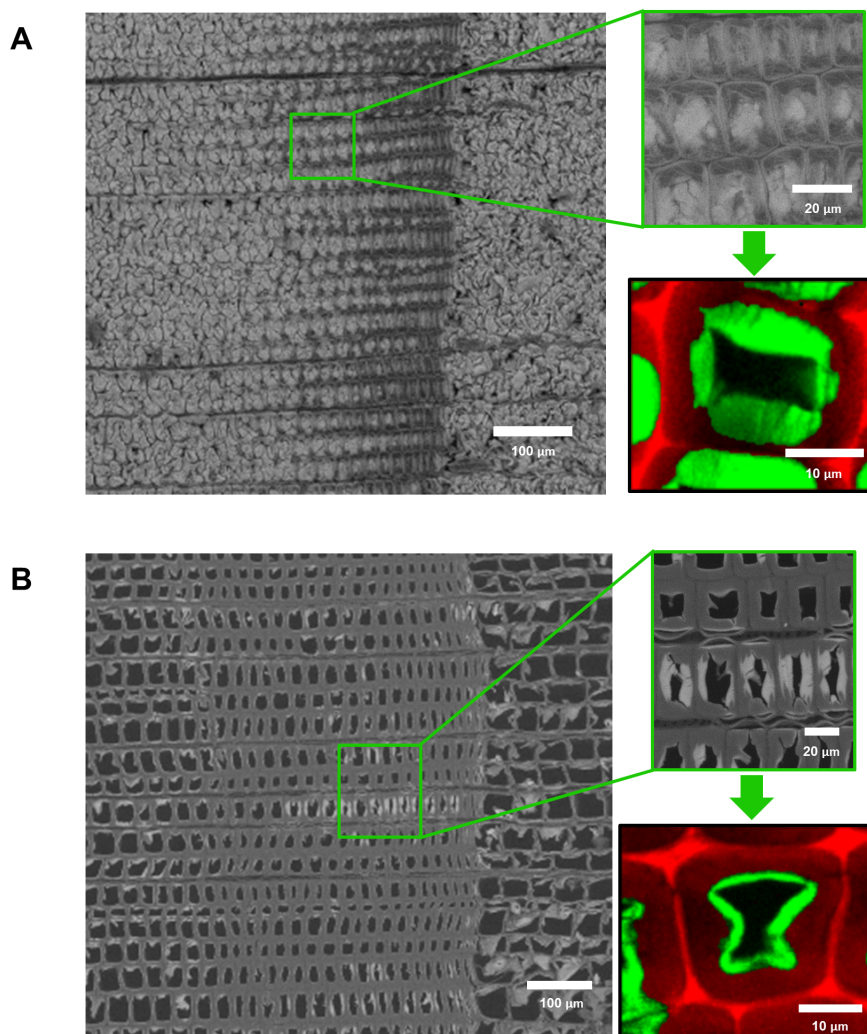


**Figure 3.3:** Raman and SEM (BSE detector) images of the BiBB distribution in the wood cell wall after modification reactions in Py (A) and DCM (B). Green areas representing W-Br vibrations and red areas representing lignin vibrations.

The SEM (BSE) images in Figure 3.3A and 3.3B indicate that the brominated compound is distributed more homogeneously in the W-Br samples modified in pyridine. In the Raman image in Figure 3.3A, a large BiBB area can be observed (in green), suggesting that the modification took place deep inside the cell wall, when reacted with pyridine. In comparison, the very clear “green rim” shown in Figure 3.3B suggests that in the case of W-Br(DCM), the reaction was limited to the lumen/cell wall interface when reacted with dichloromethane. Both SEM and Raman images confirm that we can control the distribution of BiBB in the wood scaffold at the cell wall level with a proper choice of solvent.

The SEM images also reveal that the treatment with BiBB in both solvents alters the cell wall structures, in particular in the EW regions, where the cell walls are

thin. One can easily observe that the overall cells arrangement is maintained (EW and LW regions are clearly identified), but the first layers of the cell walls can be severely damaged, with torn and swollen cell wall fragments filling up the lumen space. SEM images given in Figure S3.2 show that the solvents alone are not responsible for these cell wall alterations. Previous studies have shown that isolated cellulose fibers or crystals can dissolve in organic solvents when they are highly substituted (through acetylation for instance), which could explain the observed cell wall alterations.<sup>199</sup> However, the wood cell wall is a composite material where cellulose is not available in an isolated form: in our samples, cellulose fibers are embedded in the lignin-hemicelluloses matrix. Moreover, the calculated substitution degree for cellulose in our case is below the 0.5 critical value reported in literature (see calculations in Table S3.2). Therefore, we believe that the permanent cell wall alterations observed after the BiBB reaction are rather an indication that the alkyl bromide groups occupy space in the cell wall. In the most severe cases (highest BiBB WPGs obtained with Py), the extent of swelling is such that the wood cell wall structure might be disrupted. This phenomenon was already reported for other reactions in wood.<sup>200,201</sup> This also explains why the cell wall swelling and damage are considerably lower for the W-Br(DCM) samples, where less BiBB groups enter the cell walls.

Following the microscale investigation, we characterized the BiBB distribution at the macroscale, i.e. throughout the cubes. Penetration of liquids in wood at the macroscale is not trivial. Although the porous wood structure is designed to transport fluids over several meters, many natural openings irreversibly close upon wood felling and drying, thereby limiting transport of fluids in bulk wood materials. In our case, the geometry of the cubes is such that some tracheids will have an open end at the cube surface, but others will be entirely closed inside the bulk of the cube. Such fibers may not be fully impregnated by the BiBB solutions (regardless whether pyridine or dichloromethane is used).

To evaluate the presence of BiBB in wood at various depth, we successively removed thin cross-section slices off the cube from surface to center (i.e. from 0 to 2.5 mm), acquiring a FTIR spectrum on the fresh surface every 100  $\mu\text{m}$  (see Figure 3.4A). For the sake of clarity, only a few spectra are shown in Figure 3.4B, but the ratios calculated for all depths are given in Figure 3.4C. We asserted the presence of the BiBB modification through the C=O stretching signal at  $1737\text{ cm}^{-1}$ . This carbonyl stretching is also present in native wood, but there is a pronounced increase in absorption intensity due to the presence of BiBB after

the esterification.

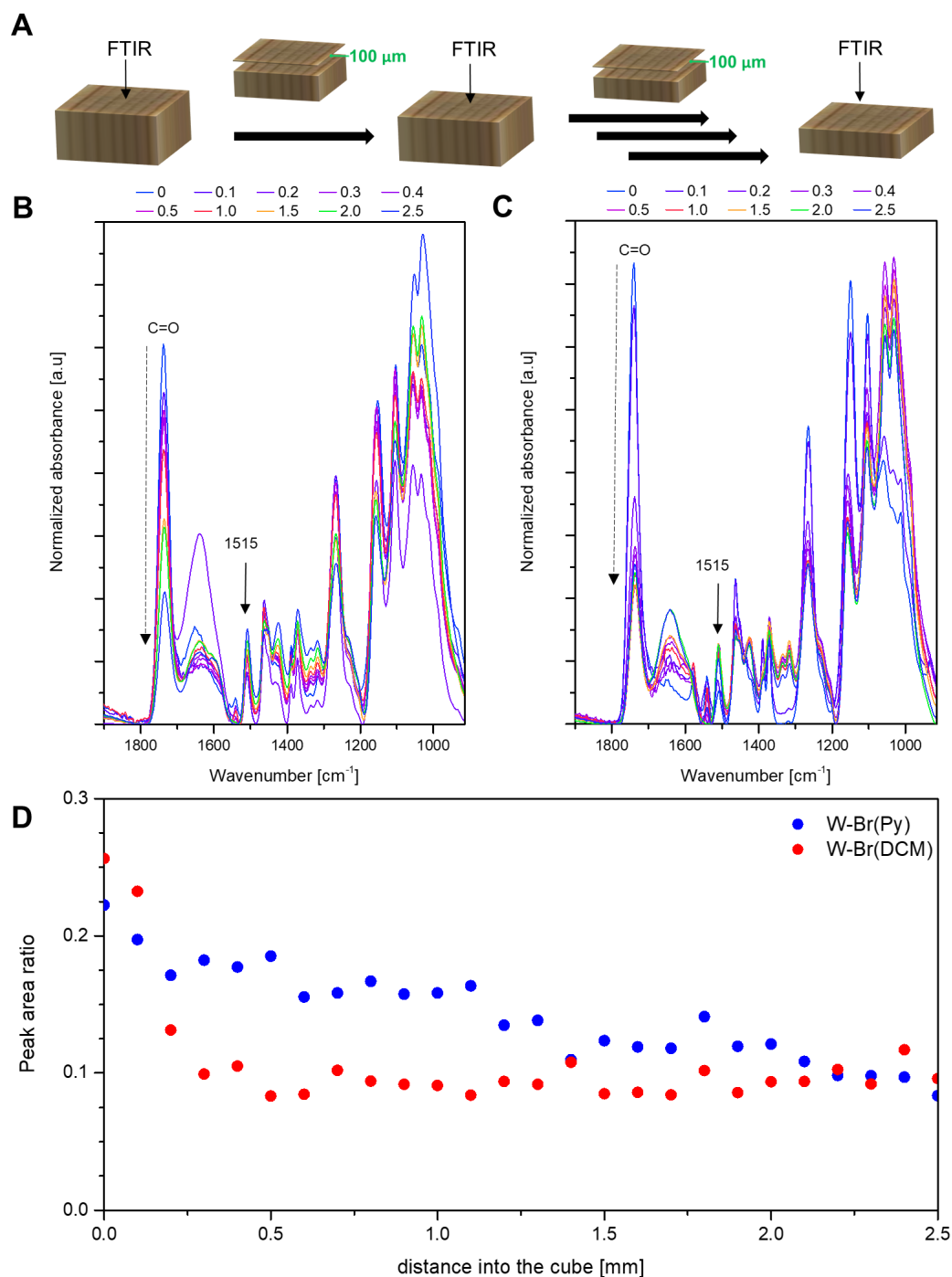


**Figure 3.4:** (A) successive removal of 100 μm thick wood slices for the FTIR study. (B) FTIR spectra of the W-Br(Py) macroinitiator at various distances from the cube surface. (C) FTIR spectra of the W-Br(DCM) macroinitiator at various distances from the cube surface. The spectra were peak area normalized through the entire spectra using MATLAB. (D) Presence of BiBB through the wood cubes shown by the ratio of the carbonyl peak area against the aromatic skeletal peak area assigned to lignin, as a function of depth.

As shown in Figure 3.4B and C, there is a clear decrease in the carbonyl peak intensity from the surface spectrum to the spectrum taken in the center of the cube, for both macroinitiators. This suggests that the modification is

not homogeneously distributed throughout the cube, regardless of the solvent used. To facilitate the interpretation of the FTIR spectra, and because FTIR is only a semi-quantitative method, we calculated the peak area ratio between the variable carbonyl peak at  $1737\text{ cm}^{-1}$  and the skeletal lignin peak ( $1515\text{ cm}^{-1}$ ) which is not affected by the esterification (see plot in Figure 3.4D).<sup>202</sup>

For the W-Br(DCM), we see a sharp decrease in the intensity ratio immediately after the surface. This is likely due to the poor swelling capabilities of DCM, which limits the penetration of BiBB molecules inside wood, not only at the cell wall level as demonstrated earlier, but also at the macroscale. Since DCM is a bad wood-swelling solvent, it is very unlikely that the solution of BiBB can soak through several cell walls and react with the -OH groups available in the closed tracheids at the center of the cube.

Contrarily, for the samples modified with the good wood-swelling solvent, pyridine, we see that the ratio decreases regularly from the surface to the center of the cube. This indicates that the modification took place throughout the cube length, with a clear gradient in intensity. This can be explained by the ability of pyridine to swell wood cell walls, and to penetrate deep inside the wood structure. In the center of the cube (2.5 mm), the ratios for both W-Br(DCM) and W-Br(Py) are similar to ratios observed for native wood, suggesting that there is little modification taking place at this depth.

### 3.2.3. Synthesis and characterization of wood-polymer materials

Following the solvent-controlled distribution of BiBB in the wood structure, we studied the *grafting from* polymerization of two monomers using the W-Br(DCM) and W-Br(Py) macroinitiators: [2-(Methacryloyloxy)ethyl]trimethyl ammonium chloride solution (METAC) and 2,2,2-Trifluoroethyl methacrylate (TFEMA). METAC and TFEMA were polymerized using the same solvent, dimethylformamide (DMF). DMF is an excellent wood-swelling solvent, used to ensure that the monomers were effectively transported inside the wood samples and reached the available alkyl bromide initiating sites. Raman microscopy and SEM with EDX and WDX analysis were performed on the samples to study the distribution of these two polymers.

To analyze the distribution of the polymers at the cell wall level in the different samples, vertex component analysis (VCA) was performed in the spectral range from  $200$  to  $1800\text{ cm}^{-1}$  on the respective Raman spectroscopy mappings. The analysis was performed with five endmembers for the TFEMA-modified

samples and six for the METAC-modified samples. The cell wall component (CW – with contribution from lignin and cellulose), the compound middle lamellae component (CML – mainly lignin), and the modification components (W-Br-PTFEMA or W-Br-PMETAC – encompassing the spectral signatures from wood, BiBB and the corresponding polymers) are shown in Figure 3.5 and Figure 3.6. The corresponding endmember spectra are given in the corresponding figures.

In these two figures, the compound middle lamellae (CML), mainly consisting of lignin, can be clearly seen in the VCA for all the data sets. The presence of lignin is shown by the aromatic skeletal vibrations at  $1607\text{ cm}^{-1}$ , the main lignin marker band.<sup>72</sup> The cell wall component (CW) can be detected by the C-C-C ring deformation at  $380\text{ cm}^{-1}$ , or by the C-O-C glycosidic asymmetric and symmetric vibrations between  $1070$  and  $1140\text{ cm}^{-1}$ , all attributed to cellulose.<sup>72,75</sup>

In the case of the W-Br(Py)-TFEMA samples, it is not possible to differentiate two different endmembers within the cell wall because of the overlapping of characteristic cell wall vibrations with TFEMA polymer vibrations between  $1000$  and  $1140\text{ cm}^{-1}$  over the entire cell wall area. Since the VCA could not be used to identify the CW endmember for this sample, we instead produced an image of the cell wall by integrating one of the cellulose characteristic bands between  $1070$  and  $1140\text{ cm}^{-1}$  (see Figure 3.5, image labelled with \*). Although this band also contains fluorine bands, it serves as a guidance to the position of the cell wall in the mapping.<sup>72,75,203</sup>

To characterize PTFEMA, we used signals from the methacrylate such as the carbonyl band (C=O) at  $1740\text{ cm}^{-1}$  and the C-CH<sub>3</sub> asymmetric bending band at  $1453\text{ cm}^{-1}$ . More characteristic of the PTFEMA are several C-F vibrations bands, between  $1400$  and  $1000\text{ cm}^{-1}$  and at  $660\text{ cm}^{-1}$ , and (sat)-C-F<sub>3</sub> vibrations bands at both  $845$  and  $300\text{ cm}^{-1}$ .<sup>203,204</sup>

For the PMETAC, the characteristic methacrylate bands of the carbonyl vibration and the C-CH<sub>3</sub> asymmetric bending could be used again. More characteristic vibrations of PMETAC are the N<sup>+</sup>(CH<sub>3</sub>)<sub>3</sub> asymmetric bending at  $955\text{ cm}^{-1}$  and the C-N symmetric stretch at  $720\text{ cm}^{-1}$ . Vibrations from tertiary bromoalkanes from the initiator are detected at  $530\text{ cm}^{-1}$ .<sup>204,205</sup>

In Figure 3.5 and Figure 3.6, respectively, it is possible to observe polymer growth deep into the cell wall structure for both polymer reactions performed on

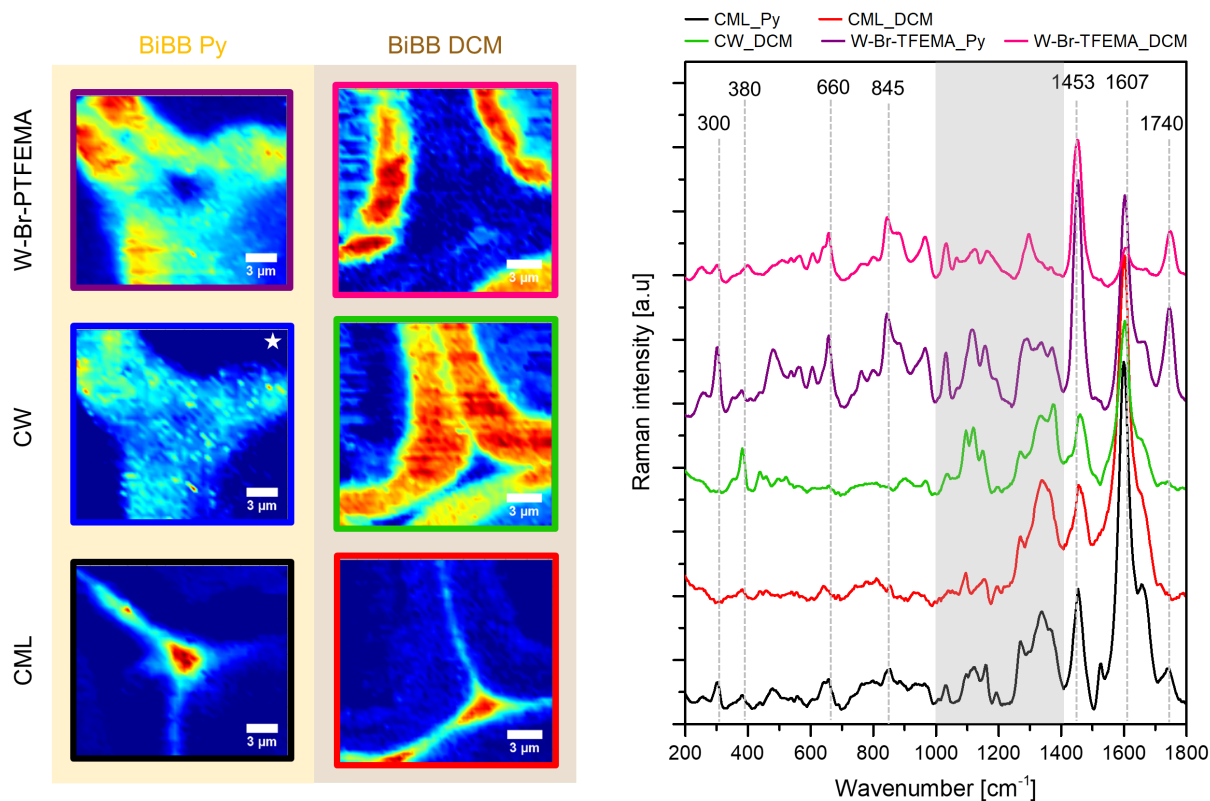


**Figure 3.5:** Raman analysis of the samples modified by PTFEMA with both W-Br(Py) and W-Br(DCM) macroinitiator sets. VCA was performed on the Raman mappings for each modification from 200 to 1800  $\text{cm}^{-1}$ . The spectra represent the different endmembers obtained from the VCA. All images result from the VCA analysis except for the image labeled with \*, resulting from the cellulose integration (1070-1140  $\text{cm}^{-1}$ ) on the W Br(Py) PTFEMA sample.

W-Br(Py) macroinitiators (W-Br(Py)-PTFEMA and W-Br(Py)-PMETAC). In the case of the set of samples obtained from the W-Br(DCM) macroinitiators, both polymer modifications (W-Br(DCM)-PTFEMA and W-Br(DCM)-PMETAC) show a similar distribution: as opposed to the W-Br(Py) Polymer samples, the modification is only observed at the lumen/cell wall interface. The results obtained by Raman spectroscopy were confirmed through SEM with EDX and WDX detectors, for PTFEMA and PMETAC respectively (see Figure S3.3 and Figure S3.4, Supporting Information). The EDX results show the intensities of the Fluorine element (present in PTFEMA) throughout the cell walls for the W-Br(Py)-PTFEMA samples and at the lumen/cell wall interface for the W-Br(DCM)-PTFEMA samples.

Detecting the presence of nitrogen through x-ray energies in electron microscopy is a challenge, especially when the main scaffold mainly consists in carbon and oxygen rich polymers, due to overlapping of the nitrogen peak with the two other elements. In our samples, the nitrogen signal could not be properly detected with neither EDX nor WDX. However, in the METAC monomer, the quaternary nitrogen has a chlorine counter-ion, which emits at higher x-ray

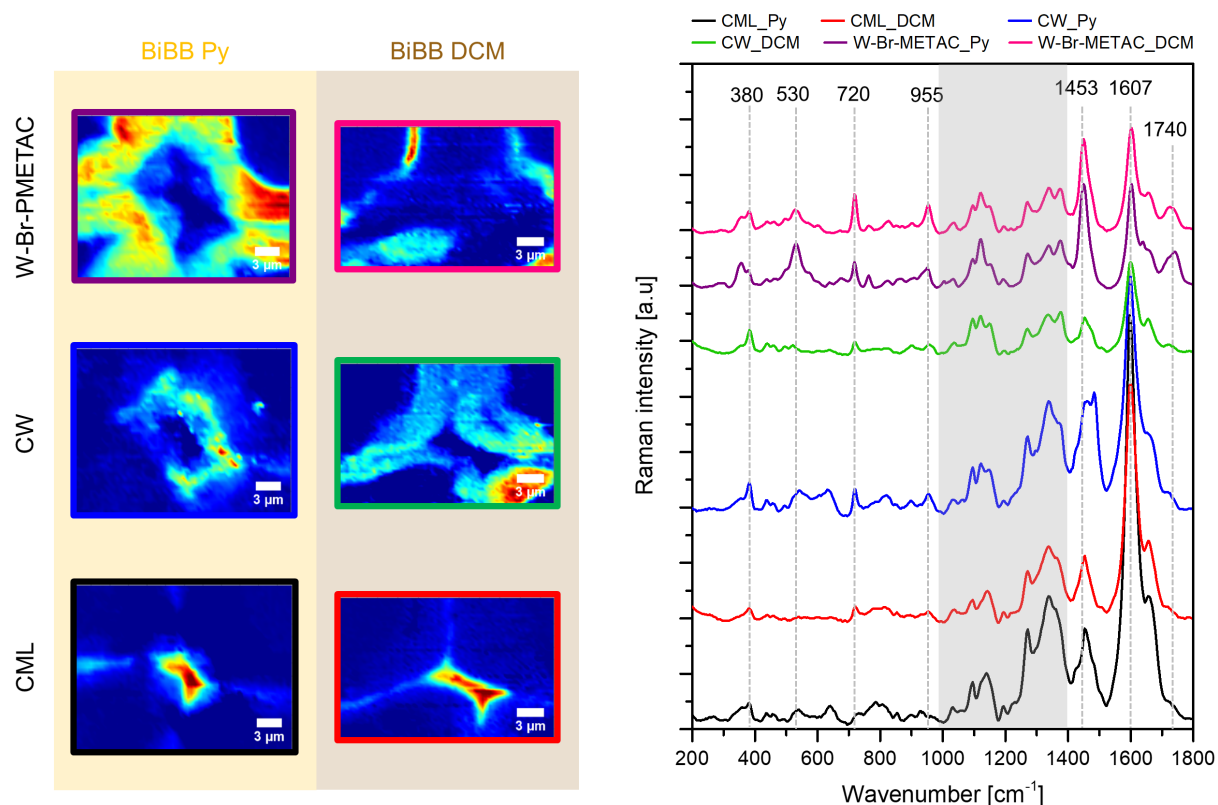


**Figure 3.6:** Raman analysis of the samples modified by PMETAC with both W-Br(Py) and W-Br(DCM) macroinitiator sets. VCA was performed on the Raman mappings for each modification from 200 to 1800  $\text{cm}^{-1}$ . The spectra represent the different endmembers obtained from the VCA

energies. Using Cl, we could properly detect the presence of the PMETAC polymer. The images of the W-Br(Py)-PMETAC show the presence of chlorine inside the cell wall. In the W-Br(DCM)-PMETAC samples, chlorine may only be seen at the lumen/cell wall interface. Although this is an indirect method to detect the covalently grafted PMETAC chains, the results clearly confirm the Raman observations.

With these studies, we observed clear overlapping distributions in between the initiator and the polymers. We could therefore confirm that the polymers were grafted from the BiBB moieties anchored in the cell wall structure, regardless of the wettability properties of the monomer. These results show that it is possible to control the polymer distribution in the wood structure at the microscale. According to the initiator WPGs and assuming that the macroscale polymer distribution at matches with the macroscale distribution of the initiator, we expected higher polymer WPGs for the samples derived from the pyridine macroinitiators. Strikingly, the results given in Table 3.1 show that there is no significant difference in the polymer WPGs.



Table 3.1: Initiator and polymer weight percent gains in the wood samples.

Sample ID	WPG BiBB [%]	WPG polymer [%]
W-Br(DCM)-PTFEMA	15.5	42.9
W-Br(Py)-PTFEMA	25.0	43.4
W-Br(DCM)-PMETAC	15.5	16.4
W-Br(Py)-PMETAC	25.0	18.4

To understand this result, we characterized the distribution of polymers at the macroscale using the FTIR method described previously for the BiBB-modified samples. To compile the graphs shown in Figure 3.7, we calculated the peak area ratio between the polymer signature peaks and the aromatic skeletal peak ( $1515\text{ cm}^{-1}$ ), attributed to lignin. For the fluorinated polymer, the C-F signal at  $1280\text{ cm}^{-1}$  was used, and for the PMETAC, the quaternary amine peak was used ( $955\text{ cm}^{-1}$ ). The corresponding FTIR spectra can be found in Figure S3.5.

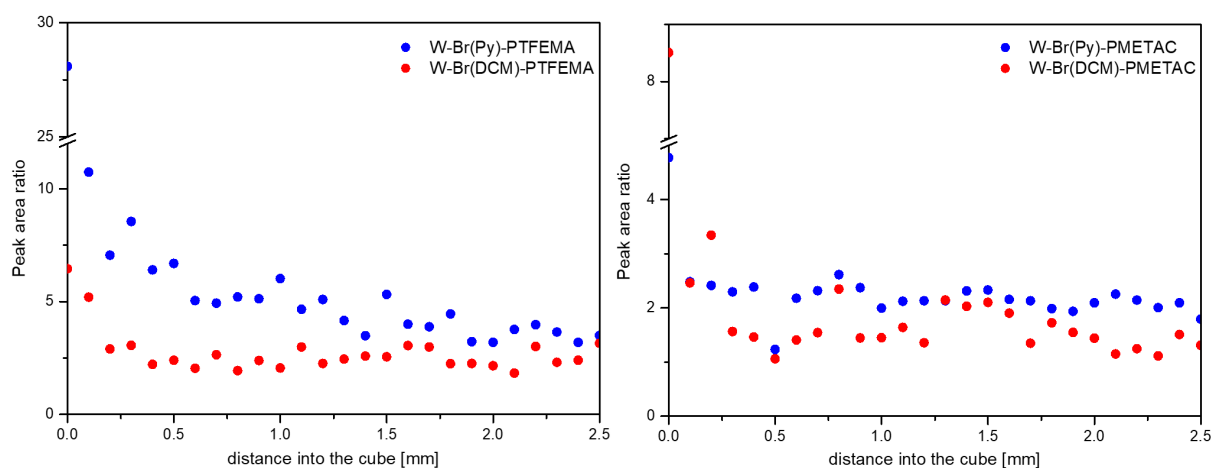


Figure 3.7: Macroscale distribution of the polymer modifications (TFEMA and METAC) using both W Br(Py) and W Br(DCM) macroinitiators. The plots show the peak area ratio between the polymer signature peaks and the aromatic skeletal peak attributed to lignin as a function of depth.

According to Figure 3.7, the profiles obtained for W-Br(DCM)-PTFEMA and W-Br(DCM)-PMETAC are similar to the W-Br(DCM) profile shown in Figure 3.4D. Most of the polymer is present directly at the surface, then the signal drops until  $300\text{ }\mu\text{m}$ , where it reaches a plateau, indicating only trace amounts of polymer in the cube center. This correlates well with the BiBB distribution obtained from the experiment in dichloromethane.

In the case of the wood-polymer samples generated from W-Br(Py) (i.e. W-Br(Py)-PTFEMA and W-Br(Py)-PMETAC), the FTIR ratio profiles do not exactly match with the W-Br(Py) profiles. Instead of the expected regular decrease

seen in Figure 3.4D, the polymer content sharply decreases after the first cuts (500 and 200  $\mu\text{m}$  below the surface for PTFEMA and PMETAC modification, respectively). Deeper into the cube, although a slight gradient is visible, low amounts of polymer modification are detected.

Therefore, regardless of the solvent used in the first modification step, the plots in Figure 3.7 indicate that most of the polymerization takes place at the surface of the wood cubes and in the first few hundred microns. In the end, both the W-Br(Py) and W-Br(DCM) macroinitiators generate wood-polymer materials with similar polymer distributions at the macroscale, and this explains the comparable percent gains obtained. The limited polymerization inside the wood cube likely results from a diffusion issue. The polymerization immediately starts at the wood cube surface, and the growing polymer chains will “densify” the wood surface, slowing down the penetration of the solution inside the wood bulk, and affecting the kinetics of the polymerization.

In principle, we can also estimate the chain length of the tethered polymer chains in wood. Assuming that all grafted alkyl bromide groups initiate the growth of a polymer chain, we calculated degrees of polymerization that are smaller than the targeted ones (see Table S3.3).

However, according to the results shown in this study, it is clear that only a fraction of the BiBB moieties actually generate polymer chains (most of the polymerization takes place close to the surface, i.e. most BiBB molecules present deep inside the wood do not react). Therefore, if we consider that no significant polymer content is found after the first 500  $\mu\text{m}$  (on both sides, which is consistent with the results shown in Figure 3.7), then we can infer that only about 20% of the cube really contains grafted polymer. If we apply this 20% correction to the fraction of BiBB reacting, we can estimate more realistic DPs, i.e. closer to the targeted DPs (see Table S3.3). This table also shows that the polymerization of METAC was less controlled. Although it would need more investigations, we believe that the electrostatic interactions generated by the positively charged METAC units and growing METAC chains, as well as the positively charged ATRP catalyst could explain this observation.

### 3.3. Conclusions

We demonstrated the possibility to control the spatial distribution of the polymer chains grafted via SI-AGET-ATRP inside wood materials, through the use of solvents with different wood-swelling capabilities. With Raman spectroscopy and SEM (BSE, EDX, WDX) we could show that a good swelling solvent (e.g. pyridine) enables the introduction of molecules such as the ATRP initiator (BiBB) deep inside the cell wall structure. Conversely, a bad swelling solvent (e.g. dichloromethane) limits the diffusion of the molecule from the lumen into the cell wall structure, resulting in modification at the lumen/cell wall interface. The control over the initiator distribution allows for the control of the polymerization of two different monomers.

In addition, we showed that the use of different solvents also allows controlling the modification distribution at the macroscale. This is particularly notable for the initiator distribution. The distribution of the polymer is somewhat less controlled, as the difference between the two W-Br-Polymer sets is less noticeable. This is due to a diffusion issue, related to the growth of the polymer chains at the surface of the wood samples. However, this issue could probably be addressed by carefully studying the kinetics of impregnation inside the wood samples.

To conclude, this study allows for a better understanding of the parameters involved in polymer modifications on wood, focusing on SI-AGET-ATRP. In many applications envisioned for functional lignocellulosic materials, the distribution of the modification is a key issue influencing the performance of the material. This study yielded important results and information for further investigations on the modification of wood, and will be of great use to design and optimize polymerization processes where a control over the distribution is needed. This will facilitate the production of wood-based materials with new functionalities for specific applications.

### 3.4. Experimental section

**Materials.** Norway spruce (*Picea abies*) was cut into cubes of  $10 \times 10 \times 5 \text{ mm}^3$ , Radial  $\times$  Tangential  $\times$  Longitudinal dimensions. Throughout the experiments, the samples used had similar earlywood/latewood distributions. Before the first functionalization step, the samples were Soxhlet extracted and dried in an oven under vacuum at  $65 \text{ }^\circ\text{C}$  until a constant mass was reached.

Monomers [2-(Methacryloyloxy)ethyl]trimethylammonium chloride solution (METAC) and 2,2,2-Trifluoroethyl methacrylate (TFEMA), initiator  $\alpha$ -bromoisobutyryl bromide (BiBB), reducing agent Tin(II) 2-ethylhexanoate ( $\text{Sn}(\text{Oct})_2$ ), copper complex  $\text{Cu}(\text{II})\text{Br}_2$ , ligand N,N,N',N'',N'''-Pentamethyldiethylenetriamine (PMDETA), as well as solvents N,N-dimethylformamide (DMF, anhydrous grade) and dichloromethane (DCM, anhydrous grade) were purchased from Sigma-Aldrich and used as received. Pyridine (Py, anhydrous grade) was purchased from VWR and used as received.

**Synthesis of wood macroinitiator.** Oven dried wood samples were placed under vacuum ( $10^{-2}$  mbar) in a Schlenk flask capped with a septum. A BiBB solution (in either anhydrous Py or anhydrous DCM) was added with a syringe. When we used DCM as solvent, a small amount of pyridine was added (1:1 molar equivalent with BiBB), in order to remove the hydrogen bromide byproduct. The amounts of BiBB engaged in reactions were calculated according to the formulas given in SI information. The reaction was stirred at room temperature for a given amount of time. The reacted wood cubes were withdrawn and washed with methanol and sonicated in methanol and acetone to remove any unreacted material. After the washing, the cubes (W-Br) were dried in an oven under vacuum at  $65 \text{ }^\circ\text{C}$  until constant mass was reached. The samples produced in this step are named W-Br(Py) and W-Br(DCM), according to the reaction solvent used.

**AGET SI-ATRP of TFEMA and METAC using W-Br as macroinitiator.** Both TFEMA and METAC were polymerized in DMF with the W-Br macroinitiators, using the following concentration ratio: [Monomer]:[W-Br]:[ $\text{Cu}(\text{II})\text{Br}_2$ ]:[PMDETA]:[ $\text{Sn}(\text{Oct})_2$ ]=10:1:1:2:2. W-Br samples were placed in a Schlenk flask, capped with a septum, together with the  $\text{Cu}(\text{II})\text{Br}_2$ . The flask was evacuated until it reached low vacuum (ca.  $10^{-2}$  mbar). DMF was added and the flask was placed in an oil bath at  $80 \text{ }^\circ\text{C}$ . In a separate flask cooled with ice, ligand and monomer were dissolved in DMF. The content of the flask was sparged with nitrogen for an hour, and then added to the heated Schlenk flask containing the wood samples. The reducing agent ( $\text{Sn}(\text{Oct})_2$ ) was added slowly during the first 40h of polymerization using a syringe pump, and the total reaction time was 48h. The reacted wood cubes were withdrawn and washed with ethanol and sonicated in ethanol and acetone, and water for PMETAC samples, to remove any unreacted material, as well as non-grafted polymer chains. After the washing, the cubes were dried in an oven under vacuum at  $65 \text{ }^\circ\text{C}$  until constant mass was reached. The W-Br(Py) and W-Br(DCM) samples reacted with TFEMA in this step are named W-Br(Py)-PTFEMA and W-Br(DCM)-PTFEMA, respectively. The W-Br(Py) and W-Br(DCM) samples reacted with METAC in this step are named W-Br(Py)-PMETAC and W-Br(DCM)-PMETAC, respectively.

**Weight Percent Gain (WPG, %) calculation.** The WPG represents the amount of modification

introduced into the cube at each modification step. . To estimate the WPG, the weight of the dried wood cubes was measured before ( $W_{BM}$ ) and after the modification ( $W_{AM}$ ), and the WPG is calculated as follows:

$$WPG(\%) = \frac{W_{AM} - W_{BM}}{W_{BM}} \times 100 \quad (3.1)$$

**Raman microscopy.** Wood samples were polished using a rotary microtome, removing the first 200  $\mu\text{m}$  of material. The measurements of the W-Br macroinitiators were performed with a confocal Raman microscope (Renishaw inVia, Wotton-under-Edge, England) using a 532 nm laser, an oil immersion objective (Nikon, 100x, NA = 1.3, 0.17 mm coverslip corrected) and an 1800 l/mm grating. As mapping parameters, an integration time of 1.5s with circa 5 mW, and a step width of 300 nm were used. The measurements of the TFEMA and METAC polymerized samples were performed with the same Raman microscope using a 633 nm laser, a water immersion objective (Olympus, 60x, NA = 1) and a 600 l/mm grating. As mapping parameters, an integration time between 5 and 10s with circa 25 mW laser power, and a step width of 400 nm were used.

**FTIR spectroscopy.** Fourier transform infrared spectroscopy (FTIR) measurements were conducted on a Tensor 27 (Bruker instruments) equipped with an ATR module. One spectrum was measured every 100  $\mu\text{m}$  below the wood cube surface until the cube center. This was done by slicing off 100  $\mu\text{m}$  cross-sections then measuring on the fresh wood cube surface (25 spectra per cube, from 0 to 2.5 mm). Spectra were baseline-corrected with the concave rubberband correction method in the OPUS software (Bruker) and peak area normalized over the whole spectrum with MATLAB. The peak area ratios, without prior normalization, were also calculated in MATLAB.

**SEM/EDX/WDX.** Wood samples were polished using a rotary microtome, removing the first 200  $\mu\text{m}$  of material. SEM images were obtained in an SEM FEI Quanta 200FEG. The measurements were carried out under low vacuum, at a working distance of 10 mm, with spot size of 4 and an acceleration voltage of 10 kV. The scanning electron microscopy (SEM) images were produced with a backscattered secondary electron detector (BSE).

The energy dispersive x-ray (EDX) mappings were acquired in an SEM Quanta 600 FEI. The samples were coated with a 20 nm layer of carbon prior to all measurements. The measurements were carried out under high vacuum, at a working distance of 10 mm, with a spot size of 4.5, and an acceleration voltage of 10 kV.

Wavelength dispersive x-ray (WDX) mappings were acquired in a JEOL JSM7100 FEG scanning electron microscope operating with the EDAX TEXS spectrometer. The TEXS HP is a parallel beam spectrometer (PBS) optimized to cover low energy and transition element energies from 150 eV up to 10 keV. The samples were coated with a 20 nm layer of carbon prior to all measurements. The measurements were carried out under high vacuum, at a constant working distance of 14 mm, at a spot size of 4 nA, and an acceleration voltage of 10 kV.

## **Acknowledgements**

This research work was supported by the Swiss National Science Foundation (grant no 160041). The authors are grateful to Dr. Karsten Kunze from ScopeM at ETH Zürich, for his support on the SEM measurements, and to Asel Maria Aguilar Sanchez from the IFB department at ETH Zürich for her support in the ESEM measurements.

## Supplementary information

### S3.1: Wood Swelling Experiments in Py and DCM

Spruce wood cubes were immersed in either DCM or Pyridine. Their weights and dimensions were measured, until constant mass was reached (equilibrium). The swelling is calculated as follows:

$$S(\%) = \frac{V_w - V_d}{V_d} * 100 \quad (\text{S3.1})$$

Where  $V_w$  is the wet volume, and  $V_d$  is the dry volume. The results are given in Figure S3.1.

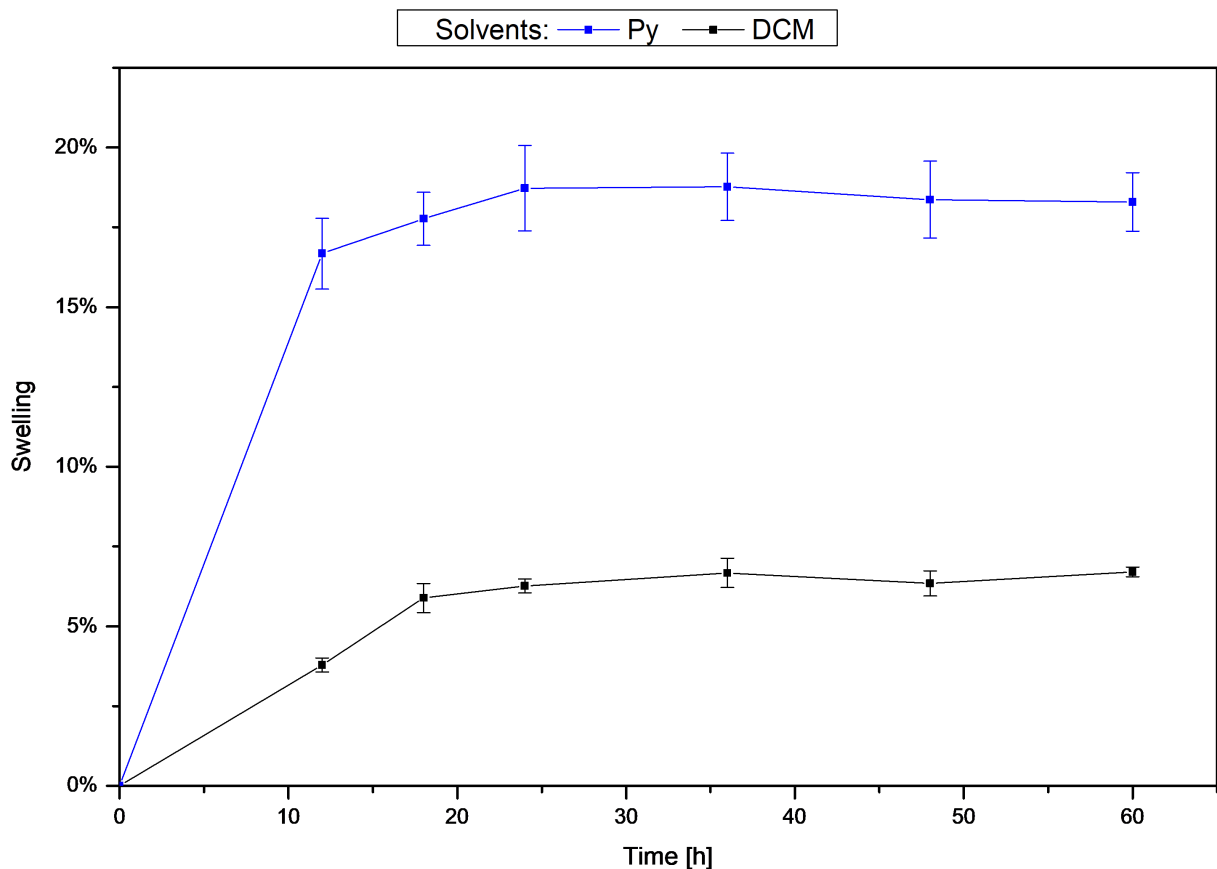
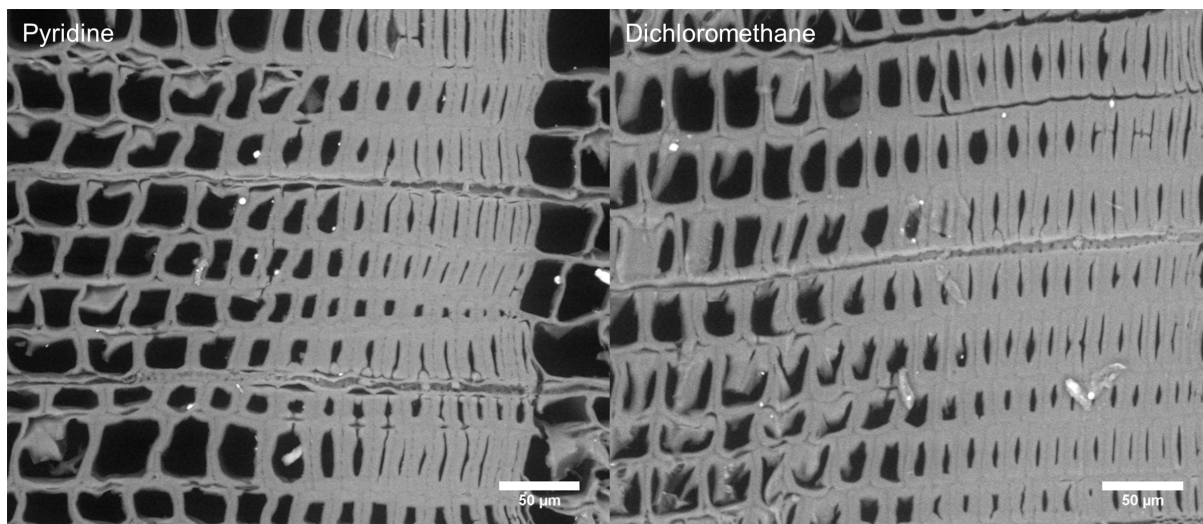


Figure S3.1: Wood swelling over time in pyridine and dichloromethane.



**Figure S3.2:** SEM images of spruce wood cross-sections after treatment with solvents (full immersion in solvent for 8h at room temperature, then washing with methanol and acetone). These conditions reproduce the esterification conditions, without the reactive compound BiBB. The images confirm that the solvent treatment does not modify the wood microstructure.

### S3.2: Theoretical WPG and substitution degree of cellulose

#### Assumptions

When considering bulk wood modification through esterification, the accessibility of wood hydroxyl groups is a key parameter. Hydroxyl groups are found on all main constituents of the wood cell wall (cellulose, hemicelluloses, and lignin).

Assuming that a wood sample is correctly impregnated (i.e. the solution of reactants fully soaks the wood structure, and penetrates inside the cell wall composite material), one could expect that all -OH groups from wood biopolymers should be engaged in the reaction.

However, an important fraction of these -OH groups are actually not accessible or poorly reactive. This is essentially the case for -OH groups that are engaged into hydrogen bonding, such as the groups found in crystalline cellulose regions. To take this into account, a few assumptions are made.

Wood is typically composed by 40 to 45% cellulose, 20 to 30% hemicellulose, and 20 to 40% lignin. For our calculations, we assumed it to be composed of 50% of cellulose (to account for the hydroxyl groups from the other components). We consider that the other 50% do not contain reactive hydroxyls. One cellulose unit, the so-called anhydroglucose unit (AGU), has a molecular weight of



162.14 g/mol, and has three –OH groups. We assume that only one of these three hydroxyl groups can react (to account both for the inaccessible groups in the crystalline phase, and also to reflect the different reactivities of the three hydroxyls from AGU).

With these assumptions, we can estimate the amount of accessible -OH groups in 1 g of spruce softwood, according to the cellulose content:

Wood cellulose content	$n_{OH}$ [mmol]
40%	7.4
45%	8.3
50%	9.3

Our numbers are consistent with the value reported in literature for another softwood (8.6 mmol/g).<sup>25,206</sup>

### Theoretical BiBB WPG

Based on these comments, the following equations can be used to calculate the amount of BiBB engaged in the reactions ( $m_{BiBB}$ ), and the maximal BiBB content ( $WPG_{grafted BiBB}$ ):

$$m_{BiBB} = \frac{0.5 \times m_{wood} \times MW_{BiBB} \times eq}{MW_{AGU}} \quad (S3.2)$$

$$WPG_{grafted BiBB} = \frac{0.5 \times m_{wood} \times MW_{grafted BiBB} \times eq}{MW_{AGU}} \quad (S3.3)$$

With  $MW_{AGU} = 162.14$  g/mol,  $MW_{BiBB} = 229.90$  g/mol, and  $MW_{grafted BiBB} = 150.00$  g/mol and  $eq$  being the molar ratio between BiBB and AGU units.

We provide an example of calculation for the esterification of 1 g of spruce wood with different equivalents of  $\alpha$ -bromoisobutryl bromide (BiBB) per AGU units in Table S3.1.

### CHAPTER 3. SOLVENT-CONTROLLED SPATIAL DISTRIBUTION OF SI-AGET-ATRP GRAFTED POLYMERS IN LIGNOCELLULOSIC MATERIALS

**Table S3.1:** example of calculation for the esterification of 1 g of spruce wood with different equivalents of *a*-bromoisobutyryl bromide (BiBB) per AGU units.

Calculation of BiBB amount engaged in the reaction						Expected maximal BiBB content	
$m_{\text{wood}}$	$m_{\text{cellulose}}$	$n_{\text{AGU}}$	$n_{\text{BiBB}}:n_{\text{AGU}}$	$n_{\text{BiBB}}$	$m_{\text{BiBB}}$	$m_{\text{BiBB,max}}$	$\text{WPG}_{\text{BiBB,max}}$
[g]	[g]	[mmol]		[mmol]	[g]	[g]	
1	0.5	3.0838	1	3.0838	<b>0.7090</b>	0.4626	<b>46.3%</b>
1	0.5	3.0838	0.5	1.5419	<b>0.3545</b>	0.2313	<b>23.1%</b>
1	0.5	3.0838	0.1	0.3084	<b>0.0709</b>	0.0463	<b>4.6%</b>

It should be noted that for esterification of wood with small molecules, for instance acetylation, it is common to obtain maximum weight percent gains around 25% (corresponding to about 5.8 mmol of  $-\text{COCH}_3$  per gram of wood). In our case, a simple calculation shows that the grafting of 5.8 mmol of  $-\text{COC}(\text{CH}_3)_2\text{Br}$  in one gram of wood would result in a 87% WPG. With our conservative assumptions, we calculated a maximal WPG of 46.3%.

#### Substitution degree of cellulose

It is well known and accepted that lignin and hemicelluloses can react upon a wood chemical treatment.<sup>207</sup> In fact, most studies related to the distribution of bonded chemicals after wood modification such as acetylation, show that lignin is highly substituted when compared to carbohydrates, and that the highest contribution to the final weight gain comes from the substitution of the abundant  $-\text{OH}$  groups from the hemicelluloses.<sup>208,209</sup>

If we would consider that cellulose is the only wood biopolymer reacting, which evidence show not to be the case, we can estimate its degree of substitution due to our reactions. As shown in the table below, using various weight percent gain scenarios (from 5 to 45%), reflecting the WPGs obtained in our study, and using various wood cellulose contents within realistic assumptions (according to most sources, spruce wood typically contains 40 to 50% cellulose), we obtain a maximum degree of substitution of 0.41. If we take a more reasonable assumption (i.e. that lignin and hemicellulose react to a larger extent than the  $-\text{OH}$  groups from cellulose), the maximum degree of substitution should be even lower.

### CHAPTER 3. SOLVENT-CONTROLLED SPATIAL DISTRIBUTION OF SI-AGET-ATRP GRAFTED POLYMERS IN LIGNOCELLULOSIC MATERIALS

**Table S3.2:** Estimation of cellulose substitution degree after reaction with BiBB.

Assumption: only cellulose reacts	Calculations are based on one gram of wood
MW of a grafted BiBB molecule	149.9 g/mol
MW of an anhydroglucose unit (AGU)	162.14 g/mol
Dry mass of native wood	1 g

Wood cellulose content [%]	Mass of cellulose [g]	$n_{AGU}$ [mmol]	$n_{OH}$ [mmol]
40	0.40	2.467	7.401
45	0.45	2.775	8.326
50	0.50	3.084	9.251

WPG <sub>BiBB</sub> [%]	Dry mass of modified wood [g]	$n_{BiBB}$ in modified wood [mmol]
5	1.05	0.334
15	1.15	1.001
25	1.25	1.668
35	1.35	2.335
45	1.45	3.002

WPG BiBB [%]	Wood cellulose content [%]	Substitution degree of cellulose
5	40	0.05
	45	0.04
	50	0.04
15	40	0.14
	45	0.12
	50	0.11
25	40	0.23
	45	0.20
	50	0.18
35	40	0.32
	45	0.28
	50	0.25
45	40	0.41
	45	0.36
	50	0.32

### S3.3: EDX mappings of the W-Br-PTFEMA samples

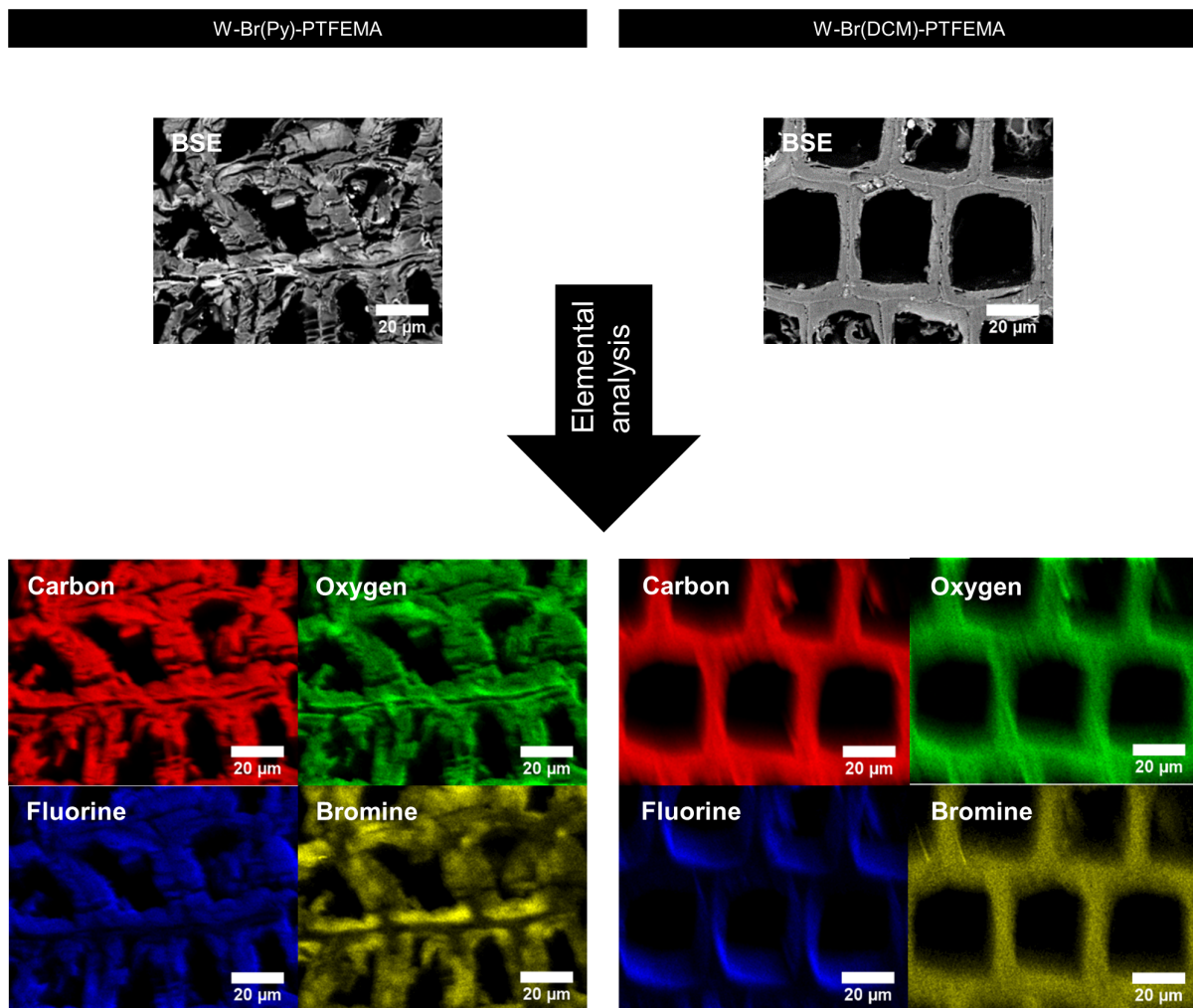


**Figure S3.3:** EDX elemental mapping results for TFEMA-polymerized samples in both BiBB sets of reaction (Py and DCM).

S3.4: WDX mappings of the W-Br-PMETAC samples

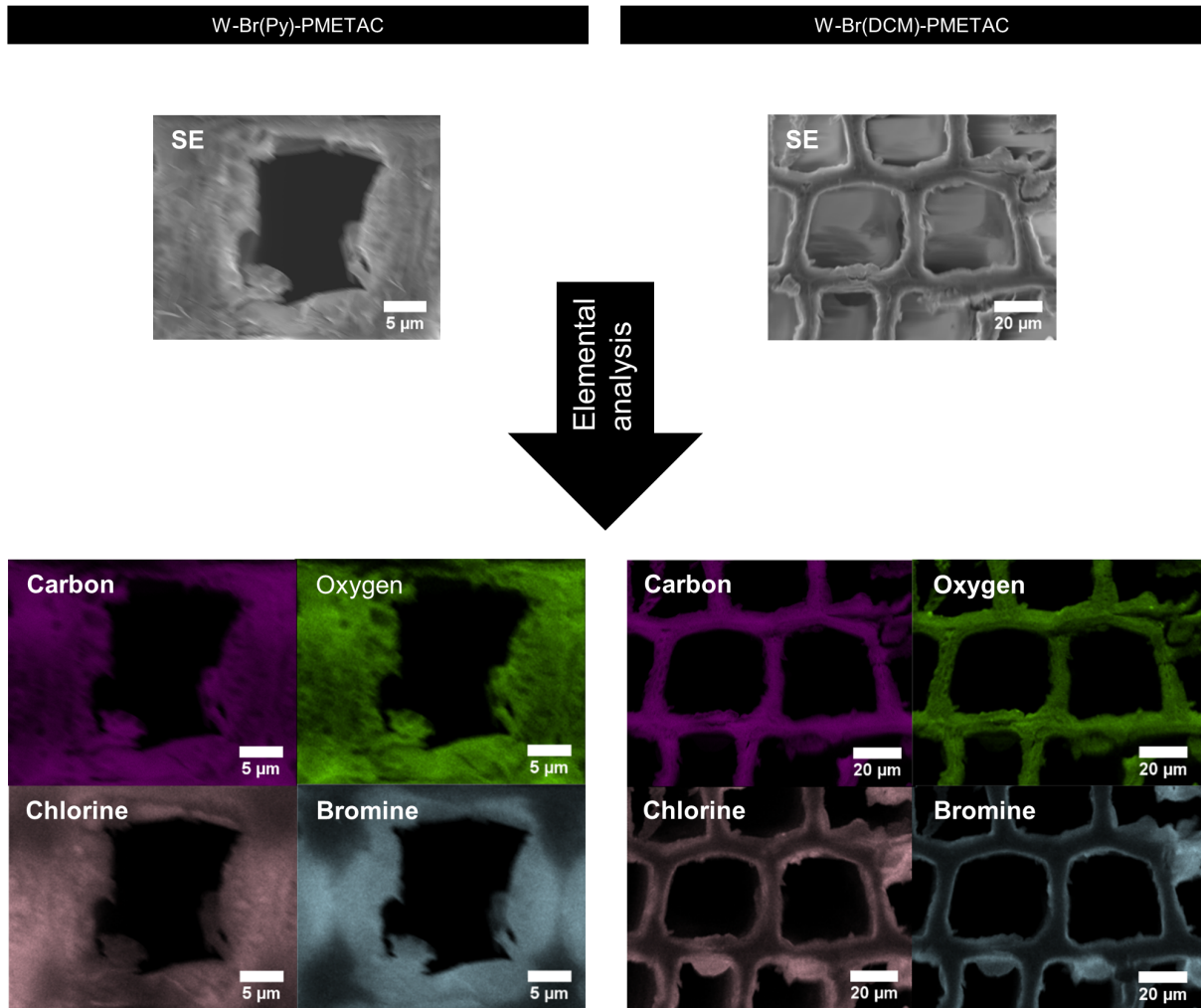


**Figure S3.4:** WDX elemental mapping results for METAC-polymerized samples in both BiBB sets of reaction (Py and DCM).

### S3.5: FTIR spectra of the W-Br-Polymer samples

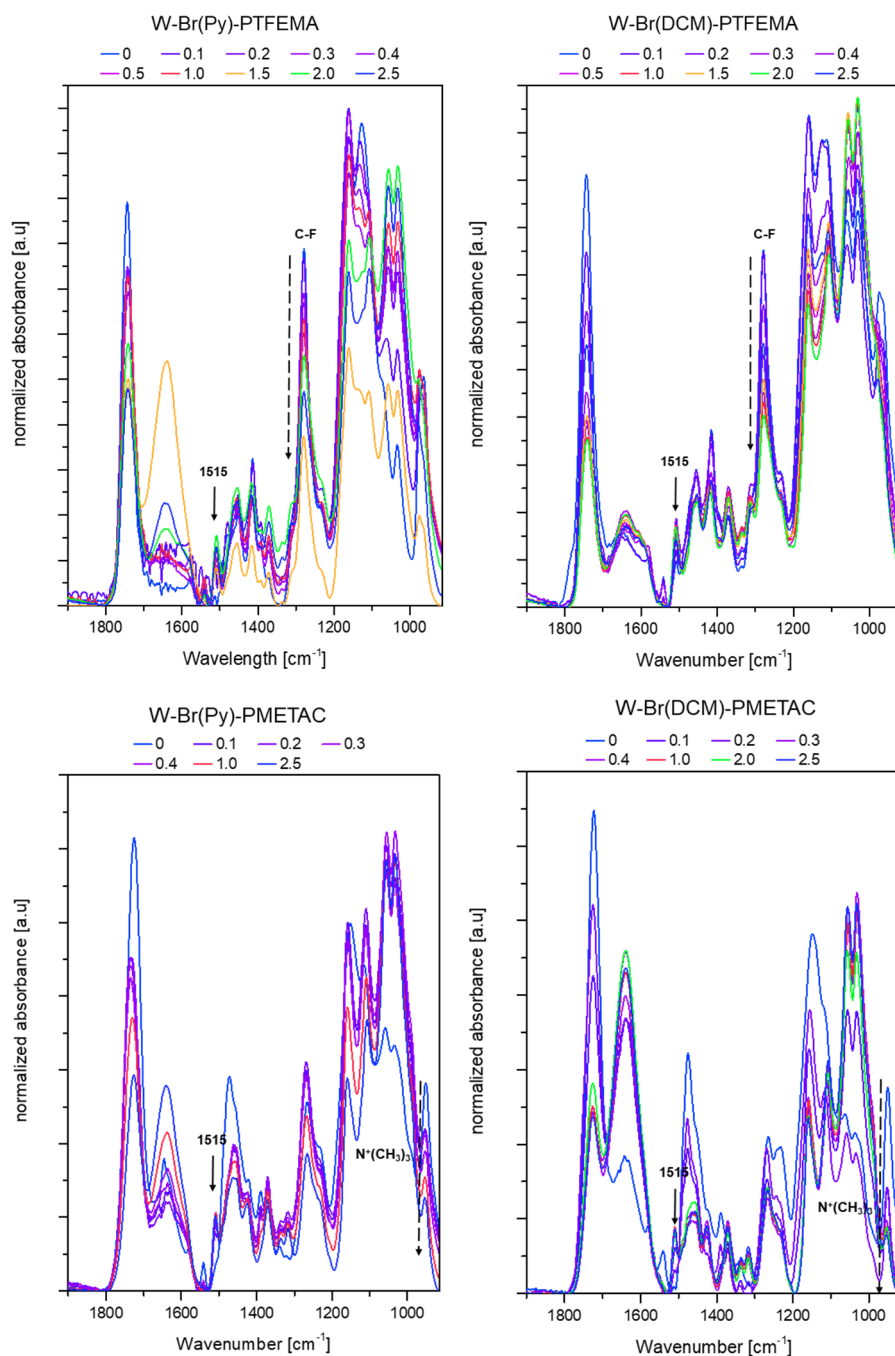


**Figure S3.5:** FTIR spectra of the different polymer modification (TFEMA and METAC monomers) in the two BiBB reacted sets (Py and DCM).

### S3.6: Targeted and estimated degrees of polymerization

*Table S3.3: Targeted and estimated degrees of polymerization.*

Sample ID	Targeted DP	Estimated DP	Estimated DP after correction
W-Br(DCM)-PTFEMA	10	2.9	14.3
W-Br(Py)-PTFEMA	10	1.9	9.7
W-Br(DCM)-PMETAC	10	0.9	4.4
W-Br(Py)-PMETAC	10	0.7	3.3





# Chapter 4

## Grafting of Amphiphilic Block Copolymers on Lignocellulosic Materials via SI-AGET-ATRP

Functionalizing bio-sourced materials is a major topic in the field of materials science. In particular, grafting polymerization techniques have been employed to change the surface properties of various substrates. Here, we report on the grafting of amphiphilic block copolymers in lignocellulosic materials using AGET-SI-ATRP. With this modification, it is possible to combine the interesting properties (anisotropy and high mechanical stability) of lightweight lignocellulosic materials, such as wood, with the special properties of the grafted block copolymers. Hydroxyl groups on wood cell wall biopolymers were used for the chemical bonding of an alkyl bromide as the initiator for AGET-SI-ATRP of a highly hydrophilic monomer ([2-(Methacryloyloxy)ethyl] trimethylammonium chloride) – METAC) and a highly hydrophobic fluorinated monomer (2,2,3,3,4,4,5,5 Octofluoropentyl methacrylate – OFPMA). The successful grafting of homopolymers and block copolymers onto the wood structure was confirmed through FTIR and Raman spectroscopy. The functionalization with the two homopolymers yielded lignocellulosic materials with opposite wettabilities, whereas by the adjustment of the ratio between the two copolymer blocks, it was possible to tune the wettability within these two extremes.

## 4.1. Introduction

The depletion of fossil resources and the ever-increasing environmental problems are critical issues for our societies leading to the urgent need for bio-sourced alternatives to produce new materials. The modification of biopolymers such as cellulose, lignin and chitosan is therefore a key research area for both academic and industry related fields.<sup>210-212</sup> A great variety of modification techniques have been used to bring new functionalities into these materials, leading to applications in packaging, adhesives, biomedicine, building materials, or composites.<sup>211,213-217</sup> In recent years, the interest for new materials based on bulk lignocellulosics (i.e. wood) has raised.<sup>28,35,46,187-190,192,193</sup> Although wood has been and still is mainly used in the furniture and construction sector, recent studies have shown its potential in a wide variety of applications going beyond its classical utilizations.

In most of these pioneering studies, the introduction of chemical functionalities into the wood structure is needed, and can be achieved through a number of techniques, which were already successfully applied to biomacromolecules.<sup>210,211</sup> In these novel wood-based materials, the unique hierarchical porous structure of wood should be maintained: it is an anisotropic lightweight material with high mechanical stability. However, the modification of a porous anisotropic scaffold with multiple length scales is not trivial. In the design of complex hierarchical materials based on wood, the spatial distribution of the modification can be a key parameter in obtaining the final desired properties.<sup>26,27</sup> Another objective is to obtain stable modifications providing reliable materials, through for instance covalent attachment of the newly added functionalities.

Surface initiated controlled polymerization techniques (SI-CRP) have been extensively used to modify bio-sourced materials.<sup>218</sup> They allow for the covalent attachment of polymer chains on surfaces, with a high control over chain length and grafting density. As an example, surface initiated atomic transfer radical polymerization (SI-ATRP), is a well-known CRP technique, capable of polymerizing a vast range of different monomer species, in a wide variety of solvents, and reaction conditions.<sup>51</sup> SI-ATRP was already applied to the most technologically relevant biopolymers, including cellulose,<sup>219</sup> lignin,<sup>220</sup> and

chitosan.<sup>221</sup> It was also performed on more complex materials, such as wood.<sup>33,49</sup> A variation of SI-ATRP, surface initiated activators generated by electron transfer atomic transfer radical polymerization (SI-AGET-ATRP) has also been used on bulk wood.<sup>49,222</sup>

ATRP also offers many possibilities in terms of polymer architecture (stars, branches, comb-like, etc...) and polymer composition (homopolymers, block copolymers, random copolymers, gradient copolymers, etc...).<sup>223</sup> The sequential co-polymerization of two or more monomers gives rise to block copolymers with unique properties, often based on the incompatibility between the blocks. According to the monomers used, the applications range from thermoplastics, drug delivery, patterning of surfaces, or synthesis of mesoporous materials.<sup>224</sup> Therefore, the modification of bio-sourced materials through the grafting of block copolymers has the potential to broaden the range of possible applications for these materials.<sup>225,226</sup>

Many block copolymerizations have been performed on single wood-based polymers, such as lignin and cellulose.<sup>220,221,227,228</sup> A few studies also report on copolymerization in lignocellulosic materials,<sup>229-231</sup> but to the best of our knowledge, only one study reports on the controlled grafting of copolymer brushes (on disintegrated wood fibers).<sup>232</sup> Grafting block copolymers on a non-ideal material such as wood is challenging. Wood is a highly hydrophilic material, it is negatively charged, and the porosity at nano- and micro-level may locally generate high curvatures on the surface. Such surface parameters are known to have an influence on the grafting of polymer chains.<sup>233,234</sup>

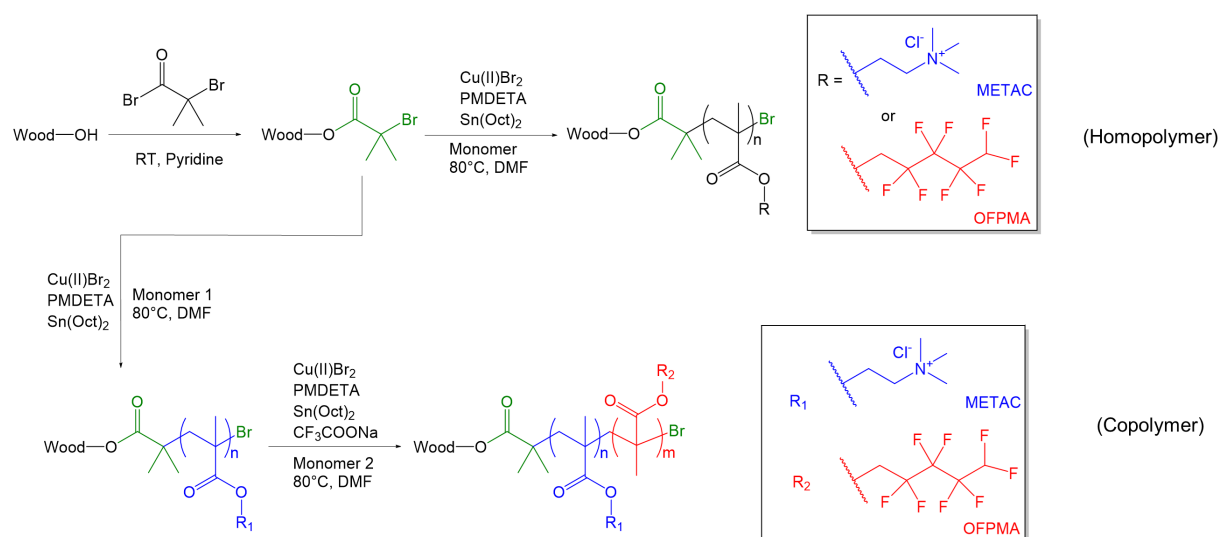
In the context of the development of advanced wood-based materials, we were interested in tuning the wettability of solid wood via grafting of amphiphilic block copolymers. Some of the applications of amphiphilic block copolymers include drug delivery, use as emulsifiers (e.g. for Pickering emulsions), and possibly special wettability properties.<sup>235-238</sup> Regarding the latter, several research groups reported that special wettabilities needed for oil/water separation challenges can be achieved through the juxtaposition of a highly hydrophilic charged domain with a low surface energy fluorinated domain.<sup>98,101</sup>

Herein, our idea was to graft bulk wood with block copolymers consisting of a highly hydrophilic polyelectrolyte, poly([2-(Methacryloyloxy)ethyl]trimethyl

ammonium chloride) (PMETAC) and a highly hydrophobic fluorinated polymer, poly(2,2,3,3,4,4,5,5-Octafluoropentyl methacrylate) (POFPMA). We proposed to graft this PMETAC-*b*-POFPMA amphiphilic block copolymer through a grafting from technique, SI-AGET-ATRP. The wood-polymer hybrid materials were characterized with FTIR and Raman spectroscopy techniques. The wettability of the wood surfaces grafted with PMETAC-*b*-POFPMA copolymers were compared to native wood and homopolymer-grafted wood. To the best of our knowledge, this is the first report of grafting block copolymers chains by a CRP technique onto the natural wood scaffold, and it contributes to the fast growing research area dealing with the functionalization of lignocellulosic materials.

## 4.2. Results and Discussion

SI-AGET-ATRP is a two-step controlled radical polymerization technique. This technique follows the same principle as classical SI-ATRP, but the addition of a reducing agent has an advantage: the reaction conditions are milder (no need for drastic oxygen-free conditions). In the first step,  $\alpha$ -Bromoisobutyryl bromide (BiBB) is covalently attached to the hydroxyl groups available in the wood cell walls, to obtain the wood macroinitiator (W-Br). In the second step, the desired polymer is grown from alkyl bromide moieties present in the macroinitiator (see Scheme 4.1).



**Scheme 4.1:** Schematic representation of the chemical modification of wood via SI-AGET-ATRP.

#### 4.2.1. Synthesis of the macroinitiator

The modification of wood through esterification of the –OH functionalities present in biopolymers is well known.<sup>14,25,239</sup> In most cases, activated carboxylic acids such as anhydrides or acid chlorides are used. It is also possible to attach ATRP initiators, such as BiBB.<sup>33,222</sup> In previous works,<sup>222</sup> we have shown the effect of different reaction parameters (reaction time, solvent, BiBB concentration, and year ring distribution) on the resulting BiBB weight percent gain. In the present study, we used samples with BiBB WPGs ranging from 9% to 32%. The FTIR spectra of unmodified wood (Ref.) and the BiBB-modified wood (W-Br), given in Figure S4.1, show the characteristic peaks observed for the BiBB modification (carbonyl peak (C=O) at  $1740\text{ cm}^{-1}$ , the ether peak (C-O) at  $1280\text{ cm}^{-1}$ , and carbon bromide peak (C-Br) at  $753\text{ cm}^{-1}$ ).<sup>202,240</sup>

#### 4.2.2. Homopolymerizations

While solution polymerizations or grafting of polymer brushes on ideal surfaces can be well controlled with CRP techniques, the hierarchical porous structure and chemical variability of wood represents a great challenge. The use of functional monomers with opposite wettabilities such as METAC and OFPMA may also require specific reaction conditions.

We therefore studied the grafting of PMETAC and POFPMA on wood before investigating the conditions for a copolymerization. Keeping in mind the different nature of the two monomers, we had to find an adequate solvent for both monomeric and polymeric species, dimethylformamide (DMF). As reported in several publications,<sup>26,32</sup> DMF is an excellent wood swelling solvent, allowing to carry reactants deep into the wood structure.

The relation between the amount of initiating sites (BiBB) available in the wood and the WPG obtained from the polymer modification was studied. The final polymer weight gain in the wood scaffold is the result of the grafting density and the length (degree of polymerization, DP) of the tethered chains. The WPGs shown in Figure 4.1 for W-PMETAC and W-POFPMA were obtained from different W-Br macroinitiators (varying amount of initiating sites), and with different targeted DPs. For an ideal controlled grafting polymerization (i.e. full monomer conversion where all initiating sites generate a polymer chain), the targeted

and obtained WPGs should be strictly equal (this is illustrated by the straight line in Figure 4.1).

Our data points deviate from this ideal behavior, indicating a mismatch in between the targeted WPGs and the obtained WPGs, for all polymerizations (see Figure 4.1). This can be attributed to two issues: either all alkyl bromide moieties do not initiate the growth of a polymer chain (i.e. the grafting density is lower than expected), or full monomer conversion is not reached (i.e. the targeted DP are not reached, and shorter chains are obtained).

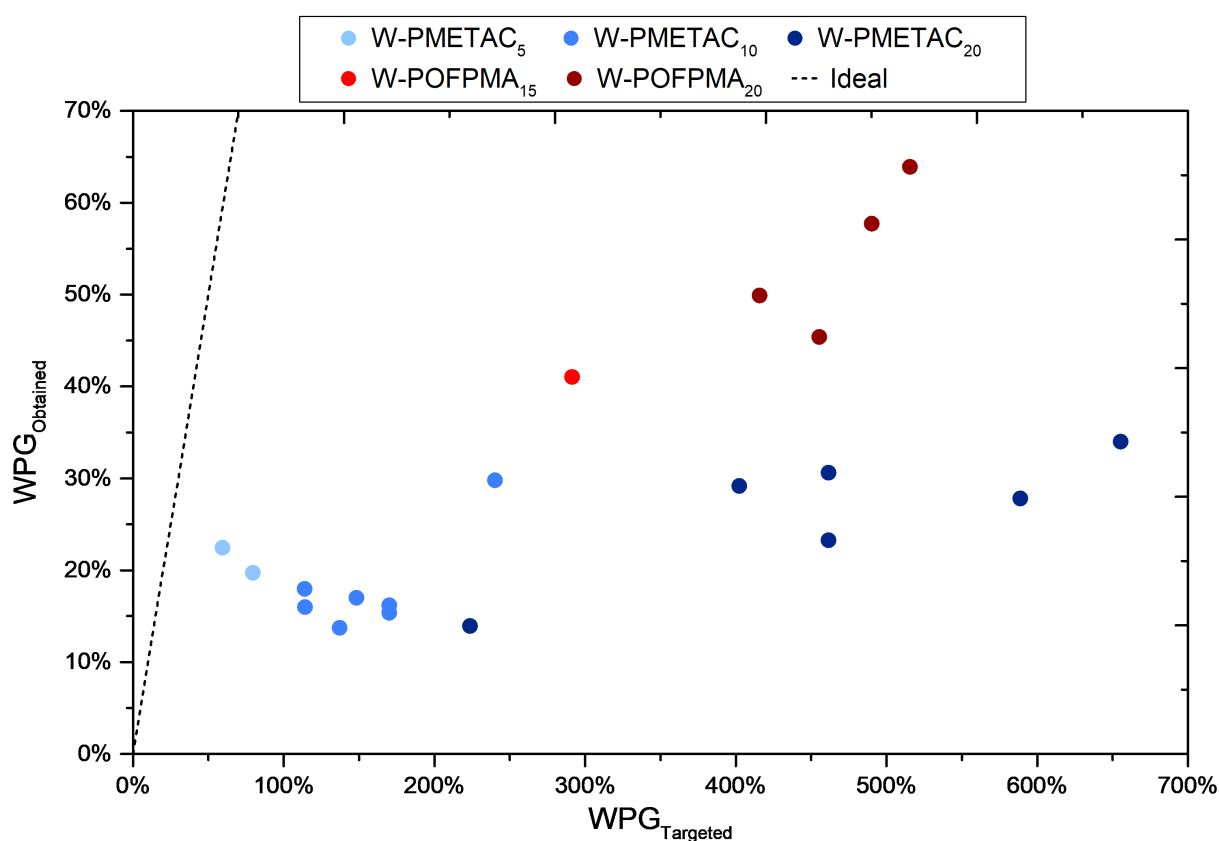
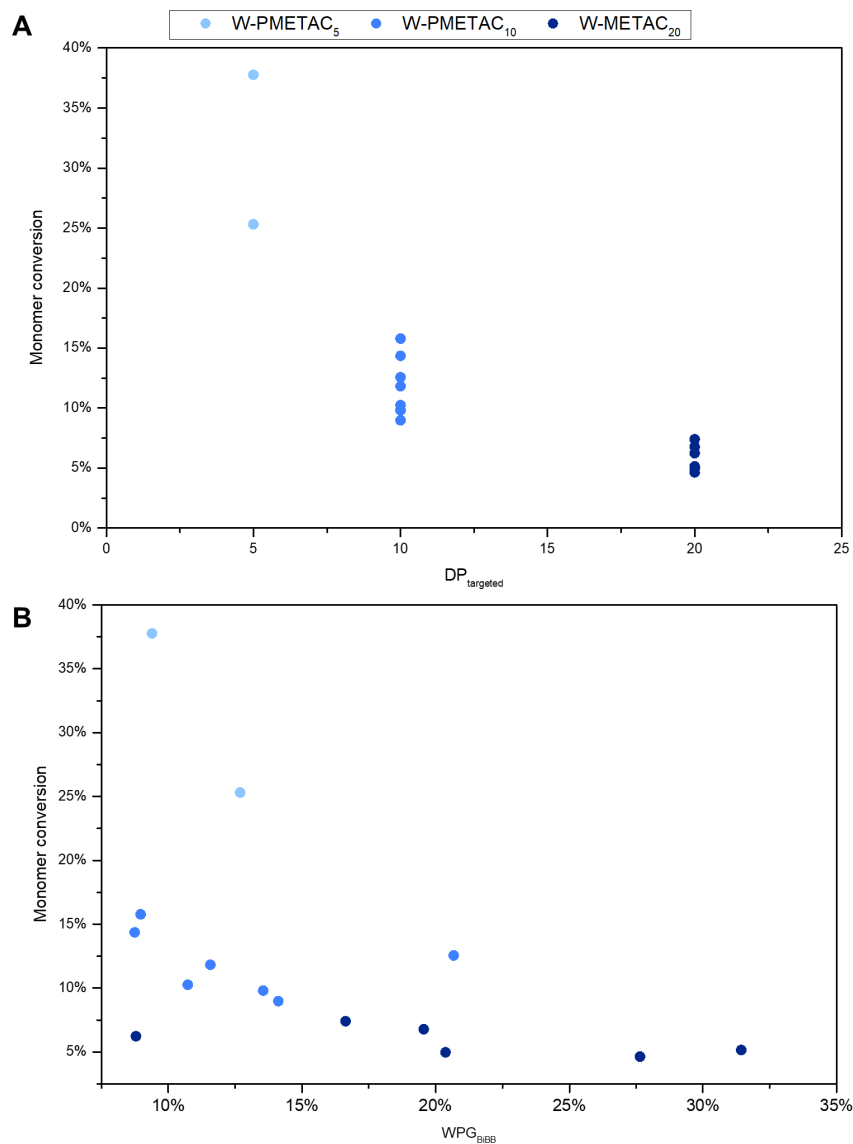


Figure 4.1: Obtained weight percent gains of each homopolymer with respect to the targeted weight percent gains.

According to previous publications, the chemical modification of a wood scaffold is not spatially homogeneous.<sup>26,241,242</sup> The distribution of the modifier in wood is affected by the extent of penetration of solutions inside the bulk of the sample, and by the diffusion of reactants inside the dense wood cell walls. In our case, the BiBB molecules are introduced inside wood with pyridine (an excellent wood swelling solvent). BiBB molecules are relatively small and highly reactive: they have been shown to react deep inside the cell wall structure.<sup>33</sup> In order to grow a polymer chain in the next step, both monomers and catalyst

complex need to reach the initiating sites. This is relatively easy when the initiator is anchored at the interface between cell wall and lumen, but if the initiator is located deep inside the cell wall, then the reactants must diffuse from the lumen through the cell wall. The result is that a large proportion of the alkyl bromide moieties cannot initiate polymerization, and the obtained weight gain is significantly lower than the targeted amount. This was also confirmed in previous work.<sup>222</sup>, and could explain our observations.

However, in the case of PMETAC, it is interesting to observe that the relation between final monomer conversion is also clearly affected by the initial targeted DP, and by the amount of BiBB in wood (see Figure 4.2).



**Figure 4.2:** Monomer conversion of METAC under (A) different targeted degrees of polymerization and (B) different BiBB WPGs.

According to the first plot (Figure 4.2A), the conversion of METAC towards W-PMETAC is higher when short chains are targeted and decreases when longer chains are targeted. In the second plot (Figure 4.2B), we can see that a higher concentration of initiating sites also leads to lower conversions. Both results point toward the following: when the growth of low grafting density (low BiBB content) short chains (DP targeted 5) is targeted, the polymerization is better controlled (closer to ideal polymerization).

In this homopolymerization, METAC monomer, the Cu(II)Br<sub>2</sub> / Ligand catalyst and the growing PMETAC chains are all positively charged. The addition of charged monomers to charged growing polymer chains was studied by Cuccato et al.<sup>243</sup> In their work, they observed that the growth of the chains was hindered after some time. They hypothesized that the electrostatic interactions between the polymer and the monomers, result in strong repulsions between the two positively charged entities, hindering further addition of monomeric units. In a similar fashion a few studies have shown that electrostatic interactions in between charged surfaces (charged growing polymer brushes) and the ATRP catalyst complex affects the grafting density of polymer chains.<sup>234,244</sup> In that case, the limitation comes from the depletion of catalyst concentration close to the surface due to the electrostatic repulsions.

In our case, we believe that after a certain grafting density is reached, the positive charges of the growing PMETAC chains generate a repulsive effect preventing the catalyst to get close to the surface (difficulties to initiate new polymer chains from remaining alkyl bromides), and slowing down the addition of new monomers (difficulties to reach higher DPs). We characterized the homopolymerizations on the lignocellulosic scaffold with FTIR spectroscopy, and the specific peaks for each polymeric species were identified (Figure 4.3). In Figure 4.3A and B, we show the spectra of the unmodified wood (Ref), the wood modified by the BiBB initiator (W-Br), and the wood grafted with the corresponding polymers (W-POLYMER). In both graphs the carbonyl peak (C=O) at 1740 cm<sup>-1</sup> and the ether peak (C-O) at 1280 cm<sup>-1</sup> corresponding to the acrylate functionality are clearly increased when compared to the W-Br spectra. In addition, the presence of the polymers can be detected through their characteristic peaks: N<sup>+</sup>(CH<sub>3</sub>)<sub>3</sub> vibration at 955 cm<sup>-1</sup> for W-PMETAC (Figure 4.3A) and C-F vibration at 820 cm<sup>-1</sup> for W-POFPMA (Figure 4.3B).<sup>204,205</sup>



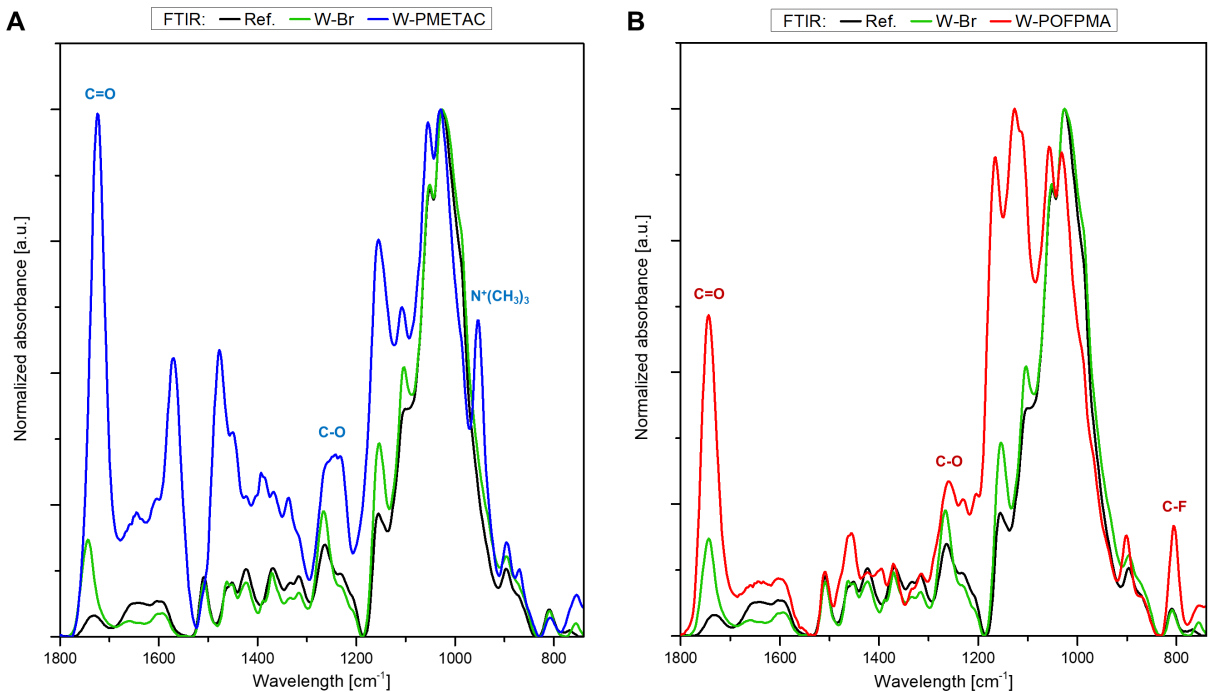


**Figure 4.3:** FTIR spectra of native wood (Ref), wood ATRP macroinitiators (W-Br), and wood grafted with methacrylates (W-PMETAC and W-POFPMA).

The polymer modifications could also be detected through Raman spectroscopy for both W-PMETAC and W-POFPMA. Figure 4.4 displays the Raman mappings and the corresponding average spectra of the marked regions of interest (ROI) for each homopolymer. The Raman mapping images shown in Figure 4.4 are obtained through the integration of the characteristic polymer peaks – N<sup>+</sup>(CH<sub>3</sub>)<sub>3</sub> for W-PMETAC between 920 and 990 cm<sup>-1</sup> and C-F for W-POFPMA between 855 and 760 cm<sup>-1</sup> – and the skeletal aromatic vibration attributed to lignin between 1570 and 1700 cm<sup>-1</sup>.<sup>75,204,205</sup>

In all the average spectra, we observe the carbonyl band (C=O) at 1740 cm<sup>-1</sup> together with typical wood bands such as the skeletal aromatic vibration at 1607 cm<sup>-1</sup>, assigned to lignin. In the spectrum of the W-PMETAC sample (purple), the N<sup>+</sup>(CH<sub>3</sub>)<sub>3</sub> asymmetric bending band at 955 cm<sup>-1</sup> and C-N vibration band at 720 cm<sup>-1</sup> are observed.<sup>205</sup> Both spectra of the W-POFPMA samples show a C-F vibration band and C-F<sub>2</sub> twist band at 820 cm<sup>-1</sup> and 300 cm<sup>-1</sup>, respectively.<sup>204,245,246</sup>

Two average spectra were taken for the W-POFPMA samples, from different regions in the Raman mapping. The first spectrum (green) was acquired in the lumen: it clearly shows the POFPMA bands. The second one (pink) was acquired

at the interface lumen/cell wall and we can clearly identify the combination of POFPMA together with wood components. The corresponding ROIs are marked on the integration mapping images for each homopolymer.

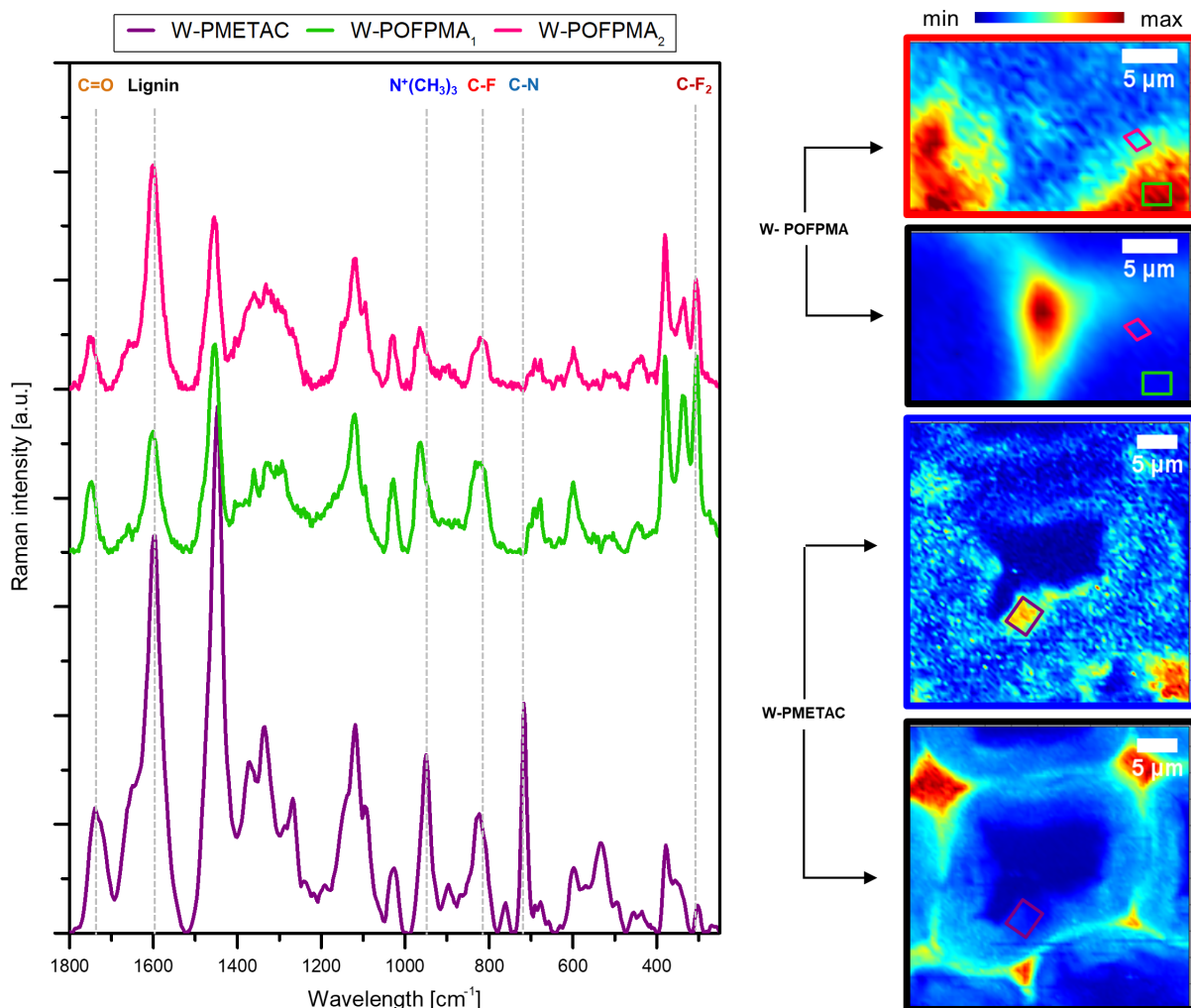


**Figure 4.4:** Average Raman spectra of the marked regions of interest in the Raman mapping images of the homopolymerized samples W-PMETAC and W-POFPMA. The Raman mapping images were obtained by integration of lignin- and polymer-specific bands.

### 4.2.3. Copolymerization

To obtain well-defined block copolymers, the copolymerization experiments were carried out sequentially. The W-Br samples were first reacted with METAC to grow PMETAC chains, then the second monomer (OPFMA) was added to extend the PMETAC grafted chains and produce the PMETAC-b-POFPMA amphiphilic block copolymers.

Initially, we directly used the homopolymerization reaction conditions described in the previous section. According to our results, it was not possible to add a

POFPMA block to the PMETAC block grafted on the wood scaffold with these conditions. We did not observe any notable weight gain after the reaction (maximum POFPMA WPG ca. 0.3%), and we could not identify the relevant FTIR signature peaks.

Following our observations on the limited growth of PMETAC chains on wood, we believe that electrostatic interactions also hinder the addition of new OFPMA monomers to extend the PMETAC block. This problem has been reported in literature, and it has been shown that in order to build amphiphilic block copolymers comprising a charged block, a salt can be used to screen the charges of the first block during the polymerization of the second block.<sup>247</sup> In our case, with the increase of the ionic strength of the reaction medium, the charges of the PMETAC should have a reduced adverse effect on the polymerization of OFPMA monomers. For this reason, in all the following copolymer syntheses, OFPMA monomers were reacted in the presence of a sodium fluoroacetate salt to screen the PMETAC charges.

To demonstrate the feasibility of the copolymerization in optimal conditions (i.e. excluding possible issues related to surface initiation from the wood macroinitiators), we synthesized a PMETAC-*b*-POFPMA block copolymer in solution. Using Ethyl  $\alpha$ -bromoisobutyrate (EBriB) as initiator (same alkyl halide structure as in our W-Br macroinitiators), we first synthesized PMETAC polymer chains in DMF, targeting 20 repeating units. Then, POFPMA chains (again targeting 20 repeating units) were grown from the purified PMETAC macroinitiators to obtain the amphiphilic block copolymers. A  $\text{CF}_3\text{COONa}$ /METAC ratio of 2 was used. After each polymerization step, we characterized the polymers through GPC (see Figure 4.5) and NMR (see Figure S4.2 in Supplementary Information). NMR spectroscopy confirmed the formation of PMETAC after the first step and the presence of PMETAC and POFPMA after the second step.

The GPC curves of the copolymer revealed a clear shift toward higher molecular weights when compared to the PMETAC macroinitiator trace (Figure 4.5). We observed an increase of about 50% (from 12 000 to 18 100 Da) for the number average molecular weight ( $M_N$ ), while the weight average molecular weight ( $M_W$ ) increased from 20 600 to 38 300 Da (measured against PMMA standards).

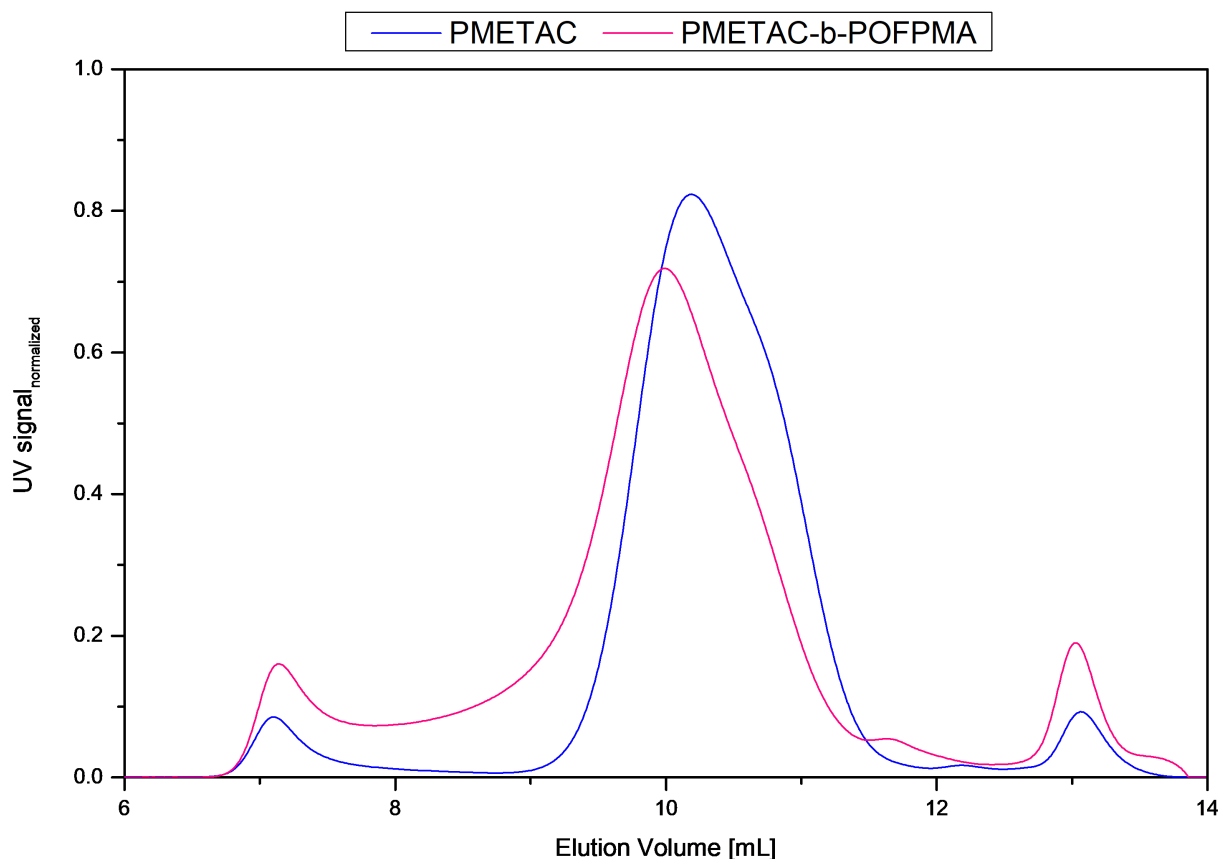


**Figure 4.5:** GPC traces of PMETAC and PMETAC-b-POFPMA chains from SI-AGET-ATRP reaction in solution.

This clear molecular weight increase indicates that the PMETAC chains could initiate the polymerization of OFPMA, yielding the targeted PMETAC-b-POFPMA copolymer.

Following the successful solution copolymerization, we proceeded with the surface-initiated grafting approach, using W-Br as macroinitiators. The first block was grown using the reaction conditions described previously. For the second step, the amount of salt was calculated in terms of equivalents with the number of moles of METAC grafted in the first step. With a 1:2 ratio of salt with respect to the PMETAC, the polymerization of OFPMA was successful, with a 6% weight increase. This indicated that the chosen salt was capable of shielding the charges of the PMETAC chains, and that the PMETAC chains could be extended with a second block (POFPMA). According to the results for both solution and surface-initiated polymerization, it is obvious that the screening of the positive charges from the METAC units was crucial.

In the surface-initiated polymerization approach, to efficiently screen these charges, it is not only important to have a sufficient salt concentration (with

respect to the amount of METAC), but the accessibility of the charges is also an important factor, that could be related to the PMETAC grafting density and to the PMETAC chain length, i.e. to PMETAC WPG.

#### 4.2.3.1. Study of the copolymerization parameters

In the next paragraphs, we report on the effect of two parameters on the copolymerization. We first discuss the effect of the amount of grafted PMETAC on the POFPMA WPG. Then we discuss the effect of the salt concentration (with respect to the PMETAC amount) and its impact on the POFPMA WPG.

To obtain W-PMETAC with various chain lengths, three polymerization batches using the same W-Br macroinitiators (9% BiBB WPG) were performed (the low BiBB WPG was chosen in order to be able to control the PMETAC growth, having in mind the limitations when using high amounts of initiator). Thus, from these three batches, W-PMETAC samples with 14%, 18%, and 22% PMETAC WPGs were produced. Each of these were further engaged in the copolymerization reactions of OFPMA (for all reactions, the targeted POFPMA repeating units was kept constant, and the METAC/salt ratio was set to 1:2). The POFPMA WPGs as a function of the targeted PMETAC chain lengths (and the actual PMETAC WPGs) resulting from these polymerizations are shown in Figure 4.6.

According to this plot, as both the targeted PMETAC chain length and the PMETAC WPGs increase, the final amount of POFPMA seems to decrease. This can be also explained through considerations regarding electrostatic and steric effects.

Polyelectrolytes in polar aprotic solvents (such as DMF) behave similarly to polyelectrolytes in polar protic solvents (such as water).<sup>248</sup> Classically, fully charged polyelectrolytes adopt an extended conformation in solution to minimize electrostatic interactions. If the charges are screened (by the addition of salt), the electrostatic interactions are suppressed and the polymer chains adopt a coiled conformation.

The same behavior was observed with polyelectrolyte brushes on flat surfaces.<sup>249</sup> In this case, the charge screening leads to chain collapsing. We can also expect a similar behavior in our W-PMETAC samples, if we consider that the

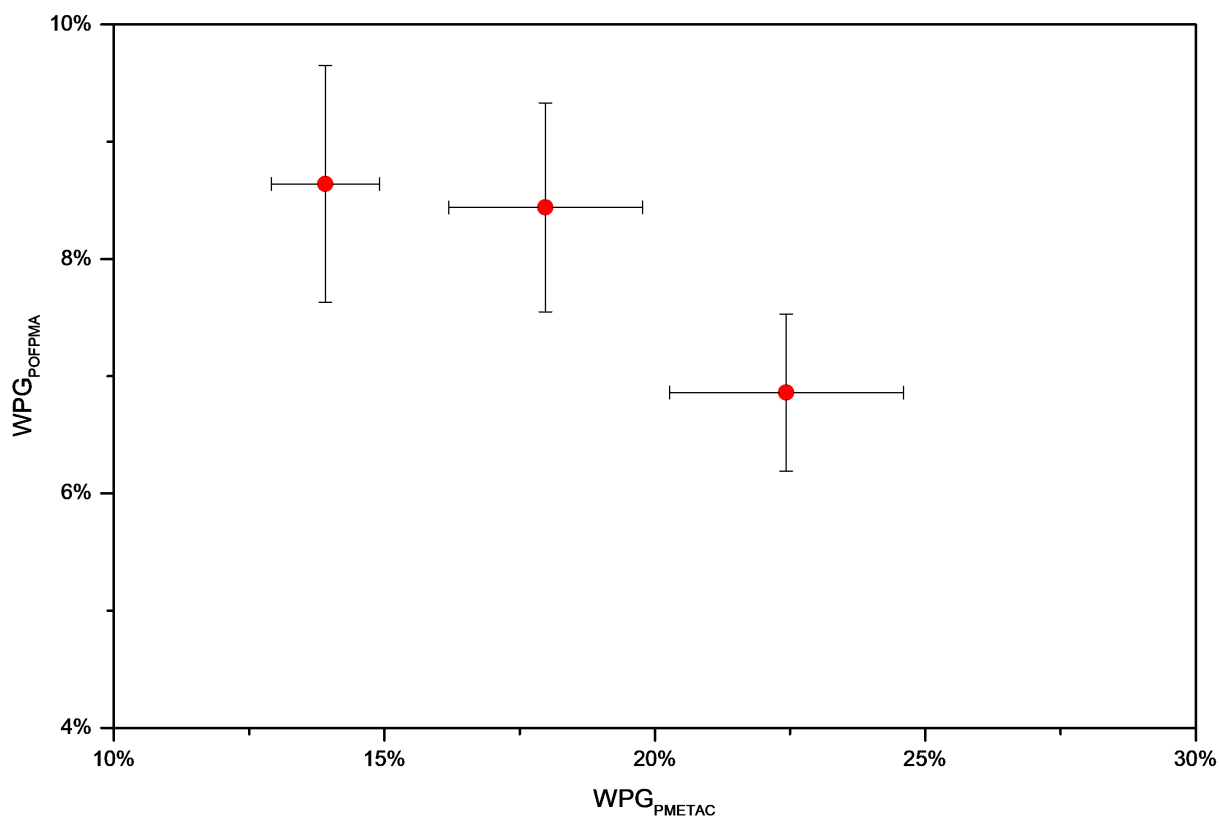


**Figure 4.6:** WPG of POFPMA with respect to different PMETAC-modification concentrations. The degree of polymerization for each point corresponds to 5, 10, and 20 with increasing PMETAC concentration.

addition of salt screens most charges. This means that the bromine end groups on the PMETAC chains might be “buried” within the collapsed brushes, i.e. their accessibility might be reduced. Moreover, the longer the PMETAC chain, the more inaccessible its end-group will be. Since these end groups are the initiating points to extend the PMETAC with the OFPMA monomers, the PMETAC collapsing could explain the trend (decrease in POFPMA WPG) observed in Figure 4.6.

Subsequently, the effect of the salt concentration on the polymerization of OFPMA was studied. First, we verified that sodium trifluoroacetate did not have an adverse effect on the homopolymerization of OFPMA. To do this, we grafted POFPMA chains directly on the wood macroinitiator (W-Br), i.e. without the interaction of the W-PMETAC brushes. The results shown in Figure 4.7 suggest that the increase in salt concentration has a positive effect on the homopolymerization of OFPMA, with an increase in the POFPMA WPG.

In the second experiment, a set of identical W-PMETAC samples was used for the OFPMA polymerization. All conditions were identical, except for the salt ratio

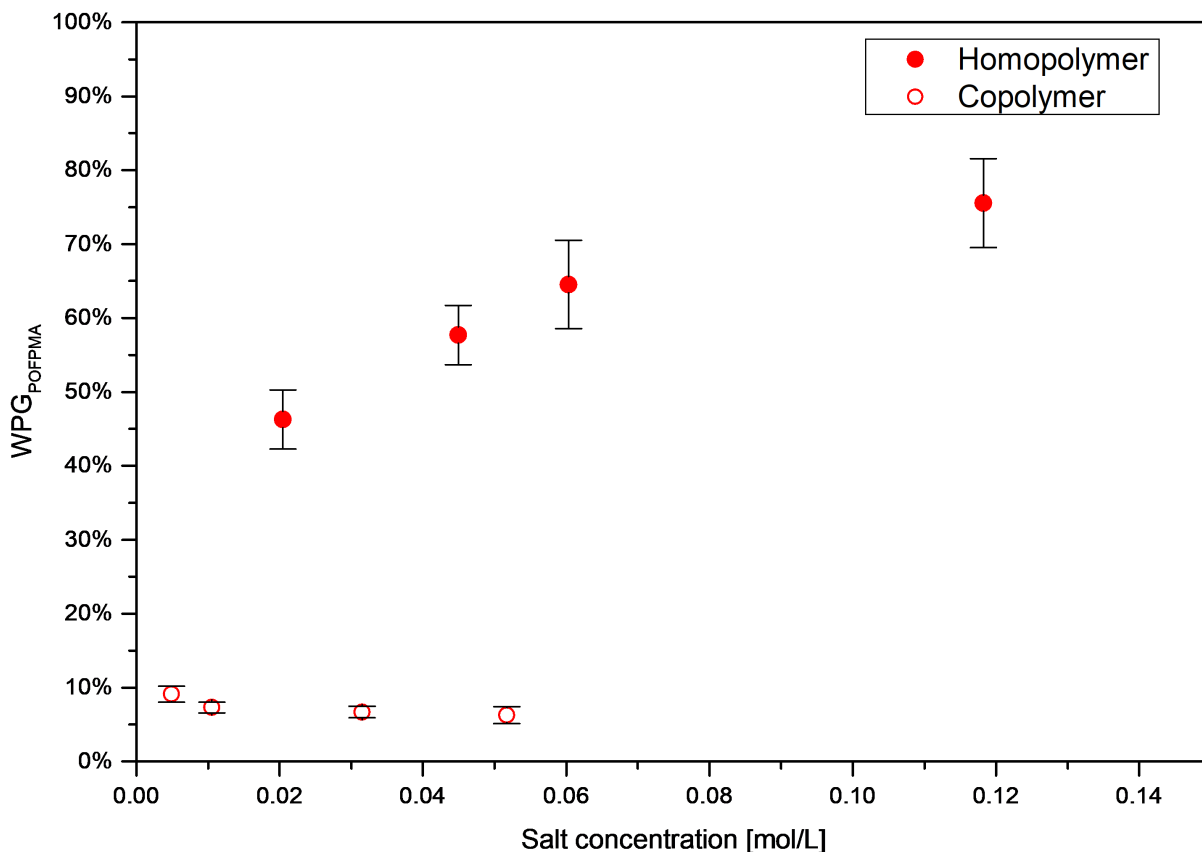


**Figure 4.7:** Effect of the concentration of salt on the polymerization of OFPMA, in the case of the homo- and co-polymerizations. For the copolymerization, the METAC/salt concentration ratio was 0.5, 1, 2, and 4 equivalents.

(from 0.5 to 4 equivalents of salt with respect to METAC). As opposed to the homopolymer samples (W-POFPMA), we observe no significant change in the POFPMA WPG for the copolymer samples (W-PMETAC-b-POFPMA).

As explained earlier, when we do not use salt, the copolymerization of OFPMA with W-PMETAC does not occur because the local concentration of monomer and catalyst complex close to growing polymer chains is low. With the addition of salt, a sufficient amount of charges are shielded, charged species can come closer to the growing polymer chains, and the polymerization can occur. However, if we increase the concentration further, the complete screening of charges likely leads to chain collapse, reducing the accessibility of initiating sites, and subsequently hindering further polymerization.

#### 4.2.3.2. Copolymer characterization

The presence of the PMETAC-*b*-POFPMA copolymer on the bulk wood scaffold was characterized with FTIR and Raman spectroscopy. The FTIR and Raman spectra are given in Figure 4.8, along with the Raman mappings.

In the FTIR and Raman spectra, we can see the carbonyl vibration (C=O) at  $1740\text{ cm}^{-1}$  and  $1720\text{ cm}^{-1}$ , the C-O vibration at  $1280\text{ cm}^{-1}$ , and the skeletal aromatic vibration at  $1607\text{ cm}^{-1}$  (attributed to lignin). The characteristic peaks of each polymer are also visible in both spectra:  $\text{N}^+(\text{CH}_3)_3$  vibration at  $955\text{ cm}^{-1}$  and C-F vibration at  $820\text{ cm}^{-1}$ . The Raman spectrum was taken from a region of interest marked in the Raman mapping images. The Raman mapping images were obtained from integrating the  $\text{N}^+(\text{CH}_3)_3$  peak between  $920$  and  $990\text{ cm}^{-1}$  for PMETAC, the C-F vibration between  $855$  and  $790\text{ cm}^{-1}$  for POFPMA, and the skeletal aromatic vibration assigned to lignin between  $1570$  and  $1700\text{ cm}^{-1}$  for the compound middle lamella (CML – mainly lignin).<sup>75,204,205</sup>

#### 4.2.4. Wettability measurements

The wettability properties of the homopolymer-grafted samples (W-PMETAC and W-POFPMA) and a set of copolymer-grafted samples (W-PMETAC-*b*-POFPMA) were characterized with contact angle measurements under air, with the sessile drop method. According to the results shown in Figure 4.9, the hydrophilicity of wood is drastically increased after the grafting of PMETAC chains: in contrast to other samples including native wood, the water drop is immediately absorbed. As expected, the introduction of POFPMA into the wood structure makes it highly hydrophobic: a very high and stable contact angle (ca.  $145^\circ$ ) is observed. The decrease of contact angle over time in the case of pure POFPMA is likely due to the evaporation of the water drop.<sup>250,251</sup>

Moreover, the CA measurements reveal that the PMETAC:POFPMA block ratio has a clear influence on the wettability. We produced three wood-copolymer samples with a fixed PMETAC amount, and a varying POFPMA amount: W-copolymer A (30% PMETAC and 9% POFPMA), W-copolymer B (30% PMETAC and 13% POFPMA), and W-copolymer C (30% PMETAC and 22% POFPMA). By adjusting the copolymerization ratio, one can tune the wettability of the wood. The contact angles characterizing the wood-copolymer surfaces range from



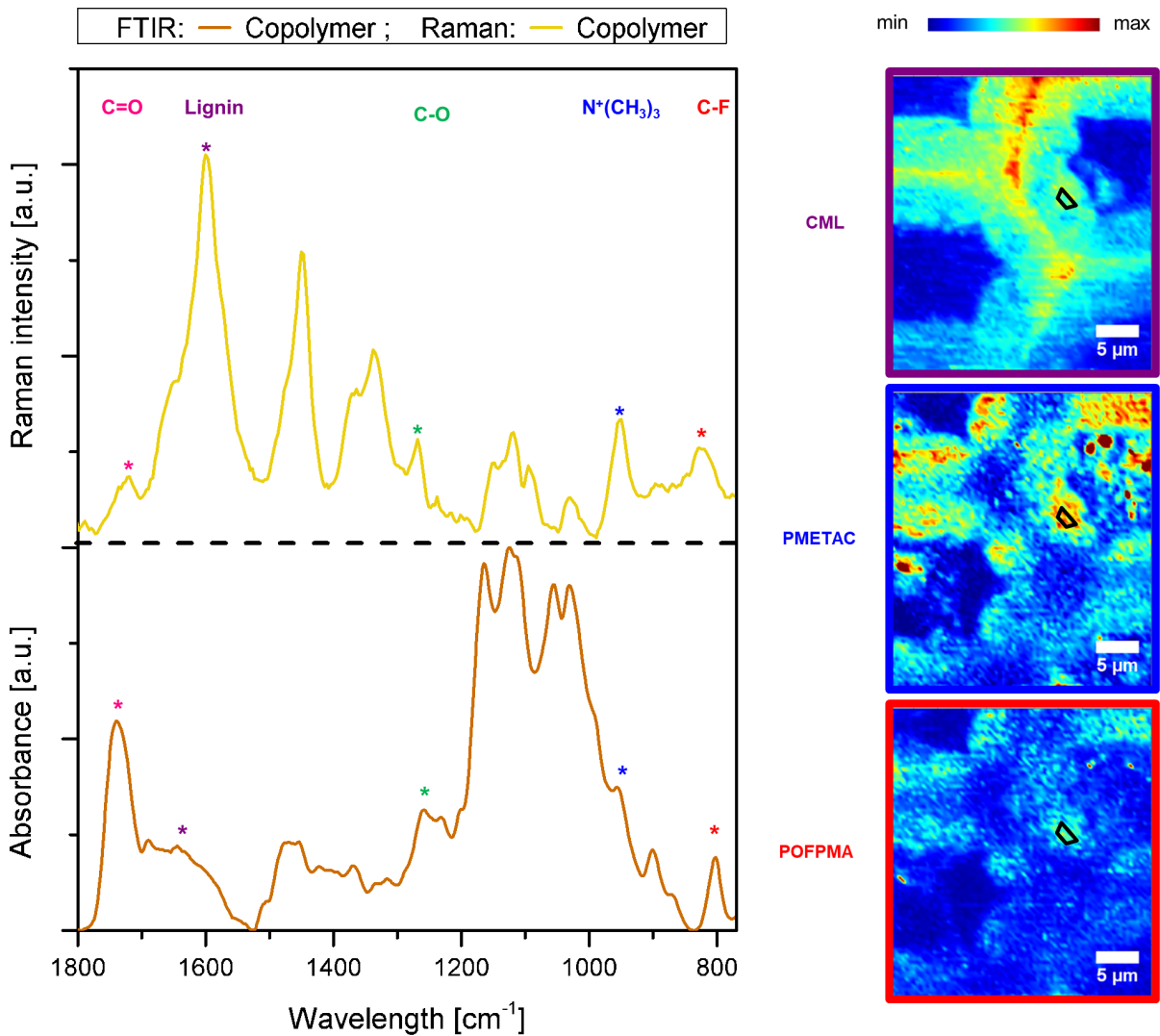


**Figure 4.8:** FTIR and Raman spectra of the copolymerized samples, and Raman mappings showing the distribution of the polymers in the wood scaffold.

close to  $0^\circ$  (W-copolymer A – short POFPMA chains) to  $145^\circ$  (W-copolymer C – longer POFPMA chains). This trend can be observed in Figure 4.9.

The control over surface wettability of materials is essential for various applications. Surfaces having a well-defined juxtaposition of charged and hydrophobic domains have been shown to have peculiar wettability properties, that are of interest for demanding oil/water separation challenges.<sup>98</sup> With the grafting of amphiphilic block copolymers, we have also shown that we can manipulate the surface wettability of a new substrate, wood. Since wood also possesses an anisotropic porous structure designed to transport liquids, similar to different devices produced for oil/water emulsion separation, we believe that a possible use for this modification could be in oil/water separation challenges. Nevertheless, further studies should be performed in order to confirm its possible

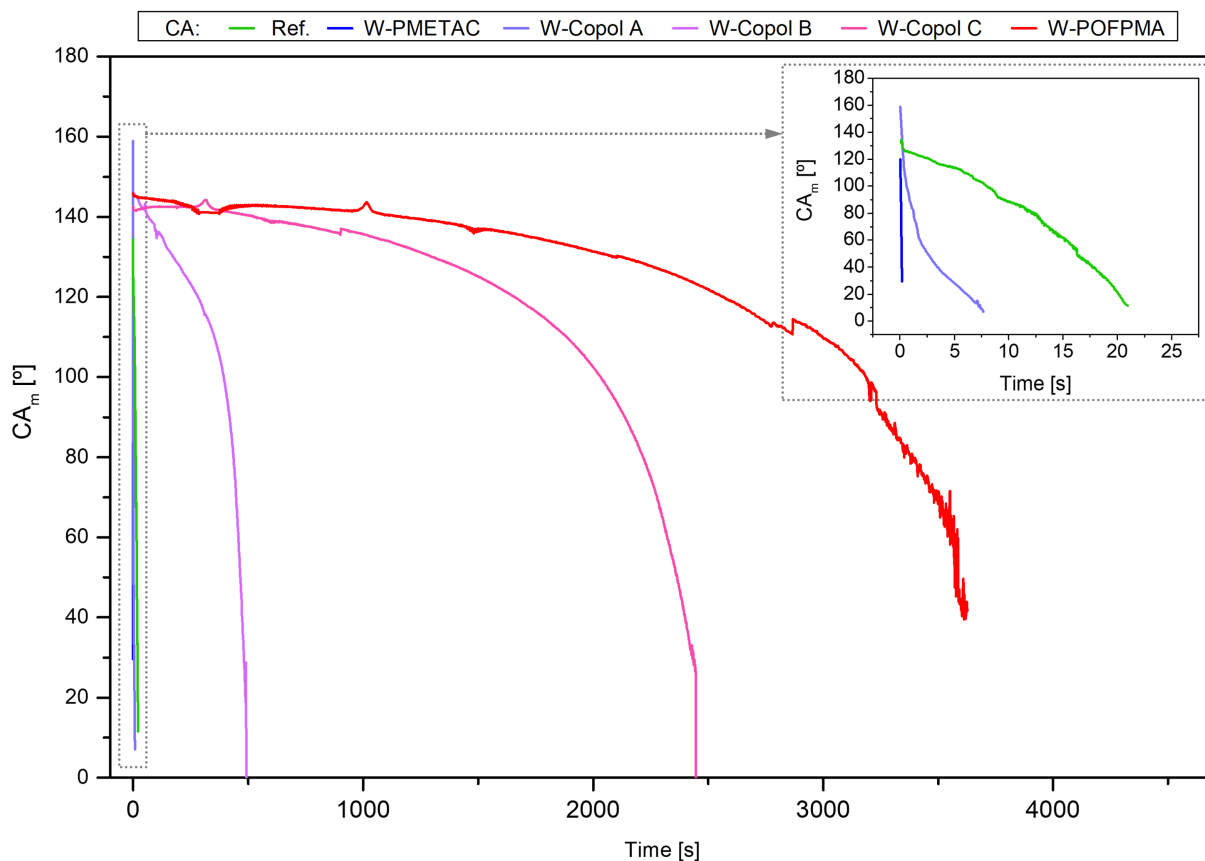


**Figure 4.9:** Contact angles (CA) through the sessile drop method of the unmodified wood (Ref.) and the different wood modifications with the corresponding WPG: PMETAC (30%), Copolymer A (30%PMETAC/9%POFPMA), Copolymer B (30%PMETAC/13%POFPMA), Copolymer C (30%PMETAC/22%POFPMA), and POFPMA (70%).

use in this field.

### 4.3. Conclusions

We demonstrated that SI-AGET-ATRP is a suitable method enabling the control over the grafting of polymer chains with various functionalities. Spruce wood samples were successfully modified through the homopolymerization of acrylates (METAC, bearing a quaternary amine, and OFPMA bearing a fluorinated side chain). Spectroscopy techniques confirmed the presence of the polymers in the bulk wood structure. In the case of PMETAC, the low WPGs obtained after polymerization resulted from electrostatic interactions generated by charged species (METAC and ATRP catalyst) affecting the full conversion of the monomers. To achieve the block copolymerization, it was necessary to screen the charges with a counter ion. The successful PMETAC chain extension with OFPMA was indirectly shown by the additional weight gain, the co-localization of PMETAC and POFPMA signals in the wood scaffold, and

finally by the changes in wettability. While W-PMETAC and W-OFPMA exhibit opposite and extreme wettabilities, we have shown that the variation of the ratio in between the hydrophilic and hydrophobic polymer block generates wood materials with wettability properties that lay between the two extremes.

The controlled grafting of block copolymers on bulk wood will contribute to the development of new wood-based advanced materials. In the future, we envisage a possible use of these copolymer-modified wood samples in oil/water separation applications. Besides, this study provides an example of grafting amphiphilic block copolymer brushes using monomers with antagonistic properties, which should be of interest to researchers preparing functional surfaces from other bio-based materials.

#### 4.4. Experimental section

##### *Materials*

Norway spruce (*Picea abies*) cross sections (1 mm thick and 20 mm diameter) were prepared from large wood cross sections obtained by circular saw cutting. Monomers [2-(Methacryloyloxy)ethyl]trimethylammonium chloride solution (METAC) and 2,2,3,3,4,4,5,5-Octafluoropentyl methacrylate (OFPMA), initiator  $\alpha$ -bromoisobutyryl bromide (BiBB), reducing agent Tin(II) 2-ethylhexanoate ( $\text{Sn}(\text{Oct})_2$ ), copper complex  $\text{Cu}(\text{II})\text{Br}_2$ , ligand N,N,N',N'',N'''-Pentamethyldiethylenetriamine (PMDETA), as well as the salt Sodium trifluoroacetate ( $\text{CF}_3\text{COONa}$ ) were purchased from Sigma-Aldrich and used as received. Pyridine (Py, anhydrous grade) and N,N-dimethylformamide (DMF, anhydrous grade) were purchased from VWR and used as received.

##### *Methods*

A table summarizing the reaction conditions for each reaction batch can be found in the Supplementary Information. **Synthesis of wood macroinitiator (W-Br).** Oven dried wood samples were placed under vacuum ( $10^{-2}$  mbar) in a Schlenk flask capped with a septum. A BiBB solution (in anhydrous pyridine) was added with a syringe. The amount of BiBB was calculated as 0.5 molar equivalent with wood glucopyranose equivalents (MW = 162 g/mol). The reaction was stirred at room temperature for 4h. The reacted wood discs were withdrawn, washed with methanol and sonicated in methanol and acetone to remove any unreacted material. After the washing, the discs (W-Br) were dried in an oven under vacuum at 65 °C until constant mass was reached.

**AGET SI-ATRP of OFPMA and METAC using W-Br as macroinitiator.** Both OFPMA and METAC were polymerized in DMF with the W-Br macroinitiator, using the following molar ratio: [Monomer]:[W-Br]:[ $\text{Cu}(\text{II})\text{Br}_2$ ]:[PMDETA]:[ $\text{Sn}(\text{Oct})_2$ ]=X:1:1:2:2, where X varied from 5 to 20. W-Br samples were placed in a Schlenk flask, capped with a septum, together with the  $\text{Cu}(\text{II})\text{Br}_2$ . The

flask was evacuated until it reached low vacuum (ca.  $10^{-2}$  mbar). DMF was added and the flask was placed in an oil bath at 80 °C. In a separate flask cooled with ice, ligand and monomer were dissolved in DMF. The content of the flask was sparged with nitrogen for an hour, and then added to the heated Schlenk flask containing the wood samples. The reducing agent ( $\text{Sn}(\text{Oct})_2$ ) was added slowly during the first 40h of polymerization using a syringe pump, and the total reaction time was 48h. The reacted wood discs were withdrawn, washed with ethanol and sonicated in ethanol and acetone, and water for PMETAC samples, to remove any unreacted material. After the washing, the discs were dried in an oven under vacuum at 65 °C until constant mass was reached. The samples produced in this step were named W-POFPMA and W-PMETAC, for the W-Br samples reacted with OFPMA and METAC respectively.

**W-PMETAC chain extension with OFPMA via SI-AGET-ATRP.** OFPMA was polymerized in DMF with various W-PMETAC samples as macroinitiators, using the following molar ratio: [Monomer]:[W-Br]:[Cu(II)Br<sub>2</sub>]:[PMDETA]:[Sn(Oct)<sub>2</sub>]=20:1:1:2:2. We followed the same reaction procedure used for the homopolymerization expect for the addition of salt. The salt concentration was calculated as molar equivalents to the concentration of PMETAC. We used different METAC/Salt ratios: 0.5, 1, 2, and 4.

**Synthesis of PMETAC-b-OFPMA amphiphilic block copolymers in solution.** PMETAC polymer chains were first polymerized in DMF, with EBriB as initiator, using the following molar ratio: [METAC]:[EBriB]:[Cu(II)Br<sub>2</sub>]:[PMDETA]:[Sn(Oct)<sub>2</sub>]=20:1:1:2:2. After 48 hours of reaction, where the reducing agent was fed for the first 40 h of reaction, the polymer was purified through repeated precipitations in acetone. Subsequently, POFPMA chains were grown from the alkyl bromide end groups on the PMETAC chains. The following molar ratio was used: [OFPMA]:[Br-PMETAC]:[Cu(II)Br<sub>2</sub>]:[PMDETA]:[Sn(Oct)<sub>2</sub>]=20:1:1:2:2, and sodium trifluoroacetate salt was added (Salt:METAC ratio of 2). After polymerization of OFPMA, the copolymer chains were purified through repeated precipitations in acetone.

### *Characterization*

**Weight Percent Gain (WPG) calculation.** The WPG represents the amount of modification introduced into the discs at each modification step. To estimate the WPG, the weight of the dried wood discs was measured before and after the modification.

**Monomer conversion calculation.** The monomer conversion represents the amount of monomer that polymerized in the wood sample. To estimate the monomer conversion, it was assumed that the increase in the wood's weight after the polymerization reaction was due only to the grafting of polymer onto the wood surface.

**Raman microscopy.** Wood samples were polished using a rotary microtome, removing the first 200  $\mu\text{m}$  of material. The measurements of the W-PMETAC and W-PMETAC-b-POFPMA reacted samples were performed with a confocal Raman microscope (Renishaw inVia, Wotton-under-Edge, England) using a 633 nm laser, a water immersion objective (Olympus, 60x, NA = 1) and a 600 l/mm grating. As mapping parameters, an integration time between 5 and 10s with circa 25 mW laser power, and a step width of 400 nm were used. The measurements of

the W-POFPMA reacted samples were performed with the same confocal Raman microscope using a 785 nm laser, an air objective (Leica, 50x, NA = 0.75) and a 600 l/mm grating. As mapping parameters, an integration time of 30s with circa 40 mW laser power, and a step width of 600 nm were used. The mappings of the homopolymers were obtained after cosmic ray removal and baseline correction of the spectra using Wire 4.1 software (Renishaw).

The average spectra of the regions of interest were obtained after cosmic ray removal with the Wire 4.1 software (Renishaw), using Cytospec, and were afterwards baseline corrected using concave rubberband correction method with the OPUS software (Bruker).

All Raman mappings were plotted using Cytospec.

**FTIR spectroscopy.** Fourier transform infrared spectroscopy (FTIR) measurements were conducted on a Tensor 27 (Bruker instruments) equipped with an ATR module. Spectra were baseline-corrected with the concave rubberband correction method and min-max normalized over the entire spectra in the OPUS software (Bruker).

**Contact angle.** Water contact angle measurements were performed using the sessile drop method (SD) on an OCA10 (Dataphysics) instrument in an acclimatized room at 20 °C. Water drops measured, of 6  $\mu$ L, were dispensed with the help of a thin needle (SNS 021/001, OD = 0.21 mm; ID = 0.11 mm; L = 51 mm, Dataphysics).

**GPC.** Gel permeation chromatography analysis of PMETAC and PMETAC-b-POFPMA were performed on an Agilent 1100 GPC using two "PFG linear M" columns from Polymer Standards Services (PSS), Germany, connected in series with an Agilent 1100 VWD/UV detector operated at 290 nm. Samples were eluted in 1,1,1,3,3,3-Hexafluoroisopropanol with 0.02 M Potassium Trifluoroacetate (KTFAC) at 1 mL/min and room temperature. Molecular weights were measured with respect to a PMMA standard calibration.

**NMR.**  $^1\text{H}$  NMR (300 MHz) spectra were recorded on a Bruker Advance III spectrometer. PMETAC spectra were recorded in  $\text{D}_2\text{O}$ , while PMETAC-b-POFPMA spectra were recorded in 1,1,1,3,3,3-Hexafluoroisopropanol- $\text{d}_2$ .

## Supplementary information

### S4.1: FTIR of the macroinitiator

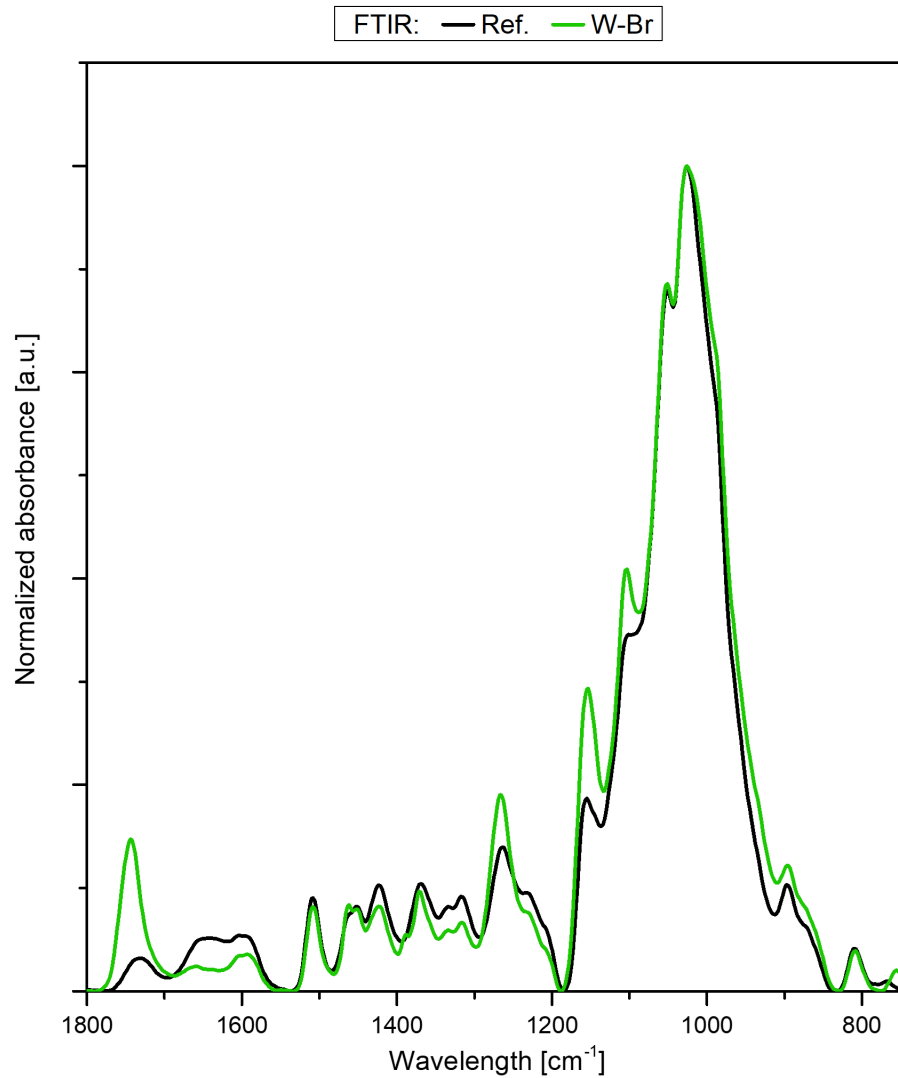


**Figure S4.1:** FTIR spectra of native wood (Ref) and the BiBB-modified wood (W-Br).

S4.2: NMR spectra of PMETAC and PMETAC-b-POFPMA polymer chains reacted in solution

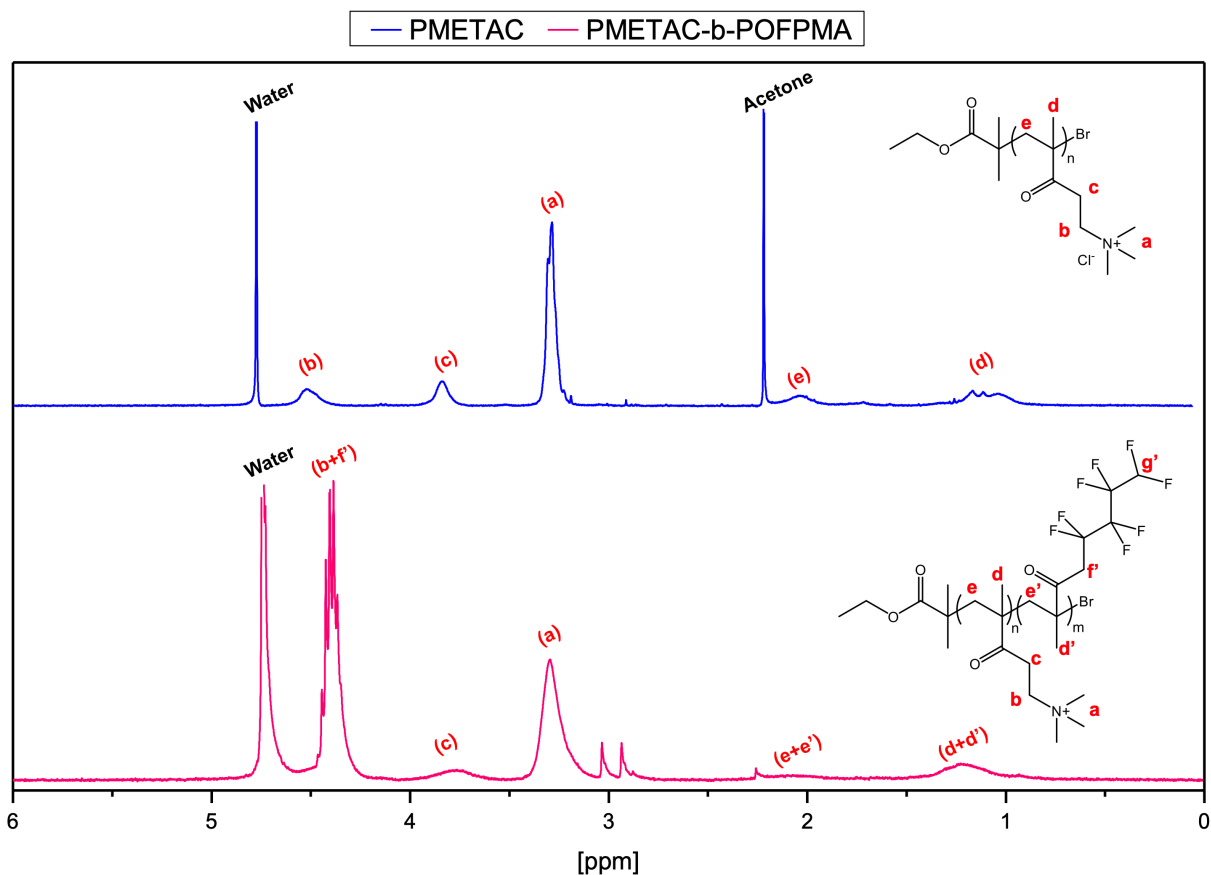


**Figure S4.2:** NMR spectra of PMETAC (top): (a) 3.3 ppm (b) 4.4 ppm, (c) 3.8 ppm, (d) 1.2 ppm, (e) 2 ppm. Typical broadening of polymer peaks visible. NMR spectra of PMETAC-b-POFPMA (bottom): (a) 3.3 ppm, (b) 4.4 ppm, (c) 3.8 ppm, (d+d') 1.2 ppm, (e+e') 2 ppm (f') 4.4 ppm. The secondary aliphatic hydrogens of the fluorinated chain are overlapping. The tertiary H of the fluorinated chain (g') is not visible anymore due to extreme broadening given by the strong coupling with the fluorine.

**S4.3: Table summarizing the different reaction conditions**

BiBB reaction	PMETAC polymerization			POFPMA polymerization			
	WPG <sub>BiBB</sub> (%)	Ratio [M]:[I]:[Cat]:[L]:[Red]	WPG <sub>PMETAC</sub> (%)	X <sub>PMETAC</sub> (%)	WPG <sub>POFPMA</sub> (%)	X <sub>POFPMA</sub> (%)	Ratio PMETAC:salt
09.39		5:1:1:2:2	22.43	37.76	06.86	02.45	1:02
12.69		5:1:1:2:2	19.72	25.30	-	-	-
08.74		10:1:1:2:2	15.97	14.35	06.69	02.41	1:02
08.97		10:1:1:2:2	17.98	15.77	08.44	03.02	1:02
10.73		10:1:1:2:2	13.73	10.24	-	-	-
11.57		10:1:1:2:2	16.98	11.82	06.28	01.77	1:04
13.55		10:1:1:2:2	16.17	09.79	07.30	01.78	1:01
14.12		10:1:1:2:2	15.35	08.96	09.11	02.12	1:0.5
20.68		10:1:1:2:2	29.78	12.55	-	-	-
08.79		20:1:1:2:2	13.91	06.22	19.46	03.05	1:02
16.63		20:1:1:2:2	29.17	07.39	-	-	-
19.56		20:1:1:2:2	30.62	06.76	-	-	-
20.37		20:1:1:2:2	23.25	04.96	-	-	-
27.65		20:1:1:2:2	27.79	04.63	-	-	-
31.44 <sup>a</sup>		20:1:1:2:2	33.98	05.13	-	-	-
11.56		-	-	-	49.91	12.00	-
12.84		-	-	-	46.27	10.16	N/A <sup>c1</sup>
13.96		-	-	-	57.70	11.77	N/A <sup>c2</sup>
14.79		-	-	-	64.53	12.51	N/A <sup>c3</sup>
14.36		-	-	-	75.50	15.02	N/A <sup>c4</sup>
10.76		-	-	-	41.03 <sup>b</sup>	14.07	-

<sup>a</sup> This BiBB reaction was performed twice under the same reaction time and conditions (4h each time).

<sup>b</sup> In this polymerization, the targeted DP was of 15. In all the rest of POFPMA polymerizations, both homopolymerization and copolymerization, the targeted DP was of 20.

<sup>c1,2,3,4</sup> Equivalence in salt concentration to Salt:PMETAC ratio of 0.5, 1, 2, and 4.



# Chapter 5

## Oil/Water Separation with Functionalized Wood-based Membranes

The use of bio-based materials for oil/water separation has been of increasing interest in the past years. We have previously reported on the use of native wood for the separation of free oil/water mixtures. However, this system does not allow for the separation of oil/water emulsions. In our last work, we reported on the modification of wood with amphiphilic block copolymers (a polyelectrolyte and a fluorinated block) and on the control of the spatial distribution of the polymers in wood using different solvents. In this chapter, preliminary work regarding the combination of these two last studies will be presented for the separation of oil/water emulsions.

## **5.1. Results and Discussion**

In previous work, we have shown that the hierarchical porous structure of wood is capable of separating free oil/water mixtures thanks to capillary forces in the wood structure.<sup>35</sup> These capillary forces allow a water layer to be retained on top of the wood structure, which in turn repels the oil phase, due to immiscibility of the two liquids. However, in oil/water emulsions, especially with the use of surfactants, the dispersed phase shows enhanced affinity towards the continuous phase, forming a macroscopically homogeneous phase. Therefore, unmodified wood is not capable of separating them.

### **5.1.1. Characteristics of the wood-based membrane for oil/water separation**

A common chemical composition used for oil/water separation devices is based on the combination of a hydrophilic polyelectrolyte and a fluorinated compound.<sup>98,101</sup> According to literature, in order to successfully separate emulsions by repelling the oil and allowing the water to pass through, the charged and fluorinated domains need to be organized in a specific manner. One possible path is to produce a block copolymer with the hydrophilic polyelectrolyte grafted onto the surface of the wood, followed by a thick fluorinated polymer layer. This polymer layer should be thick enough to retain the oil (long aliphatic chains) but still allow the water (a very small molecule) to pass through the defects of the fluorinated layer. Once the water passes through the defects of the fluorinated layer it would be rapidly absorbed by the underlying superhydrophilic polyelectrolyte layer, and would flow through the wood scaffold. This phenomenon is schematized in Figure 5.1.

In order to successfully modify the wood for oil/water emulsion separation, two main parameters need to be understood. It has been shown that the position of the modification in the wood scaffold plays an important role for the final properties of the modified material.<sup>26,27</sup> Previously, we have shown that through the use of different solvents, it is possible to control the spatial distribution of the ATRP initiator enabling the control over the spatial distribution of the

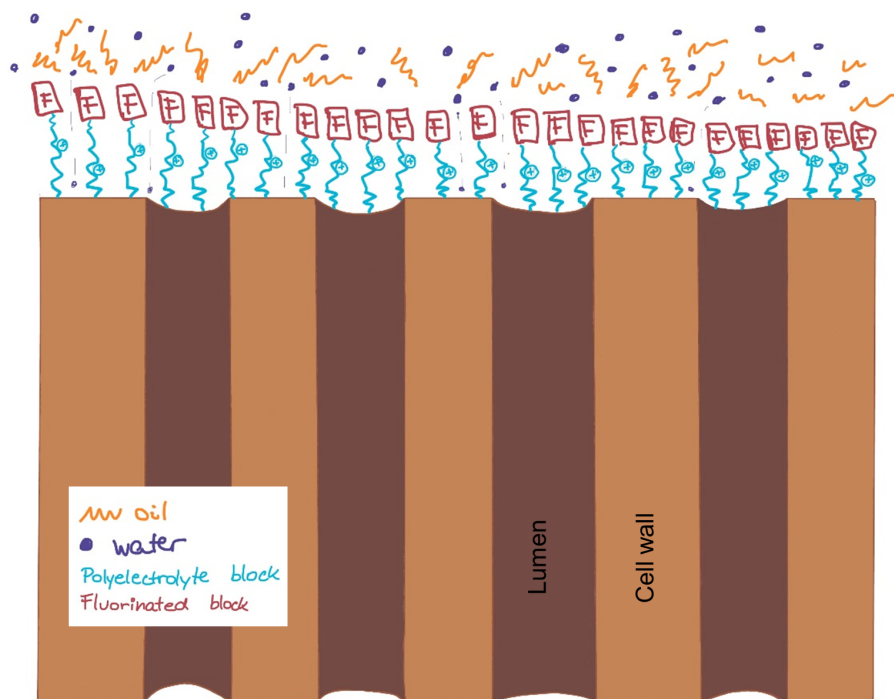


**Figure 5.1:** Scheme of the oil/water separation on the block copolymerized wood scaffolds.

polymer modification.<sup>222</sup> The other parameter was shown in a consecutive study, where we demonstrated that SI-AGET-ATRP allows for the control of the copolymerization reaction enabling different wettability performances of the modified wood.<sup>252</sup> By the combination of these two works, we expect to produce a wood cross section that is capable of separating oil/water emulsions.

The key parameters for oil/water emulsion separation are the membrane's pore size and chemical composition. For oil/water emulsions, both type of separation phenomena take place: physical (size exclusion) and chemical (intermolecular interactions). Although chemical modification can bring the adequate chemical functionalities for oil/water separation, the size of the emulsions separated will depend on the pore size of the membrane.

Through these studies, we have seen that high WPG of BiBB can result in swelling of the wood structure, thereby reducing the pore sizes. This could allow for a separation of smaller droplet sized emulsions. Nevertheless, given the size of our lumina (the membrane's pores) we do not expect to be capable of separating emulsions with sizes below 20  $\mu\text{m}$ .

### 5.1.2. Preliminary membrane characterization

In the following section the preliminary results obtained regarding the separation of free oil/water mixtures and oil/water emulsions with the copolymer-modified wood-based membranes will be discussed.

#### 5.1.2.1. Membrane wettability properties

Before starting with the emulsions, the wettability properties of the membrane were analyzed. In previous work we showed the contact angles obtained for the different membranes (Copolymers A (30%PMETAC/ 9%POFPMA), B (30%PMETAC/ 13%POFPMA), and C (30%PMETAC/ 22%POFPMA)).<sup>252</sup> The resulting contact angles ranged from more hydrophilic than unmodified wood to almost as hydrophobic as pure POFPMA.

In this work, we have tested the underwater oil contact angle (OCA) and the underwater oil-sliding angle (OSA), through the captive bubble method (CB) on the same membranes. In Figure 5.2, both results are shown.

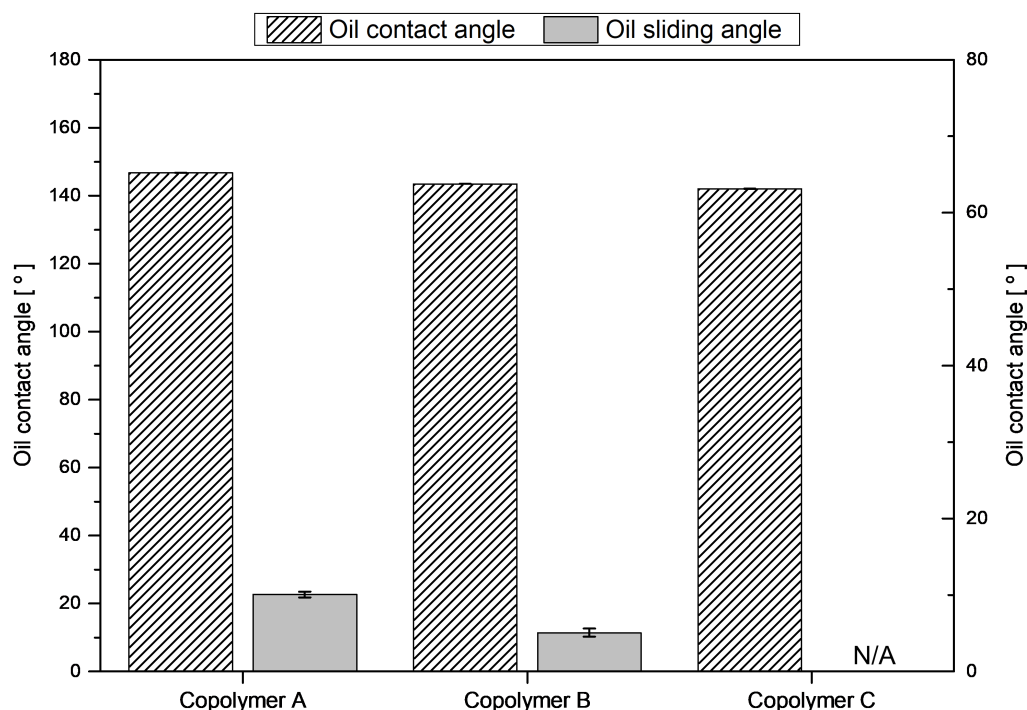


**Figure 5.2:** OCA and OSA for the three copolymer-modified wood-based membranes (Copolymer A, Copolymer B, and Copolymer C).

The OCA values remain more or less the same for all Copolymers approximately at 145°, like seen for unmodified wood, the OSA decreases as the concentration of POFPMA in the sample increases. We would expect a lower OSA value for copolymer C; however, due to the high concentration of POFPMA in the sample, the disc macroscopically bends making it impossible to measure the OSA properly.

Given the OCA and OSA results, our modified wood-based membranes should theoretically be capable of separating emulsions.

### **5.1.2.2. Free oil/water separation**

Before attempting to separate emulsions, the modified wood-based membranes separation performance was tested for free oil/water mixtures. The oil was dyed in red following previous procedures, in order to detect any traces in the permeate.<sup>35</sup> The results showed a completely clear permeate indicating that no oil or only oil in the concentrations in the ppm range was present. This was expected given the similar OCA and OSA values obtained for the membranes. However, characterization of the permeate by GC-FID, to corroborate this data is needed. Contrarily, due to the modification with POFPMA the flux reduced noticeable, with the separation time for 10 mL feed increasing from a few minutes to several hours (circa 4 hours). This was also expected from the water contact angle results shown in previous work, where the water drop (3  $\mu$ L) took more than 45 min to be absorbed with sample copolymer C.<sup>222</sup>

### **5.1.2.3. Production and separation of oil/water emulsions**

For oil/water emulsion separation, stable emulsions (long enough to be characterized and measured) are needed. Given that the separation of emulsions is partially restricted by the pore size of the membrane, and we are limited in modifying the pore size of our membrane, in order to properly characterize our membrane, the separation needs to be tested with a wide range of emulsion sizes. The production of oil/water emulsions is a difficult task.

Literature on the topic is limited, and it is difficult to find a consensus on the correct parameters to produce stable emulsions.<sup>63,135,253</sup>

Nevertheless, we produced oil-in-water emulsions of sizes ranging from approximately 300 nm to 50  $\mu\text{m}$  (see Experimental Section for more information). Given the experimental testing time required to produce stable emulsions, the results shown in this chapter are only preliminary results. Therefore, some emulsions were just characterized by white light microscopy methods.

The different emulsions produced were stable for different amounts of time, ranging from a few hours to a month depending on their size (longer time for smaller droplet size emulsions). In order to produce the emulsions, equipment providing different shearing forces was used (magnetic stirring, vortex, and bath and probe sonication) with various concentrations of different emulsifiers. Larger emulsion sizes were obtained through magnetic stirring at different concentrations of Tween20 (surfactant). However, the emulsions were stable for less than an hour, which is too short to be able to characterize and test them (circa 5 hours needed). Through vortex, emulsions in the micrometer range, using again Tween20, were obtained (circa 50  $\mu\text{m}$  droplet diameter). These were stable for approximately 3 hours; therefore, as the separation without applying any external force (pressure) takes approximately 4 hours, parts of the emulsion were already unstable when separated. An example image of the emulsions before and after separation, analyzed by white light microscopy, is shown in Figure 5.3. Although it seems that certain sizes could have been separated (below circa 10  $\mu\text{m}$ ), the results are not conclusive, as the emulsions were not stable.

By using bath and probe sonication, the emulsions obtained had sizes ranging between circa 300 nm and 3  $\mu\text{m}$ , with different sodium dodecyl sulfate (SDS) concentrations. The emulsions were produced at three different concentrations 10:90, 30:70, and 50:50 v/v oil/water and SDS concentrations ranging from 0.1 to 0.5 mg SDS per mL. These emulsions were stable for a period of at least one month. The different sizes of the emulsions produced are shown in Figure 5.4.

Whereas, it was possible to produce emulsions by just bath sonication for the

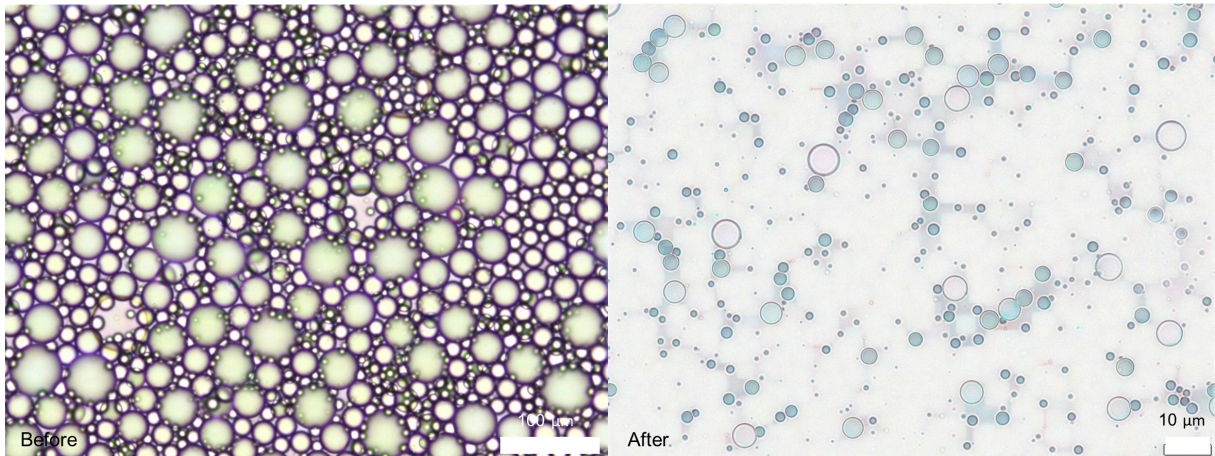


**Figure 5.3:** White light microscopy images of the Tween20 vortex-produced emulsions before and after separation (left scale bar 100  $\mu\text{m}$ , right scale bar 10  $\mu\text{m}$ ).

10:90 and 30:70 v/v oil/water, for the 50:50 v/v oil/water emulsions probe sonication was needed. The result an droplet size range from 300 nm to 1.5  $\mu\text{m}$  for the former group of emulsions, regardless of the emulsifier concentration, whereas the latter ones (also regardless of the SDS concentration) had droplet sizes between circa 800 nm and 2  $\mu\text{m}$ , as shown in Figure 5.4.

While these emulsions were stable enough to be tested with the modified

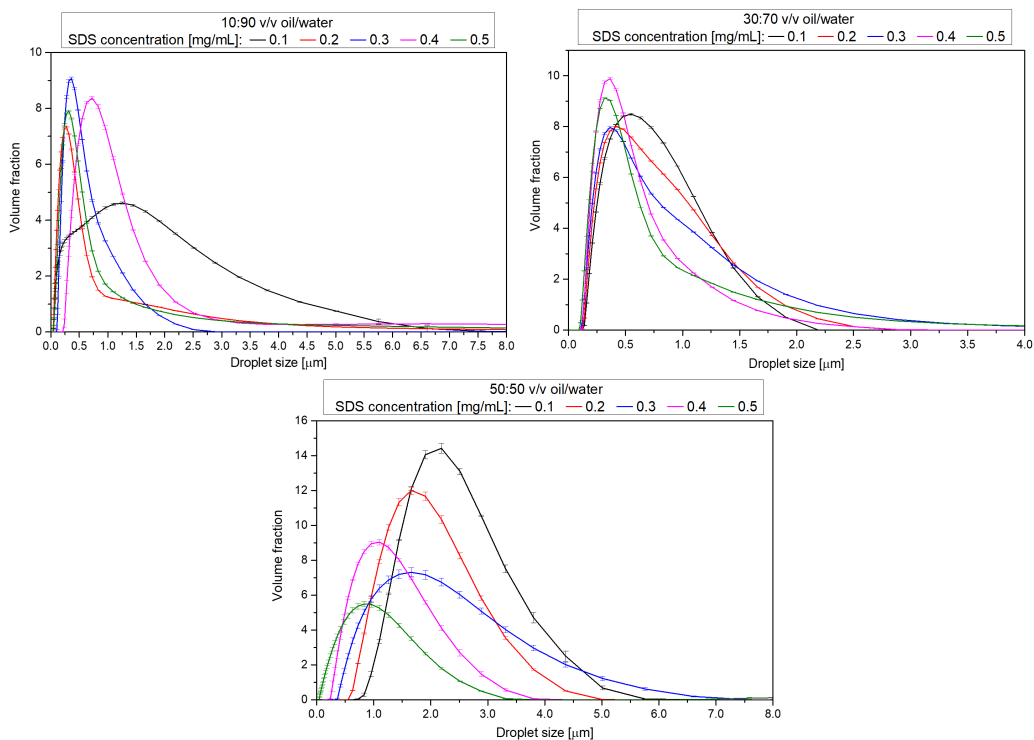


**Figure 5.4:** Emulsions droplet size of the SDS bath and probe sonication-produced emulsions, measured by small-angle light scattering.

wood-based membrane, the size ranges were too small to be separated and no differences before and after separation were observed. In future work, emulsions with bigger droplet sizes would need to be produced in order to properly test the performance of the membrane.

### 5.2. Conclusions

From this preliminary work, it can be concluded that as for the unmodified wood, copolymer-modified wood-based membranes are capable of separating free oil/water mixtures. While the separation probably yields high separation efficiencies, the flux seems to decrease considerably.

Conversely, from the preliminary results copolymer-modified wood-based membranes should be capable of separating emulsions with sizes above at least 20  $\mu\text{m}$ . Nevertheless, all these results are preliminary and further work should be carried out in order to obtain more conclusive data.

### 5.3. Experimental section

**Materials.** Copolymer-modified Norway spruce (*Picea abies*) cross sections (1 mm thick and 20 mm diameter) were prepared in previous work.<sup>222</sup> Throughout the experiments, the samples had similar EW/LW distribution. Prior to any separation experiment, the samples were soaked in water under vacuum to assure they were in a fully hydrated state.

The oil used was hexadecane (Sigma-Aldrich, >99%). Red dye Sudan III (Fluka A.G.) was used to dye the oil. The surfactants used for oil/water emulsion experiments were sodium dodecyl sulfate (SDS, Sigma-Aldrich) and Tween20 (Sigma Aldrich). All chemicals were used as received.

**Separation experiments.** The wetted wood cross section disks (1 mm thick, 2 cm diameter) were placed between two glass tubes held by a clamp. Rubber O-rings guaranteed a proper sealing between the equipment and the wood. The oil/water mixtures (50 v/v) were poured simultaneously in the upper tube. The separation was driven only by gravity; no external pressure was applied. The same procedure was followed for the oil/water emulsions. The amount of oil in the permeate was visually inspected.

**Oil contact angle (OCA) and oil sliding angle (OSA).** Oil contact angles and oil sliding angles were measured on an OCA20 (Dataphysics) instrument, installed in a climate room



with 65% humidity, at 20 °C. Wood samples were completely soaked with water prior to the experiments. The underwater measurements were performed using a glass cuvette filled with MilliQ water and the captive bubble (CB) technique. A thin curved needle (SNC 021/011 with OD = 0.21 mm; ID = 0.114 mm; Length = 57 mm; Width = 10 mm; Upwards = 7 mm, Dataphysics) was used to control the oil drop placement and size under the wood. Drops of 10 µL were used for these measurements.

**Oil-in-water emulsions.** Oil-in-water emulsions were produced in the presence of SDS with oil/water concentrations of 10:90, 30:70, and 50:50 v:v. The SDS concentrations used to produce these emulsions ranged from 0.1 to 0.5 mg/mL. The 10:90 and 30:70 v/v emulsions were produced through bath sonication at 60 °C overnight, using HUBERLAB SW 6H (400 W). The 50:50 v/v emulsions were produced through probe sonication, using Ultrasonichorn (450 W, Branson). The emulsions through probe sonication were produced with a power of circa 60 W in intervals of 0.5 seconds. The samples were sonicated for a period of 10 min.

Oil-in-water emulsions were produced in the presence of Tween20 using a Vortex instrument. The samples were produced with a 30:70 v/v ratio of oil in water and 5% w/w concentration of Tween20. The emulsions were sonicated for 10 min. Oil-in-water emulsions were produced in the presence of Tween20 by stirring at 1500 rpm. The samples were produced with 3 mg of Tween20 per milliliter with different oil to water ratios ranging from 10:90 to 50:50 v/v. Another batch of emulsions was produced through stirring with 20:80 v/v ratio of oil to water and different Tween20 concentrations, which ranged from 0.1 to 0.5 mg of Tween per milliliter.

**Emulsion characterization.** The emulsions were characterized using a white light microscope (Olympus BX51) and a small-angle light scattering instrument (Mettler Toledo). For both measurements, the samples were diluted before measuring.



# Chapter 6

## Continuous Oil/Water Separation System

In order to use a separation system at an industrial scale, the system needs to be easily scalable and economically viable (energy and material consumption). Continuous systems are most of the times the best option. In this chapter, we discuss the challenges of producing a continuous system for oil/water separation, our designing ideas to overcome these challenges, and the actual state of the continuous separation system design.

## **6.1. Design of the separation system**

In oil water separation, where the separation takes place vertically (i.e. dead-end configuration), one of the phases accumulates on top of the membrane. As shown previously, at a certain point, as the repelled phase keeps accumulating, the pressure exerted by the liquid column on the membrane reaches the breakthrough pressure and the separation no longer takes place. Moreover, if the separation should take place in large quantities (assuming an infinite value of breakthrough pressure) one would need an infinite amount of material to hold the liquid column on the membrane. As both cases are not feasible, there is a need of extracting this liquid column from the system. Another important parameter to be considered is good contact of the feed with the membrane surface in order for the separation to take place.

### **6.1.1. Lab-scale separation system**

Having these two features in mind, we produced a new separation system device. The novelty lays on the membrane holder, which has a feeding tube that finishes close to the surface of the membrane (unmodified and modified wood) and an exit for the concentrate, oil in our case, on the top of the membrane holder. This should allow for a good contact of the feed (contaminated water) with the membrane and the withdrawal of the accumulating phase (oil). The wood-based membrane is compressed between the top part of the holder and a perforated grid to allow the permeate (purified water) to pass through, avoiding any leak of the feed and concentrate through possible gaps between the holder and the membrane. To further adjust the wood in the separation holder, rubber O-rings may be used. A detailed scheme for the sample holder and the oil/water separation process taking place in the holder is shown in Figure 6.1.

For the separation to take place continuously, the separation holder needs to be mounted in series with other equipment (pumping system, valves, indicators – for pressure, temperature, and flow – and tanks, piping, etc.). For the lab-scaled

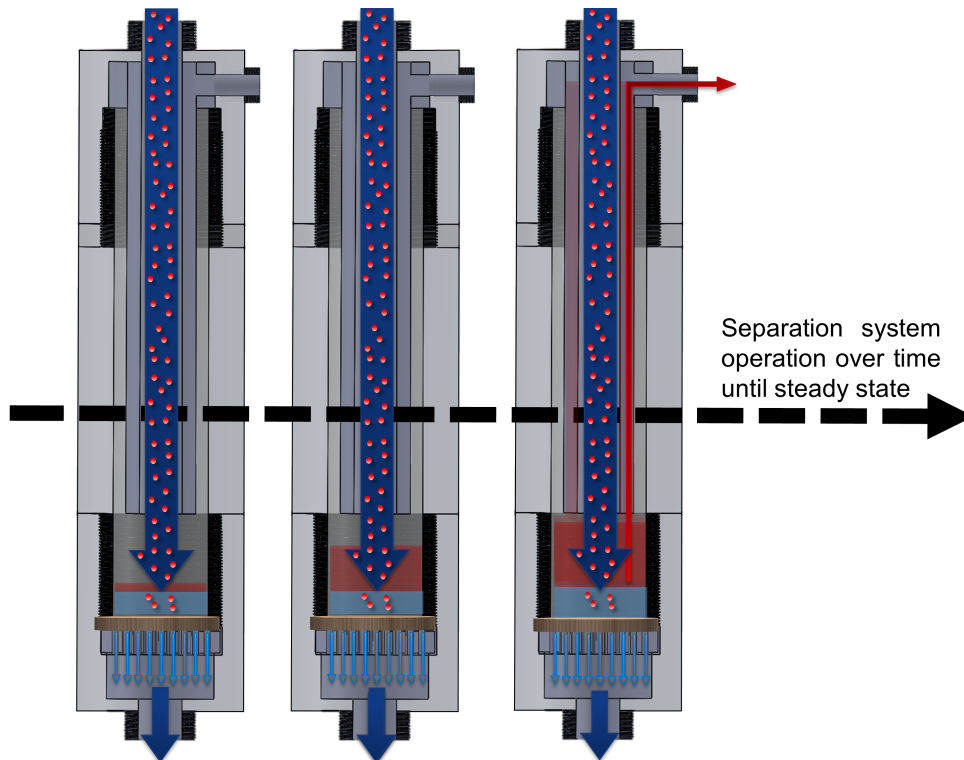


**Figure 6.1:** Schematic representation of the wood holder system. Water and oil represented in blue and red, respectively.

system, given the small flows, compressed air was selected as the pumping system. In order to control the flux and monitor any possible fouling, two pressure indicators are needed. To control the flux the pressure indicator at the feed should have a feedback loop to the valve controlling the feed flow. The process and instrumentation diagram (P&ID) of the designed scale-up system is shown in Figure 6.2. This P&ID considers possible cycle tests that could be desired in the future, thus the recycling loop.

With the designed system, apart from allowing testing the amount of separation cycles the membrane can tolerate before suffering from fouling, it would be also possible to sample if the separation efficiency decreases during the cycle test.

Before using this complex system, it was decided to try separating 2 L of contaminated water without recycling nor complex control loops. The actual separation system is shown in Figure 6.3.

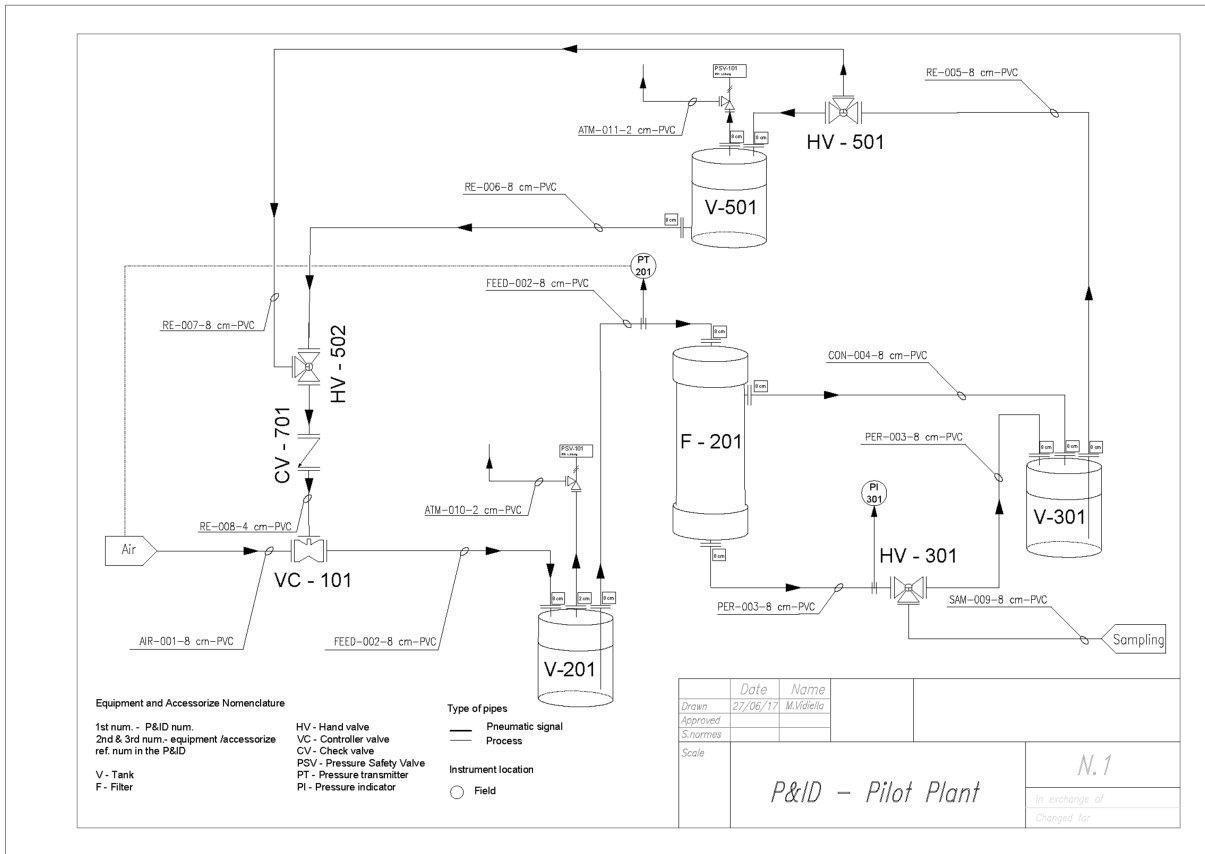


**Figure 6.2:** P&ID of the pilot plant (continuous operation) in cycle test mode. Pipes are correspondingly: feed (FEED), concentrate (CON), permeate (PER), recycle (RE), atmosphere (ATM), and sampling (SAM). The size and material is also given.

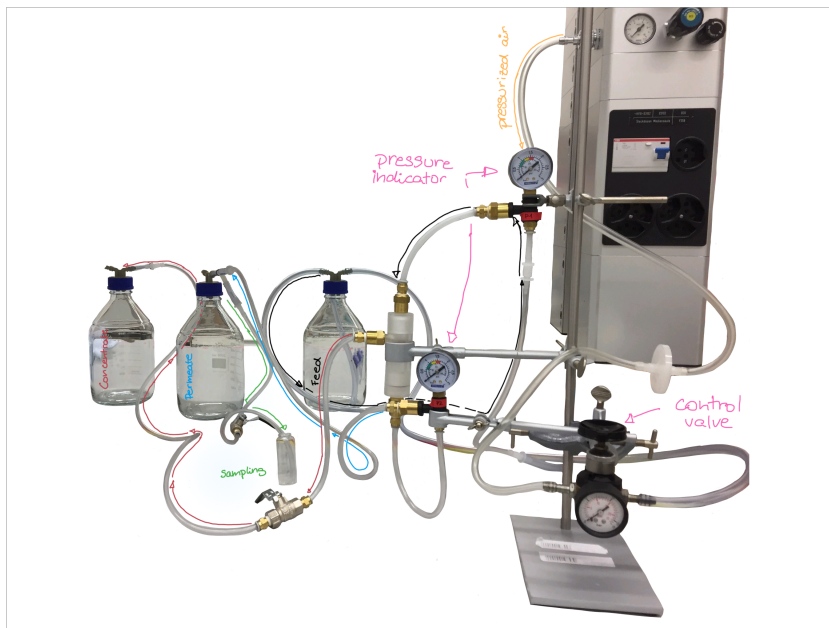


**Figure 6.3:** Image of the lab-scale separation system.

#### 6.1.1.1. Separation experiments on the lab-scale separation system

From preliminary results with the separation system shown in Figure 6.3, it was seen that it was not possible to use the separation system without a precise pressure control loop. Given the different physicochemical properties of oil and water, it was very difficult to control the pressure exercised without an adequate system. Small fluctuations in the feeding pressure would result in both liquids passing through the membrane. This is possibly also due to the  $P_B$  of our membranes with oil, which in the case of hexadecane was experimentally measured as of  $2.64 \pm 0.13$  kPa, i.e.  $2.65 \times 10^{-2}$  bar. Industrial separation systems operate between 0.5 and 1 bar. This low  $P_B$  gives small error margin and thus cannot be controlled with a manual valve.

#### 6.1.2. Separation system scale-up for industrialization

Following the drawing in Figure 6.2, it is possible to observe that the actual lab-scale separation system is mostly similar to an industrial water treatment process. One of the differences would be the pumping method, which can be easily exchanged. The other part of equipment that would need to be modified would be the membrane holder. Therefore, we expect to be able to scale up our laboratory system by only slightly modifying the membrane holder. Given the thickness of the membrane, determined as a trade-off between tracheid length and mechanical stability of the wood scaffold, the membranes are restricted in diameter (radial and tangential direction in wood structure). A possible way of increasing the active surface while maintaining mechanical stability is increasing the number of wood discs used in a membrane holder. The wood discs would have to be placed between a grid with holes close to the diameter of the discs on the top (side in contact with the feed and concentrate) and smaller holes on the bottom that would still allow water to flow. A scheme of this up-scaled membrane holder can be seen in Figure 6.4. A parameter that would be important to have in mind is the height of the membrane holder, which should not exceed 35 cm (estimated breakthrough pressure for spruce wood). The sample holder sketched in Figure 6.4 was designed to be one meter

in diameter, which would accommodate approximately 210 wood-based membrane samples.

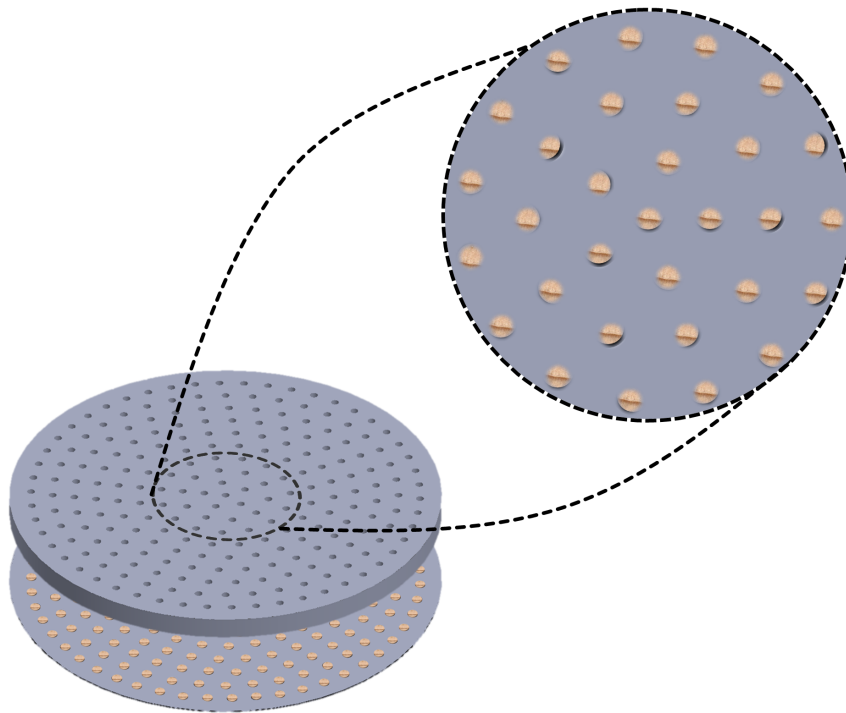


**Figure 6.4:** Schematic representation of the possible scale-up membrane holder.

Another possibility is to change the type of separation from dead-end to cross-flow. This would allow for an easier control over the pressure of feed.

## 6.2. Conclusions

From the preliminary work performed on the lab-scale system, we can conclude that a good pressure control is essential to operate the system in a dead-end configuration. To scale-up the system to an industrial water treatment plant, a few modifications would be necessary after promising results would have been achieved on the lab-scale system. Given the low breakthrough pressure of the wood membrane, if it is not possible to scale-up the system while controlling the pressure using the dead-end configuration, a cross-flow configuration could be used instead.



# Chapter 7

## General Discussion and Conclusion

The main aim of this thesis was to use wood as a scaffold for oil/water separation. As the most promising current devices for this application are membranes, one should have in mind their physical properties when choosing the wood species that will be used as a scaffold. Therefore, ideally the wood species of choice should have a structure formed with a narrow lumen size distribution (the membrane's pores). Comparing softwoods with hardwoods, the former ones tend to have narrower lumen size distributions (considering earlywood and latewood distributions separately).<sup>14</sup> Another important factor, when choosing the wood species, is the amount of extractives; as they can interact with the oil/water system and possibly with wood modification reactions, lower amounts would be desired. Species inhabiting in temperate zones tend to have lower amounts of extractives compared to tropical wood species.<sup>254</sup>

Spruce wood (*Picea abies*) is a species that fulfills the abovementioned requirements. Moreover, it is highly abundant in Switzerland and is one of the most studied wood species. Therefore, even though there could be other eligible wood species, with narrower lumen size distributions, spruce wood seemed to be a good candidate for this work.

## **7.1. Oil/water separation with native wood**

Many concepts used for oil/water separation have been inspired by nature.<sup>104,105,110,255</sup> Several articles have shown different materials that are capable of separating free oil/water mixtures, due to existing capillary forces formed in their structure.<sup>101,117,131,150,179,256</sup> In our first work (see Chapter 2), we showed that the structure of wood is also exhibiting these capillary forces, maintaining a water layer on the surface that can repel oil. It achieved high fluxes, and high separation efficiencies with low fouling. The efficiencies were based on the capability of generating these capillary forces and the immiscibility of oil with water. An important parameter to study, related to the capillary forces, was the breakthrough pressure, which is the pressure at which the capillary forces are exceeded. At that point, the water layer is no longer retained, thus, the oil is not repelled and passes through the membrane.

The breakthrough pressure depends on the interaction between the oil with water (oil/water interfacial tension,  $\gamma_{12}$ ) and the structure of the material, wood in our case (see Equation 2.1 and Figure S2.2 for more information). Surprisingly, by theoretically estimating the breakthrough pressure for different wood species it was seen that similar results for the separation of free oil/water mixtures with different wood species could be obtained (only beech wood was tested experimentally within the study). We could conclude that wood species with structural ratios between  $2R$  and  $2D$  (pore sizes and cell wall thicknesses) in the range of spruce could be possible candidates for the separation of free oil/water mixtures (not the case for oil/water emulsions). The use of local species could allow for the separation of free oil/water mixtures in the region of need by simply cutting wood cross sections of the available tree species. This could have a great impact; especially in developing countries where economic resources are scarce and imports expensive.

The wood pieces can be prepared by different processing techniques, leading to different surface roughness: microtome blade, circular saw, sanding, and band saw. In an earlier stage of the study, the separation efficiency of

wood produced by the different processing techniques was investigated. No remarkable differences in separation efficiency nor fluxes were detected, with the concentration of hexadecane (C16) detected in the permeate always below 10 ppm, except in the cases where the samples were macroscopically destroyed, e.g. during the band saw cutting process.

However, due to the different surface roughness created by these techniques, we expected that there may be some differences in terms of resistance to fouling. The exposure of broken fibers (sticking out of the cross-section plane) to the oil, e.g. in samples prepared by circular or band saw cutting, could result in greater fouling of the sample. We observed different oil sliding angle values (OSA) between the earlywood and the latewood regions. These differences were also observed with contact angle measurements (SD) between these two wood regions, which correlates with the work from Wang et.al.<sup>257</sup> We believe these observations between earlywood and latewood CA could be extended to different surface roughness produced by the different processing techniques.

Comparing different devices on the market is always difficult. There is usually a trade-off in terms of performance (efficiency, breakthrough pressure, flux, and emulsion size separated), which can be tuned by the different parameters that characterize a membrane: membrane pore size, oil contact angle (OCA), oil sliding angle (OSA) or adhesion forces (fouling properties), and wettability.

For instance, in order to achieve high fluxes, large pore sizes are needed, which can result in low breakthrough pressures. Contrarily, smaller pores, which can separate smaller emulsion sizes, can result in the need of applying high pressure for one of the phases to pass through the membrane.

Different procedures are used to measure the pore sizes, fluxes and breakthrough pressures (also called intrusion liquid pressure), which also complicates the comparison between devices. In many cases, some of the parameters cannot be accurately measured, such as pore sizes in inhomogeneous materials.<sup>117,131,150,153,179,256,257</sup>

Nevertheless, a comparison of the native wood performance to other devices available on the market shows that a good trade-off is found for each of

the native wood membrane's characteristic performance parameters for the separation of free oil/water mixtures. The fluxes of membranes available in literature range from 83 to 25 200 Lm<sup>-2</sup>h<sup>-1</sup>. Wood can reach fluxes of 3 500 to 6 500 Lm<sup>-2</sup>h<sup>-1</sup> while achieving breakthrough pressures of 2.64 to 2.12 kPa (ranges from 1 to 17 kPa in literature). However, given the high surface energy of wood and its pore size, it is not capable of separating emulsions, whereas other devices can.<sup>135</sup>

Many different synthetic and natural materials have been reported to be able to separate oil from water thanks to capillary forces.<sup>104,105,110,255</sup> These devices come with a wide range of pore sizes (from 1 to 50 μm in diameter) and in a variety of chemical compositions, which can have different surface energies and structures. All of them are capable of separating free oil/water mixtures; some of them also claim to be capable of separating emulsions. In oil/water separation, especially in the form of emulsion, the most important factor is the surface energy of the separating device. To repel oil under air, the surface energy of the repelling material has to be lower than the surface tension of oil (20 to 30 mN/m).<sup>106</sup> The lowest surface energies are achieved by using fluorinated compounds to modify the surface of the membrane scaffold, and by introducing re-entrant structures into the scaffold. The surface energy of wood is typically between 30 and 50 mN/m.<sup>84</sup> Therefore, when the oil is emulsified in water, it is difficult to separate oil from water without the presence of fluorinated compounds, by simple immiscibility of oil with water. Some of the materials cited previously contain fluorinated compounds in their structure,<sup>101,135</sup> thus, in principle they should be able to separate oil/water emulsions.

In terms of the range of oil droplet sizes the materials can separate, there is a strong dependency on the pore size of the membrane, as the oil needs to get in contact with the fluorinated compounds present in the material's structure. There are several examples in literature where it is not clear whether the membranes proposed can separate emulsions of the droplet sizes suggested, as there is no or not sufficient information regarding the pore size of the membrane.<sup>135,151,258,259</sup>

With most of these articles, it is difficult to reproduce the data following the emulsion preparation procedures, because of missing information (shearing method and its operation conditions, amount of surfactant, and ratio of oil and water used). Moreover, in some cases, where all the relevant information is mentioned,<sup>101,258</sup> the emulsions are not stable for more than a few minutes. Therefore, the results, in those cases, refer rather to free oil/water mixtures than to emulsions.

Another problem concerning the reliability of the results in terms of emulsion separation, thus hindering the comparison between devices, is related to the methods used to characterize the efficiency of the membrane for such purposes. The methods used range from simple white light microscopy observations to infrared spectrometer oil content analyzer.<sup>101,136,155,256,260–262</sup>

Characterization of emulsion separation through white light microscopy is questionable for determining the membrane's efficiency, as it is a very imprecise technique for this kind of measurement. It could likely be that the observed region is not representative for the entire sample. Moreover, this technique does not give any information in terms of mass content. The efficiency is just deduced from the ratio between the number of droplets of a certain size visible before and after the separation. Therefore, this method does not take into account the breakage and coalescence of the droplets. This phenomenon could take place by shearing of the emulsion due to membrane pore size constraints. Therefore, one could possibly conclude that a certain emulsion size is separated when in fact there has only been a breakage of the droplets to smaller sized droplets rather than effective separation through chemical interactions of the membrane with the emulsions.

Thermogravimetric analysis (TGA) is also imprecise when the oil being studied does not have a single boiling point, e.g. diesel and gasoline, as they consist of a mixture of different oils. Moreover, part of the water and oil particles may be dragged by the vapor flux during evaporation of one of the two phases.

Transmittance and density measurements can be questionable when an emulsifier is mixed with the oil/water system.

Infrared spectrometer oil content, however, can be a good and precise

technique for oil/water separation efficiency characterization.<sup>151,152,179,256,263–265</sup>

In our work we used gas chromatography with flame ionized detector (GC-FID) and high-performance liquid chromatography (HPLC) to determine the remaining oil content in the permeate. GC-FID was determined as one of the most adequate techniques for the measurement of oil in produced water by OSPAR standard (Oslo-Paris Convention).<sup>149</sup> Although these are two adequate and complimentary techniques for oil content characterization with very high resolution (in the ppm range), there are high expenses associated to them.

### 7.2. Tuning the wood's wettability through graft polymerization

Oil pollution in water can also be found in the form of oil/water emulsions, due to the weathering processes oil undergoes when in contact with the environment (see Figure 1.6). In this form, oil is miscible in water and native wood is not capable to separate the two. As mentioned previously, surface energy and structure (mainly re-entrant structures) are key for the separation of oil/water emulsions.

In order to obtain a wood cross section with oil/water separation capabilities for emulsions, we need to be able to repel the oil (only possible with a surface with very low surface energy – fluorine chemistry) while still being capable of letting the water through (hydrophilic compound). This leads to the need for wettability changes. A possible way to obtain such surfaces is through the juxtaposition of two distinct domains (a superhydrophilic polyelectrolyte and superhydrophobic one).<sup>101,156</sup>

In wood, this could be achieved through the grafting of copolymers. The copolymer should have a block structure with the hydrophilic block (e.g. a polyelectrolyte) attached to wood, and the hydrophobic block (e.g. a fluorinated polymer) sticking away from the surface. This organization is needed in order to have the oil repelled by the fluorinated polymer (top layer), while the small water molecules attracted by the superhydrophilic underlayer could still

pass through its defects. A scheme of this conformation is shown in Figure 5.1. In order to obtain such a modification, a precise control over the position of the polymer (to have all the modification at the surface of the wood) and of the polymerization reaction itself is needed.

### 7.2.1. Control over the spatial distribution of the modifying polymer in wood

The transport and positioning of chemical modifications in bulk wood is an important factor affecting the end-properties of the modified material, which still has to be better understood.

Three main pathways exist for the transport of natural biochemical compounds in the living tree: from one cell to another via pits, from lumen to cell wall via diffusion, and through the middle lamellae.<sup>10,198</sup> Although the pathways have not been directly monitored during modification, from the positioning of the modifying chemicals after reaction one can hypothesize that wood-mineralization and in-situ polymerization follow two of these three different modification pathways. Specifically, mineralization follows modification through the middle lamellae and in-situ polymerization seems to occur from the lumen into the cell wall via diffusion.<sup>33,35,192,198,266</sup>

Focusing on in-situ polymerization, one can find analogies with the positioning of extractives in heartwood. Wood in the living tree has been optimized for water transport and mechanical support. As shown in section 1.3.1 the xylem (wood) represents the biggest part of the tree trunk. The xylem consists of two parts: the sapwood (living parenchyma cells) and the heartwood (dead parenchyma cells).

Extractives can be found in the lumen or in the capillaries of the cell walls. Berlyn has shown that the hydrated S2 layers of pine tracheid cell walls have 25% free space.<sup>267</sup> Berlyn further suggested that if the free space is arranged in a suitable manner, which is the case with species with so-called "regular heartwood", extractives may penetrate the cell wall (molecule size should also be considered). Capillaries having cross sections from 16 to 60 Å, which is large enough to take molecules of considerable size (glucose molecule 6.3 Å and

flavonoid monomer 15 Å), provide the free space in wet cell walls. However, in some cases the molecules are too large to enter these capillaries. In this case, the extractives are stored in the lumen. This results in the formation of “false” heartwood. In “false” heartwood, dark coloration in the wood can be observed due to accumulation of high-molecular-weight extractives in the cell lumina. However, given that the extractives are only present in the lumen, the improvement of properties, typically dimensional stability, given by the introduction of extractives is not observed, hence the name “false” heartwood.<sup>268</sup>

The effect on shrinking and swelling of the wood due to the position and composition of the extractives, is also seen for chemical modifications.<sup>26,27</sup> Although the pathways of both types of wood modifications (natural and synthetic) are not fully understood, some of the affecting parameters for the formation and positioning of extractives (natural modification) are well documented.<sup>198,267–271</sup>

This is not the case for chemical modifications, where different positions of the modification can be targeted for different applications. Therefore, an important parameter to study was how to control the position of polymers with different wettability properties (needed for the application) in the wood structure. A possible route that was chosen, was the use of solvents with different wood-swelling capabilities.

Although there have been different works, mainly for dimensional stability, in which it was shown that the polymer position played a role on the performance of the modified wood,<sup>26,27</sup> so far no work has focused on controlling the position of the modification through the use of different solvents.

SI-AGET-ATRP, the polymerization technique used, is a two-step reaction. In the first step, the initiator (BiBB) is grafted onto the wood structure (producing the macroinitiator). In the second step, the polymer chains are grown from the covalently grafted BiBB molecules. Since the polymer will only grow from the grafted initiator, the control over its position leads to control over the position of



the polymer.

For this purpose, following the work of Mantanis et al. on the swelling properties of different solvents in wood, a good (Pyridine – Py) and a bad (Dichloromethane – DCM) wood swelling solvent were chosen.<sup>32</sup>

Considering the wood microstructure (at the cellular level), Pyridine allowed cell wall penetration (from the lumen towards the cell wall), and the use of DCM limited the modification to the lumen/cell wall interface. The control was not only limited to the cellular level but it was also seen at the macroscopic level, along the longitudinal direction. At this scale, modification through the entire length of the cube took place, although a clear gradient in amount of modification from the surface to the center of the cube could be observed. Contrarily, the modification was mainly limited to the first 300  $\mu\text{m}$  of the cube with DCM mediated reactions.

This gradient in modification along the length of the cubes (5 mm) at the macroscale, is in part due to the closing of bordered pits when the tree is felled. These bordered pits are used as means of transport in the living tree between two adjacent tracheids cells, making it possible to transport water up to tens of meters, even though the tracheids have a length of 3 mm (in spruce trees). However, as mentioned, most of these tracheids close when the tree is felled. Some of them are thought to reopen during the modification process but most of them remain closed, limiting transport between the closed ends of the tracheids, and therefore, through the length of the samples.

The control over the reaction at these two scales was observed in the same manner for both the initiator and the polymer. Nevertheless, the trend was not as pronounced for the polymer at the macroscale. The surface densified due to strong polymerization at the surface of the wood. This slowed down the diffusion of reactants and hindered polymer grafting onto the BiBB molecules present in the center of the cube.

A possible way to address diffusion limitations is to slow down the polymerization rate. This is the case for the metabolic process of polyphenols in the living tree, where it was shown that if the polymerization of this molecules occurs very

slowly, the heartwood substances may spread out through the woody tissue as soon as the semipermeable plasma membrane of the parenchyma cells has disappeared after cell death.<sup>269</sup> Another way is to allow sufficient time for the monomer/catalyst solution to diffuse and impregnate wood homogeneously, and then only to trigger the polymerization (through a temperature raise for instance).

The study of polyphenols in beech, in the living tree, showed that these substances are located in the cell lumina in the form of small droplets or layers covering the inner cell wall.<sup>269</sup> Phenolic coating of the cell wall has been shown to affect the penetration of some wood species with aqueous solutions of preservatives. Following the idea of the hydrophobic coating by phenolic compounds, it was first suspected, that the hydrophobic BiBB molecule could also form a similar layer on the cell wall. This would then prevent the hydrophilic METAC monomer from reaching the active BiBB sites within the cell wall and thus affect the spatial distribution of PMETAC. However, this was not the case and may be explained by the small size of the molecule. The system would be therefore more analogous to the introduction and polymerization of flavonoid molecules in the living tree.<sup>272-274</sup> The porous structure of the cell wall allows these molecules, which are hydrophobic, to diffuse into the cell wall even at fully hydrated state – the usual state of the living tree.

Focusing on the final application, oil/water separation, there has to be a certain positioning of the polymer modification for the separation to efficiently take place. The modification needs to be targeting a thick modification layer in the first micrometers of the wood surface, leaving the center of the wood unmodified. Therefore, the inhomogeneous grafting of polymer due to diffusion limitations from the surface to the center would not be an issue for this particular application.

During the study of the control over the spatial polymer-modification distribution in the wood through ATRP, the samples used were cubes compared to the usually used discs. The difference in geometry (discs and cubes) led to a final

observation. Although the reaction had been performed and mastered for the discs, it was a challenge to find the correct parameters to reproduce the results previously observed, mainly due to diffusion issues. We found that the initial pressure ( $\geq 1 \times 10^{-2}$  mbar), at which we were introducing our initiator and solvent for the production of the macroinitiator, strongly affected the modification result. The reaction times had to be increased to reach the same WPG with the cubes as in the discs. For the same reasons, we found out that it was difficult to reproduce results when using cubes. Due to the easier liquid penetration, the disc geometry was preferred to obtain reproducible results (in terms of WPG). However, these represent a challenge in sample preparation for surface characterization techniques. Whereas the surface of the wood cubes can be polished with a rotary microtome without further preparation of the sample, due to sample geometry constraints, the wood discs need to be fixed into a cube before polishing. This is usually done by gluing the sample onto a wood cube or through embedding.

### 7.2.2. Control over the copolymerization reaction

Several modification techniques based on the addition of synthetic polymers have been used for the production of oil/water separating devices: electrostatic deposition (layer-by-layer), in situ oxidative polymerization, spray drying, dip coating, phase inversion, and in-situ polymerization (ATRP, RAFT amongst others).<sup>95,98,101,156</sup>

Wettability properties of a material are given by its structure and chemical composition. Therefore, working with biological materials, such as wood, with high chemical variability, requires the use of controlled modification techniques, in order to have a good control over the surface chemistry and structure. Moreover, for chemical and mechanical stability of the modification, it should be covalently grafted onto the wood surface.

Several polymer-based modifications have been carried out on wood for dimensional stability (as shown in Section 1.4). Copolymerization has been performed on biological materials such as lignin, cellulose, bulk wood and

derivatives.<sup>219,229,275-277</sup> In the case of wood, most of these modifications were aiming at dimensional stability with polymers of similar wettability properties compared to wood and were not aiming for the introduction of new functional groups for added-value applications.

The copolymerization of monomers with opposite wettabilities to obtain amphiphilic block copolymers is not trivial. Monomers with opposed wettability properties are difficult to react with each other to form a copolymer in solution, as the monomers will tend to react amongst themselves rather than with each other.

Despite the great challenge, amphiphilic copolymers can be used in a wide range of applications and therefore are highly desirable.<sup>225</sup>

A *grafting from* technique such as surface-initiated atomic transfer radical polymerization (SI-ATRP), can offer the needed control over the reaction to produce block copolymers with amphiphilic properties. ATRP has been widely used in the functionalization of membranes for different applications.<sup>278-285</sup>

Biological materials have been modified through this technique and its derivatives (SI-AGET-ATRP, amongst others).<sup>33,42,59,191,195,196,219,234,286,287</sup> In some cases this technique has even been used to graft biopolymers with block copolymers, however, the examples are very limited and restricted to polymers with similar wettability properties.<sup>219-221,228,288</sup>

SI-AGET-ATRP, a derivative from SI-ATRP, is a robust and versatile technique, for polymerizing a wide range of monomers, in various solvents and reaction conditions.<sup>51</sup> Compared to normal ATRP, it is also a step closer towards an industrial process as it does not require drastic oxygen free conditions for the reaction to take place. SI-ATRP techniques have already been successfully performed on wood. Given the challenge of modifying a natural material with highly heterogeneous structure, SI-AGET-ATRP was the polymerization technique chosen.

The monomers initially chosen for the copolymerization were the hydrophilic monomer, [2-(Methacryloyloxy)ethyl] trimethylammonium chloride (METAC), which gave a good performance after modifying the wood, increasing its

hygroscopic properties; and the initial fluorinated monomer 2,2,2-Trifluoroethyl methacrylate (TFEMA), which did not fulfill the expectation of producing an oleophobic wood. In a further step, TFEMA was replaced by 2,2,3,3,4,4,5,5-Octafluoropentyl methacrylate (OFPMA), to increase the amount of fluorine in the modification, and achieve lower surface energies.

In a first trial TFEMA and METAC were copolymerized in the same reaction batch. The result was a modified wood that had wettabilities similar to native wood. The FTIR spectra of this copolymerization showed some of the peaks of each polymer but other important ones were not present and were shifted, making it difficult to determine whether both polymers were present.

Since both polymers can be reacted under the same conditions and are expected to have similar reactivity ratios, we expected to obtain random copolymers if reacted together on the same reaction step. Therefore, the only possible path to obtain a complete block co-polymer was to react them sequentially. This adds an extra step to the polymerization process. However, as mentioned before, AGET-SI-ATRP allows the process to be carried out under less oxygen free conditions, facilitating the up-scale towards an industrialization of the modification process.

In a second attempt, METAC and OFPMA were reacted in consecutive steps. In this case, we did not obtain any appreciable WPG after the OFPMA polymerization. The hypothesis was that given the different wettability properties of the two monomers, the OFPMA impeded reactions with the METAC. Therefore, we hypothesize to have a “located” copolymerization during the first attempt, where the TFEMA and the METAC formed their own chain from different available BiBB sites, forming regions of the wood with TFEMA and others with METAC. Although no examples were available concerning the modification of wood through copolymers formed by monomers with opposed wettability, examples reporting grafting on model surfaces are available. Hofer et al. showed that to react a negatively charged polymer with hydrophilic wetting properties and a fluorinated polymer with hydrophobic wetting properties it was necessary to use a salt.<sup>247</sup> The salt would allow shielding the charges of the hydrophilic polyelectrolyte enabling the reaction with the fluorinated monomer.

Following this example, a salt that could be used in the reacting media (DMF) and shows similar physicochemical properties to the fluorinated monomer was selected, sodium fluoroacetate ( $\text{CF}_3\text{COONa}$ ). By introducing the salt during the second block polymerization reaction, it was possible to produce a block copolymer with amphiphilic properties.

The copolymerization of the wood discs yield samples with wettabilities ranging from superhydrophilic to completely hydrophobic, with intermediate contact angles that decreased faster or slower over time depending on the amount of the POFPMA block in the sample (see Figure 4.9). The copolymerized samples from less to more hydrophobic were named Copolymer A, B, and C.

The abovementioned different wettability properties, characterization results of the copolymerized-wood through spectroscopy techniques, and the fact that we reacted the polymers in two sequential reactions indicate that the wood was modified by a block copolymer. However, in order to have a final proof, being able to completely characterize the polymer-modification (MW, chain length distribution, copolymer ratio, etc.) by typical polymer characterization techniques (NMR, SEC, MALDI-TOF, ...), it is necessary to cleave the polymer chains from the wood structure. This would allow determining for instance the grafting density, giving clear information on how many initiator moieties are being reacted in each modification. Preliminary experiments were carried out following available polymer cleaving literature on cellulose,<sup>234</sup> however, the complex structure of bulk lignocellulosic materials such as wood did not allow for a successful cleavage. This would be an interesting topic to be explored in the future.

The life cycle and impact of a material can be divided into three different parts: production, use and end-life or recyclability.

In terms of production, while SI-AGET-ATRP offers a high control over the polymerization of various monomers and can allow for the functionalization of complex structures with amphiphilic block copolymers, industrialization is still

limited.

Indeed, CRP techniques (including ATRP) are currently not considered to replace conventional radical polymerizations for the production of commodity polymers in large volumes. Nevertheless, there is a growing interest shown by industrial research investments focusing on the utilization of CRP techniques to produce specialty chemicals. The application of these techniques are mainly in the markets related to cosmetics, health, automotive paintings and coatings, adhesives, sealants, and membranes, amongst others.

The limitation in their application is mainly due to high cost of the CRP agents and low production volumes, though this might change in the future. Another limitation, specific to ATRP, is the high amount of catalyst complex needed and the type of solvents that can be used, which presents both an economical and environmental issue. While the increase in reactivity of the catalytic complex is being studied, there have also been some developments in regenerating these catalysts to achieve lower concentrations, such as with SI-ARGET-ATRP.<sup>289</sup>

Therefore, with some further developments in the field, it could be possible to produce functionalized wood-based membranes through this or similar techniques.

Since the modification results in covalently attached polymers chains inside the wood structure, leaching of modification chemicals during use should not be an issue.

The most challenging aspect of the life cycle of our wood-based membranes is related to the recyclability of the membranes. Since it is not possible to selectively cleave the grafted polymers from the wood membrane, the functionalized wood samples would need to be burned once the fouling cannot be removed from the wood surface. Nevertheless, as we targeted a “water-removing” configuration it should be noted that the membranes should only suffer from limited fouling, allowing for long-lasting life cycles.

### 7.3. Oil/water separation with functionalized wood-based membranes

By controlling the position of the polymer and the block copolymerization of a superhydrophilic polyelectrolyte (PMETAC) and a fluorinated superhydrophobic and oleophobic polymer (POFPMA) on the wood structure it should be possible to produce a wood-based membrane capable of separating free oil/water mixtures but also oil/water emulsions.<sup>98,101</sup>

Given the interesting wettability properties of water with wood on the various copolymer-modified samples, it was decided to test the underwater oil contact angle and sliding angles of these samples. The results were also promising, obtaining wood-based membranes that were capable of repelling the oil underwater, with oil contact angles (OCA) above 140° (see Figure 5.2). The oil-sliding angle results (OSA) ranged from 5 to 10°, decreasing as the amount of POFPMA in the samples increased. Following these two results, we expected to obtain a lower OSA value for Copolymer C. However, due to the high concentration of POFPMA in the sample, the disc macroscopically bended making it impossible to measure the OSA properly.

Nevertheless, with these encouraging results, oil/water separation was tested on the functionalized wood-based membranes, using the same separation holder system as for the unmodified wood. High separation efficiencies were obtained likewise with the unmodified wood, however, the flux rate decreased substantially with sample Copolymer C (30%METAC/22%POFPMA). This was expected due to the long time needed for the complete absorption of water with this sample during the water contact angle measurements (see Figure 4.9). Conversely, we believe that the decrease in flux could be also due to the modification, which has shown to decrease the pore size of our wood (see Figure 3.3).

In order to test the effectiveness of the membrane to separate oil/water emulsions, oil/water emulsions with various droplet sizes should be available and be stable for sufficient time to perform the tests and characterize the emulsions.



Due to the lack of adequate literature on the topic this is highly time consuming and as it was not the main goal of the thesis, only preliminary results could be obtained.

The only stable emulsions that were possible to produce were emulsions with 300 nm to 5  $\mu\text{m}$  droplet size (see Figure 5.4). The emulsions were produced with three different oil/water ratios: 10:90, 30:70 and 50:50 v/v oil/water and different SDS concentrations, ranging from 0.1 to 0.5 mg of SDS per mL.

These emulsions were tested on the functionalized wood-based membranes, however, due to the small size of the emulsions the membrane was not capable of separating the oil from water. We expect that the modified wood membrane should be capable of separating emulsions with droplet sizes above 30  $\mu\text{m}$ . It was seen that during the chemical modification the cell wall swelled (due to the introduction of new material) and the lumen pores became smaller.

Therefore, it could be possible that smaller droplet sizes (possibly above 10  $\mu\text{m}$ ) are also separated. Nevertheless, an adequate study of the maximum pore size in the modified membranes is needed.

Demulsification can be achieved through different processes. While membrane demulsification tends to be the most efficient method, other processes are available for this purpose. Such processes can be chemical demulsification, biological demulsification, electrical demulsification, and microwave or ultrasonic radiation, amongst others.<sup>290–292</sup> Nevertheless, these processes also have their limitations and can be energy intensive. Moreover, the demulsification of small droplet sized emulsions is still a challenge, due to their high stability.

#### **7.4. From a batch lab-scale to a continuous industrial set-up**

In order to use a separation system at an industrial scale, it should be economically viable and scalable to the quantities demanded by the market. Continuous processes are usually less energy intense and, therefore, more

desired. In oil/water separation, the phase repelled remains on the surface of the membrane. If this phase is not extracted, the liquid column could generate a pressure exceeding the breakthrough pressure, and the repelled phase would penetrate the membrane. Therefore, for a continuous set-up, it is important to produce a membrane holder that allows for a good contact between the feed and the membrane and where the repelled phase is extracted from the holder before  $P_B$  is reached. Our holder was designed following the two abovementioned requirements, as can be seen in Figure 6.1.

Preliminary tests were performed on the prototype separation system, the results were not conclusive as the pressure had to be controlled manually. During the experiments it was seen that, due to the different physical properties (e.g. viscosity and density) of the two liquids (oil and water) it was very difficult to control the pressure with a manual valve and an analog pressure indicator. In order to be able to test the membranes performance properly, the pressure control valve should have a feedback loop to the pressure indicator at the feed and be electronically operated. This feedback loop would need high precision at such small scale (see proposed system in Figure 6.2).

The separation system could work for large quantities (i.e. at industrial scales) provided that a few changes are done. The pumping source, which is pressurized air for the lab-scale system, should be exchanged for a centrifuge pump. This would allow refilling the feed tank without stopping operation. Otherwise, the feeding tank should be exchanged for a membrane tank. These are far more expensive than standard tanks and need high maintenance. Another challenge would be scaling-up the membrane holder. Given the natural structure of spruce wood, the geometry of the samples is restricted to certain sizes. As shown in Figure S2.1, in order to have the maximum amount of fibers opened at both ends of the membrane (through where the water flows) the membrane should be as thin as possible. Assuming that all bordered pits are closed in the spruce wood sample, the flow would decrease together with the membrane thickness due to the blocked water pathways inside the membrane. Conversely, in order to maintain mechanical stability of the membrane, a

certain thickness is required. A trade-off was found at 1 mm membrane thickness.

A further geometrical parameter would be the diameter of the membrane, as the membranes are discs. While the diameter of the membrane was initially selected considering the maximum opening size in a standard reaction flasks (for the functionalization of the membrane), this diameter cannot be much larger for a 1 mm thick cross section, due to mechanical stability reasons. Therefore, the only possibility of increasing the flow is by using a great number of the separation holders designed for the lab-scaled separation or designing a new separation holder that can hold several wood-based membranes. As the first option is very material intensive and therefore, not economical, a possible new separation holder is proposed (see Figure 6.4).

Nevertheless, for operation purposes one should still have at least three separation holders in parallel to be able to perform maintenance washings without having to interrupt the entire water purification system.

We expect that with these two changes and the correct operational parameters, this separation system would allow for separating oil/water with our wood-based membranes at larger scales.



# Chapter 8

## Outlook

Most of the materials produced by the scientific community working on oil/water separation follow a bottom-up approach. In this work, we showed that lignocellulosic materials, such as wood, with their porous hierarchical anisotropic structure are also capable of reaching similar performances. Through the modification with amphiphilic block copolymers of wood we can improve the already outstanding properties of this material. This work also provided the tools to control the position of the modification in complex porous structure such as wood. This will allow for a better tuning of the modifications to obtain the desired material properties. Conversely, we offer a possible approach for modifying porous complex surfaces with amphiphilic block-copolymers. Modification through amphiphilic block-copolymers further widens the range of applications in which this bio-sourced materials can be used. Nevertheless, the work is never finished. In the following section a few possible following studies are given.

### 8.1. Future work

The polymerization protocols for monomers with amphiphilic properties on lignocellulosic materials, their characterization and implementation for oil/water separation systems developed in this work present a promising step towards renewable resource based solutions to one of the greatest environmental problems.

While we reached several milestones, there are still a lot of challenges to be overcome.

The wood functionalization angle could be explored to greater extent. In order to go towards an industrialized process, a possibility would be trying to obtain the same polymer system through free radical polymerization (FRP). The loss of control, if tolerable, could be compensated by a more environmentally friendly and robust polymerization. Moreover, it would also be interesting, to study the viability of the polymerization reaction in more environmentally friendly solvents, such as water. If FRP is not an option, there have been some studies of ATRP in water.

Another important point in terms of the polymerization reaction onto wood scaffolds would be the formulation of a mathematical model describing the reaction. This would involve the investigation of several mechanisms: the mass transfer (diffusion) of reactants and catalysts into the scaffolds porous structure, the interaction of the different chemical species involved, and the kinetics of the polymerization. While modeling each mechanism can be relatively easy, their combination, considering the interaction between them, would lead to a multitude of parameters that would need to be fitted, which is not a simple task. However, the benefits would be a better understanding of the reactions, which would in turn lead to a better control and predictability of the outcomes. Furthermore, this study could also enable better understanding of the reaction pathways in the wood scaffold.

Concerning the oil/water separation with lignocellulosic materials, several aspects still need to be assessed. While there are no efficiency differences using wood with different surface roughness on free oil/water mixtures, the

surface roughness could affect the separation efficiency of oil/water emulsions. Moreover, we believe that the surface roughness might influence the fouling of the membrane.

During the characterization of the copolymerized samples, some changes were observed (for instance in the wettability). Lower contact angles were observed after wetting and redrying the samples compared to the original contact angle of the dried sample. Moreover, Raman spectroscopy water immersed measurements (as usually performed on bulk wood) with POFPMA-modified samples could not detect the fluorinated polymer. This however was possible under air. Our hypothesis is that there is a reorientation of the polymer resulting in these two abovementioned effects. A possible way to prove this hypothesis would be through high-resolution transmission electron microscopy (HR-TEM) imaging.

## **8.2. Current limitation in the field of oil/water separation technologies**

There are several interesting new materials being proposed for oil/water separation. However, comparing them with industrially available materials, they are far from being competitive. Moreover, it is difficult to compare novel materials in literature systematically due to the lack of standardized characterization techniques for efficiency and overall performance.

In order to test the efficiency of the membranes to separate oil water emulsions, a thorough study has to be performed in order to be able to produce stable emulsions of wide range of droplet sizes. Furthermore, the interaction of the different emulsifiers with the membranes has yet to be addressed. It would be interesting to know if the surfactants are retained, pass through, or are even adsorbed by the membrane. In the latter case, this could lead to significant efficiency losses.

### 8.3. Social impact of the work

In a world where drinking water has shown to be scarce, the need for water treatment devices is eminent. Most of the devices for water treatment developed in the last years are made of oil-based materials. In order to produce them, oil needs to be extracted and transported. During the extraction and transportation of oil, high amounts of oil leak into the environment. Oil is known to be the greatest pollutant in water and mainly due to anthropogenic causes. Therefore, by transitioning to bio-based materials and a renewable resource-based economy this contribution can be reduced to a significant extent. In this work, we show the use of a highly abundant bio-based, such as wood, for oil/water separation. Native wood could be use in developing countries, where economical resources are scares, to separate free oil/water mixtures; reducing the anthropogenic impact in the environment and contributing to a fair world.



# Chapter 9

## References

- (1) Yasui, M. In *Compr. Biomed. Phys.* 5; Elsevier: 2014; Vol. 2, pp 83–89.
- (2) Geise, G. M.; Lee, H.-S.; Miller, D. J.; Freeman, B. D.; McGrath, J. E.; Paul, D. R. Water purification by membranes: The role of polymer science. *J. Polym. Sci. Part B Polym. Phys.* **2010**, *48*, 1685–1718.
- (3) Bollmann, M. et al., *World ocean review: Living with the oceans*; maribus gGmbH: 2010.
- (4) Gossen, L. P.; Velichkina, L. M. Environmental problems of the oil-and-gas industry (Review). *Pet. Chem.* **2006**, *46*, 67–72.
- (5) Transportation Research Board and National Research, *Oil in the Sea III: Inputs, Fates, and Effects*; The National Academies Press: Washington, DC, 2003, p 277.
- (6) 2. Oil pollution and clean-up operations. *Environmentalist* **1983**, *3*, 6–12.
- (7) NATO Science for Peace and Security Series - C: Environmental Security, *Water Purification and Management*; Coca-Prados, J., Gutiérrez-Cervelló, G., Eds.; Springer: 2011; Vol. 4, p 228.
- (8) Cheryan, M.; Rajagopalan, N. Membrane processing of oily streams. Wastewater treatment and waste reduction. *J. Memb. Sci.* **1998**, *151*, 13–28.
- (9) Geyer, R.; Jambeck, J. R.; Law, K. L. Production, use, and fate of all plastics ever made. *Sci. Adv.* **2017**, *3*.
- (10) Berglund, L. A.; Burgert, I. Bioinspired Wood Nanotechnology for Functional Materials. *Adv. Mater.* **2018**, *30*, 1–15.
- (11) Fengel, D.; Wegener, G., *Wood: chemistry, ultrastructure, reactions*; Walter de Gruyter: Berlin; New York, 1983, p 626.
- (12) Navi, P.; Sandberg, D. In *Thermo-Hydro-Mechanical Process. Wood*; Lausanne: EPFL Press: 2011; Chapter 3.
- (13) Hägglund, E., *Chemistry of Wood*, 1st Editio; Academic Press, Inc.: 1951, p 631.
- (14) Rowell, R. M., *Handbook of Wood Chemistry and Wood Composites*, Second Ed.; CRC Press: 2012, pp i–668.
- (15) Meyer, R. W.; Côté, W. A. Formation of the protective layer and its role in tylosis development. *Wood Sci. Technol.* **1968**, *2*, 84–94.
- (16) De Micco, V.; Balzano, A.; Wheeler, E. A.; Baas, P. Tyloses and Gums: a Review of Structure, Function and Occurrence of Vessel Occlusion. *IAWA J.* **2016**, *37*, 186–205.
- (17) Schmitt, U.; Liese, W. Response of xylem parenchyma by suberization in some hardwoods after mechanical injury. *Trees* **1993**, *8*, 23–30.
- (18) Hoffmann, P.; Jones, M. A. In *Archaeol. wood Prop. Chem. Preserv.* American Chemical Society, Ed., 1989; Chapter 2, pp 35–65.
- (19) Greil, P. Biomorphous ceramics from lignocellulosics. *J. Eur. Ceram. Soc.* **2001**, *21*, 105–118.
- (20) Chen, H. In *Biotechnol. Lignocellul. Theory Pract.* Springer Netherlands: Dordrecht, 2014; Chapter 2, pp 25–71.
- (21) Holtzapfel, M. In *Encycl. Food Sci. Nutr.* Elsevier: 2003, pp 3060–3071.

- (22) Scheller, H. V.; Ulvskov, P., *Hemicelluloses*; 1, 2010; Vol. 61, pp 263–289.
- (23) Ren, J.-L.; Sun, R.-C. In *Cereal Straw as a Resour. Sustain. Biomater. Biofuels*; Elsevier: 2010, pp 73–130.
- (24) Tolbert, A.; Akinosho, H.; Khunsupat, R.; Naskar, A. K.; Ragauskas, A. J. Characterization and analysis of the molecular weight of lignin for biorefining studies. *Biofuels, Bioprod. Biorefining* **2014**, *8*, 836–856.
- (25) Hill, C. A. S., *Wood Modification: Chemical, Thermal and Other Processes*; John Wiley & Sons, Ltd: Chichester, UK, 2006, p 260.
- (26) Ermeydan, M. A.; Cabane, E.; Hass, P.; Koetz, J.; Burgert, I. Fully biodegradable modification of wood for improvement of dimensional stability and water absorption properties by poly( $\epsilon$ -caprolactone) grafting into the cell walls. *Green Chem.* **2014**, *16*, 3313.
- (27) Keplinger, T.; Cabane, E.; Chanana, M.; Hass, P.; Merk, V.; Gierlinger, N.; Burgert, I. A versatile strategy for grafting polymers to wood cell walls. *Acta Biomater.* **2015**, *11*, 256–263.
- (28) Kostić, S.; Berg, J. K.; Casdorff, K.; Merk, V.; Burgert, I.; Cabane, E. A straightforward thiol–ene click reaction to modify lignocellulosic scaffolds in water. *Green Chem.* **2017**, *19*, 4017–4022.
- (29) Furuno, T.; Imamura, Y.; Kajita, H. The modification of wood by treatment with low molecular weight phenol-formaldehyde resin: a properties enhancement with neutralized phenolic-resin and resin penetration into wood cell walls. *Wood Sci. Technol.* **2004**, *37*, 349–361.
- (30) Zhang, Y.; Zhang, S. Y.; Yang, D. Q.; Wan, H. Dimensional stability of wood-polymer composites. *J. Appl. Polym. Sci.* **2006**, *102*, 5085–5094.
- (31) Mathias, L. J.; Lee, S.; Wright, J. R.; Warren, S. C. Improvement of wood properties by impregnation with multifunctional monomers. *J. Appl. Polym. Sci.* **1991**, *42*, 55–67.
- (32) Mantanis, G. I.; Young, R. A.; Rowell, R. M. Swelling of Wood Part II. Swelling in Organic Liquids. *Holzforchung* **1994**, *48*, 480–490.
- (33) Cabane, E.; Keplinger, T.; Künniger, T.; Merk, V.; Burgert, I. Functional lignocellulosic materials prepared by ATRP from a wood scaffold. *Sci. Rep.* **2016**, *6*, 31287.
- (34) Keplinger, T.; Cabane, E.; Berg, J. K.; Segmehl, J. S.; Bock, P.; Burgert, I. Smart Hierarchical Bio-Based Materials by Formation of Stimuli-Responsive Hydrogels inside the Microporous Structure of Wood. *Adv. Mater. Interfaces* **2016**, *3*, 1600233.
- (35) Vidiella del Blanco, M.; Fischer, E. J.; Cabane, E. Underwater Superoleophobic Wood Cross Sections for Efficient Oil/Water Separation. *Adv. Mater. Interfaces* **2017**, *4*, 1700584.
- (36) Bruce, C. Surface Modification of Cellulose by Covalent Grafting and Physical Adsorption for Biocomposite Applications., Doctoral Thesis, KTH Royal Institute of Technology, Stockholm, 2014.
- (37) Kang, H.; Liu, R.; Huang, Y. Graft modification of cellulose: Methods, properties and applications. *Polymer (Guildf)*. **2015**, *70*, A1–A16.
- (38) Gürdağ, G.; Sarmad, S. In *Polysacch. Based Graft Copolym.* Springer Berlin Heidelberg: Berlin, Heidelberg, 2013, pp 15–57.
- (39) Kan, K. H. M.; Li, J.; Wijesekera, K.; Cranston, E. D. Polymer-Grafted Cellulose Nanocrystals as pH-Responsive Reversible Flocculants. *Biomacromolecules* **2013**, *14*, 3130–3139.
- (40) Roy, D.; Semsarilar, M.; Guthrie, J. T.; Perrier, S. Cellulose modification by polymer grafting: a review. *Chem. Soc. Rev.* **2009**, *38*, 2046.
- (41) Roy, D.; Guthrie, J. T.; Perrier, S. Graft Polymerization: Grafting Poly(styrene) from Cellulose via Reversible Addition–Fragmentation Chain Transfer (RAFT) Polymerization. *Macromolecules* **2005**, *38*, 10363–10372.

- (42) Morits, M.; McKee, J. R.; Majoinen, J.; Malho, J.-M.; Houbenov, N.; Seitsonen, J.; Laine, J.; Gröschel, A. H.; Ikkala, O. Polymer Brushes on Cellulose Nanofibers: Modification, SI-ATRP, and Unexpected Degradation Processes. *ACS Sustain. Chem. Eng.* **2017**, *5*, 7642–7650.
- (43) Okahisa, Y.; Yoshida, A.; Miyaguchi, S.; Yano, H. Optically transparent wood-cellulose nanocomposite as a base substrate for flexible organic light-emitting diode displays. *Compos. Sci. Technol.* **2009**, *69*, 1958–1961.
- (44) Zhu, M.; Song, J.; Li, T.; Gong, A.; Wang, Y.; Dai, J.; Yao, Y.; Luo, W.; Henderson, D.; Hu, L. Highly Anisotropic, Highly Transparent Wood Composites. *Adv. Mater.* **2016**, *28*, 5181–5187.
- (45) Hassel, B. I.; Trey, S.; Leijonmarck, S.; Johansson, M. A Study on the Morphology, Mechanical, and Electrical Performance of Polyaniline-modified Wood - A Semiconducting Composite Material. *BioResource* **2014**, *9*, 5007–5023.
- (46) Burgert, I.; Cabane, E.; Zollfrank, C.; Berglund, L. Bio-inspired functional wood-based materials – hybrids and replicates. *Int. Mater. Rev.* **2015**, *60*, 431–450.
- (47) Fu, Q.; Ansari, F.; Zhou, Q.; Berglund, L. A. Wood Nanotechnology for Strong, Mesoporous, and Hydrophobic Biocomposites for Selective Separation of Oil/Water Mixtures. *ACS Nano* **2018**, *12*, 2222–2230.
- (48) Zhang, X. M.; Ji, J. F.; Tang, Y. J.; Zhao, Y. Wood Pulp Fibers Grafted with Polyacrylamide through Atom Transfer Radical Polymerization. *Adv. Mater. Res.* **2011**, 396-398, 1458–1461.
- (49) Fu, Y.; Li, G.; Yu, H.; Liu, Y. Hydrophobic modification of wood via surface-initiated ARGET ATRP of MMA. *Appl. Surf. Sci.* **2012**, *258*, 2529–2533.
- (50) Klumperman, B. Reversible Deactivation Radical Polymerization., 2015.
- (51) Huang, C. F. Surface-initiated atom transfer radical polymerization for applications in sensors, non-biofouling surfaces and adsorbents. *Polym. J.* **2016**, *48*, 341–350.
- (52) Ouchi, M.; Sawamoto, M. Sequence-controlled polymers via reversible-deactivation radical polymerization. *Polym. J.* **2018**, *50*, 83–94.
- (53) Matyjaszewski, K. In *ACS Symp. Ser.* 2015; Vol. 1187, pp 1–17.
- (54) Matyjaszewski, K. Atom Transfer Radical Polymerization (ATRP): Current Status and Future Perspectives. *Macromolecules* **2012**, *45*, 4015–4039.
- (55) Matyjaszewski, K.; Xia, J. Atom transfer radical polymerization. *Chem. Rev.* **2001**, *101*, 2921–2990.
- (56) Azzaroni, O. Polymer brushes here, there, and everywhere: Recent advances in their practical applications and emerging opportunities in multiple research fields. *J. Polym. Sci. Part A Polym. Chem.* **2012**, *50*, 3225–3258.
- (57) Wang, W.; Tang, J.; Jia, Z.; Li, X.; Xiao, Z. Grafting of amphiphilic polymers containing quaternary ammonium group on SiO<sub>2</sub> surface via surface-initiated ATRP. *J. Polym. Res.* **2012**, *19*, 9804.
- (58) Huang, F.; Ding, C.; Li, J. Resisting Protein but Promoting Cell Adhesion by Choline Phosphate: A Comparative Study with Phosphorylcholine. *J. Bioresour. Bioprod.* **2018**, *3*, 3–8.
- (59) Yin, Y.; Tian, X.; Jiang, X.; Wang, H.; Gao, W. Modification of cellulose nanocrystal via SI-ATRP of styrene and the mechanism of its reinforcement of polymethylmethacrylate. *Carbohydr. Polym.* **2016**, *142*, 206–212.
- (60) Islam, M. S.; Hamdan, S.; Hassan, A.; Talib, Z. A.; Sobuz, H. R. The chemical modification of tropical wood polymer composites. *J. Compos. Mater.* **2014**, *48*, 783–789.
- (61) Mandal, M.; Maji, T. K. Comparative study on the properties of wood polymer composites based on different modified soybean oils. *J. Wood Chem. Technol.* **2017**, *37*, 124–135.
- (62) Niska, K. O.; Sanadi, A. R. In *Wood-Polymer Compos.* 1; Elsevier: 2008, pp 41–71.

- (63) Wang, G.; He, Y.; Wang, H.; Zhang, L.; Yu, Q.; Peng, S.; Wu, X.; Ren, T.; Zeng, Z.; Xue, Q. A cellulose sponge with robust superhydrophilicity and under-water superoleophobicity for highly effective oil/water separation. *Green Chem.* **2015**, *17*, 3093–3099.
- (64) Mamiński, M.; Król, M.; McDonald, A. G.; McIlroy, D. N.; Niraula, I. B.; Czechowska, J.; Parzuchowski, P. Thermally initiated solvent-free radical modification of beech (*Fagus sylvatica*) wood. *Wood Sci. Technol.* **2013**, *47*, 1019–1031.
- (65) Pin Luo, S.; zhen Cao, J.; Wang, X. Properties of PEG/thermally modified wood flour/polypropylene (PP) composites. *For. Stud. China* **2012**, *14*, 307–314.
- (66) Mamiya, Y. Scanning Electron Microscopy of Pine Seedling Wood Tissue Sections Inoculated with the Pinewood Nematode *Bursaphelenchus xylophilus* Previously Prepared for Light Microscopy. *J. Nematol.* **2012**, *44*, 255–9.
- (67) Oksman, K. Improved interaction between wood and synthetic polymers in wood/polymer composites. *Wood Sci. Technol.* **1996**, *30*, 197–205.
- (68) Hristov, V. N.; Krumova, M.; Vasileva, S.; Michler, G. H. Modified polypropylene wood flour composites. II. Fracture, deformation, and mechanical properties. *J. Appl. Polym. Sci.* **2004**, *92*, 1286–1292.
- (69) Zierdt, P.; Theumer, T.; Kulkarni, G.; Däumlich, V.; Klehm, J.; Hirsch, U.; Weber, A. Sustainable wood-plastic composites from bio-based polyamide 11 and chemically modified beech fibers. *Sustain. Mater. Technol.* **2015**, *6*, 6–14.
- (70) Egerton, R. F., *Physical principles of electron microscopy: An introduction to TEM, SEM, and AEM, second edition*, 2nd ed.; Springer Nature: 2016, pp 1–196.
- (71) Goodhew, P. J.; Humphreys, J.; Beanland, R., *Electron microscopy and analysis*, 3rd ed.; Taylor & Francis: London, 2001, 265 pp.
- (72) Gierlinger, N.; Keplinger, T.; Harrington, M. Imaging of plant cell walls by confocal Raman microscopy. *Nat. Protoc.* **2012**, *7*, 1694–1708.
- (73) Gierlinger, N. Revealing changes in molecular composition of plant cell walls on the micron-level by Raman mapping and vertex component analysis (VCA). *Front. Plant Sci.* **2014**, *5*, 1–10.
- (74) Labb, N.; Rials, T. G.; Kelley, S. S. In *Charact. Cellul. Cell Wall*; Blackwell Publishing Professional: Ames, Iowa, USA, 2006; Chapter 9, pp 110–122.
- (75) Gierlinger, N.; Keplinger, T.; Harrington, M.; Schwanninger, M. In *Cellul. - Biomass Convers.* InTech: 2013; Chapter 8, pp 159–192.
- (76) Gierlinger, N.; Schwanninger, M. The potential of Raman microscopy and Raman imaging in plant research. *Spectroscopy* **2007**, *21*, 69–89.
- (77) Atalla, R. H.; Whitmore, R. E.; Heimbach, C. J. Raman Spectral Evidence for Molecular Orientation in Native Cellulosic Fibers. *Macromolecules* **1980**, *13*, 1717–1719.
- (78) Agarwal, U. P. Raman imaging to investigate ultrastructure and composition of plant cell walls: Distribution of lignin and cellulose in black spruce wood (*Picea mariana*). *Planta* **2006**, *224*, 1141–1153.
- (79) Gierlinger, N.; Reisecker, C.; Hild, S.; Gamsjaeger, S. In *Materials Design Inspired by Nature: Function Through Inner Architecture*; The Royal Society of Chemistry: 2013; Chapter 7, pp 151–179.
- (80) Gierlinger, N. Chemical Imaging of Poplar Wood Cell Walls by Confocal Raman Microscopy. *Plant Physiol.* **2006**, *140*, 1246–1254.
- (81) Gierlinger, N.; Goswami, L.; Schmidt, M.; Burgert, I.; Coutand, C.; Rogge, T.; Schwanninger, M. In situ FT-IR microscopic study on enzymatic treatment of poplar wood cross-sections. *Biomacromolecules* **2008**, *9*, 2194–2201.
- (82) Keplinger, T.; Konnerth, J.; Aguié-Béghin, V.; Rüggeberg, M.; Gierlinger, N.; Burgert, I. A zoom into the nanoscale texture of secondary cell walls. *Plant Methods* **2014**, *10*, 1.

- (83) Brauchle, E.; Schenke-Layland, K. Raman spectroscopy in biomedicine - non-invasive in vitro analysis of cells and extracellular matrix components in tissues. *Biotechnol. J.* **2013**, *8*, 288–297.
- (84) De Meijer, M.; Haemers, S.; Cobben, W.; Militz, H. Surface Energy Determinations of Wood: Comparison of Methods and Wood Species. *Langmuir* **2000**, *16*, 9352–9359.
- (85) Yuan, Y.; Lee, T. R. In *Surf. Sci. Tech.* 1; Springer: Berlin, 2013; Vol. 51; Chapter 1, pp 3–34.
- (86) Montes Ruiz-Cabello, F. J.; Rodríguez-Valverde, M. A.; Marmur, A.; Cabrerizo-Vílchez, M. A.
- (87) Pierce, E.; Carmona, F.; Amirfazli, A. Understanding of sliding and contact angle results in tilted plate experiments. *Colloids Surfaces A Physicochem. Eng. Asp.* **2008**, *323*, 73–82.
- (88) Oil Spills — Safe Drinking Water Foundation., <https://www.safewater.org/fact-sheets-1/2017/1/23/oil-spills> (accessed 04/11/2018).
- (89) 3 Surprising Sources of Oil Pollution in the Ocean., <https://news.nationalgeographic.com/news/2014/03/140325-texas-pollution-oil-spills-animals-science/> (accessed 04/11/2018).
- (90) Global Marine Oil Pollution Information Gateway • Facts • Sources of oil to the sea., <http://oils.gpa.unep.org/facts/sources.htm> (accessed 04/11/2018).
- (91) Board, O. S.; Studies, L.; Board, M., *Responding to Oil Spills in the U.S. Arctic Marine Environment*; National Academies Press: Washington, D.C., 2014.
- (92) Padaki, M.; Murali, R. S.; Abdullah, M. S.; Misdan, N.; Moslehyani, A.; Kassim, M. A.; Hilal, N.; Ismail, A. F. Membrane Technology Enhancement in Oil–Water Separation. A Review. *Desalination* **2015**, *357*, 197–207.
- (93) Reverse Osmosis vs. Nanofiltration and Other Filtration Technologies – Water Treatment Specialists – Aqua Clear LLC., <http://aquaclearllc.com/technical-info/reverse-osmosis-vs-nanofiltration-and-other-filtration-technologies/> (accessed 06/21/2018).
- (94) Brainerd, E. L. Caught in the crossflow. *Nature* **2001**, *412*, 387–388.
- (95) Gupta, R. K.; Dunderdale, G. J.; England, M. W.; Hozumi, A. Oil/water separation techniques: a review of recent progresses and future directions. *J. Mater. Chem. A* **2017**, *5*, 16025–16058.
- (96) Zhang, E.; Cheng, Z.; Lv, T.; Qian, Y.; Liu, Y. Anti-corrosive hierarchical structured copper mesh film with superhydrophilicity and underwater low adhesive superoleophobicity for highly efficient oil–water separation. *J. Mater. Chem. A* **2015**, *3*, 13411–13417.
- (97) Jin, M.; Wang, J.; Yao, X.; Liao, M.; Zhao, Y.; Jiang, L. Underwater Oil Capture by a Three-Dimensional Network Architected Organosilane Surface. *Adv. Mater.* **2011**, *23*, 2861–2864.
- (98) Brown, P. S.; Atkinson, O. D. L. A.; Badyal, J. P. S. Ultrafast Oleophobic–Hydrophilic Switching Surfaces for Antifogging, Self-Cleaning, and Oil–Water Separation. *ACS Appl. Mater. Interfaces* **2014**, *6*, 7504–7511.
- (99) Zhang, Z. H.; Wang, H. J.; Liang, Y. H.; Li, X. J.; Ren, L. Q.; Cui, Z. Q.; Luo, C. One-step fabrication of robust superhydrophobic and superoleophilic surfaces with self-cleaning and oil/water separation function. *Sci. Rep.* **2018**, *8*, 1–12.
- (100) Yong, J.; Chen, F.; Yang, Q.; Huo, J.; Hou, X. Superoleophobic surfaces. *Chem. Soc. Rev.* **2017**, *46*, 4168–4217.
- (101) Kota, A. K.; Kwon, G.; Choi, W.; Mabry, J. M.; Tuteja, A. Hygro-Responsive Membranes for Effective Oil–Water Separation. *Nat. Commun.* **2012**, *3*, 1–8.
- (102) Tuteja, A.; Choi, W.; Ma, M.; Mabry, J. M.; Mazzella, S. a.; Rutledge, G. C.; McKinley, G. H.; Cohen, R. E. Designing superoleophobic surfaces. *Science (80- )*. **2007**, *318*, 1618–22.
- (103) Miller, D. J.; Kasemset, S.; Paul, D. R.; Freeman, B. D. Comparison of membrane fouling at constant flux and constant transmembrane pressure conditions. *J. Memb. Sci.* **2014**, *454*, 505–515.

- (104) Darmanin, T.; Guittard, F. Superhydrophobic and superoleophobic properties in nature. *Mater. Today* **2015**, *18*, 273–285.
- (105) Wong, T.-s.; Kang, S. H.; Tang, S. K. Y.; Smythe, E. J.; Hatton, B. D.; Grinthal, A.; Aizenberg, J. Bioinspired self-repairing slippery surfaces with pressure-stable omniphobicity. *Nature* **2011**, *477*, 443–447.
- (106) Liu, M.; Wang, S.; Wei, Z.; Song, Y.; Jiang, L. Bioinspired Design of a Superoleophobic and Low Adhesive Water/Solid Interface. *Adv. Mater.* **2009**, *21*, 665–669.
- (107) Srinivasan, S.; Chhatre, S. S.; Guardado, J. O.; Park, K.-C.; Parker, A. R.; Rubner, M. F.; McKinley, G. H.; Cohen, R. E. Quantification of feather structure, wettability and resistance to liquid penetration. *J. R. Soc. Interface* **2014**, *11*, 20140287–20140287.
- (108) Rijke, A. M.; Jesser, W. a. The Water Penetration and Repellency of Feathers Revisited. *Condor* **2011**, *113*, 245–254.
- (109) Bormashenko, E.; Bormashenko, Y.; Stein, T.; Whyman, G.; Bormashenko, E. Why do pigeon feathers repel water? Hydrophobicity of penna, Cassie–Baxter wetting hypothesis and Cassie–Wenzel capillarity-induced wetting transition. *J. Colloid Interface Sci.* **2007**, *311*, 212–216.
- (110) Waghmare, P. R.; Gunda, N. S. K.; Mitra, S. K. Under-water superoleophobicity of fish scales. *Sci. Rep.* **2014**, *4*.
- (111) Liu, X.; Zhou, J.; Xue, Z.; Gao, J.; Meng, J.; Wang, S.; Jiang, L. Clam's shell inspired high-energy inorganic coatings with underwater low adhesive superoleophobicity. *Adv. Mater.* **2012**, *24*, 3401–3405.
- (112) Feng, X.-Q.; Gao, X.; Wu, Z.; Jiang, L.; Zheng, Q.-S. Superior Water Repellency of Water Strider Legs with Hierarchical Structures: Experiments and Analysis. *Langmuir* **2007**, *23*, 4892–4896.
- (113) Sun, M.; Watson, G. S.; Zheng, Y.; Watson, J. A.; Liang, A. Wetting properties on nanostructured surfaces of cicada wings. *J. Exp. Biol.* **2009**, *212*, 3148–3155.
- (114) Quéré, D.; Reyssat, M. Non-adhesive lotus and other hydrophobic materials. *Philos. Trans. A. Math. Phys. Eng. Sci.* **2008**, *366*, 1539–1556.
- (115) Bush, J. W. M.; Hu, D. L.; Prakash, M. The Integument of Water-walking Arthropods: Form and Function. *Adv. In Insect Phys.* **2007**, *34*, 117–192.
- (116) Hensel, R.; Neinhuis, C.; Werner, C. The springtail cuticle as a blueprint for omniphobic surfaces. *Chem. Soc. Rev.* **2016**, *45*, 323–341.
- (117) Yong, J.; Chen, F.; Yang, Q.; Bian, H.; Du, G.; Shan, C.; Huo, J.; Fang, Y.; Hou, X. Oil-water separation: A gift from the desert. *Adv. Mater. Interfaces* **2016**, *3*, 1–7.
- (118) Lee, S. G.; Lim, H. S.; Lee, D. Y.; Kwak, D.; Cho, K. Tunable Anisotropic Wettability of Rice Leaf-Like Wavy Surfaces. *Adv. Funct. Mater.* **2013**, *23*, 547–553.
- (119) Duan, B.; Gao, H.; He, M.; Zhang, L. Hydrophobic Modification on Surface of Chitin Sponges for Highly Effective Separation of Oil. *ACS Appl. Mater. Interfaces* **2014**, *6*, 19933–19942.
- (120) Wang, G.; Zeng, Z. X.; Wu, X. D.; Ren, T. H.; Han, J.; Xue, Q. J. Three-Dimensional Structured Sponge with High Oil Wettability for the Clean-up of Oil Contaminations and Separation of Oil-Water Mixtures. *Polym. Chem.* **2014**, *5*, 5942–5948.
- (121) Chen, X.; Weibel, J. A.; Garimella, S. V. Continuous Oil-Water Separation Using Polydimethylsiloxane-Functionalized Melamine Sponge. *Ind. Eng. Chem. Res.* **2016**, *55*, 3596–3602.
- (122) Ke, Q.; Jin, Y.; Jiang, P.; Yu, J. Oil/Water Separation Performances of Superhydrophobic and Superoleophilic Sponges. *Langmuir* **2014**, *30*, 13137–13142.
- (123) Zhang, L.; Xu, L.; Sun, Y.; Yang, N. Robust and Durable Superhydrophobic Polyurethane Sponge for Oil/Water Separation. *Ind. Eng. Chem. Res.* **2016**, *55*, 11260–11268.

- (124) Stolz, A.; Le Floch, S.; Reinert, L.; Ramos, S. M.; Tuillon-Combes, J.; Soneda, Y.; Chaudet, P.; Baillis, D.; Blanchard, N.; Duclaux, L.; San-Miguel, A. Melamine-derived carbon sponges for oil-water separation. *Carbon N. Y.* **2016**, *107*, 198–208.
- (125) Cortese, B.; Caschera, D.; Federici, F.; Ingo, G. M.; Gigli, G. Superhydrophobic Fabrics for Oil–Water Separation through a Diamond Like Carbon (DLC) Coating. *J. Mater. Chem. A* **2014**, *2*, 6781–6789.
- (126) Liu, F.; Ma, M.; Zang, D.; Gao, Z.; Wang, C. Fabrication of superhydrophobic/superoleophilic cotton for application in the field of water/oil separation. *Carbohydr. Polym.* **2014**, *103*, 480–487.
- (127) Rana, M.; Chen, J.-T.; Yang, S.; Ma, P.-C. Biomimetic Superoleophobicity of Cotton Fabrics for Efficient Oil-Water Separation. *Adv. Mater. Interfaces* **2016**, *3*, 1600128.
- (128) Chen, J.; Shen, C.; Yang, S.; Rana, M.; Ma, P.-C. Acid and temperature dual-responsive cotton fabrics with polymer coating. *Compos. Commun.* **2017**, *4*, 10–15.
- (129) Liang, L.; Su, M.; Zheng, C.; Li, J.; Zhan, H.; Li, X.; Meng, X. Fabrication of hydrophobic/oleophilic cotton fabric by mussel-inspired chemistry for oil/water separation. *Fibers Polym.* **2017**, *18*, 2307–2314.
- (130) Lei, S.; Shi, Z.; Ou, J.; Wang, F.; Xue, M.; Li, W.; Qiao, G.; Guan, X.; Zhang, J. Durable superhydrophobic cotton fabric for oil/water separation. *Colloids Surfaces A Physicochem. Eng. Asp.* **2017**, *533*, 249–254.
- (131) Zhou, C.; Chen, Z.; Yang, H.; Hou, K.; Zeng, X.; Zheng, Y.; Cheng, J. Nature-Inspired Strategy toward Superhydrophobic Fabrics for Versatile Oil/Water Separation. *ACS Appl. Mater. Interfaces* **2017**, *9*, 9184–9194.
- (132) He, K.; Duan, H.; Chen, G. Y.; Liu, X.; Yang, W.; Wang, D. Cleaning of Oil Fouling with Water Enabled by Zwitterionic Polyelectrolyte Coatings: Overcoming the Imperative Challenge of Oil-Water Separation Membranes. *ACS Nano* **2015**, *9*, 9188–9198.
- (133) Fan, J.; Duan, J.; Yu, Z.; Wu, D.; Zhu, H. Oleophobicity of Chitosan/Micron-alumina-Coated Stainless Steel Mesh for Oil/Water Separation. *Water, Air, Soil Pollut.* **2016**, *227*, 163.
- (134) Li, B.; Liu, X.; Zhang, X.; Chai, W. Stainless steel mesh coated with silica for oil–water separation. *Eur. Polym. J.* **2015**, *73*, 374–379.
- (135) Zhang, W.; Shi, Z.; Zhang, F.; Liu, X.; Jin, J.; Jiang, L. Superhydrophobic and Superoleophilic PVDF Membranes for Effective Separation of Water-in-Oil Emulsions with High Flux. *Adv. Mater.* **2013**, *25*, 2071–2076.
- (136) Solomon, B. R.; Hyder, M. N.; Varanasi, K. K. Separating Oil-Water Nanoemulsions Using Flux-Enhanced Hierarchical Membranes. *Sci. Rep.* **2014**, *4*, 5504.
- (137) Jiang, Y.; Hou, J.; Xu, J.; Shan, B. Switchable oil/water separation with efficient and robust Janus nanofiber membranes. *Carbon N. Y.* **2017**, *115*, 477–485.
- (138) Lu, D.; Zhang, T.; Gutierrez, L.; Ma, J.; Croué, J.-P. Influence of Surface Properties of Filtration-Layer Metal Oxide on Ceramic Membrane Fouling during Ultrafiltration of Oil/Water Emulsion. *Environ. Sci. Technol.* **2016**, *50*, 4668–4674.
- (139) Chen, P.-C.; Xu, Z.-K. Mineral-Coated Polymer Membranes with Superhydrophilicity and Underwater Superoleophobicity for Effective Oil/Water Separation. *Sci. Rep.* **2013**, *3*, 2776.
- (140) Obaid, M.; Barakat, N. A. M.; Faddali, O. A.; Motlak, M.; Almajid, A. A.; Khalil, K. A. Effective and reusable oil/water separation membranes based on modified polysulfone electrospun nanofiber mats. *Chem. Eng. J.* **2015**, *259*, 449–456.
- (141) Zhu, Y.; Wang, D.; Jiang, L.; Jin, J. Recent progress in developing advanced membranes for emulsified oil/water separation. *NPG Asia Mater.* **2014**, *6*, e101.
- (142) Zhu, H.; Chen, D.; Li, N.; Xu, Q.; Li, H.; He, J.; Lu, J. Graphene foam with switchable oil wettability for oil and organic solvents recovery. *Adv. Funct. Mater.* **2015**, *25*, 597–605.

- (143) Gao, R.; Liu, Q.; Wang, J.; Liu, J.; Yang, W.; Gao, Z.; Liu, L. Construction of superhydrophobic and superoleophilic nickel foam for separation of water and oil mixture. *Appl. Surf. Sci.* **2014**, *289*, 417–424.
- (144) Luo, Z.-Y.; Lyu, S.-S.; Wang, Y.-Q.; Mo, D.-C. Fluorine-Induced Superhydrophilic Ti Foam with Surface Nanocavities for Effective Oil-in-Water Emulsion Separation. *Ind. Eng. Chem. Res.* **2017**, *56*, 699–707.
- (145) Verwey, E. J. W. Theory of the Stability of Lyophobic Colloids. *J. Phys. Colloid Chem.* **1947**, *51*, 631–636.
- (146) Berne, B. J.; Pecora, R., *Dynamic light scattering with application to chemistry, biology and physics*; Dover Publications, Mineola: 2000.
- (147) Roig, A. R.; Alessandrini, J. L. Particle Size Distributions from Static Light Scattering with Regularized Non-Negative Least Squares Constraints. *Part. Part. Syst. Charact.* **2006**, *23*, 431–437.
- (148) Xu, R. Light scattering: A review of particle characterization applications. *Particuology* **2015**, *18*, 11–21.
- (149) Yang, M. In *Prod. Water*, Lee, K., Neff, J., Eds.; Springer New York: New York, NY, 2011; Chapter 2, pp 57–88.
- (150) Li, J.; Li, D.; Yang, Y.; Li, J.; Zha, F.; Lei, Z. A prewetting induced underwater superoleophobic or underoil (super) hydrophobic waste potato residue-coated mesh for selective efficient oil/water separation. *Green Chem.* **2016**, *18*, 541–549.
- (151) Fan, J. B.; Song, Y.; Wang, S.; Meng, J.; Yang, G.; Guo, X.; Feng, L.; Jiang, L. Directly Coating Hydrogel on Filter Paper for Effective Oil-Water Separation in Highly Acidic, Alkaline, and Salty Environment. *Adv. Funct. Mater.* **2015**, *25*, 5368–5375.
- (152) Xue, Z.; Wang, S.; Lin, L.; Chen, L.; Liu, M.; Feng, L.; Jiang, L. A Novel Superhydrophilic and Underwater Superoleophobic Hydrogel-Coated Mesh for Oil/Water Separation. *Adv. Mater.* **2011**, *23*, 4270–4273.
- (153) Kavalenka, M. N.; Hopf, a.; Schneider, M.; Worgull, M.; Hölscher, H. Wood-based microhaired superhydrophobic and underwater superoleophobic surfaces for oil/water separation. *RSC Adv.* **2014**, *4*, 31079.
- (154) Coca, J.; Gutiérrez, G.; Benito, J. In *Water Purif. Manag.* Coca-Pardos, J., Gutiérrez-Cervelló, G., Eds.; Springer Netherlands: Dordrecht, 2011; Chapter 1, pp 1–55.
- (155) Dunderdale, G. J.; Urata, C.; Sato, T.; England, M. W.; Hozumi, A. Continuous, High-Speed, and Efficient Oil/Water Separation using Meshes with Antagonistic Wetting Properties. *ACS Appl. Mater. Interfaces* **2015**, *23*, 1–5.
- (156) Brown, P. S.; Bhushan, B. Mechanically durable, superomniphobic coatings prepared by layer-by-layer technique for self-cleaning and anti-smudge. *J. Colloid Interface Sci.* **2015**, *456*, 210–218.
- (157) Liu, H.; Raza, A.; Aili, A.; Lu, J.; AlGhaferi, A.; Zhang, T. Sunlight-Sensitive Anti-Fouling Nanostructured TiO<sub>2</sub> Coated Cu Meshes for Ultrafast Oily Water Treatment. *Sci. Rep.* **2016**, *6*, 25414.
- (158) Zhang, L.; Zhong, Y.; Cha, D.; Wang, P. A Self-Cleaning Underwater Superoleophobic Mesh for Oil-Water Separation. *Sci. Rep.* **2013**, *3*, 2326.
- (159) Zhang, Z.; Sèbe, G.; Rentsch, D.; Zimmermann, T.; Tingaut, P. Ultralightweight and flexible silylated nanocellulose sponges for the selective removal of oil from water. *Chem. Mater.* **2014**, *26*, 2659–2668.
- (160) Zhu, Q.; Pan, Q. Mussel-Inspired Direct Immobilization of Nanoparticles and Application for Oil-Water Separation. *ACS Nano* **2014**, *8*, 1402–1409.
- (161) Zhang, J.; Seeger, S. Polyester materials with superwetting silicone nanofilaments for oil/water separation and selective oil absorption. *Adv. Funct. Mater.* **2011**, *21*, 4699–4704.



- (162) Jung, Y. C.; Bhushan, B. Wetting behavior of water and oil droplets in three-phase interfaces for hydrophobicity/philicity and oleophobicity/philicity. *Langmuir* **2009**, *25*, 14165–14173.
- (163) Cheng, Q.; Li, M.; Zheng, Y.; Su, B.; Wang, S.; Jiang, L. Janus interface materials: superhydrophobic air/solid interface and superoleophobic water/solid interface inspired by a lotus leaf. *Soft Matter* **2011**, *7*, 5948–5951.
- (164) Cai, Y.; Lu, Q.; Guo, X.; Wang, S.; Qiao, J.; Jiang, L. Salt-Tolerant Superoleophobicity on Alginate Gel Surfaces Inspired by Seaweed (*Saccharina japonica*). *Adv. Mater.* **2015**, *27*, 4162–4168.
- (165) Howarter, J. A.; Genson, K. L.; Youngblood, J. P. Wetting behavior of oleophobic polymer coatings synthesized from fluorosurfactant-macromers. *ACS Appl. Mater. Interfaces* **2011**, *3*, 2022–2030.
- (166) Paul, U. C.; Fragouli, D.; Bayer, I. S.; Athanassiou, A. Functionalized cellulose networks for efficient oil removal from oil-water emulsions. *Polymers (Basel)*. **2016**, *8*.
- (167) Peng, H.; Wu, J.; Wang, Y.; Wang, H.; Liu, Z.; Shi, Y.; Guo, X. A facile approach for preparation of underwater superoleophobicity cellulose/chitosan composite aerogel for oil/water separation. *Appl. Phys. A Mater. Sci. Process.* **2016**, *122*.
- (168) Yang, J.; Song, H.; Yan, X.; Tang, H.; Li, C. Superhydrophilic and superoleophobic chitosan-based nanocomposite coatings for oil/water separation. *Cellulose* **2014**, *21*, 1851–1857.
- (169) Lu, F.; Chen, Y.; Liu, N.; Cao, Y.; Xu, L.; Wei, Y.; Feng, L. A fast and convenient cellulose hydrogel-coated colander for high-efficiency oil–water separation. *RSC Adv.* **2014**, *4*, 32544.
- (170) Zhou, X.; Zhang, Z.; Xu, X.; Guo, F.; Zhu, X.; Men, X.; Ge, B. Robust and durable superhydrophobic cotton fabrics for oil/water separation. *ACS Appl. Mater. Interfaces* **2013**, *5*, 7208–7214.
- (171) Singh, V.; Jinka, S.; Hake, K.; Parameswaran, S.; Kendall, R. J.; Ramkumar, S. Novel natural sorbent for oil spill cleanup. *Ind. Eng. Chem. Res.* **2014**, *53*, 11954–11961.
- (172) Engelund, E. T.; Thygesen, L. G.; Svensson, S.; Hill, C. A. S. A critical discussion of the physics of wood-water interactions. *Wood Sci. Technol.* **2013**, *47*, 141–161.
- (173) Fahlén, J.; Salmén, L. On the Lamellar Structure of the Tracheid Cell Wall. *Plant Biol.* **2002**, *4*, 339–345.
- (174) Donaldson, L.; Bardage, S.; Daniel, G. Three-dimensional imaging of a sawn surface: A comparison of confocal microscopy, scanning electron microscopy, and light microscopy combined with serial sectioning. *Wood Sci. Technol.* **2007**, *41*, 551–564.
- (175) Ross, R. J.; USDA Forest Service., F. P. L. *Wood handbook : wood as an engineering material*; tech. rep.; 2010, p 508.
- (176) Bixler, G. D.; Bhushan, B. Biofouling: lessons from nature. *Philos. Trans. R. Soc.* **2012**, *370*, 2381–2417.
- (177) Tirmizi, N. P.; Raghuraman, B.; Wiencek, J. Demulsification of Water / Oil / Solid Emulsions by Hollow-Fiber Membranes. *AIChE J.* **1996**, *42*, 1263–1276.
- (178) Tuteja, A.; Choi, W.; Mabry, J. M.; McKinley, G. H.; Cohen, R. E. Robust Omniphobic Surfaces. *Proc. Natl. Acad. Sci.* **2008**, *105*, 18200–18205.
- (179) Gao, X.; Xu, L. P.; Xue, Z.; Feng, L.; Peng, J.; Wen, Y.; Wang, S.; Zhang, X. Dual-scaled porous nitrocellulose membranes with underwater superoleophobicity for highly efficient oil/water separation. *Adv. Mater.* **2014**, *26*, 1771–1775.
- (180) Mantanis, G. I.; Young, R. a. Wetting of wood. *Wood Sci. Technol.* **1997**, *31*, 339–353.
- (181) Gérardin, P.; Petrič, M.; Petrič, M.; Lambert, J.; Ehrhardt, J. J. Evolution of wood surface free energy after heat treatment. *Polym. Degrad. Stab.* **2007**, *92*, 653–657.

- (182) Gindl, M.; Reiterer, A.; Sinn, G.; Stanzl-Tschegg, S. E. Effects of surface ageing on wettability, surface chemistry, and adhesion of wood. *Holz als Roh- und Werkst.* **2004**, *62*, 273–280.
- (183) Rodríguez-Valverde, M. A.; Cabrerizo-Vílchez, M. A.; Rosales-López, P.; Páez-Dueñas, A.; Hidalgo-Álvarez, R.; Rosales-López, P.; Páez-Dueñas, A.; Hidalgo-Lvarez, R. Contact angle measurements on two (wood and stone) non-ideal surfaces. *Colloids Surfaces A Physicochem. Eng. Asp.* **2002**, *206*, 485–495.
- (184) Chen, P.-Y.; McKittrick, J.; Meyers, M. A. Biological materials: Functional adaptations and bioinspired designs. *Prog. Mater. Sci.* **2012**, *57*, 1492–1704.
- (185) Wegst, U. G. K.; Bai, H.; Saiz, E.; Tomsia, A. P.; Ritchie, R. O. Bioinspired structural materials. *Nat. Mater.* **2015**, *14*, 23–36.
- (186) Darmanin, T.; Guittard, F. Recent advances in the potential applications of bioinspired superhydrophobic materials. *J. Mater. Chem. A* **2014**, *2*, 16319–16359.
- (187) Lv, S.; Fu, F.; Wang, S.; Huang, J.; Hu, L. Novel wood-based all-solid-state flexible supercapacitors fabricated with a natural porous wood slice and polypyrrole. *RSC Adv.* **2015**, *5*, 2813–2818.
- (188) Trey, S.; Jafarzadeh, S.; Johansson, M. In situ polymerization of polyaniline in wood veneers. *ACS Appl. Mater. Interfaces* **2012**, *4*, 1760–1769.
- (189) Li, Y.; Fu, Q.; Yu, S.; Yan, M.; Berglund, L. Optically Transparent Wood from a Nanoporous Cellulosic Template: Combining Functional and Structural Performance. *Biomacromolecules* **2016**, *17*, 1358–1364.
- (190) Wang, Y.; Tian, T.; Cabane, E. Wood Composites with Wettability Patterns Prepared by Controlled and Selective Chemical Modification of a Three-Dimensional Wood Scaffold. *ACS Sustain. Chem. Eng.* **2017**, *5*, 11686–11694.
- (191) Cabane, E.; Keplinger, T.; Merk, V.; Hass, P.; Burgert, I. Renewable and Functional Wood Materials by Grafting Polymerization Within Cell Walls. *ChemSusChem* **2014**, *7*, 1020–1025.
- (192) Merk, V.; Chanana, M.; Keplinger, T.; Gaan, S.; Burgert, I. Hybrid wood materials with improved fire retardance by bio-inspired mineralisation on the nano- and submicron level. *Green Chem.* **2015**, *17*, 1423–1428.
- (193) Frey, M.; Widner, D.; Segmehl, J. S.; Casdorff, K.; Keplinger, T.; Burgert, I. Delignified and Densified Cellulose Bulk Materials with Excellent Tensile Properties for Sustainable Engineering. *ACS Appl. Mater. Interfaces* **2018**, *10*, 5030–5037.
- (194) Norimoto, M.; Gril, J.; Rowell, R. M. Rheological properties of chemically modified wood: relationships between dimensional and creep stability. *Wood Fiber Sci.* **1992**, *24*, 25–35.
- (195) Zampano, G.; Bertoldo, M.; Bronco, S. Poly(ethyl acrylate) surface-initiated ATRP grafting from wood pulp cellulose fibers. *Carbohydr. Polym.* **2009**, *75*, 22–31.
- (196) Yu, H.; Fu, Y.; Li, G.; Liu, Y. Antimicrobial surfaces of quaternized poly[(2-dimethyl amino)ethyl methacrylate] grafted on wood via ARGET ATRP. *Holzforschung* **2013**, *67*, 455–461.
- (197) Park, Y. I.; Spiecker, H. Variations in the tree-ring structure of Norway spruce (*Picea abies*) under contrasting climates. *Dendrochronologia* **2005**, *23*, 93–104.
- (198) Segmehl, J. S.; Lauria, A.; Keplinger, T.; Berg, J. K.; Burgert, I. Tracking of Short Distance Transport Pathways in Biological Tissues by Ultra-Small Nanoparticles. *Front. Chem.* **2018**, *6*, 1–9.
- (199) Okajima, K.; Kowsaka, K.; Kamide, K. An explanation of the solubility behaviour of cellulose acetate in various solvents in terms of supermolecular structure formed by introduction of a substituent group into the glucopyranose unit. *Polym. Int.* **1992**, *29*, 47–59.
- (200) Rowell, R. M.; Ellis, W. D. In *Urethane Chem. Appl.* 1981; Chapter 19, pp 263–284.

- (201) Rowell, R. M.; Gutzmer, D. I.; Sachs, I. B.; Kinney, R. E. Effects of alkylene oxide treatments on dimensional stability of wood. *Wood Sci.* **1976**, *9*, 51–54.
- (202) Schwanninger, M.; Rodrigues, J.; Pereira, H.; Hinterstoesser, B. Effects of short-time vibratory ball milling on the shape of FT-IR spectra of wood and cellulose. *Vib. Spectrosc.* **2004**, *36*, 23–40.
- (203) Raihane, M.; Ameduri, B. Radical copolymerization of 2,2,2-trifluoroethyl methacrylate with cyano compounds for dielectric materials: Synthesis and characterization. *J. Fluor. Chem.* **2006**, *127*, 391–399.
- (204) Socrates, G., *Infrared and Raman characteristic group frequencies*; John Wiley & Sons, Ltd: 2001, p 347.
- (205) Anastassopoulou, J. D. In *Chem. Prop. Biomol. Syst.* Rizzarelli, E., Theophanides, T., Eds.; Topics in Molecular Organization and Engineering, Vol. 8; Springer Netherlands: Dordrecht, 1991, pp 1–9.
- (206) Hill, C.; Jones, D. The dimensional stabilization of Corsican pine sapwood by reaction with carboxylic acid anhydrides. *Holzforschung* **1996**, *50*, 457–462.
- (207) Rowell, R. M. In *Chem. Solid Wood*, 1984; Chapter 4, pp 175–210.
- (208) Rowell, R. M. Distribution of reacted chemicals in southern pine modified with methyl isocyanate. *Wood Sci.* **1980**, *13*, 102–110.
- (209) Truksne, D.; Svalbe, K. Study of the content of bound acetyl groups in the main components of acetylated wood. *Latv. Lauksaimn. Akad. Raksti* **1977**, *130*, 32–39.
- (210) Habibi, Y.; Lucia, L. A.; Rojas, O. J. Cellulose Nanocrystals: Chemistry, Self-Assembly, and Applications. *Chem. Rev.* **2010**, *110*, 3479–3500.
- (211) Laurichesse, S.; Avérous, L. Chemical modification of lignins: Towards biobased polymers. *Prog. Polym. Sci.* **2014**, *39*, 1266–1290.
- (212) Mourya, V.; Inamdar, N. N. Chitosan-modifications and applications: Opportunities galore. *React. Funct. Polym.* **2008**, *68*, 1013–1051.
- (213) Jedvert, K.; Heinze, T. Cellulose modification and shaping – a review. *J. Polym. Eng.* **2017**, *37*, 845–860.
- (214) Zhang, X.; Qu, T.; Mosier, N. S.; Han, L.; Xiao, W. Cellulose modification by recyclable swelling solvents. *Biotechnol. Biofuels* **2018**, *11*, 191.
- (215) Fatona, A.; Berry, R. M.; Brook, M. A.; Moran-Mirabal, J. M. Versatile Surface Modification of Cellulose Fibers and Cellulose Nanocrystals through Modular Triazinyl Chemistry. *Chem. Mater.* **2018**, *30*, 2424–2435.
- (216) Anterola, A. M.; Lewis, N. G. Review Trends in lignin modification: a comprehensive analysis of the effects of genetic manipulations/mutations on lignification and vascular integrity. *Phytochemistry* **2002**, *61*, 221–294.
- (217) Umezawa, T. Lignin modification in planta for valorization. *Phytochem. Rev.* **2018**.
- (218) Zoppe, J. O.; Ataman, N. C.; Mocny, P.; Wang, J.; Moraes, J.; Klok, H. A. Surface-Initiated Controlled Radical Polymerization: State-of-the-Art, Opportunities, and Challenges in Surface and Interface Engineering with Polymer Brushes. *Chem. Rev.* **2017**, *117*, 1105–1318.
- (219) Carlmark, A.; Malmström, E. E. ATRP Grafting from Cellulose Fibers to Create Block-Copolymer Grafts. *Biomacromolecules* **2003**, *4*, 1740–1745.
- (220) Diao, B.; Zhang, Z.; Zhu, J.; Li, J. Biomass-based thermogelling copolymers consisting of lignin and grafted poly(N-isopropylacrylamide), poly(ethylene glycol), and poly(propylene glycol). *RSC Adv.* **2014**, *4*, 42996–43003.
- (221) Tang, F.; Zhang, L.; Zhu, J.; Cheng, Z.; Zhu, X. Surface Functionalization of Chitosan Nanospheres via Surface-Initiated AGET ATRP Mediated by Iron Catalyst in the Presence of Limited Amounts of Air. *Ind. Eng. Chem. Res.* **2009**, *48*, 6216–6223.

- (222) Vidiella del Blanco, M.; Gomez, V.; Keplinger, T.; Grafulha, L. F.; Cabane, E. Solvent-Controlled Spatial Distribution of SI-AGET-ATRP Grafted Polymers in Lignocellulosic Materials. (*accepted in Biomacromolecules*) **2018**.
- (223) Matyjaszewski, K.; Tsarevsky, N. V. Nanostructured functional materials prepared by atom transfer radical polymerization. *Nat. Chem.* **2009**, *1*, 276–288.
- (224) Feng, H.; Lu, X.; Wang, W.; Kang, N.-G.; Mays, J. Block Copolymers: Synthesis, Self-Assembly, and Applications. *Polymers (Basel)*. **2017**, *9*, 494.
- (225) Alexandridis, P. Amphiphilic copolymers and their applications. *Curr. Opin. Colloid Interface Sci.* **1996**, *1*, 490–501.
- (226) Hansen, N. M. L.; Gerstenberg, M.; Haddleton, D. M.; Hvilsted, S. Synthesis, characterization, and bulk properties of amphiphilic copolymers containing fluorinated methacrylates from sequential copper-mediated radical polymerization. *J. Polym. Sci. Part A Polym. Chem.* **2008**, *46*, 8097–8111.
- (227) Malmström, E.; Carlmark, A. Controlled grafting of cellulose fibres – an outlook beyond paper and cardboard. *Polym. Chem.* **2012**, *3*, 1702–1713.
- (228) Castelvetro, V.; Geppi, M.; Giaiacopi, S.; Mollica, G. Cotton Fibers Encapsulated with Homo- and Block Copolymers: Synthesis by the Atom Transfer Radical Polymerization Grafting-From Technique and Solid-State NMR Dynamic Investigations. *Biomacromolecules* **2007**, *8*, 498–508.
- (229) Ellis, W. D.; O'Dell, J. L. Wood-polymer composites made with acrylic monomers, isocyanate, and maleic anhydride. *J. Appl. Polym. Sci.* **1999**, *73*, 2493–2505.
- (230) Devi, R. R.; Maji, T. K. Chemical modification of simul wood with styrene–acrylonitrile copolymer and organically modified nanoclay. *Wood Sci. Technol.* **2012**, *46*, 299–315.
- (231) Li, Y.; Wu, Q.; Li, J.; Liu, Y.; Wang, X.-M.; Liu, Z. Improvement of dimensional stability of wood via combination treatment: swelling with maleic anhydride and grafting with glycidyl methacrylate and methyl methacrylate. *Holzforschung* **2012**, *66*, 59–66.
- (232) Tastet, D.; Save, M.; Charrier, F.; Charrier, B.; Ledeuil, J.-B.; Dupin, J.-C.; Billon, L. Functional biohybrid materials synthesized via surface-initiated MADIX/RAFT polymerization from renewable natural wood fiber: Grafting of polymer as non leaching preservative. *Polymer (Guildf)*. **2011**, *52*, 606–616.
- (233) Cheesman, B. T.; Neilson, A. J. G.; Willott, J. D.; Webber, G. B.; Edmondson, S.; Wanless, E. J. Effect of colloidal substrate curvature on pH-responsive polyelectrolyte brush growth. *Langmuir* **2013**, *29*, 6131–6140.
- (234) Zoppe, J. O.; Xu, X.; Känel, C.; Orsolini, P.; Siqueira, G.; Tingaut, P.; Zimmermann, T.; Klok, H. A. Effect of Surface Charge on Surface-Initiated Atom Transfer Radical Polymerization from Cellulose Nanocrystals in Aqueous Media. *Biomacromolecules* **2016**, *17*, 1404–1413.
- (235) Xiong, X.-B.; Binkhathlan, Z.; Molavi, O.; Lavasanifar, A. Amphiphilic block co-polymers: Preparation and application in nanodrug and gene delivery. *Acta Biomater.* **2012**, *8*, 2017–2033.
- (236) Adams, M. L.; Lavasanifar, A.; Kwon, G. S. *Amphiphilic block copolymers for drug delivery*; tech. rep. 7; 2003, pp 1343–1355.
- (237) Xu, J.; Sun, Y.; Chen, J.; Zhong, S. Novel application of amphiphilic block copolymers in Pickering emulsions and selective recognition of proteins. *New J. Chem.* **2018**, *42*, 3028–3034.
- (238) Qian, W.; Song, X.; Feng, C.; Xu, P.; Jiang, X.; Li, Y.; Huang, X. Construction of PEG-based amphiphilic brush polymers bearing hydrophobic poly(lactic acid) side chains via successive RAFT polymerization and ROP. *Polym. Chem.* **2016**, *7*, 3300–3310.
- (239) Mantanis, G. I. Wood chemical modification. *BioResources* **2017**, *12*, 4478–4489.
- (240) Roghani-Mamaqani, H.; Haddadi-Asl, V.; Khezri, K.; Salami-Kalajahi, M. Polystyrene-grafted graphene nanoplatelets with various graft densities by atom transfer radical polymerization from the edge carboxyl groups. *RSC Adv.* **2014**, *4*, 24439–24452.

- (241) Drafz, M. H. H.; Franz, A.; Namyslo, J. C.; Kaufmann, D. E. Chemistry and Spectroscopy of Renewable Materials, Part 1: Imaging the Penetration Depth of Covalent Wood Modification. *ACS Sustain. Chem. Eng.* **2015**, *3*, 566–568.
- (242) Mahltig, B.; Swaboda, C.; Roessler, A.; Böttcher, H. Functionalising wood by nanosol application. *J. Mater. Chem.* **2008**, *18*, 3180.
- (243) Cuccato, D.; Storti, G.; Morbidelli, M. Experimental and Modeling Study of Acrylamide Copolymerization with Quaternary Ammonium Salt in Aqueous Solution. *Macromolecules* **2015**, *48*, 5076–5087.
- (244) Kizhakkedathu, J. N.; Brooks, D. E. Synthesis of Poly(N,N-dimethylacrylamide) Brushes from Charged Polymeric Surfaces by Aqueous ATRP: Effect of Surface Initiator Concentration. *Macromolecules* **2003**, *36*, 591–598.
- (245) Hannon, M. J.; Boerio, F. J.; Koenig, J. L. Vibrational Analysis of Polytetrafluoroethylene. *J. Chem. Phys.* **1969**, *50*, 2829–2836.
- (246) Shimoaka, T.; Sonoyama, M.; Amii, H.; Takagi, T.; Kanamori, T.; Hasegawa, T. Study of Perfluoroalkyl Chain-Specific Band Shift in Infrared Spectra on the Chain Length. *J. Phys. Chem. A* **2017**, *121*, 8425–8431.
- (247) Hofer, C. J.; Zlateski, V.; Stoessel, P. R.; Paunescu, D.; Schneider, E. M.; Grass, R. N.; Zeltner, M.; Stark, W. J. Stable dispersions of azide functionalized ferromagnetic metal nanoparticles. *Chem. Commun.* **2015**, *51*, 1826–1829.
- (248) Jousset, S.; Bellissent, H.; Galin, J. C. Polyelectrolytes of High Charge Density in Organic Solvents. Synthesis and Viscosimetric Behavior. *Macromolecules* **1998**, *31*, 4520–4530.
- (249) Biesalski, M.; Johannsmann, D.; Rühle, J. Electrolyte-induced collapse of a polyelectrolyte brush. *J. Chem. Phys.* **2004**, *120*, 8807–8814.
- (250) Guan, J. H.; Wells, G. G.; Xu, B.; Mchale, G.; Wood, D.; Martin, J.; Stuart-Cole, S. Evaporation of Sessile Droplets on Slippery Liquid-Infused Porous Surfaces (SLIPS). *Langmuir* **2015**, *31*, 11781–11789.
- (251) Misyura, S. Y. Evaporation of a sessile water drop and a drop of aqueous salt solution. *Sci. Rep.* **2017**, *7*, 14759.
- (252) Vidiella del Blanco, M.; Gomez, V.; Keplinger, T.; Cabane, E. Grafting of Amphiphilic Block Copolymers on Lignocellulosic Materials via SI-AGET-ATRP. (*submitted*) **2018**.
- (253) Kagawa, Y.; Ishigami, T.; Hayashi, K.; Fuse, H.; Mino, Y.; Matsuyama, H. Permeation of concentrated oil-in-water emulsions through a membrane pore: numerical simulation using a coupled level set and the volume-of-fluid method. *Soft Matter* **2014**, *10*, 7985–7992.
- (254) Hakkila, P., *Utilization of Residual Forest Biomass*, 1989, pp 352–477.
- (255) Brown, P. S.; Bhushan, B. Bioinspired, roughness-induced, water and oil super-philic and super-phobic coatings prepared by adaptable layer-by-layer technique. *Sci. Rep.* **2015**, *5*, 14030.
- (256) Chen, J.; Li, K.; Zhang, H.; Liu, J.; Wu, S.; Fan, Q.; Xue, H. Highly Efficient and Robust Oil/Water Separation Materials Based on Wire Mesh Coated by Reduced Graphene Oxide. *Langmuir* **2017**, *33*, 9590–9597.
- (257) Wang, K.; Yiming, W.; Saththasivam, J.; Liu, Z. A flexible, robust and antifouling asymmetric membrane based on ultra-long ceramic/polymeric fibers for high-efficiency separation of oil/water emulsions. *Nanoscale* **2017**, *9*, 9018–9025.
- (258) Wang, C.-f.; Huang, H.-c.; Chen, L.-f. Protonated Melamine Sponge for Effective Oil/Water Separation. *Sci. Rep.* **2015**, *5*, 14294.
- (259) Yu, Q.; Zhang, W.; Zhao, X.; Cao, G.; Liu, F.; Di, X.; Yang, H.; Wang, Y.; Wang, C. A Simple, Green Method to Fabricate Composite Membranes for Effective Oil-in-Water Emulsion Separation. *Polymers (Basel)*. **2018**, *10*, 323.

- (260) Chaudhary, J. P.; Vadodariya, N.; Nataraj, S. K.; Meena, R. Chitosan-Based Aerogel Membrane for Robust Oil-in-Water Emulsion Separation. *ACS Appl. Mater. Interfaces* **2015**, *7*, 24957–24962.
- (261) Shi, Z.; Zhang, W.; Zhang, F.; Liu, X.; Wang, D.; Jin, J.; Jiang, L. Ultrafast Separation of Emulsified Oil/Water Mixtures by Ultrathin Free-Standing Single-Walled Carbon Nanotube Network Films. *Adv. Mater.* **2013**, *25*, 2422–2427.
- (262) Zhang, Q.; Liu, N.; Wei, Y.; Feng, L. Facile fabrication of hydrogel coated membrane for controllable and selective oil-in-water emulsion separation. *Soft Matter* **2018**, *14*, 2649–2654.
- (263) Cao, Y.; Liu, N.; Fu, C.; Li, K.; Tao, L.; Feng, L.; Wei, Y. Thermo and pH Dual-Responsive Materials for Controllable Oil/Water Separation. *ACS Appl. Mater. Interfaces* **2014**, *6*, 2026–2030.
- (264) Li, J.; Bai, X.; Tang, X.; Zha, F.; Feng, H.; Qi, W. Underwater superoleophobic/underoil superhydrophobic corn cob coated meshes for on-demand oil/water separation. *Sep. Purif. Technol.* **2018**, *195*, 232–237.
- (265) Zhang, Q.; Cao, Y.; Liu, N.; Zhang, W.; Chen, Y.; Lin, X.; Tao, L.; Wei, Y.; Feng, L. A Facile Approach for Fabricating Dual-Function Membrane: Simultaneously Removing Oil from Water and Adsorbing Water-Soluble Proteins. *Adv. Mater. Interfaces* **2016**, 1–5.
- (266) Ermeydan, M. A. Wood Cell Wall Modification With Hydrophobic Molecules., Ph.D. Thesis, Universität Potsdam, 2014.
- (267) Berlyn, G. P. Microspectrophotometric investigations of free space in plant cell walls. *Am. J. Bot.* **1969**, *56*, 498–506.
- (268) Hillis, W. E. Distribution, properties and formation of some wood extractives. *Wood Sci. Technol.* **1971**, *5*, 272–289.
- (269) Bosshard, H. H. On the Formation of Facultatively Colored Heartwood in *Beilschmiedia tawa*. *Wood Sci. Technol.* **1968**, *2*, 1–12.
- (270) Felhofer, M.; Prats-Mateu, B.; Bock, P.; Gierlinger, N. Antifungal stilbene impregnation: transport and distribution on the micron-level. *Tree Physiol.* **2018**, *00*, 1–12.
- (271) Belt, T.; Keplinger, T.; Hänninen, T.; Rautkari, L. Cellular level distributions of Scots pine heartwood and knot heartwood extractives revealed by Raman spectroscopy imaging. *Ind. Crops Prod.* **2017**, *108*, 327–335.
- (272) *Wood Formation in Trees: Cell and Molecular Biology Techniques*; Chaffey, N. J., Ed.; London: CRC Press: 2002, p 384.
- (273) Magel, E.; Jay-Allemand, C.; Ziegler, H. Formation of heartwood substances in the stemwood of *Robinia pseudoacacia* L. II. Distribution of nonstructural carbohydrates and wood extractives across the trunk; tech. rep. 4; 1994, pp 165–171.
- (274) Magel, E. A.; Drouet, A.; Claudot, A. C.; Ziegler, H. Formation of heartwood substances in the stem of *Robinia pseudoacacia* L. I Distribution of phenylalanine ammonium lyase and chalcone synthase across the trunk. *Trees* **1991**, *5*, 203–207.
- (275) Kai, D.; Zhang, K.; Jiang, L.; Wong, H. Z.; Li, Z.; Zhang, Z.; Loh, X. J. Sustainable and Antioxidant Lignin–Polyester Copolymers and Nanofibers for Potential Healthcare Applications. *ACS Sustain. Chem. Eng.* **2017**, *5*, 6016–6025.
- (276) Joubert, F.; Musa, O. M.; Hodgson, D. R. W.; Cameron, N. R. The preparation of graft copolymers of cellulose and cellulose derivatives using ATRP under homogeneous reaction conditions. *Chem. Soc. Rev.* **2014**, *43*, 7217–7235.
- (277) Kong, L.; Guan, H.; Wang, X. In Situ Polymerization of Furfuryl Alcohol with Ammonium Dihydrogen Phosphate in Poplar Wood for Improved Dimensional Stability and Flame Retardancy. *ACS Sustain. Chem. Eng.* **2018**, *6*, 3349–3357.
- (278) Ran, J.; Wu, L.; Zhang, Z.; Xu, T. Atom transfer radical polymerization (ATRP): A versatile and forceful tool for functional membranes. *Prog. Polym. Sci.* **2014**, *39*, 124–144.

- (279) Liu, Y. L.; Han, C. C.; Wei, T. A. C.; Chang, Y. Surface-initiated atom transfer radical polymerization from porous poly(tetrafluoroethylene) membranes using the C-F groups as initiators. *J. Polym. Sci. Part A Polym. Chem.* **2010**, *48*, 2076–2083.
- (280) Shen, X.; Liu, J.; Feng, X.; Zhao, Y.; Chen, L. Preliminary investigation on hemocompatibility of poly(vinylidene fluoride) membrane grafted with acryloylmorpholine via ATRP. *J. Biomed. Mater. Res. - Part A* **2015**, *103*, 683–692.
- (281) D'Souza, S.; Murata, H.; Jose, M. V.; Askarova, S.; Yantsen, Y.; Andersen, J. D.; Edington, C. D.; Clafshenkel, W. P.; Koepsel, R. R.; Russell, A. J. Engineering of cell membranes with a bisphosphonate-containing polymer using ATRP synthesis for bone targeting. *Biomaterials* **2014**, *35*, 9447–9458.
- (282) Chu, C.-W.; Higaki, Y.; Cheng, C.-H.; Cheng, M.-H.; Chang, C.-W.; Chen, J.-T.; Takahara, A. Zwitterionic polymer brush grafting on anodic aluminum oxide membranes by surface-initiated atom transfer radical polymerization. *Polym. Chem.* **2017**, *8*, 2309–2316.
- (283) Wang, W.-C.; Wang, J.; Liao, Y.; Zhang, L.; Cao, B.; Song, G.; She, X. Surface initiated ATRP of acrylic acid on dopamine-functionalized AAO membranes. *J. Appl. Polym. Sci.* **2010**, *21*, 534–541.
- (284) Liu, P.-S.; Chen, Q.; Liu, X.; Yuan, B.; Wu, S.-S.; Shen, J.; Lin, S.-C. Grafting of Zwitterion from Cellulose Membranes via ATRP for Improving Blood Compatibility. *Biomacromolecules* **2009**, *10*, 2809–2816.
- (285) Han, Y.; Song, S.; Lu, Y.; Zhu, D. A method to modify PVDF microfiltration membrane via ATRP with low-temperature plasma pretreatment. *Appl. Surf. Sci.* **2016**, *379*, 474–479.
- (286) Glasing, J.; Champagne, P.; Cunningham, M. F. Graft modification of chitosan, cellulose and alginate using reversible deactivation radical polymerization (RDRP). *Curr. Opin. Green Sustain. Chem.* **2016**, *2*, 15–21.
- (287) Garcia-Valdez, O.; Champagne, P.; Cunningham, M. F. Graft modification of natural polysaccharides via reversible deactivation radical polymerization. *Prog. Polym. Sci.* **2018**, *76*, 151–173.
- (288) Wang, Z.-H.; Zhu, Y.; Chai, M.-Y.; Yang, W.-T.; Xu, F.-J. Biocleavable comb-shaped gene carriers from dextran backbones with bioreducible ATRP initiation sites. *Biomaterials* **2012**, *33*, 1873–1883.
- (289) Destarac, M. Controlled radical polymerization: Industrial stakes, obstacles and achievements. *Macromol. React. Eng.* **2010**, *4*, 165–179.
- (290) Mohsin, M.; Meribout, M. Oil-water de-emulsification using ultrasonic technology. *Ultrason. Sonochem.* **2015**, *22*, 573–579.
- (291) Leppchen, K.; Dausmann, T.; Curvers, S.; Bertau, M. Microbial De-emulsification: A Highly Efficient Procedure for the Extractive Workup of Whole-Cell Biotransformations. *Org. Process Res. Dev.* **2006**, *10*, 1119–1125.
- (292) Zolfaghari, R.; Fakhru'l-Razi, A.; Abdullah, L. C.; Elnashaie, S. S.; Pendashteh, A. Demulsification techniques of water-in-oil and oil-in-water emulsions in petroleum industry. *Sep. Purif. Technol.* **2016**, *170*, 377–407.





# Marta Vidiella del Blanco



## CONTACT INFORMATION

DATE OF BIRTH: 23.08.1991

NATIONALITY: Spanish

ADDRESS: Birchstrasse 34,  
8057 Zürich (SWITZERLAND)

TEL. (+41) 768 191 554

EMAIL: marta.vidiella@gmail.com

Residence Permit: B

## PROFESSIONAL EXPERIENCE

### ❖ *PhD Candidate*

October 2015/ 2018 (exp.). Wood Material Science.

ETH Zürich, Zürich, Switzerland

#### *Main responsibilities*

- Development of chemically functionalized lignocellulosic-based membranes for oil/water separation.
- Understanding of the SI-ATRP polymerization parameters on lignocellulosic materials.
- Supervision of students (master, bachelor and chemistry apprentice).

**Demonstrated Skills:** Innovation, team leadership and interpersonal skills, analysis and problem solving, project management and organization, research and information management, self-paced project management.

### ❖ *Research Assistant*

June/ September 2015. Research group of Prof. Dr. Morbidelli.

ETH Zürich, Zürich, Switzerland.

#### *Main responsibilities*

- Continuation and documentation of the work done during the master thesis.

**Demonstrated Skills:** Forensic analysis of experimental data, documentation and intellectual property evaluation, communication and presentation skills.

### ❖ *Summer Internship*

July/ September 2012. Europe Polyolefins Research Centre.

The Dow Chemical Company. Terneuzen, The Netherlands.

#### *Main responsibilities*

- Development of a predictive process model for an R&D experimental plant operation.
- Design and implementation of a predicting software based on process kinetics.
- Modelling of product variations.

**Demonstrated Skills:** Understanding of a multinational company structure (divisions and procedures), teamwork and global networking.

## CURRICULUM VITAE

---

### ❖ *Summer Internship*

July/ August 2011. DÜO PLAST A.G.

Lauterbach and Sünna, Germany.

#### *Main responsibilities*

- Gathering polymer extrusion and polymer characterization experience.
- Support on operations and quality control of polymer film production and confection.
- Collaboration on quality control analysis and statistical evaluations.

***Demonstrated Skills:*** Teamwork, market focus and product quality value chain understanding.

## EDUCATION

---

2015/ 2018 (exp) Dr. Sc. ETH Zürich  
ETH Zürich – Switzerland.  
***PhD thesis: Functionalization of Wood Materials for Novel Membranes in Oil/Water Separation Technology*** at ETH, Zürich Switzerland

2013/2015 MSc. in Chemical Engineering  
Institut Químic de Sarrià (IQS)- Universitat Ramon Llull (URL),  
Barcelona - Spain.  
***Master thesis: PVDF-HFP/TiO<sub>2</sub> nano-composites-based polymer electrolyte for Li batteries*** at ETH, Zürich Switzerland – Period: *July 2014 to April 2015.*

2013/2015 BSc. in Chemical Engineering  
University Rovira i Virgili (URV), Tarragona - Spain.  
***Graduate project: Ultrafiltration Fibers Cleaning Process Optimization and Scale Up*** at The Dow Chemical Co Global Water Development Centre. Tarragona, Spain – Period: *February to May 2013*

## LANGUAGES

---

Catalan: Fluent - (Native language)

English: Fluent (C2)

Spanish: Fluent - (Native language)

German: Advanced (C1)

## ADDITIONAL TRAININGS

---

Certified Coach – High Develop Business School Barcelona, Spain.

User knowledge of Microsoft Office Suite.

User of math emulators and mechanical design software (AUTOCAD, ASPEN HYSYS, POLYMATH and MATLAB).

EXTRA-CURRICULAR ACTIVITIES

---

- 2016- 2017            Member of the organizing committee of the annual MaP Graduate Symposium.
- 2017                    Invited speaker at the ESEM 2017 Workshop, ETH Zürich (Switzerland).
- 2011-2018            Member of the organizing committee of the annual QMS Concert (Spain)  
Fundraising initiative in support to NGO's alleviating poverty and social exclusion of children.

AWARDS

---

- 2014                    MOBINT Scholarship from the Agency for Management of University and Research Grants (AGUR) - Generalitat de Catalunya (Catalan Government)
- May 2018              Best poster presentation ex-aequo award: *Solvent-Controlled Modification on Lignocellulosic Materials via SI-ATRP*, Macro Awards - Macromolecular Journals

Best poster presentation ex-aequo award: *Solvent-Controlled Modification on Lignocellulosic Materials via SI-ATRP*, Macro Awards - Macromolecular Journals

PERSONAL INTERESTS

---

- Music                    Piano (studies until 4th grade of Professional Music School).
- Sports                    Badminton, hiking.

## List of Publications

**Vidiella del Blanco, M.**, Fischer, E. J., and Cabane, E., *Underwater Superoleophobic Wood Cross Sections for Efficient Oil/Water Separation*, Adv. Mater. Interfaces **4**, 1700584 (2017).

Wang, Y., Yan, W., Frey, M., **Vidiella del Blanco, M.**, Schubert, M., Adobes-Vidal, M., and Cabane, E., *Liquid-like SiO<sub>2</sub>-g-PDMS coatings on wood surfaces with underwater durability, anti-fouling, anti-smudge and self-healing properties*, Adv. Sustainable Syst., 1800070 (2018)

**Vidiella del Blanco, M.**, Gomez, V., Grafulha, L.G.M., Keplinger, T., and Cabane, E., *Solvent-Controlled Spatial Distribution of SI-AGET-ATRP Grafted Polymers in Lignocellulosic Materials* (accepted in Biomacromolecules).

**Vidiella del Blanco, M.**, Gomez, V., Keplinger, T., and Cabane, E., *SI-AGET-ATRP Grafting of Block Copolymers with Amphiphilic Properties on Lignocellulosic Materials* (submitted).

## List of Conferences

**Oral and Poster:** *Tuning wood surface wettability by grafting-from ATRP*, Nature Inspires Creativity Engineers (NICE), Nice – France, 2016

**Poster:** *Wood membrane for oil-water separation*, Materials and Processes (MaP) Graduate Symposium, ETH Zürich – Switzerland, 2016

**Oral:** *Modifying the Surface Properties of Wood using ATRP Grafting Polymerization*, American Institute of Chemical Engineers (AIChE), San Francisco – USA, 2016

**Oral:** *Wood Membranes for Oil-Water Separation*, International Conference on Biobased Materials and Composites (ICBMC), Nantes – France, 2017

**Invited Oral:** *Evaluation of Treatment on Wood Surfaces*, 1<sup>st</sup> PCBM workshop: Environmental Scanning Electron Microscopy, ETH Zürich – Switzerland, 2017

**Poster:** *Controlled Modification on Wood via SI-ATRP*, Bio-inspired materials, Potsdam – Germany, 2018

**Oral:** *Wood Membranes for Oil/Water Separation*, Materials and Processes (MaP) Graduate Symposium, ETH Zürich – Switzerland, 2018

**Oral:** *Underwater Superoleophobic Wood Cross Sections*, Superhydrophilicity and Wetting Symposium (SWS), Aalto University – Finland, 2018

**Oral:** *SI-ARGET-ATRP Grafting of Block Copolymers with Amphiphilic Properties on Lignocellulosic Materials*  
and

**Poster:** *Solvent-Controlled Modification on Lignocellulosic Materials via SI-ATRP: towards a Wood Membrane for Oil/Water Separation*, Polymer Reaction Engineering (PRE) X, Punta Cana – Dominican Republic, 2018 – **Poster Price Awarded**

---

## Declaration

I, Marta Esther Vidiella del Blanco, declare that this thesis is my own work and has not been submitted in any form for another degree or diploma at any university or other institute. Information derived from the published and unpublished work of others has been acknowledged in the text and a list of references is given in the bibliography.

## Erklärung

Hiermit erkläre ich, Marta Esther Vidiella del Blanco, dass ich die vorliegende Arbeit selbständig und unter Verwendung keiner anderen als den von mir angegebenen Quellen und Hilfsmitteln verfasst habe. Ferner erkläre ich, dass ich bisher weder an der ETH ZÜRICH noch anderweitig versucht habe, eine Dissertation einzureichen oder mich einer Doktorprüfung zu unterziehen.



Zürich, September 19, 2018